



**HAL**  
open science

## Self adhesion of uncrosslinked polar elastomers

Valentine Hervio

► **To cite this version:**

Valentine Hervio. Self adhesion of uncrosslinked polar elastomers. Material chemistry. Université Paris sciences et lettres, 2019. English. NNT : 2019PSLET035 . tel-02896761

**HAL Id: tel-02896761**

**<https://pastel.hal.science/tel-02896761>**

Submitted on 23 Oct 2020

**HAL** is a multi-disciplinary open access archive for the deposit and dissemination of scientific research documents, whether they are published or not. The documents may come from teaching and research institutions in France or abroad, or from public or private research centers.

L'archive ouverte pluridisciplinaire **HAL**, est destinée au dépôt et à la diffusion de documents scientifiques de niveau recherche, publiés ou non, émanant des établissements d'enseignement et de recherche français ou étrangers, des laboratoires publics ou privés.



**THÈSE DE DOCTORAT**  
**DE L'UNIVERSITÉ PSL**

Préparée à l'Ecole Supérieure de Physique et de  
Chimie Industrielles de la ville de Paris (ESPCI)

**Autohésion d'élastomères polaires non-vulcanisés**

Self-adhesion of uncrosslinked polar elastomers

Soutenue par

**Valentine HERVIO**

Le 19 décembre 2019

Ecole doctorale n° 397

**Physique et Chimie des Matériaux**

Spécialité

**Chimie des matériaux**

Composition du jury :

Anke, LINDNER Professeur, Sorbonne Université	<i>Présidente du jury</i>
Pierre-Antoine, ALBOUY Directeur de recherche, Université Paris-sud	<i>Rapporteur</i>
Christophe, DEMAIL Professeur, Université de Pau et des Pays de l'Adour	<i>Rapporteur</i>
Annie, BRULET Ingénieure de recherche, CEA Saclay	<i>Examinatrice</i>
Ilias, ILIOPOULOS Directeur de recherche, ENSAM	<i>Examineur</i>
Costantino, CRETON Directeur de recherche, ESPCI	<i>Directeur de thèse</i>

# **Autohésion d'élastomères polaires non-vulcanisés**

---

- Résumé de la thèse en français -

## **Introduction**

Le procédé de fabrication de réservoirs d'hélicoptères implique la superposition de pièces de caoutchoucs non-vulcanisés, et l'ensemble peut être gardé pendant quelques jours à température ambiante avant le cycle de vulcanisation. Une adhérence suffisante entre les différentes couches est nécessaire afin d'empêcher le décollement et l'apparition de défauts. Lors de cette thèse, le matériau d'étude est le caoutchouc nitrile (« Nitrile Butadiene Rubber », NBR), le poly(acrylonitrile-co-butadiène).

Les principaux objectifs de cette thèse sont les suivants :

- Développer une méthode reproductible et discriminante permettant de caractériser les propriétés autohésives de caoutchouc
- Comprendre les phénomènes physico-chimiques régissant l'adhésion, et l'autohésion, de caoutchouc polaires
- Proposer des stratégies afin d'améliorer les performances adhésives du matériau étudié

Dans le cadre de cette thèse, le caoutchouc nitrile étudié est fourni par la société Safran sans indication spécifique quant à sa composition ou ses propriétés. Il est comparé à un grade Sigma-Aldrich (« Sigma NBR ») afin de s'assurer que les résultats ne sont pas propres au matériau industriel.

Lors de ce résumé, les matériaux étudiés seront d'abord caractérisés, et la méthode utilisée pour analyser l'autohésion du NBR sera détaillée. Les résultats observés seront expliqués grâce à une étude de la microstructure du matériau. Enfin, certaines stratégies envisagées pour augmenter ces propriétés autohésives seront détaillées.

## **1. Caractérisation des matériaux**

### **1.1 Détermination du taux d'acrylonitrile**

Les élastomères étudiés ont d'abord été caractérisés par DSC (Dynamic Scanning Calorimetry) et ATG (Analyse Thermo-Gravimétrique) afin de déterminer leur taux d'acrylonitrile. Les résultats sont montrés sur la Figure 1.

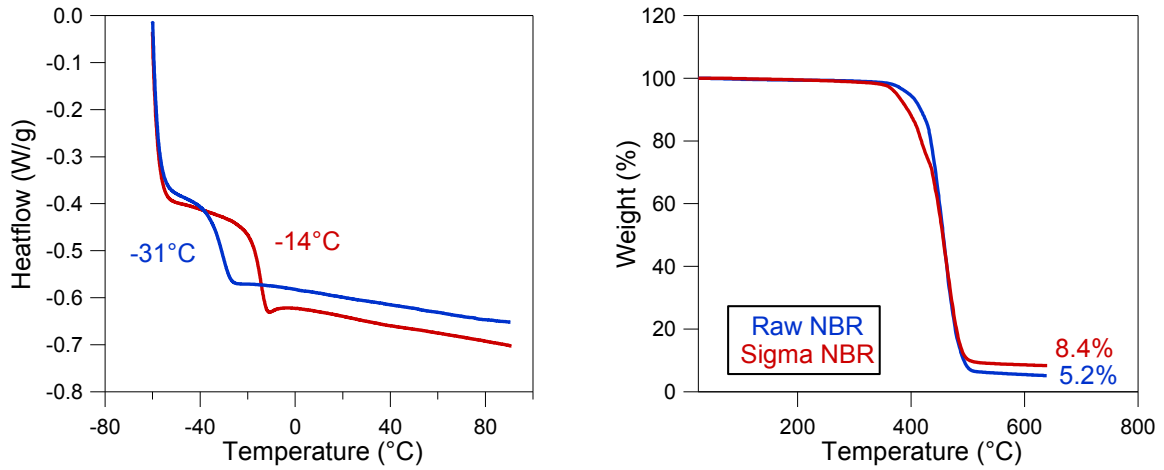


Figure 1 Courbes de DSC (gauche) et ATG (droite) pour NBR brut (courbes bleues) et pour NBR-SA (courbes rouges)

En s'appuyant sur les travaux de Sircar [1], il est possible d'estimer le taux d'ACN dans chaque élastomère pour les deux matériaux :

Matériau	Taux d'ACN	Tg (°C)
Raw NBR	32 +/- 2%	-31
Sigma NBR	43 +/- 1%	-14

Tableau 1 Propriétés des NBR étudiés

## 1.2 Propriétés mécaniques

Les propriétés mécaniques ont été étudiées dans le régime linéaire, et l'utilisation de l'équivalence temps-température (TTS) a permis de tracer une courbe maîtresse à température ambiante (Figure 2).

Les propriétés mécaniques en grande déformation ont également été étudiées en effectuant des tests en traction uniaxiale (Figure 3), et le module d'Young a été estimé à  $0.5 \pm 0.1 \text{ MPa}$  ( $\dot{\epsilon} = 0.017 \text{ s}^{-1}$ ).

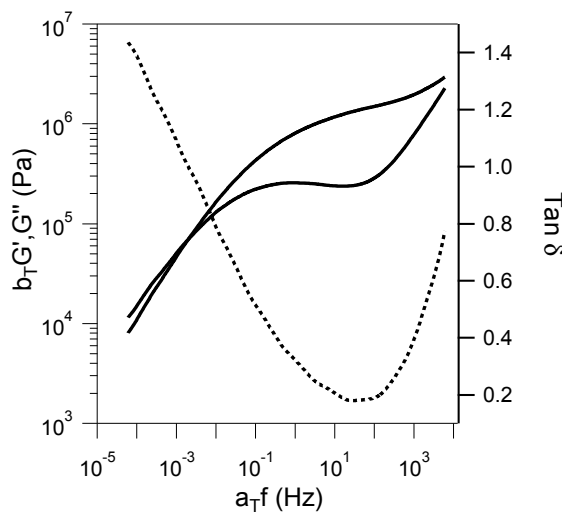


Figure 2 Courbe maîtresse du NBR (extrudé) à  $T_0=25^\circ\text{C}$

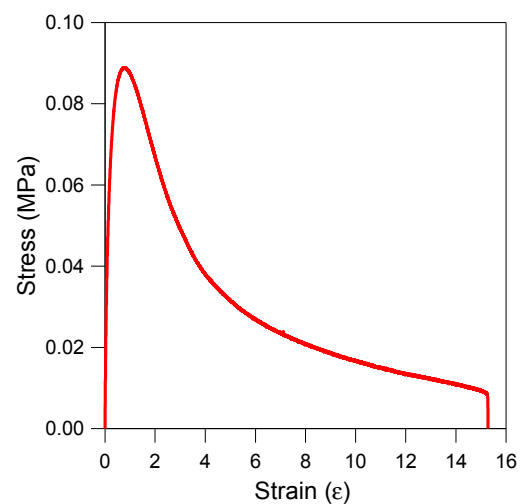


Figure 3 Traction uniaxiale sur NBR (extrudé)

### 1.3 Caractérisation des propriétés adhésives

Afin de caractériser les propriétés adhésives des élastomères, la méthode du Probe-Tack (bien détaillée dans la littérature [2]) a été le point de départ.

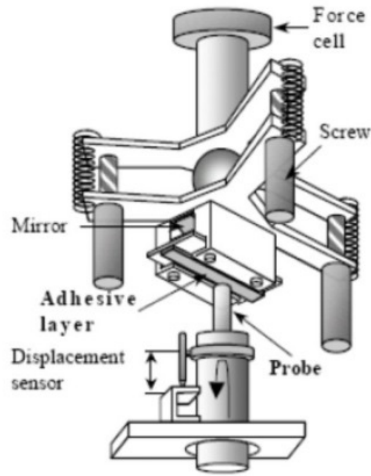


Figure 4 Machine du Probe-tack

Lors de ces essais types, un poinçon de 9.7mm de diamètre est mis en contact, à 1MPa, avec un adhésif déposé sur une plaque de verre. Après un certain temps de contact noté  $t_c$ , le poinçon se rétracte et le couple force-déplacement nécessaire pour le décollement est mesuré. Un miroir orienté à 45° permet d'observer les mécanismes de décollement à l'interface et de vérifier que le poinçon et la plaque sont bien alignés.

Lors de l'étape de décollement, la contrainte  $\sigma$  et la déformation  $\varepsilon$  sont calculées à partir de la force  $F$  et du déplacement  $l$  :

$$\sigma = \frac{F}{A}$$
$$\varepsilon = \frac{l - h_o}{h_o}$$

Avec  $h_o$  l'épaisseur initiale du système adhésive et  $A$  l'aire de contact. L'énergie d'adhésion  $W_{adh}$  ( $J/m^2$ ) est ensuite calculée telle que :

$$W_{adh} = h_o \int \sigma d\varepsilon$$

Cette méthode a été largement utilisée pour étudier l'adhésion de couche fine de matériaux mous types PSAs sur du verre [3][4][5].

Dans le cadre de cette thèse, nous avons mesuré l'adhésion entre une fine couche (~10microns) de NBR déposée sur la plaque de verre, et une couche plus épaisse (~500microns) collée sur le poinçon. La méthode du Probe-tack est utilisée pour étudier des temps de contacts de l'ordre de quelques dizaines de secondes (500 secondes maximum). L'autohésion du NBR mesurée pour de tels temps de contact étant très faible ( $W_{adh} \sim 30J/m^2$  pour 500 secondes), une nouvelle méthodologie d'essai a été définie. Celle-ci permet de séparer l'étape de formation du contact et

celle du décollement. Le contact est effectué à faible pression (0.3 bars), pendant des temps de contact compris entre une heure et plusieurs jours.

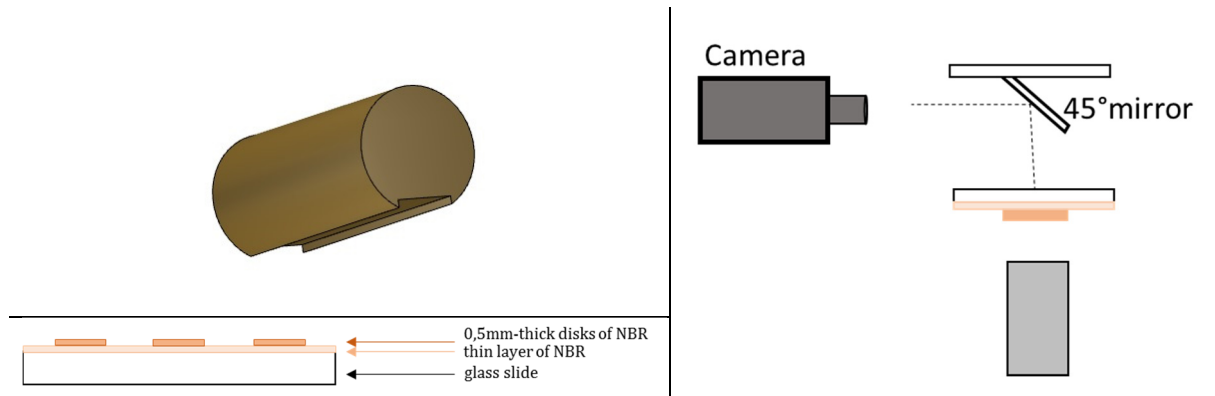


Figure 5 Illustration du poids appliqué (haut gauche), des échantillons (bas gauche) et du montage expérimental (droite)

Les propriétés autohésives du NBR augmentent faiblement avec le temps de contact. Contrairement à ce qui a été trouvé sur des matériaux apolaires type SBR (Styrene Butadiene Rubber) dans les études de Schach [4][6], il n'y a ici aucune corrélation entre l'évolution des propriétés adhésives avec le temps, et les temps caractéristiques de relaxation mesurés en rhéologie linéaire. Par ailleurs, aucun plateau n'est observé aux longs temps de contact.

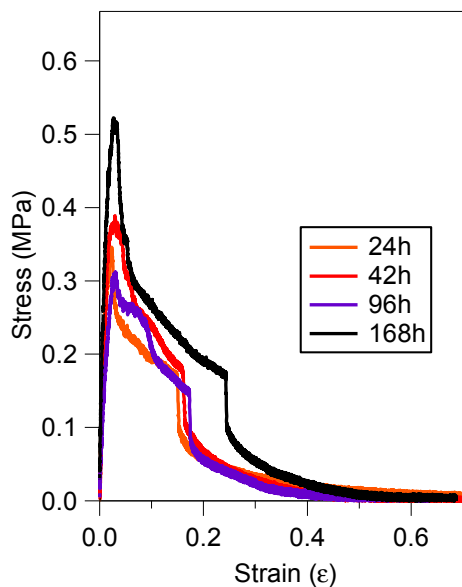


Figure 6 Evolution des propriétés autohésives (courbe contrainte-déformation) du NBR en fonction du temps de contact

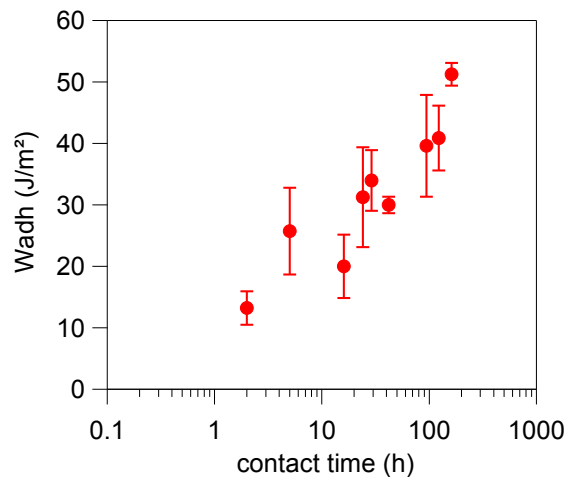


Figure 7 Evolution de l'énergie d'autohésion  $W_{adh}$  du NBR avec le temps de contact

## 2. NBR comme matériau supramoléculaire

### 2.1 Observation d'une microstructure

Ces faibles propriétés autohésives sont liées à l'existence d'une structure supramoléculaire au sein du matériau. En effet, deux états sont comparés : directement après extrusion (« *NBR-ext* »), puis après solubilisation et séchage lent (« *NBR-solub* »). Ces matériaux s'avèrent être complètement différents, notamment en rhéologie linéaire (voir Figure 8) : là où *NBR-ext* s'écoule

(dans le sens où un temps terminal de relaxation est mesurable,  $\tan \delta > 1$ ), NBR-solub se comporte comme un gel physique et le facteur de perte reste supérieur à 1 même aux faibles fréquences.

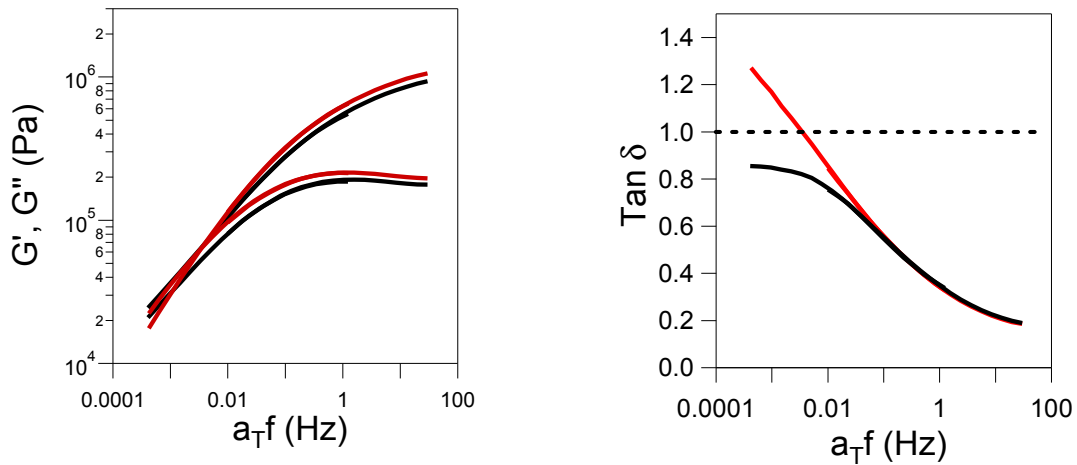


Figure 8 Propriétés rhéologiques linéaires pour NBR-ext (rouge) et NBR-solub (noir). Gauche: modules de stockage  $G'$  et de perte  $G''$ . Droite: Facteur de perte

Des études en diffraction de rayons-X (SAXS) ainsi qu'en AFM (Atomic Force Microscopy) ont notamment pu confirmer l'existence d'une structuration au sein du matériau. En effet, la Figure 9 montre l'existence de deux structures lamellaires à  $q=0.1366$  et  $q=0.1458 \text{ \AA}^{-1}$ , correspondant respectivement à des tailles de 4.6 et 4.3 nm. Sur l'échantillon extrudé, cette structure est détruite et un pic amorphe (lié à une structure mal définie) est observé proche de  $0.2 \text{ \AA}^{-1}$ . Cette structure réapparaît lorsque l'échantillon extrudé NBR-ext est laissé pendant plusieurs mois à température ambiante (voir Figure 10).

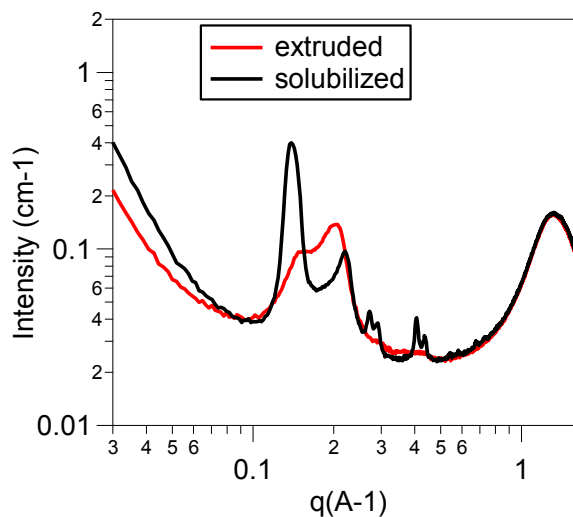


Figure 9 Courbes de SAXS sur du NBR fraîchement extrudé et du NBR solubilisé

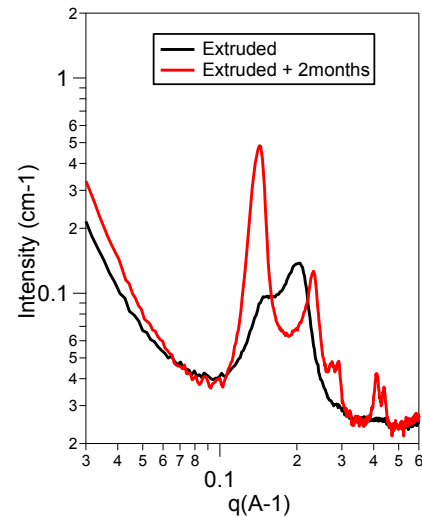
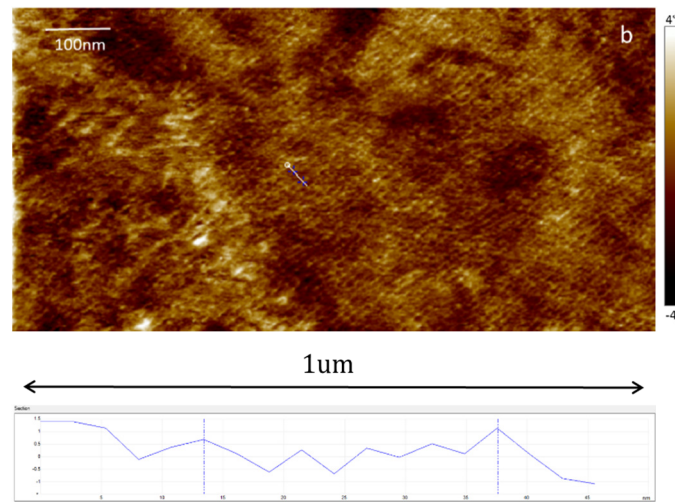


Figure 10 Effet du vieillissement sur la microstructure observée en SAXS

Ces lamelles sont également observées en AFM (Figure 11). Avec les incertitudes inhérentes à la méthode de mesure, une distance caractéristique de  $6.3 \pm 1.2\text{nm}$  est mesurée.



Profile d'intensité

Figure 11 Observation de la structure lamellaire en AFM

## 2.2 Utilisation de la RMN pour comprendre cette microstructure

Une étude détaillée en RMN  $^1\text{H}$  en solution nous a permis d'estimer la statistique du copolymère étudié. Il a été trouvé que le monomère acrylonitrile existe seulement en alternance avec des unités butadiènes, alors que le butadiène peut exister sous forme de blocks. Ainsi, il est suggéré que le matériau initialement supposé statistique est, en réalité, un copolymère à block avec des

blocks de polybutadiène, et des blocks avec des unités butadiène et acrylonitrile alternées. Une chaîne de NBR est schématisée en Figure 12.



Figure 12 Schéma illustrant une chaîne de NBR

Les monomères acrylonitrile et butadiène étant fortement immiscible, les chaînes vont s'organiser afin de limiter ce coût enthalpique, et ainsi former des lamelles (Figure 13).

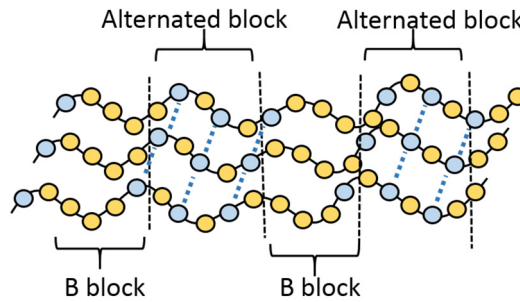


Figure 13 Organisation du NBR en lamelles

Des interactions intramoléculaires fortes entre groupement nitrile, ainsi que l'immiscibilité des blocks, empêche la migration de chaînes et peut ainsi expliquer le comportement rhéologique observé et les faibles propriétés autohésives mesurées.

### 3. Stratégies proposées pour augmenter propriétés autohésives du NBR

#### 3.1 Effet de la température

L'effet de la température a été étudié entre 40 et 120°C. Il semblerait que la destruction à haute température de l'une des structures lamellaires observées en SAXS (Figure 14) permet la migration de chaînes polymères à l'interface, et donc une nette augmentation des propriétés autohésives (Figure 15).

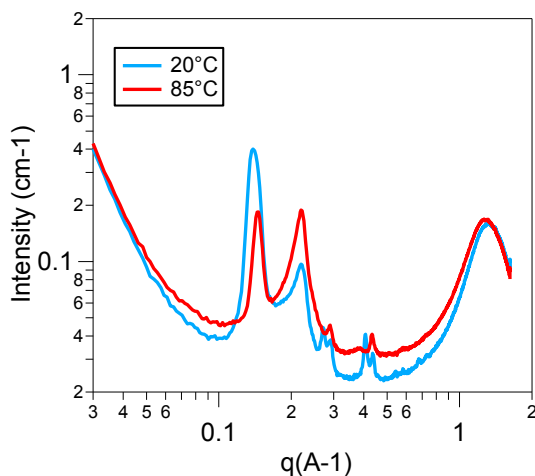


Figure 14 Observation par SAXS de l'évolution de la structure du NBR en fonction de la température

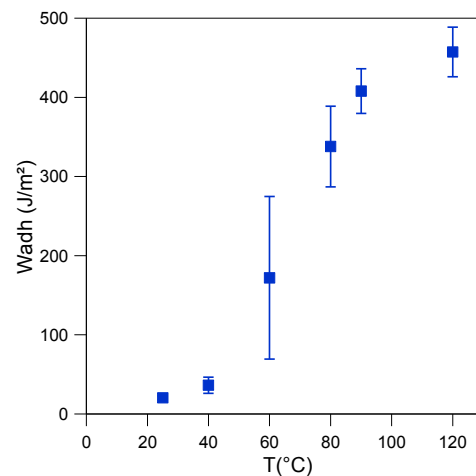


Figure 15 Evolution des propriétés autohésives du NBR en fonction de la température de contact

### 3.2 Ajout de résines tackifiantes

Afin d'améliorer les propriétés autohésives du NBR à température ambiante de la résine tackifiante a été ajoutée au NBR à l'aide d'une extrudeuse. Deux résines, l'une phénolique (polaire) et l'autre hydrocarbonée (apolaire), ont été étudiées, à différentes concentrations. Pendant ces travaux, deux régimes ont été examinés : les faibles (3%) et fortes (>10%) concentrations.

Des temps de contact allant de 1 heure à plusieurs jours ont été étudiés.

Les travaux réalisés ont permis de montrer que pour les faibles concentrations, la nature chimique de la résine est clef. En effet, aux longs temps de contact, une nette amélioration des propriétés auto-hésives du NBR est observée avec l'ajout de résine phénolique (voir Figure 16). Un mécanisme, reposant sur la capacité des molécules polaires à perturber les interactions intermoléculaires  $C\equiv N$ , est proposé pour expliquer une telle augmentation.

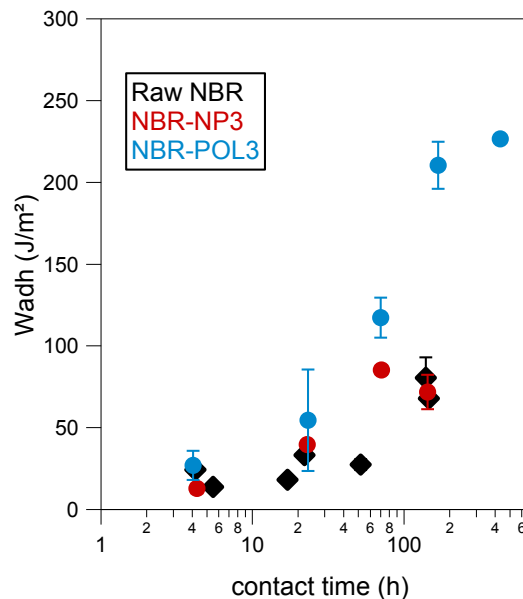


Figure 16 Evolution de l'énergie d'adhésion Wadh en fonction du temps de contact, pour les 3 matériaux considérés

A plus forte concentration (10 et 20%), la nature chimique de la résine tackifiante influence peu les propriétés autohésives du NBR. Une nette amélioration est cependant observée, aux faibles temps de contact, lorsque la concentration est augmentée de 10 à 20%. Des caractérisations mécaniques sont effectuées afin de discuter ces résultats. Par ailleurs, des analyses en SAXS montrent que l'ajout de telles concentrations perturbe fortement la microstructure du NBR. Il est suggéré que, pour des considérations de coût entropique, à forte concentration la résine apolaire migre dans les lamelles polaires et perturbe également les liaisons intermoléculaires. L'évolution de ces structures dans le temps est discutée, ainsi que l'influence de celle-ci sur les propriétés auto-hésives des matériaux.

Ainsi, le choix de la nature ainsi que de la concentration de la résine dépend fortement de l'application souhaitée. En effet, si un fort collant est nécessaire à faible temps de contact, alors il semble nécessaire d'introduire 20% de résine, et la nature chimique de celle-ci n'a que peu d'influence. Au contraire, si le collant est nécessaire aux temps longs, alors seulement 3% de résine peut suffire, et il est alors nécessaire de s'orienter vers une résine polaire. La Figure 17 montre l'effet de la concentration de chaque résine, pour deux temps de contact considérés.

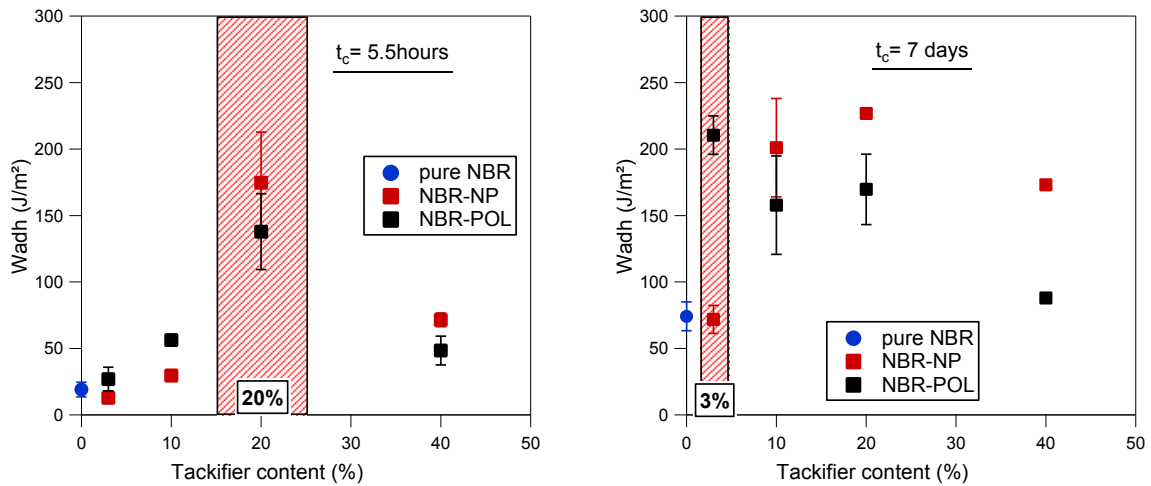


Figure 17 Evolution de l'énergie d'adhésion en fonction de la quantité de résine tackifiante introduite, pour les deux types de résine. Gauche: temps de contact=5.5 heures. Droite: temps de contact = 7 jours

### 3.3 Avivage par solvant

Cette stratégie est inspirée du procédé industriel, et consiste à utiliser l'ajout de solvant à l'interface afin de la souder et de permettre une adhésion forte entre les deux couches non vulcanisées. La Figure 18 compare les propriétés autohésives du NBR brut sans et avec avivage (avec du butanone).

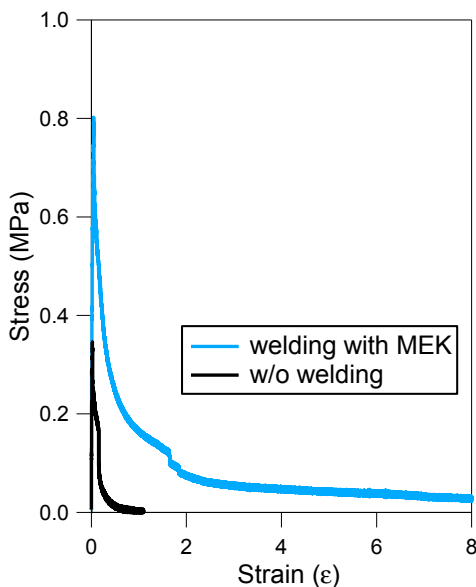


Figure 18 Influence de l'avivage sur les propriétés autohésives du NBR pour  $t_c=24h$

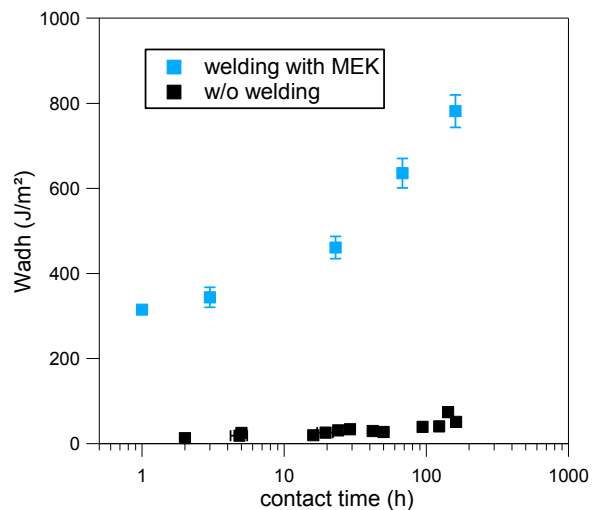


Figure 19 Evolution de l'énergie d'autohésion en fonction du temps de contact pour NBR avec et sans avivage au MEK

L'énergie d'adhésion mesurée est significativement augmentée ( $W_{adh} = 470 \text{ J/m}^2$  vs  $30 \text{ J/m}^2$  sans avivage pour 24 heures de contact). En effet, l'ajout de solvant permet non seulement d'assurer un contact *parfait* (aire de contact maximale) entre les deux surfaces, mais surtout de perturber la structure lamellaire présente en surface des couches. Ainsi, la migration des chaînes polymères est facilitée et l'interface renforcée. Une forte dissipation d'énergie est possible grâce à la formation de fibrilles. La Figure 19 montre l'évolution de l'énergie d'autohésion  $W_{adh}$  pour différents temps de contact après avivage au MEK.

Afin de comprendre quels sont les propriétés clés du solvant à utiliser afin d'augmenter au maximum le collant des deux couches mises en contact, une étude systématique a été réalisée sur douze solvants, pour un temps de contact de 3 heures.

L'influence de la qualité du solvant pour le NBR, estimé par des mesures de gonflement, a d'abord été investiguée. Cette étude nous a montré que les meilleurs solvants pour le polymère n'étaient pas nécessairement les meilleurs solvants pour l'avivage. D'autres paramètres tels que la température d'ébullition, l'affinité spécifique pour un monomère de ce copolymère à multi-blocks (acrylonitrile ou butadiène) et le moment dipolaire ont été étudiés. Les solvants avec des moments dipolaires élevés et présentant des températures d'ébullition intermédiaires ( $50^{\circ}\text{C} < T_{\text{eb}} < 150^{\circ}\text{C}$  dans cette étude) semblent être optimaux. Cependant, malgré une connaissance approfondie du copolymère à block NBR, et de sa microstructure, prévoir exactement l'influence d'un solvant sur les propriétés d'autohésion de cet élastomère reste délicat.

## **4. Conclusion**

Lors de cette thèse, une adaptation de la méthode du Probe-Tack a été proposée afin de caractériser les propriétés autohésives de matériaux mous pour de faibles pressions et longs temps de contact. Cette nouvelle méthodologie permet de dissocier les étapes de formation du contact, et de décollement, particulièrement pertinent pour étudier l'influence de la température sur ces propriétés d'interface.

Il est montré que les propriétés autohésives du NBR sont faibles et évoluent peu avec le temps de contact. Cette particularité est attribuée à la présence de lamelles de tailles nanométriques dans les échantillons. La formation de cette microstructure est due à la statistique du matériau étudié qui n'est non pas statistique mais à block, avec des blocks de monomère butadiène et des blocks formés d'unités butadiène et acrylonitrile alternées. La très faible miscibilité de ces deux monomères, ainsi que la présence d'interaction intermoléculaire  $\text{C}\equiv\text{N}$  entre groupements nitriles, rend la diffusion de chaînes à l'interface thermodynamiquement très peu favorable.

Plusieurs méthodes ont été proposées afin d'améliorer ces propriétés autohésives. Le choix d'une méthode plutôt que l'autre dépend fortement de l'application considérée et notamment du temps de contact qu'il est possible d'atteindre. Les mécanismes par lesquels chaque méthode (température, ajout d'une résine tackifiante, avivage par solvant) est efficace sont étudiés et débattus en s'appuyant sur des essais de caractérisation mécanique, sur des observations microscopiques, ainsi que sur des analyses de diffraction en rayon X.

Enfin, l'ajout de particules de PVC envisagé afin de renforcer mécaniquement le matériau NBR. Il est montré que cette molécule polaire change considérablement les propriétés autohésives de l'élastomère, et l'effet de la résine tackifiante est plus complexe à expliquer.

## 5. References

- [1] R. Schach, Y. Tran, A. Menelle, and C. Creton, "Role of chain interpenetration in the adhesion between immiscible polymer melts," *Macromolecules*, vol. 40, no. 17, pp. 6325–6332, 2007.
- [2] H. Lakrout and P. Sergot, "Direct Observation of Cavitation and Fibrillation in a Probe Tack Experiment on Model Acrylic Pressure- Sensitive-Adhesives," no. 1999, pp. 37–41.
- [3] C. Creton and H. Lakrout, "Micromechanics of flat-probe adhesion tests of soft viscoelastic polymer films," *J. Polym. Sci. Part B Polym. Phys.*, vol. 38, no. 7, pp. 965–979, 2000.
- [4] C. Creton and R. Schach, "Adhesion at interfaces between highly entangled polymer melts," *J. Rheol. (N. Y. N. Y.)*, vol. 52, no. 3, pp. 749–767, 2008.
- [5] F. Tanguy, L. U. Pierre, and E. T. Marie, "Debonding mechanisms of soft adhesives : toward adhesives with a gradient in viscoelasticity Debonding Mechanisms of Soft Adhesives : Toward Adhesives with a Gradient in Viscoelasticity," 2014.
- [6] Sircar, "Analysis of Elastomer Vulcanizate Composition by TG-DTG Techniques." 1991.

# TABLE OF CONTENTS

---

List of abbreviations

**GENERAL INTRODUCTION .....1**

## **CHAPTER 1 – From molecular dynamics to strong self-adhesion properties**

<b>1</b>	<b>Elastomers and their molecular dynamics.....</b>	<b>8</b>
1.1	Processing and key properties of elastomers.....	8
1.2	Physics of rubber elasticity.....	9
1.3	Dynamics of viscoelastic materials.....	13
<b>2</b>	<b>Introduction to the adhesion of soft materials .....</b>	<b>16</b>
2.1	Adhesive performance of soft materials .....	17
2.2	Macroscopic characterization of adhesion.....	18
2.3	Comments.....	19
<b>3</b>	<b>Formation of a strong interface.....</b>	<b>19</b>
3.1	Molecular theories.....	19
3.2	Formation of intimate contact.....	20
3.3	Polymer interfaces between polymer melts.....	23
<b>4</b>	<b>Energy dissipation as key to boost adhesion strength .....</b>	<b>29</b>
4.1	Introduction to debonding in soft materials .....	30
4.2	Predicting debonding mechanisms from linear rheology .....	31
4.3	Non-linear fibrillation.....	33
4.4	End of the story: final detachment .....	34
<b>5</b>	<b>Effect of molar mass on adhesion .....</b>	<b>34</b>
<b>6</b>	<b>Nitrile Butadiene Rubber (NBR) .....</b>	<b>35</b>
6.1	Introduction to poly(acrylonitrile-co-butadiene).....	35
6.2	Adhesion and self-adhesion properties of NBR .....	38
<b>7</b>	<b>Conclusion.....</b>	<b>40</b>
<b>8</b>	<b>References.....</b>	<b>41</b>

## CHAPTER 2 – Characterization of nitrile rubber

<b>1. Material characterizations .....</b>	<b>49</b>
1.1 Average molecular weight .....	49
1.2 Acrylonitrile content .....	49
<b>2. Characterization of mechanical properties.....</b>	<b>52</b>
2.1 Linear rheology.....	52
2.1 Uniaxial tensile tests.....	56
<b>3. Characterization of adhesion properties .....</b>	<b>57</b>
3.1 Choice of the characterization method.....	57
3.2 Probe-tack tests.....	58
3.3 Samples' preparation .....	61
3.4 Self-adhesion properties.....	62
<b>4. Conclusions and discussion .....</b>	<b>65</b>
4.1 Discussion.....	65
4.2 Conclusions .....	68
<b>5. References.....</b>	<b>69</b>

## CHAPTER 3 – NBR as supramolecular rubber

<b>1. Supramolecular behavior of NBR .....</b>	<b>73</b>
1.1. Ageing of the materials at room temperature .....	73
1.2. Dissolution of NBR in a solvent to accelerate ageing process .....	77
1.3. Conclusions .....	79
<b>2. Study of structure formation in NBR .....</b>	<b>80</b>
2.1. Literature .....	80
2.2. X-Ray Scattering .....	82
2.3. Atomic Force Microscopy .....	88
2.4. Transmission Electron Microscopy .....	91
2.5. <sup>1</sup> H NMR study .....	91
2.6. Conclusions and discussion .....	93
<b>3. “Self”-adhesion properties .....</b>	<b>94</b>
3.1. Literature on block copolymers.....	94
3.2. Influence of NBR structure on its self-adhesion properties.....	97
3.3. Self-adhesion properties of freshly extruded NBR.....	101
<b>4. Conclusions .....</b>	<b>103</b>
<b>5. References.....</b>	<b>104</b>

## CHAPTER 4 – Influence of tackifiers on the self-adhesion of nitrile rubber

<b>1. Literature on the blending of tackifiers .....</b>	<b>109</b>
1.1. General picture .....	109
1.2. Influence of the nature and the amount of tackifier.....	109
1.3. Additives in phase-separated materials.....	111
1.4. Conclusion and discussion.....	112
<b>2. Introduction .....</b>	<b>113</b>
2.1. Materials.....	113
2.2. Sample preparation .....	114
2.3. Objectives.....	115
<b>3. Blending of 3% tackifier in NBR.....</b>	<b>115</b>
3.1. Self-adhesion properties.....	116
3.2. Bulk properties and structure.....	118
3.3. Conclusion and discussion.....	120
<b>4. Blending of a high tackifier content in NBR .....</b>	<b>122</b>
4.1. Self-adhesion properties.....	122
4.2. Properties of the high concentration blends.....	126
<b>5. Conclusion.....</b>	<b>132</b>
<b>6. References.....</b>	<b>134</b>

## CHAPTER 5 – Surface effects on the self-adhesion of nitrile rubber

<b>1. Introduction to solvent welding</b> .....	<b>137</b>
1.1. Literature .....	137
1.2. Methods .....	138
<b>2. Influence of solvent welding on the adhesion and cohesion of NBR</b> .....	<b>140</b>
2.1. Adhesion of welded NBR on glass.....	140
2.2. Self-adhesion of welded NBR.....	140
<b>3. Influence of the solvent</b> .....	<b>144</b>
3.1. Presentation of the different solvents.....	144
3.2. Influence of solvent's quality for the polymer.....	144
3.3. Importance of solvents' vapor pressure .....	147
3.4. Site-specific swelling for welding .....	148
3.5. Influence of the dipole moment.....	149
3.6. Conclusions .....	150
<b>4. Effect of microstructure on solvent-welded NBR</b> .....	<b>151</b>
4.1. Introduction .....	151
4.2. Influence of microstructure of self-adhesion of NBR.....	151
4.3. Conclusion .....	153
<b>5. Influence of drying conditions</b> .....	<b>154</b>
5.1. Effect on the self-adhesion properties .....	154
5.2. Investigations .....	155
5.3. Discussion .....	158
<b>6. Conclusions</b> .....	<b>159</b>
<b>7. References</b> .....	<b>160</b>

## CHAPTER 6 – First insights into PVC-blended nitrile rubbers (NBR/PVC)

<b>1. Literature: Blending of PVC in NBR</b> .....	<b>165</b>
1.1. Introduction to NBR/PVC.....	165
1.2. Composition-dependent properties.....	165
1.3. Nanoscale heterogeneity .....	166
<b>2. Samples preparation and characterization</b> .....	<b>167</b>
2.1. Blends preparation .....	167
2.2. Mechanical properties of NBR/PVC blends .....	168
2.3. Structural organization .....	170
<b>3. Self-adhesion properties of NBR/PVC</b> .....	<b>173</b>
3.1. Samples' preparation .....	173
3.2. Influence of contact time on the self-adhesion properties of NBR/PVC blends.....	173
3.3. Solvent welding to enhance self-adhesion properties .....	175
3.4. Conclusions and discussion.....	177
<b>4. Addition of tackifiers to NBR/PVC</b> .....	<b>178</b>
4.1. Self-adhesion properties of NBR/PVC with tackifiers.....	179
4.2. Mechanical properties of NBR/PVC with tackifiers .....	181
4.3. Discussion .....	183
<b>5. General conclusions and discussion</b> .....	<b>184</b>
<b>6. References</b> .....	<b>185</b>
<b>CONCLUSIONS AND PERSPECTIVES</b> .....	<b>187</b>

## ANNEXES

<b>1. Characterizations of the materials</b> .....	<b>193</b>
1.1 NMR of NBR-SA.....	193
1.2 SEC curve of raw NBR in toluene .....	194
1.3 Method to check concentration of PVC in blends.....	194
<b>2. Determination of NBR linear regime</b> .....	<b>195</b>
<b>3. Structure observation</b> .....	<b>196</b>
3.1 SAXS of Tackifier + 3%: solubilized and aged.....	193
3.2 SAXS- Drying conditions .....	194
<b>4. Influence of welding solvent on the self-adhesion of NBR</b> .....	<b>197</b>



## List of abbreviations

NBR	Nitrile Butadiene Rubber
SBR	Styrene Butadiene Rubber
Tg	Glass Transition Temperature
Phr	Parts per hundred of rubber
PB	Polybutadiene
MEK	Methyl Ethyl Ketone = Butanone
PSA	Pressure Sensitive Adhesives
ACN	Acrylonitrile
DSC	Dynamic Scanning Calorimetry
SAXS	Small Angle X-Ray Scattering

# - GENERAL INTRODUCTION -

---

## **1. Industrial interest and fabrication process**

Safran produces different types of equipment for the aerospace industry, and among them helicopter fuel tanks. Because of its application, very well defined specifications are set and key requirements exist. First, the product, and therefore the used materials, must be resistant enough to withstand the mechanical stresses (induced by vibrations and fluid's movement) present in a helicopter. Moreover, fuel tanks have to be flexible, because of the need to optimize space in the aircraft. Indeed, in a helicopter, the tanks occupy all the space free of use after seats and equipment. Last but not least, the tank has to be lightweight and fuel-resistant, which implies specific properties regarding the used materials. For all the above reasons, Safran creates a very complex assembly with different polymer layers, and especially polar elastomers. To understand this work's problematics well, it is necessary to focus on the fuel tanks' fabrication process.

### **Materials storage**

The elastomers used are provided by an external supplier by batches of several hundreds of kilograms and are then kept in a storehouse inside the factory. The storage temperature is that of the storehouse, and can possibly vary from 0°C in the winter to up to 40°C in the summer. Materials are used in the year following their reception.

### **Materials processing**

The rubbers are first compounded through an internal mixer and then calendered at 80°C, where up to fifteen different additives such as anti-oxidants, plasticizers, fillers and tackifiers are blended. A second calendering at 100°C is performed to reach thinner sheets, with a final thickness of about 400 micrometers. Right after the calendering process, the sheets are enrolled, between two protective plastic liners to avoid any adhesion between the different layers. The sheets are then kept aside, at room temperature, until used for fuel tank fabrication.

### **Fuel tank fabrication**

The size and the geometry of each fuel tank is specific for a given helicopter. To produce a tank, an adequate metallic mold is needed (see Figure 1). The process consists in overlaying different sheets of materials, either rubber or coated fabric, in a very accurate way. In between each layer, the surfaces are scrubbed with a rag impregnated with solvent. Once the assembly is completed, the fuel tank is covered with a vacuum bag and is placed in the autoclave for the vulcanization cycle. During this vulcanization step, the elastomer chains are crosslinked with sulphur.



Figure 1 Pictures of a fuel tank mold (left) and of a helicopter fuel tank (right)

Changes in materials (rubber + additives) as well as changes in the processing conditions can modify the contact strength between the unvulcanized layers. In the industry, it is important to have a fine understanding of the adhesion mechanisms to be able to adapt the bonding strategy.

## 2. Thesis challenges

One of the polar elastomers used by Safran is the poly(acrylonitrile-co-butadiene), most commonly called “nitrile rubber” (NBR). The present study is focused on this material. As the industrial process is very complex, representative (and simplified) contact conditions will be determined to characterize the adhesion properties of such materials.

### Self-adhesion characterization method

The goal is to develop a methodology to reproducibly and quantitatively characterize self-adhesion properties of uncrosslinked nitrile rubbers. This method must be as relevant as possible for the industrial process. Therefore, the different time scales as well as the processing and storage conditions need to be taken into account for the method development:

Fabrication step	Processing conditions	Storage time	Storage conditions (T,P)
Materials storage	NA	< 2 years	0°C < T < 40°C
First calendering	80°C	15 days	Cold chamber (10°C)
Second calendering	100°C	< 5 months	Room temperature
Total fuel tank before vulcanization	NA	< 3 days	Room temperature

Table 1 Different processing and storage conditions for each fabrication step

One of the method’s key requirements is to confirm that the experimental observations noticed by the workers during the manufacturing process are well reproduced by the testing method.

### Scientific challenge

To the best of our knowledge, the adhesion and self-adhesion of unvulcanized polar elastomers have not been reported in the literature. Although the inter-diffusion mechanisms of polymer chains at the interface is well documented (see Chapter 2), all these studies have focused on non-polar, linear and monodisperse materials. Yet during this work, an industrial grade of polymer is studied, with additional complexities such as a poorly controlled molar mass distribution and molecular architecture. The goal of this project is to determine the main materials and processing parameters influencing the self-adhesion of a given polar polymer, and to understand the physics and chemical process implied.

### **3. Scope of the manuscript**

A general overview on elastomers and their dynamic properties, as well as an introduction to their adhesion, and self-adhesion, properties is presented in Chapter 1. The rest of the manuscript follows the thesis' chronology. In chapter 2, the methods to characterize both thermal and mechanical properties are presented and used to measure nitrile rubber's behavior. The material's self-adhesion properties are first characterized using a classical Probe-tack device, and a new protocol, better adapted for this material is then developed. Chapter 3 focuses on the development of a microstructure in the bulk, which explains the particular behaviors probed in Chapter 2. Several characterization techniques are used to observe and understand the formation of such organization. Chapter 3 also gives an insight on the relation between structure and self-adhesion properties. In the chapters that follow, two strategies to enhance the rubbers' self-adhesion properties are exposed, and explained in light of the structure-property scheme exposed in Chapter 3. A first strategy consists in blending small molecules called "tackifiers" inside NBR, and is detailed in Chapter 4. The use of solvent to weld the interface is then thoroughly studied in Chapter 5. Finally, poly(vinyl chloride) particles are blended into NBR and its influence on the structure and the self-adhesion properties are studied in Chapter 6.

In addition to the general literature on elastomers and adhesion presented in Chapter 2, appropriate state-of-the art and relevant references are detailed in the beginning of each chapter to comprehend the new concepts needed to analyze the results.



# **- CHAPTER 1 -**

## **FROM MOLECULAR DYNAMICS TO STRONG SELF-ADHESION PROPERTIES**

---

The objective of this chapter is to provide the reader with the thesis' key notions, and to set its general framework.

A simple physical analysis of elastomers' elasticity and viscoelasticity is first presented, and the dynamics of their melts are analyzed in light of rheological measurements. The relaxation processes introduced are key to understand the interdiffusion responsible for the formation of a strong interface between two polymer melts. The extent of energy dissipation during the debonding process, and failure mechanisms are then discussed. The effect of molecular weight as a trade-off between the development of a strong interface and the bulk dissipation between debonding is presented. Finally, an introduction on Nitrile Butadiene Rubber (NBR)'s processing and on its adhesion properties is presented.

<b>1</b>	<b>Elastomers and their molecular dynamics.....</b>	<b>8</b>
1.1	Processing and key properties of elastomers.....	8
1.1.1	Formulation and shaping of elastomer.....	8
1.1.2	Basics of elastomers mechanical properties.....	8
1.2	Physics of rubber elasticity.....	9
1.2.1	Thermodynamics of rubber (entropic elasticity).....	10
1.2.2	Rubber elasticity in a crosslinked network.....	11
1.2.3	Entangled rubber elasticity.....	12
1.2.4	Strain hardening.....	12
1.3	Dynamics of viscoelastic materials.....	13
1.3.1	Introduction to linear viscoelasticity.....	13
1.3.2	Unentangled polymer dynamics ( $M < M_e$ ).....	14
1.3.3	Entangled polymer dynamics ( $M > 2M_e$ ).....	15
1.3.4	Rheology of entangled polymer melts.....	15
<b>2</b>	<b>Introduction to the adhesion of soft materials .....</b>	<b>16</b>
2.1	Adhesive performance of soft materials.....	17
2.1.1	Pressure Sensitive Adhesives (PSA) as soft adhering materials.....	17
2.1.2	Introduction to the tack behavior of elastomers.....	17
2.2	Macroscopic characterization of adhesion.....	18
2.3	Comments.....	19
<b>3</b>	<b>Formation of a strong interface.....</b>	<b>19</b>
3.1	Molecular theories.....	19
3.2	Formation of intimate contact.....	19
3.2.1	Cavitation.....	20
3.2.2	Parameters influencing microscopic contact.....	20
3.2.3	Adhesion on glass.....	21
3.2.4	Comments.....	22
3.3	Polymer interfaces between polymer melts.....	22
3.3.1	Methods to observe motions.....	22
3.3.2	Adhesion of immiscible polymers: a thermodynamic study.....	24
3.3.3	Self-adhesion of polymers: kinetics.....	26
3.3.4	Conclusion and comments.....	29
<b>4</b>	<b>Energy dissipation as key to boost adhesion strength.....</b>	<b>30</b>
4.1	Introduction to debonding in soft materials.....	30
4.1.1	Need for dissipation.....	30
4.1.2	Types of cavities growth.....	30
4.2	Predicting debonding mechanisms from linear rheology.....	31
4.2.1	From materials elastic behavior.....	31
4.2.2	Considering viscoelastic dissipation.....	32
4.3	Non-linear fibrillation.....	33
4.4	End of the story: final detachment.....	34
<b>5</b>	<b>Effect of molar mass on adhesion .....</b>	<b>34</b>
5.1.1	Influence of molar mass on interface dynamics.....	34
5.1.2	Influence of molar mass on the green strength.....	35
5.1.3	Trade-off between tack and green strength.....	35

<b>6</b>	<b>Nitrile Butadiene Rubber (NBR)</b> .....	<b>36</b>
6.1	Introduction to poly(acrylonitrile-co-butadiene).....	36
6.1.1	Presentation .....	36
6.1.2	Manufacturing .....	36
6.2	Adhesion and self-adhesion properties of NBR .....	38
6.2.1	Adhesion of NBR to other materials.....	38
6.2.2	Self-adhesion of NBR.....	39
<b>7</b>	<b>Conclusion</b> .....	<b>40</b>
<b>8</b>	<b>References</b> .....	<b>41</b>

# 1 Elastomers and their molecular dynamics

Polymers are large molecules, macromolecules, composed of many repeating subunits called “monomers”. Elastomers (rubbers) are a specific type of polymer, with very weak intermolecular forces, used at temperatures well above that of their glass transition. Crosslinking of the rubbery chains are needed for the material to show its great mechanical properties. They are stretchable to high strains in a reversible way, and have a low Young’s modulus (~MPa). During this first part, an introduction to rubbers’ great elasticity and a rapid study of their dynamics in melt is proposed.

## 1.1 Processing and key properties of elastomers

In the rubber industry, manufacturers themselves prepare the blends on specific tools and therefore control all the processing parameters, as well as the formulation [1].

### 1.1.1 Formulation and shaping of elastomer

#### i. Formulation

The main component is, of course, the uncrosslinked rubber itself. It is either natural rubber, or synthesized by polymerization of oil-based monomers (ethylene, propylene, butadiene, styrene...). The polymerization technique as well as the used catalysts determine the structure and the molecular mass of the polymer. Different additives are blended, among which: fillers, plasticizers, stabilizers and vulcanizing agents. The nature and the amount of each additive is well controlled and optimized to satisfy the specifications.

Additives	Role
Vulcanizing agents	Forming the three dimensional elastic network
Fillers	Reinforcement and/or dilution
Plasticizers	Processing agent, flexibility, glass transition temperature
Stabilizers	Protection against aging, heat, UV, ozone...
Others	Flame retardant, foams, adhesion, colors...

*Table 1 The role of the most common additives blended in rubber*

Blending is performed in two steps:

- On an internal mixer to add fillers and oils. These tools operate discontinuously. During this step, temperature can rise up to 180°C due to viscous heating
- On cylinder mixers, also called “calenders”, at a much lower temperature to blend the vulcanizing agents without risking a premature crosslinking

#### ii. Shaping

Once the blend is ready, it is shaped using polymer molding classical techniques: injection, extrusion or compression. In the case of tires- and helicopter fuel tanks- shaping consists in overlaying the bands of raw (unvulcanized) rubber bands, and the structure relies on each layers’ specific function and positioning. The assembly is then vulcanized in appropriate presses.

### 1.1.2 Basics of elastomers mechanical properties

#### i. Vulcanization

Vulcanization is the final step of the fabrication process. It consists in fixing the three-dimensional structure through chemically crosslinking the polymer chains. The reactions are thermally triggered. The vulcanized rubber cannot be modified afterwards and heating leads to its pyrolysis

rather than its fusion. There are mainly two types of chemical agents for vulcanization: peroxides and sulfur compounds [2][3]. Sulfur bridging of polymer chains is illustrated in Figure 1.

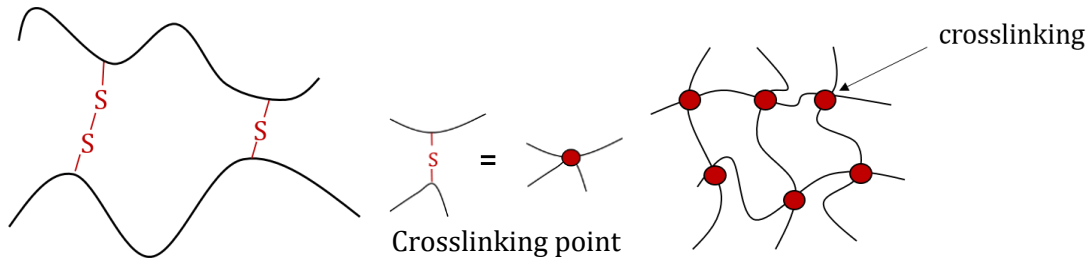


Figure 1 Vulcanization of polymer chains through sulfur bridges (crosslinking points)

Elastomers are used in this crosslinked state, which is referred to as “cured”.

ii. Mechanical properties

Elastomers are a specific kind of polymer, with very weak intermolecular forces, used at temperatures well above that of their glass transition (which is lower than 0°C). Their modulus drops of several orders of magnitude (from GPa to MPa) at this specific temperature (see Figure 2) and vulcanization prevents their flow at very high temperature. In fact, once crosslinked, elastomers –similarly to other thermosets- are not re-shapable, which is the main reason for their difficult recyclability. Figure 3 shows the difference in uniaxial tensile testing between uncrosslinked and crosslinked elastomers. Although properties in the linear regime are similar, materials have very different behavior at large strains.

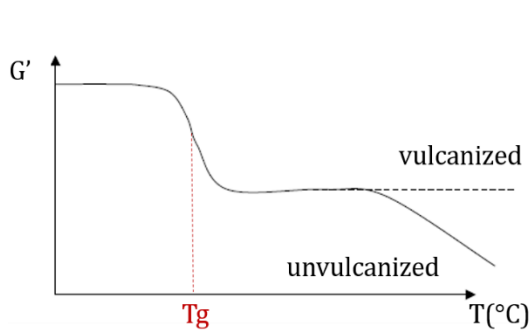


Figure 2 Linear mechanical properties of elastomers

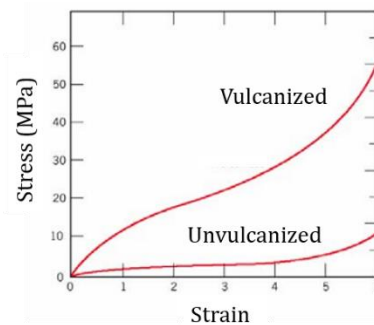


Figure 3 Effect of crosslinking on the large strain behavior of elastomers.

The physical origin of this mechanical behavior is introduced in the following paragraph.

**1.2 Physics of rubber elasticity**

To understand the physics of rubber elasticity, a brief reminder of the definition of a polymer chain and its characteristic length scales is useful. A flexible polymer is described as the assembly of  $n+1$  bonded atoms (see Figure 4).

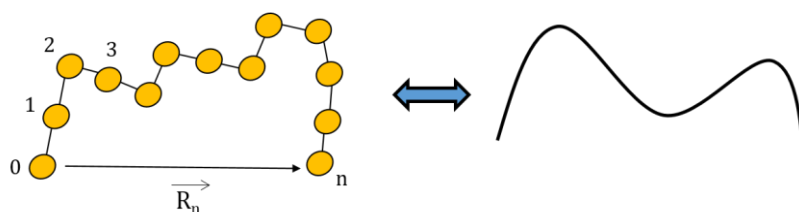


Figure 4 Schematic of a polymer chain

The end-to-end vector is the sum of all  $n$  bond vectors, and the simplest average non-zero distance is the mean-square end-to-end distance (see equation 1. 1). The latter is often used to characterize the size of linear chains.

$$\langle R^2 \rangle \equiv \langle R_n^2 \rangle \quad 1. 1$$

For an ideal chain, this value is proportional to the product of the number of bonds ( $N$ ) and the square of the monomer length  $b$  (or Kuhn length) such that:

$$\langle R^2 \rangle = b^2 N \quad 1. 2$$

In the case of an ideal linear chain, the radius of gyration  $R_g$  also scales directly with  $b^2 N$ .

The particular origin of their elasticity is first detailed, and its implication on unentangled and entangled polymer melts are then presented.

### 1.2.1 Thermodynamics of rubber (entropic elasticity)

The first law of thermodynamics states that for a transformation in any closed system, the change in energy is equal to that exchanged with the surrounding environment by thermal transfer (heat) and by mechanical transfer (work). The change in internal energy may therefore be written as:

$$dU = TdS - pdV + fdL \quad 1. 3$$

With  $T$  the temperature,  $S$  the entropy,  $p$  the pressure,  $V$  the volume,  $f$  the force for deformation and  $L$  length of deformation.  $TdS$  represents the heat added to the system,  $(-pdV)$  the work done to change the network's volume and  $fdL$  the work done upon network deformation. From the Helmholtz free energy  $F = U - TS$ , and its variation  $dF = -SdT - pdV + fdL$ , the following equalities are set:

$$\left(\frac{\partial F}{\partial T}\right)_{V,L} = -S; \left(\frac{\partial F}{\partial V}\right)_{T,L} = -p; \left(\frac{\partial F}{\partial L}\right)_{T,V} = f \quad 1. 4$$

As second derivatives of the Helmholtz free energy do not depend on the order of differentiation, the following Maxwell's relation can be obtained:

$$-\left(\frac{\partial S}{\partial L}\right)_{T,V} = \left(\frac{\partial f}{\partial T}\right)_{V,L} \quad 1. 5$$

Which shows that the force  $f$  applied to deform a network consists of two contributions

$$f = \left(\frac{\partial F}{\partial L}\right)_{T,V} = \left[\frac{\partial(U - TS)}{\partial L}\right]_{T,V} = \left(\frac{\partial U}{\partial L}\right)_{T,V} - T\left(\frac{\partial S}{\partial L}\right)_{T,V} = \left(\frac{\partial U}{\partial L}\right)_{T,V} + T\left(\frac{\partial f}{\partial T}\right)_{V,L} \quad 1. 6$$

and is the sum of an energetic term  $f_E$ , and an entropic one  $f_S$  with

$$f_E = \left(\frac{\partial U}{\partial L}\right)_{T,V} \quad 1. 7$$

$$\text{and } f_S = T\left(\frac{\partial f}{\partial T}\right)_{V,L} = -T\left(\frac{\partial S}{\partial L}\right)_{T,V} \quad 1. 8$$

In typical crystalline solids the energetic contribution dominates due to the increase in internal energy when crystalline lattices are distorted from their equilibrium position. In an ideal rubber network above  $T_g$ , there is no energetic contribution to elasticity, i.e.  $f_E=0$ . In rubbers, the entropic contribution to the force is more important than the energetic one. This entropic elasticity explains their very particular mechanical properties in which the equilibrium states corresponds to the chains' maximal entropy. When stressed, chains unfold to a great extent

and thus decrease the system's entropy  $\left(\frac{\partial S}{\partial L}\right)_{T,V} < 0$ . As soon as the stress is removed, the chains tend to come back to their initial equilibrium state. Whereas for typical crystalline solids the force decreases weakly with increasing temperature, equation 1. 8 shows that for elastomers the force increases with increasing temperature.

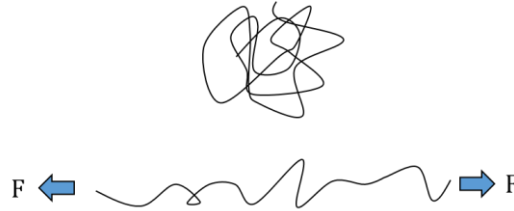


Figure 5 Illustration of the change in entropy for the large deformation of elastomers

### 1.2.2 Rubber elasticity in a crosslinked network

The simplest model to account for this elastic deformation is the affine network model, which states that the relative deformation of each network strand is the same as the macroscopic deformation imposed on the whole network. Indeed, the overall network is stretched with the same  $\lambda$  coefficients (in the three space directions) as each molecular strand (see Figure 6), and the entropic change due to the network's deformation is therefore the sum of all entropic contributions for the polymer strands.

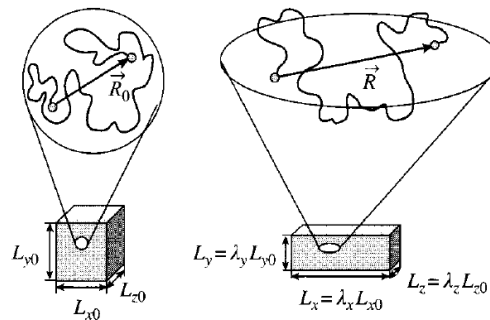


Figure 6 Each network strand adopts the relative deformation of the macroscopic network. Picture from [4]

From 1. 4, the force required to deform a network is the rate of change of its free energy with respect to its elongational deformation. As enthalpic contributions may be ignored, the change in the materials free energy is considered to be only due to entropic changes. Due to elastomers' incompressibility, deformation occurs at constant volume, and a relation for the evolution of stress  $\sigma$  with deformation is proposed:

$$\sigma = \frac{nkT}{V} \left( \lambda - \frac{1}{\lambda^2} \right) \quad 1. 9$$

With  $v=n/V$  the number of strands per unit volume,  $\lambda=\lambda_x$  (due to incompressibility  $\lambda_x\lambda_y\lambda_z=1$ ) and  $kT$  the thermal energy.

The shear modulus  $G$  is then expressed as:

$$G = \frac{nkT}{V} = \nu kT = \frac{\rho RT}{M} \quad 1.10$$

With  $\rho$  the network's density,  $M$  the average molar mass of a network strand and  $R$  the gas constant. This relation confirms that the modulus increases with temperature and shows that it increases linearly with the number density of strands.

### 1.2.3 Entangled rubber elasticity

In the above presented affine network model, the ends of each network strand are fixed in space and cannot fluctuate. In real networks of long polymers, since chains cannot cross one another, they impose topological constraints to their neighbors. These constraints are called entanglements, and Edwards proposed the tube model to account for the collective effect of all surrounding chains on a given polymer strand. The idea of such a model is to replace the network strand by an entanglement strand- which corresponds to the part of polymer in between two entanglement points- and therefore to deduce an expression for the rubbery plateau modulus of high molar mass, entangled, polymer melts:

$$G_e = \frac{\rho RT}{M_e} \quad 1.11$$

With  $M_e$  the molar mass between two entanglements such that  $M_e = N_e M_0$ , with  $N_e$  the number of monomers (of molar mass  $M_0$ ) in an entanglement strand.

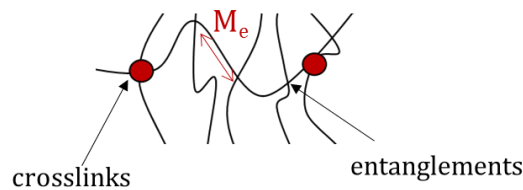


Figure 7 Illustration of crosslinks and entanglements in entangled polymer melts

### 1.2.4 Strain hardening

At high deformations, due to the chains finite extensibility, it is harder to stretch the material and a strain hardening, i.e. an increase in the measured stress at high strains, is measured. This force divergence (see Figure 9) occurs when the crosslinks strands approach their limiting extensibility. Figure 8 illustrates the chain stretching in the horizontal direction and shows its limited extensibility.

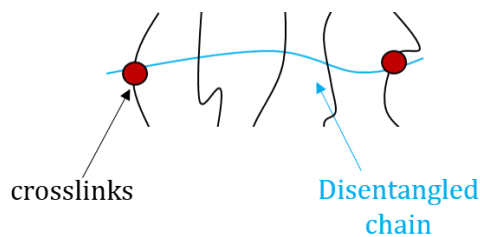


Figure 8 Illustration of a chain's limit extensibility

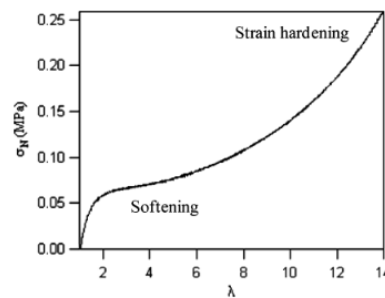


Figure 9 Uniaxial tensile curve of a strain hardening material

Another possible source of hardening in some network is the stress-induced crystallization.

It is now interesting to investigate the different tools available to characterize and model the mechanical behavior of elastomers.

### 1.3 Dynamics of viscoelastic materials

#### 1.3.1 Introduction to linear viscoelasticity

Materials deform upon stressing, and the extent of this deformation may be predicted. In the hypothesis of small deformations, two extreme cases are considered. The first one is that of an elastic solid, determined by Hooke's law. In an isotropic material, the stress  $\sigma$  is directly linked to the deformation  $\epsilon$  by a linear law:

$$\sigma = E * \epsilon \tag{1.12}$$

where E is the Young's modulus of the material.

The other case is that of a Newtonian liquid, in which the stress is not linked to the strain, but to the strain rate  $\dot{\epsilon}$ :

$$\sigma = \eta * \frac{d\epsilon}{dt} \tag{1.13}$$

with  $\eta$  the viscosity of the liquid.

Polymers usually do not show these limiting behaviors, but rather an intermediate one, called viscoelastic. A macroscopic picture of the mechanical behavior of viscoelastic materials is suggested in Figure 10 (left). When stressed, such materials are able to store and return some energy (called "elastic" or "stored" energy), but a certain amount of the total work done on the system is lost ("dissipated" energy).

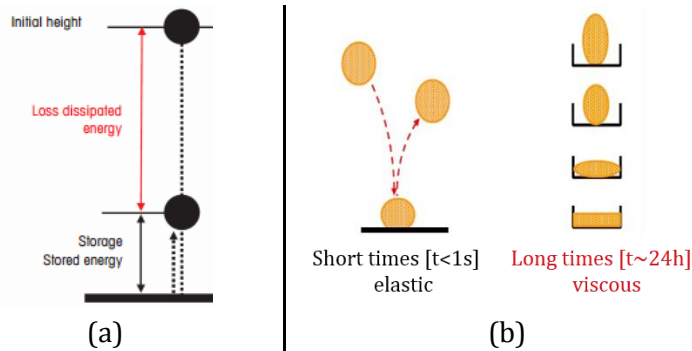


Figure 10 Illustration of typical viscoelastic materials behavior: (a) existence of dissipated and stored energy (b) time-dependent mechanical properties

This behavior is described phenomenologically with several models, such as Maxwell's and Kelvin-Voigt's model, and lead to the determination of a unique relaxation time  $\tau = \eta/G$  with G the modulus of the material. Yet polymers do not show a unique relaxation time but rather a distribution of relaxation times. The Boltzmann principle states that the response of a material to different loadings is the sum of each individual loading, and may be used to predict the relaxation times of a material. A sinusoidal stress is imposed and the polymer's response is studied. The sinusoid's frequencies are assumed to be directly linked to the relaxation times.

Let us consider a deformation  $\epsilon(t) = \epsilon_0 \cos(\omega t)$ , and a resulting stress  $\sigma(t) = \sigma_0 \cos(\omega t + \delta)$ , with a pulsation  $\omega$  and a phase difference  $\delta$ . The elastic response of a solid does not cause any

phase shift ( $\delta=0$ ), whereas in the case of a Newtonian liquid a phase delay is probed  $\delta=\pi/2$ . For viscoelastic materials, an intermediate behavior exists such that  $0 \leq \delta \leq \pi/2$ , and the resulting stress has a component in phase with the deformation (elastic behavior), and one in phase quadrature (viscous behavior). The overall stress is therefore sinusoidal but out-of-phase regarding the original deformation. The complex shear modulus is defined as  $G^* = G' + iG''$ , with  $G'(\omega)$  the elastic modulus - characterizing the stored (and restored) energy during each cycle- , and  $G''(\omega)$  the loss modulus characterizing the dissipated energy.

The loss factor is defined as  $\tan \delta = \frac{G''}{G'}$ , with

$$G' = \frac{\sigma_o}{\epsilon_o} \cos \delta \quad 1.14$$

$$G'' = \frac{\sigma_o}{\epsilon_o} \sin \delta \quad 1.15$$

Due to the viscoelastic behavior of polymers, these moduli are strongly time and frequency-dependent, and the effect on the macroscopic properties of these materials is illustrated in Figure 10 (right). The study of the time-dependent relaxation processes is presented in the next paragraph for unentangled and entangled systems.

### 1.3.2 Unentangled polymer dynamics ( $M < M_e$ )

When the polymer melt's molar mass  $M$  is lower than its mass between entanglements  $M_e$  ( $M < M_e$ ), the system is considered as unentangled, and its dynamics are described by the Rouse model. The Rouse time  $\tau_R$  is defined as the longest relaxation time of the chain, and scales as

$$\tau_R = R_g^2 / D \quad 1.16$$

$$D \sim kT / N\zeta \quad 1.17$$

with  $R_g$  the radius of gyration of the chain,  $D$  the diffusion coefficient,  $N\zeta$  is the total friction in the chain and  $kT$  thermal energy.

$\tau_R$  is of the order of 0.5ms and can be expressed as

$$\tau_R \sim \frac{b^2 \zeta}{kT} N^2 = \tau_o N^2 \quad 1.18$$

$$\tau_o = b^2 \zeta / kT \quad 1.19$$

Where  $\tau_o$  is the microscopic relaxation time of a Kuhn segment ( $\sim 10^{-10}$ s), and  $b$  the Kuhn length.

For times shorter than the Rouse relaxation time, for  $\tau_o < t < \tau_R$ , some parts of the chains are able to relax on their own. The unrelaxed segments contribute to the modulus with an energy  $kT$  and lead to a scaling of the modulus with frequency  $\omega$ :

$$G'(\omega) \sim G''(\omega) \sim \omega^{\frac{1}{2}} \quad 1.20$$

For  $t > \tau_R$  the whole polymer chain has relaxed and the behavior is that of a Newtonian viscous liquid

$$G'(\omega) \sim \omega^2 \quad 1.21$$

$$G''(\omega) \sim \omega^1 \quad 1.22$$

If the molar mass  $M$  of the polymer melt is higher than the mass between entanglement  $M_e$  (typically for  $M > 2M_e$ ), topological constraints- entanglements- will greatly modify the diffusion of the chains.

### 1.3.3 Entangled polymer dynamics ( $M > 2M_e$ )

From the tube model introduced in 1.2.3, De Gennes [5] and Doi & Edwards [6] proposed a description of the relaxation of entangled chains in the restricted tube: the reptation process. The idea of such a representation is that for a polymer chain to relax from its initial state, it has to find a way out of the tube.

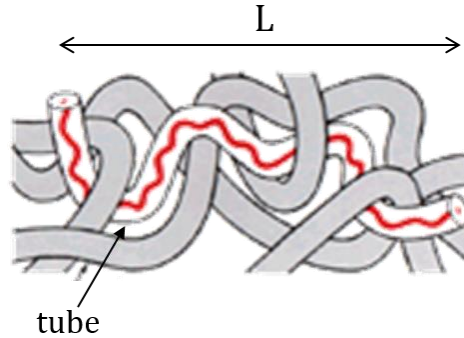


Figure 11 Illustration of the reptation model, with  $L$  the total length of the tube

At short times, the polymer chain does not feel the effect of the tube, and the segments between two entanglements (called “entanglement strand”) of  $N_e$  monomers relax following the Rouse dynamic of unentangled chains with the relaxation time  $\tau_e$ , such that from equation 1. 18:

$$\tau_e = \tau_0 N_e^2 \quad 1. 23$$

$\tau_e$  is of the order of  $10^{-6}$  to  $10^{-4}$ s.

At long times, reptation, which is the diffusion of the whole chain over the length  $L$  of the tube, takes place, with a characteristic time called the reptation time  $\tau_{REP}$ . In Figure 11, the red polymer chain has to disentangle from other chains which act as temporary obstacles.  $\tau_{REP}$  is the longest relaxation time and is sometimes referred to as  $\tau_D$  (terminal relaxation time):

$$\tau_{Rep} = \frac{L^2}{D} \propto N^3 \quad 1. 24$$

with  $N$  the polymerization index and  $D$  the diffusion coefficient. In fact, whereas theoretically  $\tau_{REP}$  scales as  $M^3$ , experiments measured a dependence as  $M^{3.4}$  [4].

At intermediate times, if entanglements are considered as fixed in time, a rubbery plateau for which  $G'$  remains constant is probed, and the expression of  $G_e$  was given earlier (see equation 1. 11).

### 1.3.4 Rheology of entangled polymer melts

All these characteristic timescales can be experimentally determined using linear rheology. For some polymers, a general equivalence has been observed between the response to stress at low temperature and to that at high frequency (or short times). Similarly, an equivalence between the response at high temperature and that at a low frequency (long times) is observed. This Time-temperature principle is true only in systems where the relaxation processes all vary with the same temperature-dependency. If so, it is possible to probe the mechanical response of a material at different temperatures and to draw a unique frequency-dependent master curve at a given temperature. This concept will be further detailed in the next chapter. Figure 12 plots, at  $25^\circ\text{C}$ , the

storage and loss modulus  $G'$  and  $G''$  as a function of reduced frequency and shows all the above-mentioned relaxation times of 1,4-polybutadiene [7].

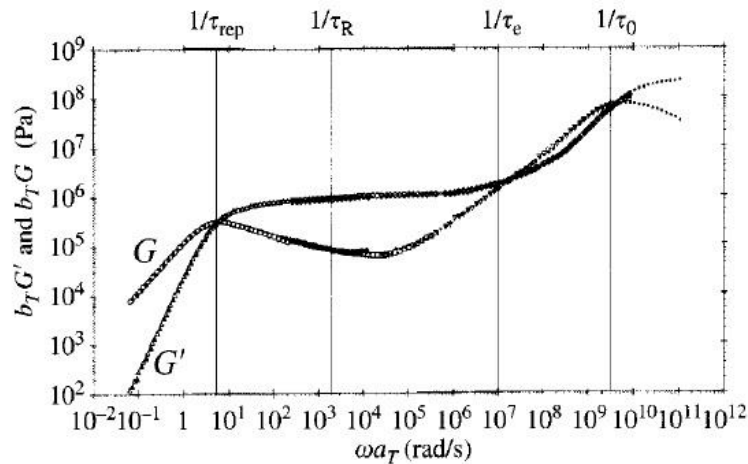


Figure 12 Master curve represented at a reference temperature of 25°C for a 1,4-polybutadiene sample. Figure from Colby [7]

Prior to showing the relevance of polymer dynamics on their adhesion behavior, let us introduce the key concept underlying my thesis.

## 2 Introduction to the adhesion of soft materials

Two materials brought in contact interact, and Dupré proposed an expression for the thermodynamic work of adhesion in the case of ideal interface separation:

$$W_{adh} = \gamma_1 + \gamma_2 - \gamma_{12} \quad 1.25$$

With  $\gamma_1$  and  $\gamma_2$  the surface energies of materials 1 and 2, and  $\gamma_{12}$  their interfacial energy.

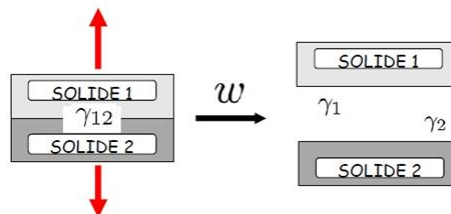


Figure 13 Illustration of an ideal interface separation between two solids, and their corresponding surface energies

Yet if one considers two stiff materials (metal plates for example) and bring them into contact, hardly any energy is needed to debond them. On the opposite, adhesion properties of two very viscous materials (fluids for example) are also barely measurable. Why? In the first case, solids are rough surfaces, and if they are not able to deform, intimate contact between both surfaces is hardly achievable, hence weak macroscopic adhesion properties. On the other side, viscous materials are able to deform to create intimate contact but are not able to resist any mechanical loading due to their poor bulk properties. These examples show that for materials to exhibit high adhesion strength, they must be deformable enough to maximize contact area, and at the same time resistant enough to withstand high stresses. Therefore, viscoelastic soft materials are ideal for such applications and among them, the adhesive strength of Pressure Sensitive Adhesives (PSAs) and elastomers have been widely investigated.

## 2.1 Adhesive performance of soft materials

### 2.1.1 Pressure Sensitive Adhesives (PSA) as soft adhering materials

PSAs are soft materials that are able to adhere to any kind of surfaces through the application of light pressure. Their adhesion strength is due to very important number of physical interactions at the interface, without any chemical reaction or solvent evaporation, and to adequate rheological properties. Dahlquist [8] indeed proposed several criterias for PSAs to show optimum bonding properties. He suggested that the best application temperature is 50-70°C above the glass transition temperature of the material, and that the material must have a shear elastic modulus  $G'$  at the bonding frequency lower than 0.1MPa for the layer to create intimate contact within the contact time. PSAs are highly deformable and are therefore able dissipate a high amount of energy during their debonding, thus exhibiting very high adhesion strength [9][10][11].

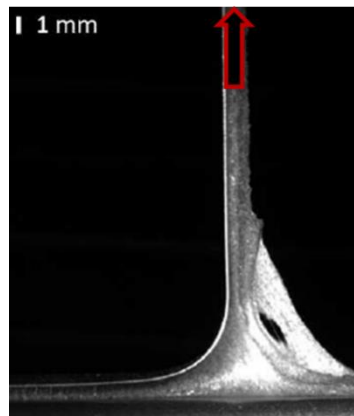


Figure 14 Image of a 90°-peeling test on a PSA.

In this thesis, another category of soft materials is studied: uncrosslinked elastomers. Yet whereas PSAs have modulus of the order of 0.1MPa, uncrosslinked elastomers are much more entangled and therefore much stiffer when tested at the 1s time scale; they exhibit moduli one order of magnitude higher than PSAs. This change in bulk properties is therefore expected to considerably change the contact formation. Moreover, PSAs are used on rigid surfaces, whereas this work is focused on the adhesion between two polymer melts. Therefore, even if the studies on PSAs are insightful for adhesion phenomenon, it is key to remember that the physics behind the bond formation and detachment of elastomers is expected to substantially differ.

### 2.1.2 Introduction to the tack behavior of elastomers

Tack is defined as the ability of two materials to resist separation after bringing them into contact for a short time under light pressure. If one considers two identical polymer melts in contact, that had had sufficient time to completely heal such that there are no interface, debonding leads to the measurement of the so-called green strength, which is the rubber's mechanical resistance to deformation and fracture prior to vulcanization. Hamed has extensively studied the self-adhesion properties of uncured elastomers [12][13][14], and suggested that for rubbers to exhibit high tack, three main conditions needed to be fulfilled [15]. First, the two materials must come in intimate contact. If adsorbed gases are present (such as moisture or impurities), the effective molecular contact between the materials is reduced, preventing a sufficient flow of the polymer chains across the interface (see Figure 15).

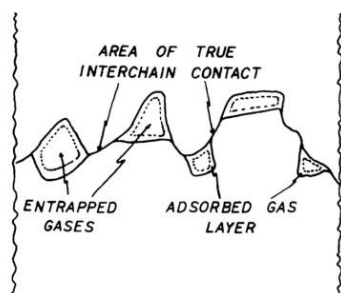


Figure 15 Illustration of adsorbed gases at the interface. Picture from Hamed [15]

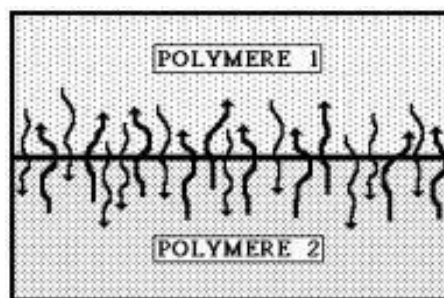


Figure 16 Illustration of the interdiffusion of polymer chains across an interface

Furthermore, once contact between surfaces is achieved, polymeric chains are able to flow across the interface. This inter-diffusion enables healing of the interface, resulting in good adhesion properties [16][17]. Not only are good contact area and sufficient inter-diffusion of chains needed to reach good properties, but a high cohesive strength is also crucial. Indeed, during the debonding of a joint, both the interface and the bulk of the material are strained.

The extent of these three criteria for adhesion and self-adhesion of elastomer will be extensively detailed in this chapter, and used throughout the thesis.

## 2.2 Macroscopic characterization of adhesion

Several tests have been developed in order to characterize the adherence between two materials. The appropriate test for a specific application should be chosen with regard to the type of material tested, but also to the performances that one needs to evaluate.

During the “rolling ball test” (also called “marble test”), a steel ball is dropped from an angled surface to a plane surface with the tested material. For a given thickness and modulus, the material’s adhesive properties are inversely related to the marble’s distance on the surface. The experimental parameters of this test are hardly controllable, it is therefore challenging to deduce an effective energy of adhesion. Yet it is a simple way to compare several adhesives and is used in some industries. Another way of measuring adhesive properties is the loop tack test: a loop of adhesive is brought into contact with a substrate and then removed at a constant speed. The force needed to remove the loop is measured and the failure energy can be evaluated [18]. In the adhesive community, the most common test is the peel test [19][20][21]. The material and its stiff backing are adhered to the substrate and its extremities are clamped to a tensile machine. Different test geometries are possible, depending on the angle between the applied force and the substrate. The adhesion energy is computed by measuring the force necessary to keep a certain debonding speed. Contact times from tens of seconds to several minutes (and hours) are reached.

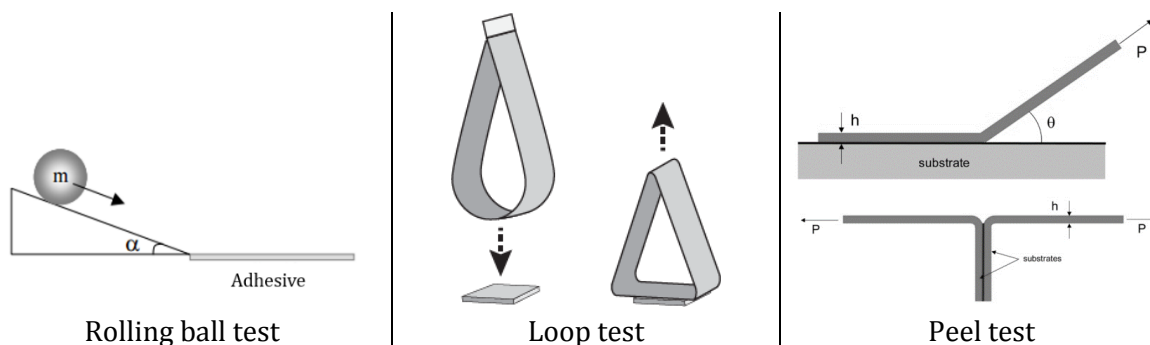


Figure 17 Means of characterizing adhesion properties: rolling ball test, loop test and peel tes,

During this work, the adhesion properties are characterized with a probe tack device [10] which will be presented more in details in Chapter 3.

## 2.3 Comments

During this part, it was shown that adhesion of two elastomers depends on several material-related properties, and several methods have been presented to characterize them. The characterization of adhesive joints is a two-stage process: bond formation and bond rupture. The mechanisms related to the contact- or interface- formation can thus be analyzed separately from those related to the debonding process. Both must be finely controlled for elastomers to exhibit high tack strength. The following paragraph will first focus on the formation of a strong interface and section 4 then introduces the energy dissipation processes needed to develop high adhesion.

## 3 Formation of a strong interface

As mentioned previously, materials must create intimate contact on a molecular scale, and form interfacial interactions to exhibit high tack properties. Several theories have been proposed to explain the origin of these interactions and the development of adhesion between two surfaces on the molecular scale.

### 3.1 Molecular theories

Among the past hundred years, several theories have tried to explain the very complex phenomenon occurring at the interface between two contacting materials to explain their adhesion energy. Among those, the adsorption theory [22] considers adhesion as a purely surface process caused by intermolecular forces when the materials are close enough. These intermolecular forces include dispersion forces and hydrogen bonding. Nevertheless, this theory is unable to justify for several observed phenomenon: it cannot account for high adhesion energies between two nonpolar materials, and the adhesion energies expected from molecular forces are several magnitudes lower than that measured with peel tests. To account for these facts, the electric theory of adhesion was developed by Derjagin and Krotova [23], and suggest that adhesion is due to charges interactions at the surface. This theory cannot alone provide an explanation for polymer-to-polymer adhesion, and more specifically to polar polymers. Voyutskii and coworkers [16][24] developed the diffusion theory to explain adhesion in such systems. This theory states that the controlling mechanisms for adhesion between two polymer layers is the interdiffusion of polymer chains across the interface. Anand and coworkers [25] argue that polymer flow occurs only once intimate contact is occurred. In fact, in their contact theory, it is suggested that the main controlling mechanism for the adhesion between polymers is the contact stage.

Both the contact and diffusion theory are widely discussed in the literature, and their relevance regarding the self-adhesion of polymer melts are studied.

### 3.2 Formation of intimate contact

According to Anand and coworkers, self-adhesion (also called “autohesion”) consists of two main steps: a first one during which the contact between both surfaces is established, followed by a bond formation step i.e. development of interfacial forces. The first step, creation of intimate contact, is tackled during this section whereas the extent by which intermolecular forces (and especially interdiffusion) develop tack strength is dealt with in the next section (3.3).

### 3.2.1 Cavitation

To truly understand what are the parameters limiting the formation of a strong interface, one must first appreciate the initiation mechanisms of failure in a joint. Lakrout and coworkers [10] performed an intensive study on the observation of probe-tack experiments for PSAs under various experimental conditions. They revealed that in all cases, the maximum in stress during the debonding process is related to the formation of cavities, and that these cavities appear randomly on the surface of the probe surface due to the negative hydrostatic pressure applied during the debonding step. Cavities are shown on Figure 18 and are the first visible signs of the beginning of failure.

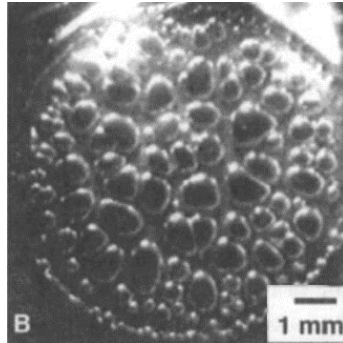


Figure 18 Observation of spherical cavities at the interface during debonding. Photo from Lakrout [10]

Therefore, preventing their earlier appearance is key to strengthen the interface. Cavities are due to presumably microscopic air pockets entrapped during the contact stage, which act as defects between the two contacting surfaces. Fine control of the surface roughness and the contact force has been identified as fundamental to enhance contact quality [26].

### 3.2.2 Parameters influencing microscopic contact

#### i. Roughness

Most, if not all, surfaces are rough, with a size and height-distribution of asperities. Roughness, which is the deviation in height from the average thickness of a surface, is a multi-scale measurement [27] and controls the microscopic contact of two materials (see illustrations in Figure 19 and Figure 20). In fact, when two rough surfaces are brought into contact, cavities are trapped at the interface and these defects strongly influence the adhesive strength of materials [28][26]. The size and distribution of these surface defects influence the cavitation process during debonding, and Chiche and coworkers [28] showed that the cavitation stress decreases with roughness, suggesting that their nucleation is easier.

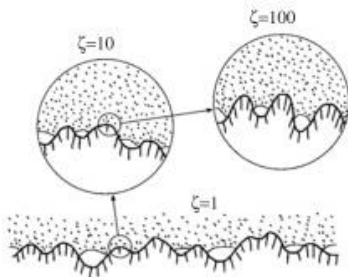


Figure 19 Substrates have roughnesses on many different lengthscales. Illustration from [27]

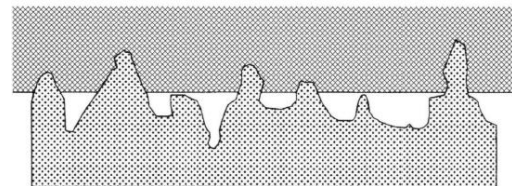


Figure 20 Contact of a rough and a smooth surface. Illustration from [26]

Roughness can be responsible for limited contact if the materials are not able to accommodate, yet if adequate bulk properties or adequate contact conditions force complete contact, the contact area is increased compared to a completely flat surface.

A way to increase the effective contact area is to increase the contact pressure.

## ii. Contact pressure

To remove these defects (trapped air) from the interface, authors [29][30] have showed that the application of pressure to force intimate contact is effective and promotes better contact. Figure 21, from Bothe [30], shows that for a given contact time, there is a certain contact pressure above which the adhesive strength does not evolve. This plateau is reached for a pressure called “saturation pressure”. Under the application of a pressure, enlargement of effective contact occurs by flow.

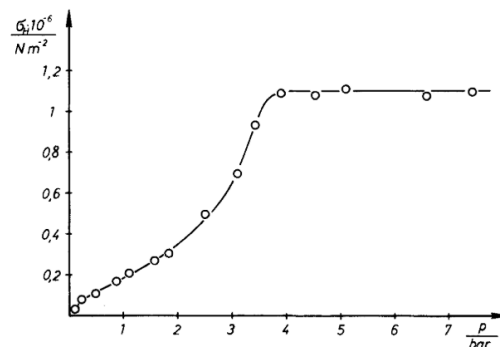


Figure 21 Adhesive strength of polychlorobutadiene as a function of contact pressure (for a contact time of 5 minutes). Figure from [30]

This effect of pressure on adhesive strength is coherent with Anand’s contact theory. Yet it is important to keep in mind that very high pressures (such as that encountered in polymer processing) can also affect the free volume necessary for Brownian motion and therefore decrease the self-diffusion of polymer chains [31].

Creton et al [32] studied the extent of contact formation between polymer melts and rigid surfaces for short contact times ( $< \tau_D$ ) and relatively low pressure ( $\sim 10^4$  Pa). Authors distinguished two situations: “large” and “small” applied pressures. In the latter, the effect of surface forces (i.e. thermodynamic work of adhesion) on contact formation are considered whereas in the former, pressures are large enough to neglect surface forces. They showed that in this case of large pressure, contact area is inversely proportional to the polymer’s elastic modulus and proportional to the applied pressure. During this thesis, contact forces were applied such that the case of “large” pressure was always considered.

### 3.2.3 Adhesion on glass

To study the effect of contact time on the adhesion strength between two polymer melts, it is complicated to separate effects due to increase of contact area and those due to interdiffusion of polymer chains across the interface. To separate both, studying adhesion of a soft material on a rigid surface gives insights on the time-related mechanisms. Smitthipong and coworkers [33] studied the adhesion of two rubbers, polyisoprene (IR) and hydrogenated acrylonitrile butadiene (HNBR), as well as a blend of both, on glass and results are shown on Figure 22. Figure 23 shows stress-strain debonding curves for the adhesion of SBR on glass for various contact times [34].

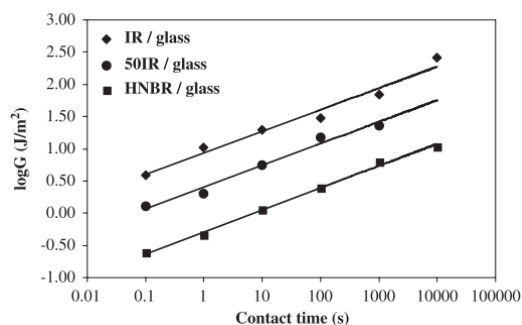


Figure 22 Variation of adhesion energy  $G$  of pure rubbers (IR and HNBR) and of a rubber blend (50IR) on glass surface as a function of contact time. Figure from [33]

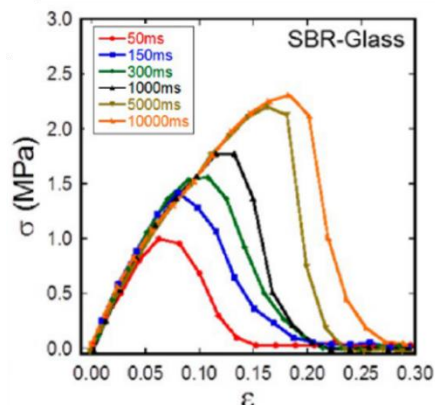


Figure 23 Stress-strain debonding curves for the adhesion of SBR on glass for various contact times. Figure from [34]

In both cases, the adhesion properties of the materials on glass increase with time. As glass prevents any diffusion of polymer chains, this boost is due to the materials' ability to maximize interfacial interactions with the substrate by re-arranging, and to an increase in the contact's quality area by flow and diffusion of air defects away from the interface. Let us quickly comment that the surface energies of HNBR and IR are similar such that the difference in their adhesion energy is due to their different mechanical properties.

### 3.2.4 Comments

The degree of confinement and the thickness of the layer [28] have also been identified as parameters influencing cavitation, yet as they were kept constant during this thesis they are not detailed in this chapter. Furthermore, a reduced contact area can also be caused by the adsorption of impurities (dust for example) on the surfaces prior to contact and it was demonstrated that low elastomer viscosity, and rapid diffusion of the impurities into the bulk of the rubber increases tack [17]. The mechanical properties of the material are also, of course, key to control its spreading on the substrate [26][28][35]. Yet as they also influence the debonding stage they were not treated independently in this section.

Once full mechanical contact is established, interfacial interactions between the surfaces must occur to provide strong adhesion. These interfacial interactions can be of different types, and of different forces, from Van Der Waals (<1kJ/mol) to polar (~2kJ/mol) or H-bonding (5 - 40 kJ/mol) forces. In the case of adhesion between two unvulcanized elastomers above their glass transition temperature, interdiffusion is the governing mechanism [15][16][24].

## 3.3 Polymer interfaces between polymer melts

### 3.3.1 Methods to observe motions

Several experimental techniques exist to investigate interfaces between polymer melts, and Stamm [36] and Russell [37] have summarized the most common ones. The big categories include ion beam analysis and X-Ray or Neutron Reflectivity.

Ion beam analysis methods such as Forward Recoil Spectrometry (FRES), and Rutherford Backscattering spectrometry (RBS) are based on the collision between surface nuclei and an incident beam of ions ( $\text{He}^{2+}$ ). The principle of FRES is illustrated in Figure 24: a monoenergetic beam of He ions reach the sample with an incidence angle. The incident ions undergo elastic

collision with the sample's nuclei which results in the removing of some nuclei. An energy-sensitive detector records the number of recoiling nuclei as a function of energy. Depending on the depth of the atom targeted, the amount of energy loss through electronic excitation during its collision with the ion beam is modified. In the case of RBS, the energy of the backscattered  $\text{He}^{2+}$  ions is studied. Both methods detection are strongly dependent on the depth of the studied nuclei, as well as on its mass. Therefore, these techniques have been extensively used [38], in particular by Green and coworkers [39][40], to study diffusion in polymer melts.

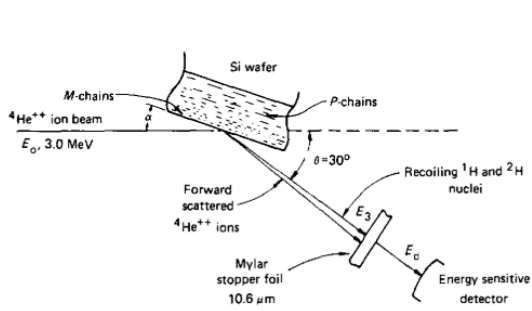


Figure 24 Illustration of the FRES experiment from [39]

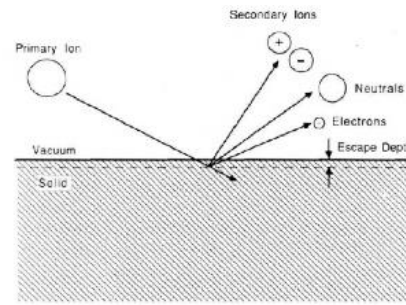


Figure 25 DSIMS: Schematic of the sputtering process caused by an impinging primary ion. Illustration from [41]

Another well known method is Dynamic Secondary Ion Mass Spectroscopy (DSIMS). The ion beam sputters neutral and ionized particles from the surface such as illustrated in Figure 25. The secondary ions are extracted, and analyzed with a mass spectrometer. This method was first used by Whiltlow [41] to study diffusion between two layers of polystyrenes (one of whom is deuterated), and Russell and coworkers [42] studied the diffusion of triblock, partially deuterated, polystyrene polymers. Their experimental study confirmed the reptation theory according to which the chain ends are responsible for the chain's center of mass motion through a reptating motion.

Neutron Reflectivity (NR) is used for its optimal resolution of the interfacial width (typically  $< 1\text{nm}$ ) and a schematic is proposed in Figure 26. The method consists in studying the number of reflected neutrons after radiation on the surface, and relies on the big difference in scattering length densities between hydrogen and deuterium which enables a good contrast between the polymer layers. It has been widely employed for the study of interdiffusion of polymers (both glassy and elastomers) [43][44][45], in which one of the layers has been deuterated.

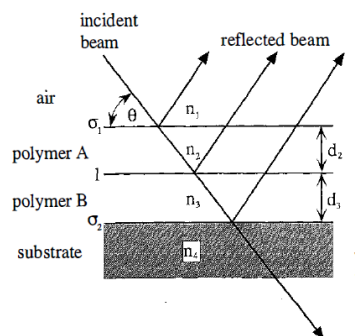


Figure 26 Schematic of a neutron reflection experiment. Illustration from [36]

### 3.3.2 Adhesion of immiscible polymers: a thermodynamic study

The thermodynamic equilibrium of the interface between two (different) polymers, well above their glass transition temperature, with a fixed molar mass is investigated. The equilibrium structure results from a balance between the enthalpic penalty of mixing two chemically distinct polymers and the entropic gain of accessing more configurations upon interdiffusion. Dynamics of entangled polymers have been presented previously (section 1.3), and their diffusion strongly depends on the affinity between the two contacting layers. Indeed, miscibility of two polymers is possible only if the difference in their solubility parameters  $\delta$  (or their Flory interaction parameter  $\chi_{12}$ ) is weak such that the enthalpy cost of mixing both is low:

$$\Delta H_{mix} \propto (\delta_1 - \delta_2)^2 \propto \chi_{12} \quad 1.26$$

i. Interfacial width  $w = f(\chi)$

Broseta and coworkers [46] have studied the influence of the Flory parameter  $\chi$  between several immiscible polymers on their interfacial width and tensions. They showed that at thermodynamic equilibrium, the interfacial width  $w$  between two polymers A and B is given by:

$$w = w(N = \infty) \frac{1}{\sqrt{1 - 2 \ln 2 * \left( \frac{1}{\chi N_A} + \frac{1}{\chi N_B} \right)}} \quad 1.27$$

Where  $N_A$  and  $N_B$  are the polymerization indexes of polymers A and B, and  $w(N = \infty)$  the prediction from Helfand's theory [47] with the assumption of infinite chain length, and scales as:

$$w(N = \infty) = \frac{b}{\sqrt{c\chi}} \quad 1.28$$

where  $b$  is the Kuhn segment length, and  $c$  is a constant which has a value of 6 or 9 depending on whether the interface is in the weak or strong segregation limit.

These theoretical considerations have been confirmed experimentally thanks to the methods presented earlier. Schach and coworkers [45] have run studies on uncrosslinked elastomers, and measured the volume fraction of a deuterated polybutadiene (PB120K-D) as a function of distance along the interface with various polymers. Figure 27 shows the volume fraction of PB120K-D,  $\Phi_{PB120K-D}$ , in Styrene Butadiene Rubber (SBR), polyisobutylene (PIB), ethylene-propylene-diene copolymer (EPDM) and poly(dimethylsiloxane) (PDMS) as a function of distance  $z$  along the interface. The measurements have been performed after thermodynamic equilibrium was reached and results (see Table in Figure 27) clearly show that the interfacial width  $w$  is large ( $\sim 20\text{nm}$ ) for low Flory parameters, and strongly decreases ( $\sim 2\text{nm}$ ) for strongly immiscible polymers melts (high  $\chi$  value).

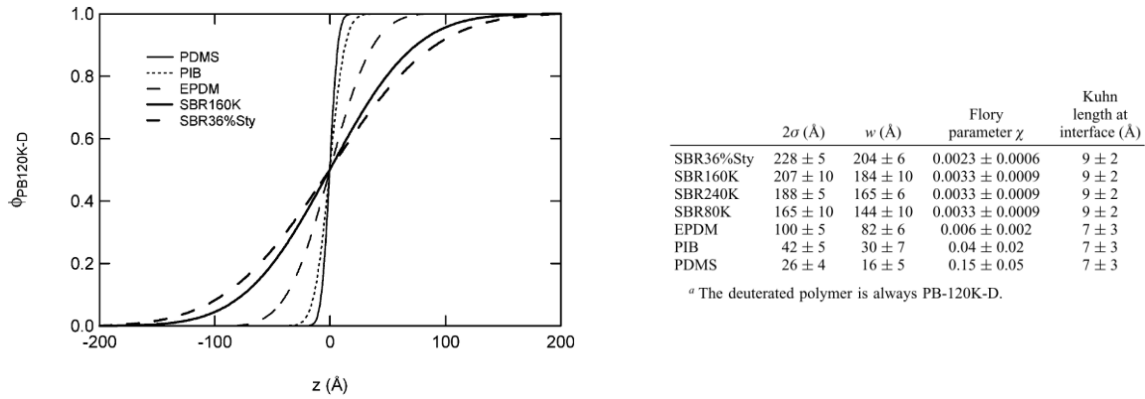


Figure 27 Left: Volume fraction of deuterated monomer as a function of distance along the interface between PB-120K-D and other polymer melts. Right: Corresponding relevant characteristics of the polymer-polymer interfaces. From [45]

## ii. Adhesive strength = $f(w)$

Several authors have then looked for a correlation between the interfacial width measured and the adhesion strength. First results [48] have focused on glassy polymers that were brought into contact above their glass transition temperature to enable diffusion, and then quenched to lower temperature to perform debonding tests through asymmetric double cantilever beam (ADCB) tests. Figure 28 shows that the adhesion energy  $G_c$  of polystyrene (PS) to poly(p-methylstyrene) (PpMS) increases as a function of interfacial width  $a_i$  (measured for various molar masses). The same trend was observed for the adhesion of uncrosslinked linear elastomers [45]. From the interfacial width  $w$  measured between PB420K-H and several elastomers in the previous section, adhesion tests were performed on a Probe-Tack device and the corresponding adhesion energies  $W_{adh}$  are shown in Figure 29.

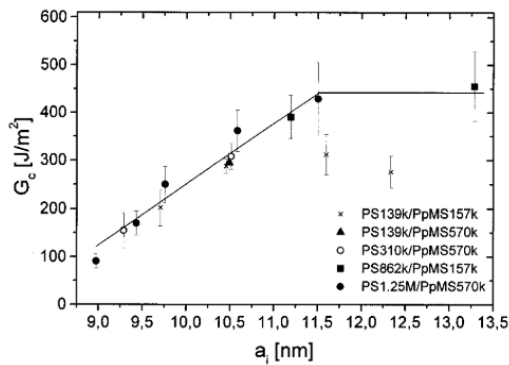


Figure 28 Adhesion energy of different samples of PS/PpMS as a function of interfacial width ( $a_i$ ). The solid line is drawn as a guide to the eye. Figure from [48]

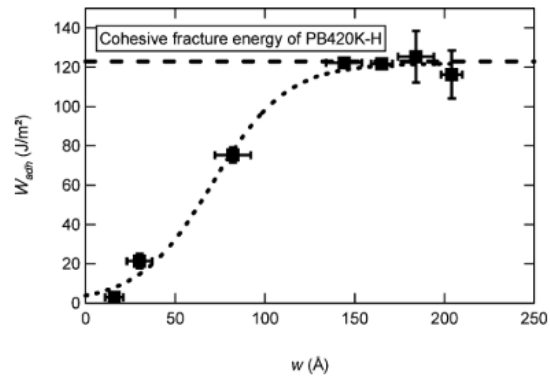


Figure 29 Adhesion energy  $W_{adh}$  of interfaces between PB420K-H and different polymers as a function of interpenetration width at the interface  $w$ . Figure from [45]

Both results show that for high molecular weight polymers ( $M \gg M_e$ ), the interfacial width is the main parameter controlling the adhesion strength and that above a certain width, the strength reaches a maximum. Nevertheless, whereas in the case of glassy polymers (Figure 28) this threshold value is attained for distances close to the molecular weight between entanglements (11-12nm), it is reached after a penetration of four to five entanglements lengths (15nm) in the case of Schach study on elastomers (Figure 29). The explanation for such a difference lies in the tested materials themselves. Schnell and coworkers [48] tested polymers in their glassy state, and showed that diffusion of polymer chains over a short distance is sufficient to activate plasticity. In this case, debonding occurs through chain rupture. In the other study, elastomers are tested at room temperature which is well above their  $T_g$ , and viscoelastic dissipation is responsible for the

high adhesion strength. In this case, debonding occurs through disentanglement of the chains at the interface.

These studies have been performed once thermodynamic equilibrium at the interfaces was reached. To study their kinetics of formation, symmetric interfaces have been thoroughly studied.

### 3.3.3 Self-adhesion of polymers: kinetics

Previous paragraphs have focused on interface after thermodynamic equilibrium. During this section, we focus on the formation of such equilibrate interface through a kinetic study.

#### i. Interfacial width as a function of time

Neutron reflectivity measurements have been performed [49] to study the diffusive motion of a deuterated polymer (polystyrene) at the interface with a hydrogenated PS of the same molecular weight, at high temperature ( $>T_g$ ). The average displacement of a chain at the interface (root mean square half-width) is plotted as a function of reduced time in Figure 30, and reveals four different regimes. The reduced time was calculated using Williams, Landel and Ferry (WLF) horizontal shift factor  $a_T$  with regard to the annealing temperature. Russell [37] used reptation arguments of Doi & Edwards to fit these regimes with the material's characteristic relaxation time, i.e. the relaxation time between entanglements  $\tau_e$  (unentangled dynamic), the Rouse relaxation time of the whole molecule  $\tau_R$ , and the reptation time  $\tau_d$ .

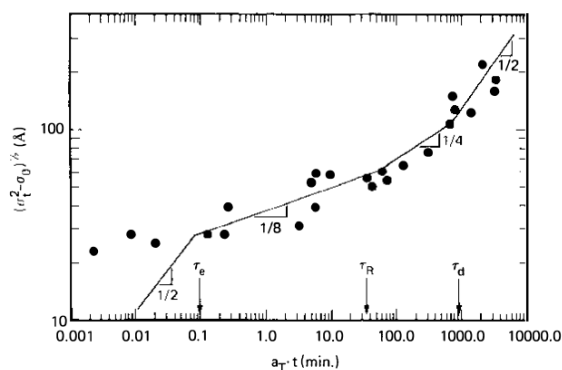


Figure 30 Average displacement of a chain at the interface as a function of reduced time at a reference temperature of 120°C. Figure from [37]

At the early stages of diffusion ( $t < \tau_e$ ), the motion of the chain is not yet influenced by entanglements. Since diffusion theories have been developed on the motion of chains in the bulk, the difference between the theoretical fit and the experimental data for short times might be explained by local relaxation of the polymer chains due to interfacial effects. For diffusion times above  $\tau_e$ , motion is restricted by entanglements and chains move following a  $t^{1/8}$  power law. Above the Rouse relaxation time, it is considered that motions of the whole chain start to be correlated and that most of the chain has escaped from its initial tube ( $\sim t^{1/4}$ ). Above the reptation time, the chain has completely relaxed from its initial tube and Fickian diffusion occurs ( $\sim t^{1/2}$ ).

#### ii. Correlation between adhesive strength and interfacial width

Similarly to what they have measured for asymmetric systems, Schnell and coworkers [48] showed that above a threshold interfacial width (close to 12nm), a jump in adhesion energy is probed and a plateau is reached, corresponding to the cohesive strength of the material (here polystyrene). Figure 31 shows the adhesion energy  $G_c$  and the interface width  $a_i$  as a function of

reduced annealing time  $t_{\text{red},120^\circ\text{C}}$  (calculated as the contact time divided by a shift coefficient from WLF equations).

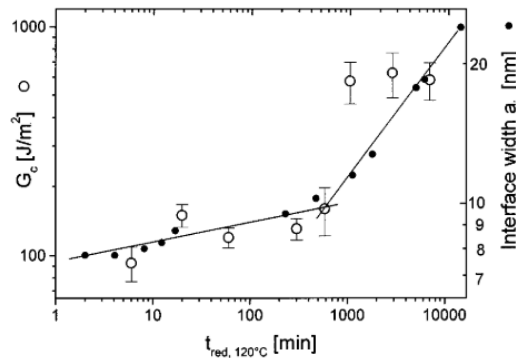


Figure 31 Double logarithmic plot of the adhesion energy ( $G_c$ ) and interfacial width ( $a_i$ ) of PS/PS as a function of the reduced annealing time. Figure from [48]

### iii. Adhesive strength vs contact time

#### Trends

Adhesion strength can be defined either using an energy-related or a stress-related criteria. If tack is calculated as the critical fracture stress  $\sigma$  for chain disentanglement, then authors [31] find that

$$\sigma \propto l(t)^{\frac{1}{2}} \quad 1.29$$

with  $l(t)$  the average monomer segment interpenetration distance, such that

$$\sigma \propto t^{\frac{1}{4}} M^{-\frac{1}{4}} \quad 1.30$$

with  $M$  the molecular weight, and  $t$  the contact time. Figure 32 shows results from Skewis on the adhesion, and self-adhesion, of uncured polymer pairs (SBR and butyl rubber, with  $M_{\text{SBR}}=260\text{kg/mol}$  and  $M_{\text{butyl}}=2250\text{kg/mol}$ ). Self-adhesion levels follow the power law of eq. 1.30, and the adhesion strength of SBR on butyl rubber is much lower since both polymers are incompatible.

Nevertheless, it is most common to consider a fracture energy criteria, in which the critical strain energy  $G_c$  follows the trend:

$$G_c \propto t^{\frac{1}{2}} M^{-\alpha} \quad 1.31$$

The value of the exponent  $\alpha$  depends on the type of debonding that occurs; either solely through chain disentanglement ( $\alpha=1/2$ ) or simultaneously with bond rupture ( $\alpha=3/2$ ). This  $t^{1/2}$  power law has been experimentally found by numerous authors [30][40][50]. Peeling tests on uncrosslinked polyisobutylene (PIB) were performed and their adhesion energy studied as a function of contact time. The results are shown on Figure 33 and confirms the time-dependence of eq. 1.31.

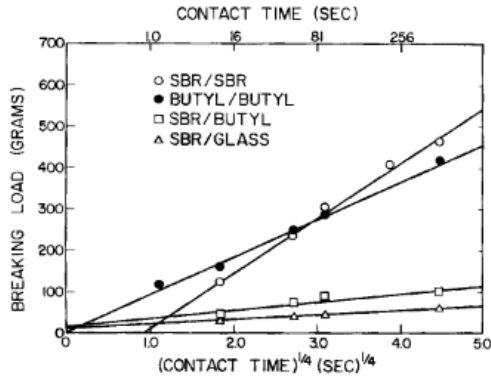


Figure 32 Tack (breaking load) as a function of  $t^{1/4}$  for several uncured polymer-polymer pairs. Figure from Wool [31]

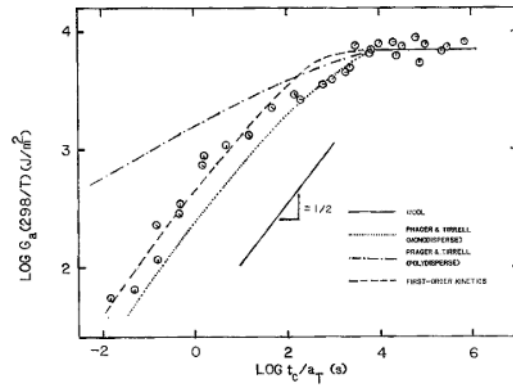


Figure 33 Log plot of the fracture resistance  $G_a$  of PIB material as a function of reduced contact time  $t_c/a_r$ . Figure from [50]

For very short contact times

Gurney and coworkers [51] studied the self-adhesion properties of linear, monodisperse, random copolymers of SBR with three different molecular weights (100, 170 and 250kg/mol) for a wide range of relatively short contact times (from 10ms to 10s). They characterized the materials' linear mechanical properties over twelve orders of frequency, and measured the characteristic times of the three systems. They showed that for very short contact times, typically 10ms ( $\tau_e < t << \tau_{REP}$ ), the self-adhesion properties of the studied NBR are independent of their molecular weight and the debonding are mainly controlled by the existence of defects at the interface during the contact formation (air entrapment). Nevertheless, individual segments still have time to relax and authors estimate that chains have diffused over 2-3 entanglements. For increasing contact time (300ms), more (7-12) entanglements relax but this (weak) diffusion length depends on the molecular weight. Finally, for contact times of the order of seconds, the diffusion is strongly related to fraction of chains that have diffused, which is directly correlated to the materials' reptation time. They thus suggested this characteristic time as a rescaling parameter, and showed that the debonding energy may be predicted thanks to the construction of a master curve (see Figure 34).

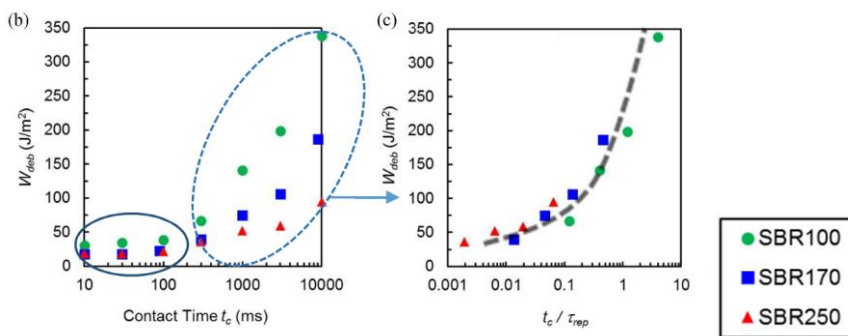
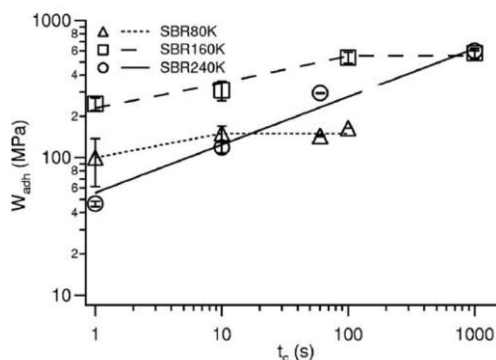


Figure 34 Work of debonding  $W_{adh}$  for SBR-SBR systems as a function of contact time  $t_c$  (left) and as a function of  $t_c/\tau_{REP}$  (right). Figures from [51]

This study shows that at very short contact times, adhesion is independent of molecular weight and the microscopic formation of intimate contact is key which is consisted with Anand's contact theory. Authors were able to estimate the degree of diffusion thanks to linear rheology measurements.

### Reptation time for healing

The existence of a plateau in adhesion energy for long enough contacts has been experimentally shown in numerous studies [21][33][52]. Schach and coworkers [53] performed an extensive study on three uncrosslinked monodisperse (80, 160 and 240 kg/mol) SBRs of different molar masses and Figure 35 shows the evolution of the self-adhesion energy of the materials  $W_{adh}$  as function of contact time  $t_c$ . Authors showed that the contact time  $t_c$  at which this plateau appeared correspond to the reptation time measured in linear rheology.



Polymer	Reptation time (s)
SBR80K	13
SBR160K	140
SBR240K	1170

Figure 35 Adhesion energy  $W_{adh}$  as a function of contact time  $t_c$  at high debonding speed (100um/s) for three SBR. Corresponding reptation times are shown on the table (right). Figure and table from [53]

### 3.3.4 Conclusion and comments

During this part, the different stages (contact and diffusion) inherent to strong interface formation were developed. Contact formation strongly depends on roughness and contact pressure, and its optimization often relies on modifying materials composition which also affects the bulk properties. Among the strategies that have been developed to solely strengthen the interface without altering bulk properties, the use of adhesion promoters [54][55] or specific surface treatment [56] can be considered. The diffusion phenomenon is strongly dependent on the materials in contact and on contact time. For very short contact times, adhesion strength is governed by interfacial defects and independent of molecular weight. For longer contact, diffusion appears to be strongly dependent on molecular weight as well as on miscibility between the considered polymers. Increasing contact temperature can lead to faster interdiffusion and hence to an enhanced adhesion performance for the same contact time [16][52] through increased thermal motion of the chains. It was also shown that diffusion phenomena is magnified when the polymer exhibits an important fraction of chain ends, and in particular in a branched structure [57].

Theories have been proposed to correlate the adhesion energy to the interfacial width, and to the contact time, and diffusion was shown to be directly correlated to linear rheological measurements. Yet these measurements, and theoretical approaches, were done for well-defined linear monodisperse polymers, which is not the case of most industrial polymers. Furthermore, linear rheology gives an indication of the polymer chains dynamics but does not provide information on the large strain regime, and particularly of the dissipative mechanisms needed for high strength properties. This will be detailed in the next section.

## 4 Energy dissipation as key to boost adhesion strength

Once a strong interface between two materials is established, it should resist high stresses during the debonding process.

### 4.1 Introduction to debonding in soft materials

#### 4.1.1 Need for dissipation

Adhesive joints exhibit fracture energies in the range of a few 100J/m<sup>2</sup> to a few 1000J/m<sup>2</sup>, and such levels cannot be explained by bond scission and creation of new interfaces alone [58]. To account for such values, one must consider viscoelastic materials ability to dissipate energy when strained. In the literature, researchers have investigated several innovative routes to enhance the bulk dissipation of their material, and in particular for the fracture of soft materials. Among these strategies, let us briefly introduce two of them. The first one, which will be of particular interest in Chapter 4, consists in increasing viscoelastic dissipation through a dynamic breaking-reforming process of labile bonds [59]. This labile bonds can be combined with covalent bonds [60][61] such that their association provides the material with both a solid character and an important deformation. Without developing further, it is important to note that the balance between the rate at which labile bonds are exchanged, and that of stretching the network is of paramount importance. The second strategy, initially developed by Jian Ping Gong [62][63][64], and extensively studied in our laboratory is the use of double (or more) interpenetrated networks as a source of energy dissipation. The difference in elastic and large strain behavior of the two network provides the material with both high stiffness and high extensibility.

For the adhesion-related problem, the design of an ideal material must not only maximize energy dissipation and strength, but also consider its interfacial properties. Indeed, when debonding a material from a surface (be it rigid or soft), there is a competition between the interfacial strength and the bulk mechanical properties. With appropriate conditions (see Dahlquist's criterias), PSAs form a perfect microscopic contact with a rigid substrate, and their transparency enables visualization of the debonding mechanisms. They are therefore a great tool to investigate the debonding mechanisms in soft materials.

#### 4.1.2 Types of cavities growth

In probe-tack experiments, once cavities have appeared, due to growth of a defect at the interface upon application of a tensile stress, two distinct situations can occur. Cavities can either grow and propagate at the interface, with hardly any bulk deformation, or grow in the bulk of the materials. Both situations, respectively called crack propagation and crack blunting, are illustrated in Figure 36.

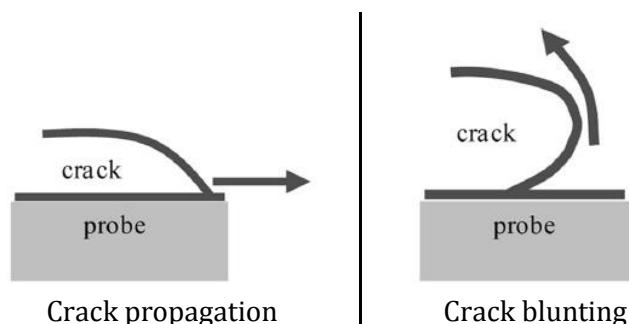


Figure 36 Schematic of a crack growth at the interface between the probe and the adhesive layer. Illustration from [65]

These two situations lead to different debonding behaviors of the material. If crack propagation at the interface occurs, a sharp decrease of the force (or stress) after cavitation is observed on the stress-strain curve; whereas important deformation and high strains are reached in the case of crack blunting. These two scenarios are illustrated in Figure 37.

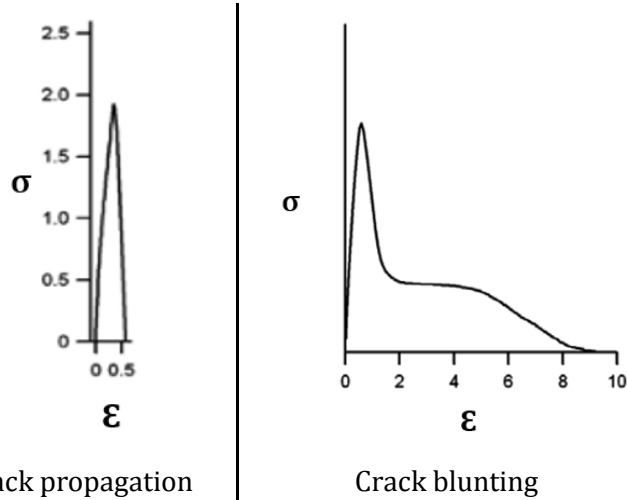


Figure 37 Debonding stress-strain curves as a function of cavity propagation mechanism (crack propagation and crack blunting)

## 4.2 Predicting debonding mechanisms from linear rheology

### 4.2.1 From materials elastic behavior

Within the framework of linear elasticity, the interfacial growth of a crack is governed by the critical energy release rate  $G_c$  (critical energy above which a crack propagates at the interface) and the bulk properties are controlled by the elastic modulus  $E$ . Webber et al [66] showed that for elastic layers, the ratio of the critical energy release rate and the elastic modulus,  $G_c/E$ , could be used to predict the type of adhesive failure. This length scale is compared to two characteristic sizes of the system: the thickness of the adhesive layer  $h$ , and the size  $r$  of an initial defect. Figure 38 shows that for  $G_c/E$  smaller than  $r$ , only interfacial crack propagation occurs and is controlled and limited by  $G_c$ . For  $G_c/E$  larger than  $h$ , crack blunting occurs and deformation in the bulk is observed. In between both extremes, a transition regime is probed.

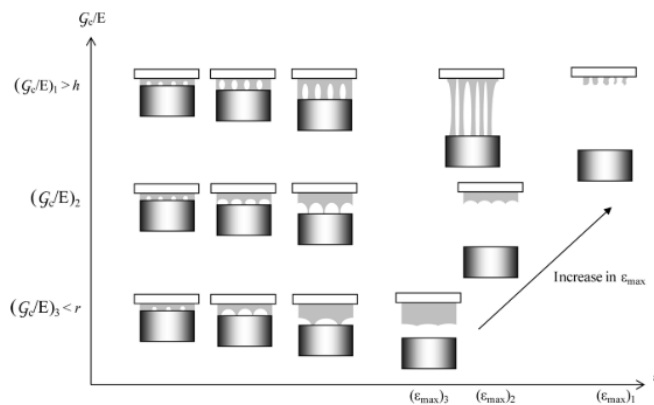


Figure 38 Schematics of the debonding process involved during probe-tack test depending on the value of the ratio  $G_c/E$ . From left to right: increase of the debonding strain. Figure from [65]

### 4.2.2 Considering viscoelastic dissipation

Viscoelastic materials exhibit, for strain- and frequency-related experimental conditions, additional dissipative mechanisms. To account for this dissipation, Maugis and Barquins [67] suggested that the critical energy release rate  $G_c$  follow the empirical equation:

$$G_c = G_o (1 + \varphi(a_T V)) \quad 1.32$$

Where  $G_o$  is the resistance to crack propagation at extremely low crack velocity, and  $\varphi(a_T V)$  characterizes the dissipative mechanisms at the tip of the crack. Authors suggested that for elastomers and relatively weakly adhering materials with only Van der Waals interactions, the dissipative factor can be approximated as:

$$\varphi(a_T V) = k * \tan \delta \quad 1.33$$

With  $k$  a constant and  $\tan \delta$  the loss factor.

Deplace and al [65] proposed an extension model presented in the previous section for elastic linear materials to take into account viscoelasticity. They suggested that the Young's modulus  $E$  can be replaced by the elastic component of the shear modulus  $G'(\omega)$  such that:

$$\frac{G_c}{E} = \frac{G_o (1 + \varphi(a_T V))}{G'(\omega)} = \frac{G_o(1 + k * \tan \delta(\omega))}{G'(\omega)} \quad 1.34$$

And

$$\frac{G_c}{E} \approx k \frac{G_o * \tan \delta(\omega)}{G'(\omega)} \quad 1.35$$

Therefore, although it does not have the dimension of a distance, the ratio  $\tan \delta(\omega)/G'(\omega)$  should play the same role as  $G_c/E$  in the elastic model, and can be experimentally obtained from rheological measurements. To do so, an assumption on the value of  $\omega$  is thus needed. In probe-tack experiments, the strain rate in the adhesive layer is heterogeneous both spatially and temporally, and the chosen frequency  $\omega$  can thus only be an approximation. Authors [65] suggested the use of the value  $2\pi V_{deb}/h_o$  where  $V_{deb}$  is the velocity of the probe and  $h_o$  the initial thickness of the layer.

In principle, this ratio enables, thanks to linear rheological measurements, to predict whether the crack will propagate at the interface or cavitate inside the bulk. The value of  $\tan \delta/G'$  at which the transition occurs depends on the  $G_o$  of the probe-adhesive interface, and a deformation map is proposed in Figure 39. The exact value of the transition point needs to be determined experimentally as the constant  $k$  in éq. 1.35 is unknown, but it is possible to predict a lower critical value of  $\tan \delta/G'$  on stainless steel than on polyethylene surface from comparison of their  $G_o$ .

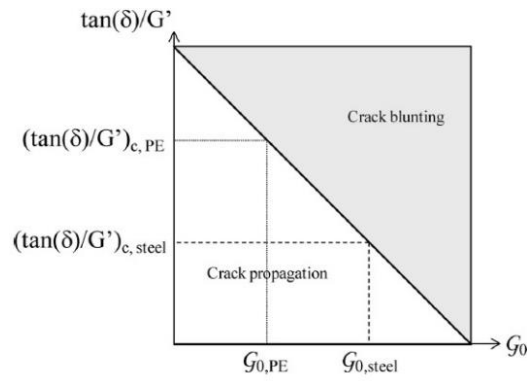


Figure 39 Prediction of a transition from interfacial propagation of a crack to cavitation from  $\tan \delta/G'$  values. Figure from [65]

Yet once a crack grows in the bulk, nonlinear deformation occurs and linear properties are not sufficient to describe the materials behavior.

### 4.3 Non-linear fibrillation

In order to have high tack, not only must the interface be resistant enough, but also the material must be able to dissipate a large amount of energy during debonding. In the case of adhesive, this energy dissipation is often associated with the growth of fibrils in the bulk of the material, which strongly deforms. This process of cavity growth in the bulk is illustrated in Figure 40.

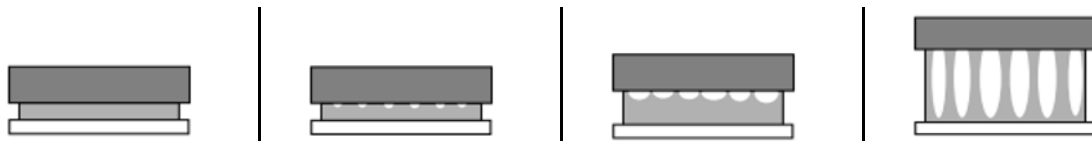


Figure 40 Illustration of the fibrillation process. From left to right: elastic deformation of the bonding layer, apparition of the first cavities at the interface, volume expansion of the cavities.

Fibrillation was first observed in peel tests by Kaelbe [19], and extensively studied on a probe-tack test by Zosel [9]. The fibrils' diameter is estimated between 10 and 100 $\mu\text{m}$ , and the maximum length can reach 500-1000 $\mu\text{m}$ . This process being mainly due to chain disentanglement, the stress needed for the material's extension is lower for polymers with high molecular mass between entanglements  $M_e$ . Furthermore, for high strains, chains can reach their extensibility limit (if they are crosslinked for example) and a strain-hardening is therefore measured.

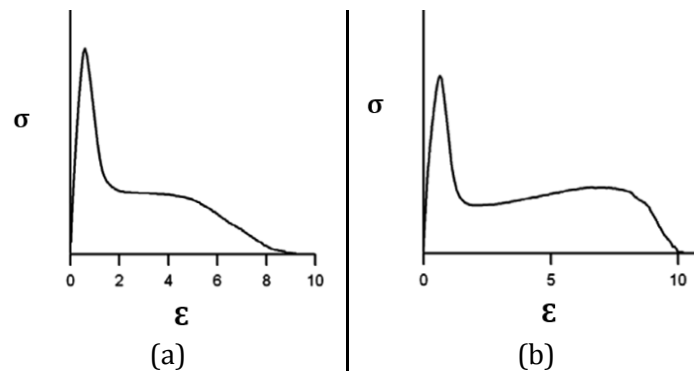


Figure 41 Stress-strain debonding curves for PSA with crack blunting and bulk deformation, without (a) and with (b) strain hardening.

Figure 41 shows that in such a situation, a shouldering is observed at high strains on the stress-strain debonding curve. Uniaxial tensile tests are therefore a good tool to investigate the large strain behavior of the material and to estimate its softening and strain hardening capacity.

Finally, the adhesive eventually debonds and different types of failure are observed.

#### 4.4 End of the story: final detachment

It was previously mentioned that during the whole debonding process, a competition between the interfacial strength (controlled by the critical energy release rate) and the materials (linear and non-linear) bulk properties occurs. If cavities are unable to propagate in the material, interfacial rupture occurs after elastic stretching, and an adhesive failure is observed (see Figure 42 (a)). If energy dissipation through fibrils formation is possible, two failure mechanisms can occur. Either fibrils eventually break and a cohesive debonding is measured (b), in which case residues of the material are present on both the probe and the glass slide, or one of the interfaces is weaker in the sense that it is unable to withstand the imposed stress, and an adhesive failure (c) is observed.

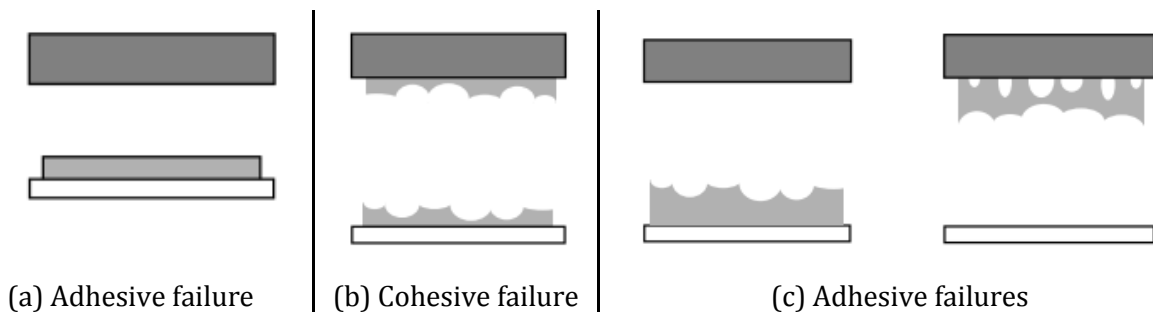


Figure 42 Different types of failure mechanisms

## 5 Effect of molar mass on adhesion

The effect of molar mass on the adhesion between two polymer melts is not straight-forward as it influences both interfacial dynamics and bulk dissipation. It has been thoroughly studied [15][57] and is a good illustration of the tradeoff between tack and green strength.

### 5.1.1 Influence of molar mass on interface dynamics

In fact, according to Voyutskii's theory, the migration of polymer chains at the interface occurs through diffusion of the free ends, and is therefore more likely to happen for short chains. As molecular mass increases, the relative proportion of end segments decreases, and for steric reasons such materials are less likely to develop tack properties. In fact, Skewis [68] measured the self-diffusion coefficient  $D$  of rubbery polymers and shows that it decreased with increasing molar mass  $M$ . It is shown that  $D$  scales as [31]:

$$D \propto \frac{1}{M^2} \quad 1.36$$

Moreover, it was mentioned in the previous part (1.3.3), that the time needed for a chain to diffuse out of its original constraining tube increases such that in theory  $\tau_{REP} \propto M^3$ . Experimentally, this time scales as  $M^{3.4}$ .

Thus, for a given contact time lower than the time needed to fully heal the interface, the adhesion strength decreases with increasing molecular weight  $M$ . In fact, Figure 43 shows the peel strength of butadiene-acrylonitrile copolymers (NBR) to polyamide (which composition is not detailed)

decreases with increasing NBR molecular weight. The authors did not fit any model to this experiment. Wool [31] suggested that, for a given contact time, the fracture energy  $G$  (from peeling experiments) evolves with the inverse of the square root of the molecular weight  $G \propto M^{-\frac{1}{2}}$ .

### 5.1.2 Influence of molar mass on the green strength

Nevertheless, high molar mass materials show great mechanical properties, and if sufficient contact time is reached (or if diffusion is enhanced through high temperature bonding or other strategies [56]) such that migration of the long macromolecules are possible, their elevated green strength boosts the joint's resistance through high energy dissipation. In fact, the fracture energy of the green strength  $G_{\infty}$ , corresponding to the pullout of chains from uncrosslinked rubbers, scales as  $G_{\infty} \propto M^{\frac{1}{2}}$ .

### 5.1.3 Trade-off between tack and green strength

This balance between tack (before thermodynamic equilibrium) and green strength (interface at thermodynamic equilibrium) for high molecular weight materials is illustrated in Figure 44 [15]. When increasing molecular weight, macromolecules do not have time to diffuse through the interface at short contact times and the tack properties are thus decreased. Yet at the same time, increase in the molecular weight leads to strengthened bulk mechanical properties and thus high green strength.

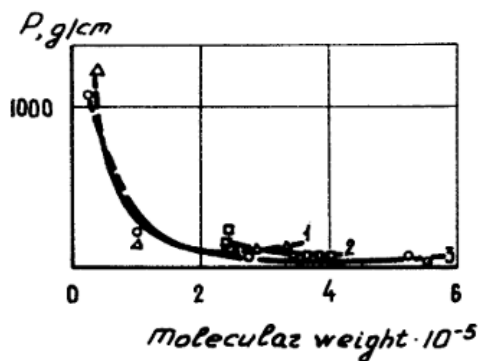


Figure 43 Peeling strength of bonded samples of PA with NBR as a function NBR molecular weight. Figure from [16]

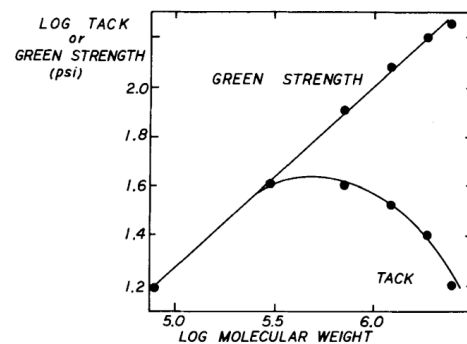


Figure 44 Tack and green strength of natural rubber as a function of molecular weight. Figure from [15]

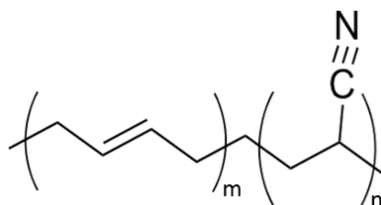
These studies have been launched on monodisperse polymers of various molecular mass. Yet for a material with a broad distribution of molecular weight, all the chains will not diffuse at the same speed. Composto and coworkers [38] studied the diffusion coefficients of deuterated, pure polystyrene and poly(xylenyl ether) (PXE), of various molecular weight, on a layer of the blend. They showed that the mutual diffusion of a polymer blend is controlled by the diffusion of its faster moving species, consistent with the “fast theory”.

## 6 Nitrile Butadiene Rubber (NBR)

### 6.1 Introduction to poly(acrylonitrile-co-butadiene)

#### 6.1.1 Presentation

Nitrile Butadiene Rubbers (NBR) are copolymers of butadiene (PB) and acrylonitrile (ACN) also referred to as poly(acrylonitrile-co-butadiene).



#### Nitrile Butadiene Rubber

They are widely used in oil seals, automotive hose and other applications, and their properties highly depend on the acrylonitrile content [69][70]. A high acrylonitrile to butadiene monomer ratio increases polarity and therefore leads to a better resistance to aromatic and aliphatic non polar hydrocarbons [71]. Nevertheless, such an increase significantly reduces the NBRs low temperature flexibility.

Butadiene monomer copolymerizes into three different structures [72]: 1,4-trans (~78% in a typical nitrile), 1,4-cis (~12%) and 1,2 (~10%), as illustrated in Figure 45. The acrylonitrile groups are inserted in a statistical pattern: head-tail, head-head and tail-tail.

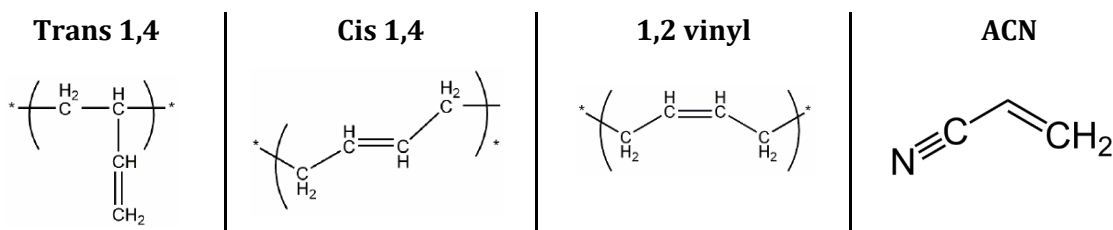


Figure 45 Different monomers involve in the polymerization of nitrile rubber

The glass transition temperature of polybutadiene highly depends on the concentration of each structure [73], from around  $-110^{\circ}\text{C}$  when the polymer is composed mainly of cis1,4 units and increased to close to  $0^{\circ}\text{C}$  when the chain is almost completely in the form of 1,2-vinyl.

#### 6.1.2 Manufacturing

Nitrile rubbers are synthesized by radical emulsion polymerization [74][75].

##### i. Radical emulsion polymerization

In the emulsion polymerization process (illustrated in Figure 46), monomers (water-insoluble) are dispersed as fine droplets into a water-based continuous media. These 100um-size droplets are emulsified thanks to surfactants. Polymerization takes place in this latex particles thanks to the presence of initiators, and each micelle acts as a micro-reactor. Radical polymerization consists in the successive addition of free-radical to monomer building blocks, thus growing the polymer chain. Emulsion polymerization offers the possibility to make high molecular weight polymers at fast polymerization rates (due to excellent heat conduction of the continuous water phase), with a viscosity of the reaction medium close to that of water and are therefore commonly used to manufacture commercial polymers.

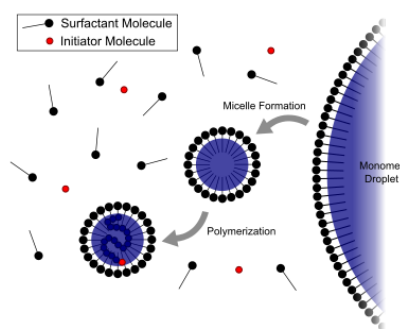
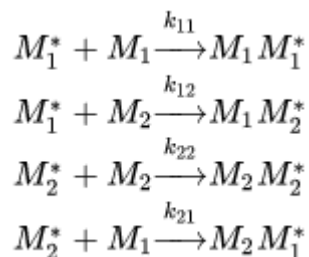


Figure 46 Illustration of emulsion polymerization

The use of this emulsion polymerization process for the synthesis of block copolymers is frequent, yet it is important to consider each monomers distribution between the aqueous continuous phase and the organic reactors. In fact, acrylonitrile is one of the monomers with a substantial solubility in aqueous media.

### ii. Reactivity ratio

During the synthesis of copolymers, two monomers  $M_1$  and  $M_2$  can each react with the two reactive chain end  $M_1^*$  and  $M_2^*$ , each with a given reaction rate constant  $k$ , as illustrated below:



The reactivity ratio  $r$  for each propagating chain is defined as the ratio between the rate constant  $k$  for the addition of a monomer to the reactive chain with the same end monomer (for example for the addition of  $M_1$  to  $M_1^*$ ), and the rate constant  $k$  of the addition of the other monomer ( $M_2$ ) to the same reactive chain ( $M_1^*$ ):

$$\begin{aligned}
 r_1 &= k_{11}/k_{12} \\
 r_2 &= k_{22}/k_{21}
 \end{aligned}
 \tag{1.37}$$

In the literature, several authors [76][77][75] have reported reactivity ratios for acrylonitrile and butadiene, referred to as  $r_{AN}$  and  $r_{BU}$ . Ambler [76] used  $r_{AN}=0.02$  and  $r_{BU}=0.39$  from Mayo's study [78] whereas Ono and coworkers [79] have considered  $r_{AN}=0.03$  and  $r_{BU}=0.2$ . Although the exact values slightly differ, they all show that the reactivity ratios are lower than unity, meaning that formation of alternating sequences is favored. Moreover, the reactivity ratio of acrylonitrile is extremely low suggesting that the acrylonitrile units react almost entirely with butadiene radicals.

### iii. Comments

Due to both monomers different solubility in reactions media, and their different reactivity ratio, it is likely that the industrial synthesis of poly(acrylonitrile-co-butadiene) leads to a wide range of polymer chain compositions. Furthermore, several authors [76][80][81] showed the existence of multiple glass transitions in acrylonitrile-butadiene rubbers at low ACN content, and these two

temperature move further apart as the acrylonitrile content decreases. The second (lower) glass transition temperature is assumed to be due to the formation of a phase richer in butadiene.

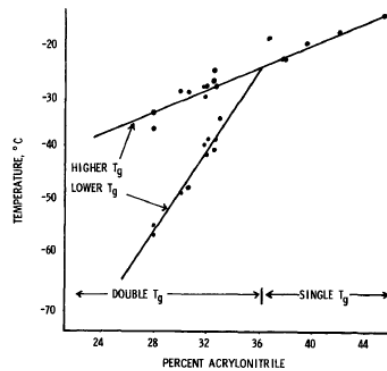


Figure 47 Glass transition temperature of NBR as a function of acrylonitrile content (%). Figure from [76]

## 6.2 Adhesion and self-adhesion properties of NBR

### 6.2.1 Adhesion of NBR to other materials

Voyutskii [16] et al studied the influence of the acrylonitrile content on the adhesion between 1. NBR and polyamide (polar polymer), and 2. NBR and polyisobutylene (nonpolar polymer). As illustrated on Figure 48, they showed that when increasing the acrylonitrile content in the copolymer, the high temperature adhesion properties on polyamide first increase and then drastically drop. The first trend is assumed to be due to more polar interactions, strengthening the bond between the two surfaces. Authors suggest that the decrease that follows is due to the poor diffusion of the chains at high polar content as a consequence of a loss of the macromolecules mobility with the presence of intermolecular forces.

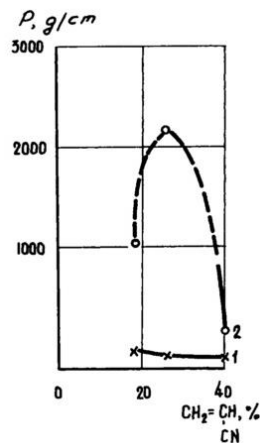


Figure 48 Peeling strength  $P$  of NBR on polyamide, as a function of acrylonitrile content for 1. Non-heated samples and 2. Bonded samples heated à  $150^{\circ}\text{C}$  for 30min. Figure from [16]

This lack of mobility explains the very poor adhesion probed at room temperature (see curve 1 in Figure 48). The adhesion of NBR to nonpolar polymer was also studied in the same article and shown to be very low and independent of the amount of polar groups. This is explained by the non-compatibility of the two materials, which is consistent with the influence of the Flory parameter on the penetration depth mentioned previously.

### 6.2.2 Self-adhesion of NBR

Bothe and Rehage [30] studied the self-adhesion properties of lightly crosslinked NBR (0.5 phr of peroxide) and suggested similar conclusions: the higher the acrylonitrile content the higher the adhesion, but the longer the time needed to reach it, from 6 to more than 10 hours (see Figure 50). In any case, when contacting the two surfaces for sufficient time, the self-adhesion reaches the cohesive strength of the material.

To the best of our knowledge, few authors have studied the self-adhesion properties of unvulcanized NBR. Forbes and coworkers [82] have the tack strength of several industrial polymers, among which nitrile rubber. Their tack measurements were performed after milling of the polymers, and for 30 seconds of contact. They demonstrated that the tack strength depended on the polymerization conditions, but that in all studied cases, long contact times, from 5 minutes to 12 hours, were needed to reach complete healing. Ansarifar et al [21] also investigated the self-adhesion properties of uncrosslinked NBR as a function of time. The materials were masticated before contact. Nitrile rubber's cohesive strength was reached after tens of contacting hours, and the energy associated was of around a hundred of  $\text{kJ/m}^2$ . The relatively long time need for NBR to approach its cohesive strength is explained by its rather high glass transition temperature ( $-23^\circ\text{C}$ ).

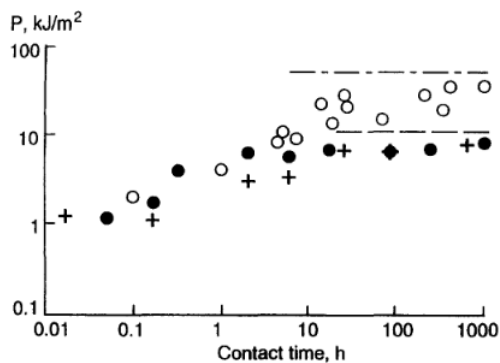


Figure 49 Variation of self- and mutual adhesion for NBR and ENR with contact time. Self-adhesion NBR ( $\circ$ ), ENR ( $\bullet$ ) and mutual adhesion (+). Figure from [21]

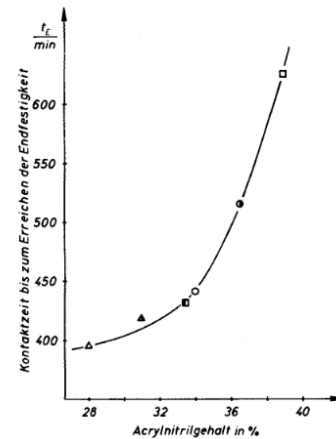


Figure 50 Time necessary to reach maximum adhesion as a function of acrylonitrile content. Figure from [30]

## **7 Conclusion**

During this chapter, a presentation of the mechanical properties of elastomers- from the entropic origin of their elasticity to the dynamics of their melts- was developed. The mechanisms by which interface strength was monitored were exposed, and the diffusion of polymer chains was correlated to their dynamics in linear rheological properties. It was shown that a strong interface had to be coupled with important energy dissipation upon debonding in order to reach high adhesion strength. Few strategies, such as surface treatment or adhesion promoters, enables a modification of one (better surface of contact) without imparting the other (bulk dissipation), yet most of the efforts made to enhance adhesion affect both. In fact, the addition of small molecules called “tackifiers” is very common in the rubber industry yet its influence on surface and bulk are hardly dissociable. A more extensive research on their effect is proposed at the beginning of Chapter 5. The present chapter also revealed that the polarity of nitrile butadiene rubber slows its chain migration and therefore affect their adhesion properties, which will be of particular interest in Chapter 4.

This state-of-the-art gives the main tool to understand the different scientific challenges encountered during this work. The material of focus is a very high molar mass, industrial polar rubber; and it is studied in its unvulcanized state.

During this manuscript, adequate literature is introduced at the beginning of each chapter.

## 8 References

- [1] Y. De Zélicourt, "Caoutchoucs : méthodes d'obtention et propriétés," *Tech. l'ingénieur*, vol. 33, no. 0, 2015.
- [2] J. Kruželák, R. Sýkora, and I. Hudec, "Sulphur and peroxide vulcanisation of rubber compounds-overview," *Chem. Pap.*, vol. 70, no. 12, pp. 1533–1555, 2016.
- [3] P. R. Dlužneski, "Peroxide Vulcanization of Elastomers," *Rubber Chem. Technol.*, vol. 74, no. 3, pp. 451–492, 2001.
- [4] M. Rubinstein and R. H. Colby, "Polymer Physics," 2003, p. 1.
- [5] P. G. De Gennes, "Reptation of a polymer chain in the presence of fixed obstacles," *J. Chem. Phys.*, vol. 55, no. 2, pp. 572–579, 1971.
- [6] M. Doi and S. F. Edwards, "Dynamics of concentrated polymer systems," *J. Chem. Soc., Faraday Trans. 2*, vol. 74, pp. 1802–1817, 1978.
- [7] R. H. Colby, L. J. Fetters, and W. W. Graessley, "Melt Viscosity-Molecular Weight Relationship for Linear Polymers," *Macromolecules*, vol. 20, no. 9, pp. 2226–2237, 1987.
- [8] D. C., "Adhesion Fundamentals and Practice." pp. 143–151, 1969.
- [9] A. Zosel, "The effect of fibrillation on the tack of pressure sensitive adhesives," *Int. J. Adhes. Adhes.*, vol. 18, no. 4, pp. 265–271, 1998.
- [10] H. Lakrout and P. Sergot, "Direct Observation of Cavitation and Fibrillation in a Probe Tack Experiment on Model Acrylic Pressure- Sensitive-Adhesives," no. 1999, pp. 37–41.
- [11] C. Creton and M. Ciccotti, "Fracture and adhesion of soft materials: a review," *Reports Prog. Phys.*, vol. 79, no. 4, p. 046601, 2016.
- [12] G. R. Hamed, "Autohesion and cohesion of uncrosslinked elastomers." 1988.
- [13] G. R. Hamed and C.-H. Shieh, "Relationship between the cohesive strength and the tack of elastomers." 1985.
- [14] G. R. Hamed and C.-H. Shieh, "Flow criterion for elastomer tack." 1982.
- [15] G. R. Hamed, "Tack and Green Strength of Elastomeric Materials," *Rubber Chem. Technol.*, vol. 54, no. 3, pp. 576–595, 1981.
- [16] S. S. Voyutskii and V. L. Vakula, "The Role of Diffusion Phenomena in Polymer-to-Polymer Adhesion," vol. 7, pp. 475–491, 1963.
- [17] G. R. Hamed and C.-H. Shieh, "Relationship between the cohesive strength and the tack of elastomers," *J. Polym. Sci. Polym. Phys. Ed.*, vol. 21, no. 8, pp. 1415–1425, 1983.
- [18] R. H. Plaut, N. L. Williams, and D. A. Dillard, "Elastic analysis of the loop tack test for pressure sensitive adhesives," *J. Adhes.*, vol. 76, no. 1, pp. 37–53, 2001.
- [19] D. H. Kaelble, "Peel Adhesion: Micro-Fracture Mechanics of Interfacial Unbonding of Polymers," *Trans. Soc. Rheol.*, vol. 9, no. 2, pp. 135–163, 1965.
- [20] D. W. Aubrey and M. Sherriff, "Peel adhesion and viscoelasticity of rubber-resin blends," *J. Polym. Sci. Polym. Chem. Ed.*, vol. 18, no. 8, pp. 2597–608, 1980.
- [21] M. A. Ansarifard, K. N. G. Fuller, and G. J. Lake, "Adhesion of unvulcanized elastomers," *Int. J. Adhes. Adhes.*, vol. 13, no. 2, pp. 105–110, 1993.
- [22] R.-J. Chang and A. N. Gent, "Effect of Interfacial Bonding on the Strength of Adhesion of

- Elastomers," vol. 19, pp. 1619–1633, 1981.
- [23] B. V. Derjaguin and V. P. Smilga, "Electronic theory of adhesion," *J. Appl. Phys.*, vol. 38, no. 12, pp. 4609–4616, 1967.
- [24] S. S. Voyutskii and V. L. Vakula, "Self-Diffusion and Inter-Diffusion in Polymer Systems," *Rubber Chem. Technol.*, vol. 37, no. 5, pp. 1153–1177, 1964.
- [25] J. N. Anand, H. J. Kabam, T. Dow, and C. Company, "Interfacial Contact and Bonding in Autohesion I- Contact Theory," no. December 2014, pp. 37–41.
- [26] A. Zosel, "The effect of bond formation on the tack of polymers," *Int. J. Adhes. Adhes.*, vol. 18, no. December 1997, pp. 265–271, 1998.
- [27] B. N. J. Persson, O. Albohr, U. Tartaglino, a I. Volokitin, and E. Tosatti, "On the nature of surface roughness with application to contact mechanics, sealing, rubber friction and adhesion.," *J. Phys. Condens. Matter*, vol. 17, no. 1, pp. R1–R62, 2005.
- [28] A. Chiche, J. Dollhofer, and C. Creton, "Cavity growth in soft adhesives," *Eur. Phys. J. E*, vol. 17, no. 4, pp. 389–401, 2005.
- [29] R. K. Beckwith, L. M. Welch, J. F. Nelson, A. L. Chaney, and E. A. McCracken, "Tack of Butyl and Natural Rubbers," *Rubber Chem. Technol.*, vol. 23, no. 4, pp. 933–944, Dec. 1950.
- [30] L. Bothe and G. Rehage, "Autohesion of Elastomers," *Rubber Chem. Technol.*, vol. 55, no. 5, pp. 1308–1327, Nov. 1982.
- [31] R. P. Wool, B. -L Yuan, and O. J. McGarel, "Welding of polymer interfaces," *Polym. Eng. Sci.*, vol. 29, no. 19, pp. 1340–1367, 1989.
- [32] C. Creton and L. Leibler, "How does tack depend on time of contact and contact pressure?," *J. Polym. Sci. Part B Polym. Phys.*, vol. 34, no. 3, pp. 545–554, 1996.
- [33] W. Smitthipong, M. Nardin, J. Schultz, and K. Suchiva, "Adhesion and self-adhesion of immiscible rubber blends," *Int. J. Adhes. Adhes.*, vol. 29, no. 3, pp. 253–258, 2009.
- [34] C. S. Davis, F. Lemoine, T. Darnige, D. Martina, C. Creton, and A. Lindner, "Debonding mechanisms of soft materials at short contact times," *Langmuir*, vol. 30, no. 35, pp. 10626–10636, 2014.
- [35] A. Zosel, "Adhesion and tack of polymers: Influence of mechanical properties and surface tensions," *Colloid Polym. Sci.*, vol. 263, no. 7, pp. 541–553, 1985.
- [36] M. Stamm and D. W. Schubert, "Interfaces Between Incompatible Polymers," *Annu. Rev. Mater. Sci.*, vol. 25, no. 1, pp. 325–356, Aug. 1995.
- [37] T. P. Russell, "The Characterization of Polymer Interfaces," *Annu. Rev. Mater. Sci.*, vol. 21, no. 1, pp. 249–268, Aug. 1991.
- [38] R. J. Composto, E. J. Kramer, and D. M. White, "Fast macromolecules control mutual diffusion in polymer blends," *Nature*, vol. 328, no. 6127, pp. 234–236, Jul. 1987.
- [39] P. F. Green, P. J. Mills, and E. J. Kramer, "Diffusion studies in polymer melts by ion beam depth profiling of hydrogen," *Polymer (Guildf)*, vol. 27, no. 7, pp. 1063–1066, 1986.
- [40] P. F. Green, C. J. Palmstrom, J. W. Mayer, and E. J. Kramer, "Marker Displacement Measurements of Polymer-Polymer Interdiffusion," *Macromolecules*, vol. 18, no. 3, pp. 501–507, 1985.
- [41] S. J. Whitlow and R. P. Wool, "Investigation of Diffusion in Polystyrene Using Secondary Ion Mass Spectroscopy," *Macromolecules*, vol. 22, no. 6, pp. 2648–2652, 1989.

- [42] T. P. Russell *et al.*, "Direct observation of reptation at polymer interfaces," *Nature*, vol. 365, no. 6443, pp. 235–237, 1993.
- [43] a. Karim, G. P. Felcher, and T. P. Russell, "Interdiffusion of Polymers at Short Times," *Macromolecules*, vol. 27, no. 23, pp. 6973–6979, 1994.
- [44] C. M. Roland and G. G. A. Bohm, "Macromolecular Diffusion and the Autoadhesion of Polybutadiene," *Macromolecules*, vol. 18, no. 6, pp. 1310–1314, 1985.
- [45] R. Schach, Y. Tran, A. Menelle, and C. Creton, "Role of chain interpenetration in the adhesion between immiscible polymer melts," *Macromolecules*, vol. 40, no. 17, pp. 6325–6332, 2007.
- [46] D. Broseta, G. H. Fredrickson, E. Helfand, and L. Leibler, "Molecular Weight and Polydispersity Effects at Polymer-Polymer Interfaces," *Macromolecules*, vol. 23, no. 1, pp. 132–139, 1990.
- [47] E. Helfand and Y. Tagami, "Theory of the interface between immiscible polymers. II," *J. Chem. Phys.*, vol. 56, no. 7, pp. 3592–3601, 1972.
- [48] R. Schnell, M. Stamm, and C. Creton, "Direct correlation between interfacial width and adhesion in glassy polymers," *Macromolecules*, vol. 31, no. 7, pp. 2284–2292, 1998.
- [49] A. Karim, A. Mansour, G. P. Felcher, and T. P. Russell, "Short-time relaxation at polymeric interfaces," *Phys. Rev. B*, vol. 42, no. 10, pp. 6846–6849, Oct. 1990.
- [50] R. G. Stacer and H. L. Schreuder-Stacer, "Time-dependent autohesion," *Int. J. Fract.*, vol. 39, no. 1–3, pp. 201–216, 1989.
- [51] R. Gurney, A. Henry, R. Schach, A. Lindner, and C. Creton, "Molecular Weight Dependence of Interdiffusion and Adhesion of Polymers at Short Contact Times," *Langmuir*, p. acs.langmuir.6b03972, 2017.
- [52] A. Sarkar, M. L. Mukherjee, and A. K. Bhowmick, "Tack and diffusion of silicone and EPDM rubbers," *J. Mater. Sci. Lett.*, vol. 11, no. 13, pp. 924–927, 1992.
- [53] C. Creton and R. Schach, "Adhesion at interfaces between highly entangled polymer melts," *J. Rheol. (N. Y. N. Y.)*, vol. 52, no. 3, pp. 749–767, 2008.
- [54] W. Thiedman, F. C. Tolan, P. J. Pearce, and M. Morris, "Silane Coupling Agents as Adhesion Promoters for Aerospace Structural Film Adhesives," *J. Adhes.*, vol. 22, no. 3, pp. 197–210, 1987.
- [55] W. J. van Ooij and M. E. F. Biemond, "Novel Class of Rubber To Steel Tire Cord Adhesion Promoters," *Rubber Chemistry and Technology*, vol. 57, no. 4, pp. 686–702, 1984.
- [56] G. L. Jialanella, *Advances in bonding plastics*, no. 3. Woodhead Publishing Limited, 2010.
- [57] V. L. Vakula, H. Yun-tsui, V. E. Gul, and S. S. Voyutskii, "Adhesion of High Polymers. VI. The Effect of Molecular Weight of NBR Copolymers of Various Polarities on Adhesion to Polar and Nonpolar Materials," *Rubber Chemistry and Technology*, vol. 34, no. 2, pp. 562–570, 1961.
- [58] L. Léger and C. Creton, "Adhesion mechanisms at soft polymer interfaces.," *Philos. Trans. A. Math. Phys. Eng. Sci.*, vol. 366, no. 1869, pp. 1425–1442, 2008.
- [59] R. P. Sijbesma *et al.*, "Reversible polymers formed from self-complementary monomers using quadruple hydrogen bonding," *Science (80-. )*, vol. 278, no. 5343, pp. 1601–1604, 1997.
- [60] L. Carlsson, S. Rose, D. Hourdet, and A. Marcellan, "Nano-hybrid self-crosslinked PDMA/silica hydrogels," *Soft Matter*, vol. 6, no. 15, pp. 3619–3631, 2010.

- [61] W. C. Lin, W. Fan, A. Marcellan, D. Hourdet, and C. Creton, "Large strain and fracture properties of poly(dimethylacrylamide)/silica hybrid hydrogels," *Macromolecules*, vol. 43, no. 5, pp. 2554–2563, 2010.
- [62] J. P. Gong, Y. Katsuyama, T. Kurokawa, and Y. Osada, "Double-network hydrogels with extremely high mechanical strength," *Adv. Mater.*, vol. 15, no. 14, pp. 1155–1158, 2003.
- [63] J. P. Gong, "Why are double network hydrogels so tough?," *Soft Matter*, vol. 6, no. 12, pp. 2583–2590, 2010.
- [64] Y. Tanaka, R. Kuwabara, Y. H. Na, T. Kurokawa, J. P. Gong, and Y. Osada, "Determination of fracture energy of high strength double network hydrogels," *J. Phys. Chem. B*, vol. 109, no. 23, pp. 11559–11562, 2005.
- [65] F. Deplace, C. Carelli, S. Mariot, and H. Retsos, "Fine Tuning the Adhesive Properties of a Soft Nanostructured Adhesive with Rheological Measurements," pp. 18–54, 2009.
- [66] R. E. Webber, K. R. Shull, A. Roos, and C. Creton, "Effects of geometric confinement on the adhesive debonding of soft elastic solids," *Phys. Rev. E*, vol. 68, p. 021805, 2003.
- [67] M. Barquins and D. Maugis, "Tackiness of Elastomers." 1981.
- [68] J. D. Skewis, "Self-diffusion coefficients and tack of some rubbery polymers." 1966.
- [69] M. Böhm, W. v. Soden, W. Heinrich, and A. A. Yehia, "Influence of crosslinking on mechanical and dielectric properties of nitrile-butadiene-rubber," *Colloid Polym. Sci.*, vol. 265, no. 4, pp. 295–303, 1987.
- [70] G. M. Bartenev, S. V. Baglyuk, and V. V. Tulinova, "Relaxational transitions of poly(butadiene-acrylonitrile) above the glass transition temperature," *Polym. Sci. U.S.S.R.*, vol. 30, no. 4, pp. 834–843, 1988.
- [71] J. L. Graham, R. C. Striebich, K. J. Myers, D. K. Minus, and W. E. Harrison, "Swelling of nitrile rubber by selected aromatics blended in a synthetic jet fuel," *Energy and Fuels*, vol. 20, no. 2, pp. 759–765, 2006.
- [72] D. L. Hertz, H. Bussem, and T. W. Ray, "Nitrile rubber- past, present and future," *Rubber Chem. Technol.*, p. 116, 1995.
- [73] N. Makhiyanov and E. V. Temnikova, "Glass-transition temperature and microstructure of polybutadienes," *Polym. Sci. - Ser. A*, vol. 52, no. 12, pp. 1292–1300, 2010.
- [74] W. H. Embree, J. M. Mitchell, and H. L. Williams, "Compositional Heterogeneity of Butadiene-Acrylonitrile Copolymers Prepared in Emulsion At 5°C," *Can. J. Chem.*, vol. 29, no. 3, pp. 253–269, 2006.
- [75] G. A., G. J., G. C., and L. M.F., "Controlled Composition in Emulsion Copolymerization Application to Butadiene- Acrylonitrile Copolymers," no. December 2014, pp. 37–41.
- [76] M. R. Ambler, "Studies on the nature of of Multiple Glass Transitions in low acrylonitrile, butadiene-acrylonitrile rubbers," vol. 11, pp. 1505–1515, 1973.
- [77] A. R. Katritzky and D. E. Weiss, "Carbon-13 nuclear magnetic resonance spectroscopy of polymers. Part II. Determination of monomer sequence distribution in butadiene-acrylonitrile copolymer," *J. Chem. Soc. Perkin Trans. 2*, no. 13, pp. 1542–1547, 1974.
- [78] F. R. Mayo and C. Walling, "Copolymerization," no. 100, 1949.
- [79] H. Ono, H. Fujiwara, and S. Nishimura, "Nanoscale heterogeneous structure of polyacrylonitrile-co-butadiene with different molecular mobilities analyzed by spin-spin relaxation time," *Polym. J.*, vol. 45, no. 10, pp. 1027–1032, 2013.

- [80] L. A. Chandler and E. A. Collins, "Multiple Glass Transitions in Butadiene-Acrylonitrile Copolymers," *J. Appl. Polym. Sci.*, vol. 13, pp. 1585–1593, 1969.
- [81] A. H. Jorgensen, L. A. Chandler, and E. A. Collins, "Multiple glass transitions in butadiene-acrylonitrile copolymers. II. Formation of incompatible phases during copolymerization." 1973.
- [82] W. G. Forbes and L. A. McLeod, "Dependence of tack strength on molecular properties." 1959.



## **- CHAPTER 2 -**

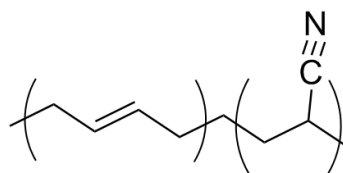
### **CHARACTERIZATION OF NITRILE RUBBER**

---

In order to properly study and understand the rubber's adhesion – and self-adhesion - performance, it is necessary to first extensively characterize it. The molecular weight and the acrylonitrile content are first determined, and the mechanical properties (both in the linear and non-linear regimes) are then analyzed. The method used to characterize the material's self-adhesion properties is then detailed and the first results are explained with regard to the mechanical properties.

<b>1. Material characterizations .....</b>	<b>49</b>
1.1 Average molecular weight .....	49
1.2 Acrylonitrile content .....	50
1.2.1 Dynamic Scanning Calorimetry .....	50
1.2.2 Thermogravimetric analysis .....	50
1.2.3 Comparison with literature .....	51
<b>2. Characterization of NBR mechanical properties .....</b>	<b>52</b>
2.1 Linear rheology.....	52
2.1.1 Instrumentation .....	52
2.1.2 Linear regime .....	52
2.1.3 Time-temperature superposition .....	53
2.1.4 Result .....	55
2.2 Uniaxial tensile tests.....	56
2.2.1 Instrument and test conditions .....	56
2.2.2 Results .....	56
<b>3. Characterization of self-adhesion properties.....</b>	<b>57</b>
3.1 Choice of the characterization method.....	57
3.2 Probe-tack tests.....	58
3.2.1 Instrumentation .....	58
3.2.2 Debonding behaviors .....	59
3.2.3 Understanding debonding curves .....	60
3.3 Samples preparation .....	61
3.3.1 Glass slides' preparation: .....	61
3.3.2 Rubber disks' preparation: .....	62
3.4 Self-adhesion properties.....	62
3.4.1 Classical Probe-tack method .....	62
3.4.2 New method for tack testing .....	63
<b>4. Conclusion and discussion .....</b>	<b>65</b>
4.1 Discussion .....	65
4.1.1 Comparison with SBR.....	65
4.1.2 Comparison with literature .....	66
4.1.3 Link between linear rheology and self-adhesion .....	67
4.2 Conclusions .....	68
<b>5. References.....</b>	<b>69</b>

In order to define a clear working frame, we decided to focus on only one grade of nitrile-butadiene rubber, free of any additives. The NBR studied is directly provided by the supplier and no particular information is given.



**Nitrile Butadiene Rubber**

This industrial material will be compared with NBR purchased from Sigma-Aldrich (referred to as “**NBR-SA**”) in order to make sure that the observations are not specific to the “industrial” rubber. Both materials were first characterized by means of chromatography and thermal analytical techniques, and then tested mechanically with the use of uniaxial tensile tests and rheology. The adhesion, and more specifically self-adhesion, properties of NBR were probed using a Probe-Tack device.

As the industrial processing of rubbers involves a calendaring step, the received rubber was extruded at 120°C during 5 minutes to be as consistent as possible with the desired application process. The extruding instrumentation is presented in depth in Chapter 4, section 2.2.

## **1. Material characterizations**

### **1.1 Average molecular weight**

Size exclusion chromatography (SEC) is a chromatographic method in which molecules in solution are separated by their size or molecular weight. It consists in passing the polymer in solution in a column (“stationary phase”) with different-sizes’ holes. The smaller molecules are trapped in these pores whereas the bigger ones cross the column at once, i.e. the larger the particles, the faster the elution, the shorter the retention time.

The SEC experiments were performed by the Institut Charles Sadron (Strasbourg, France). The device was calibrated with polystyrene, using nine Polymer Lab standards with molar masses between 2400 and 370 000g/mol. The materials were solubilized during 48h in toluene at concentrations around 4mg/mL and filtrated on a PP filter (Dynagard) of 0.2microns before injecting it into the column. During the analysis, approximately 20wt% of the material could not be analyzed because the chains were too large (>400kDa) to go through the column. Therefore, the molar mass (as well as the polydispersity index) considered are under-estimated.

The raw material (the 80wt% that could be analyzed), has a weight average molar mass  $M_w = 126\,850$  g/mol and a polydispersity index of 1.98.

The NBR supplied by Sigma Aldrich was not soluble in any suitable solvent for SEC and was therefore not analyzed.

## 1.2 Acrylonitrile content

DSC and TGA were used to determine the acrylonitrile content of both nitrile rubbers.

### 1.2.1. Dynamic Scanning Calorimetry

#### i Method

Dynamic Scanning Calorimetry (DSC) is a thermo-analytical technique in which we measure the additional heat flow necessary to raise (or decrease) the temperature of a sample to maintain the same temperature as that of a reference cell. The principle is illustrated in Figure 1.

During this thesis, DSC measurements were performed on a TA Instruments Q200 device. The reference pan was empty. The samples weigh approximately ten milligrams. The materials were first heated from  $-60^{\circ}\text{C}$  to  $100^{\circ}\text{C}$ , then cooled down to  $-60^{\circ}\text{C}$ , and a last heating cycle to  $100^{\circ}\text{C}$  was then performed. All cycles were performed at a speed of  $20^{\circ}\text{C}/\text{minute}$ .

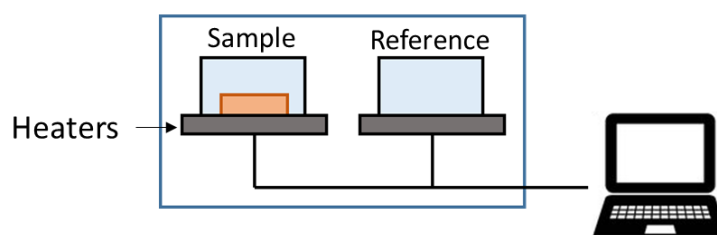


Figure 1 Illustration of Dynamic Scanning Calorimetry (DSC)

#### ii DSC results

Curves are shown in Figure 2 (left). The glass transition temperature of NBR is  $-31^{\circ}\text{C}$ , and that purchased from Sigma-Aldrich is  $-13.7^{\circ}\text{C}$ .

### 1.2.2. Thermogravimetric analysis

#### i Method

Thermogravimetric analysis (TGA) is an analysis method which consists in measuring the mass of a sample over time as temperature changes. It provides information of both physical phenomena (absorption, adsorption,...) and chemical ones (thermal decomposition, oxidations...). The phenomenon are probed using a precision balance, a furnace with a programmable control temperature, and under a variety of atmospheres (among which ambient air, vacuum, inert gas...). During this work, TGA measurements were performed on a TA Instruments SDT Q600 device, under nitrogen flow. The samples were studied between  $20$  and  $650^{\circ}\text{C}$ , at a heating rate of  $20^{\circ}\text{C}/\text{min}$ .

#### i TGA results

TGA was used as a tool to quantify the amount of acrylonitrile (ACN) inside both materials. Results are shown on Figure 2 (right). A huge mass loss ( $> 90\text{wt } \%$ ) is measured between  $350$  and  $500^{\circ}\text{C}$  and is ascribed to the degradation of the elastomer. The high-temperature residues are related to the nitrogen content and are detailed in the next paragraph.

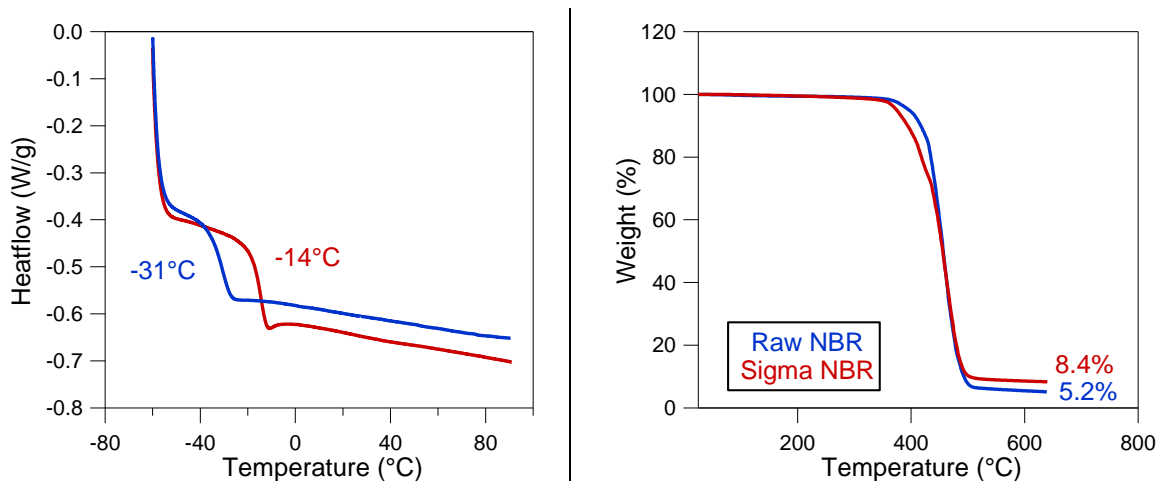


Figure 2 DSC (left) and TGA (right) curves of raw NBR (blue) and NBR-SA (red)

### 1.2.3. Comparison with literature

Sircar [1] performed a thermal analysis of NBR vulcanizates and showed that the Tg and the carbon residues at high temperature is a function of the nitrile content. Authors data enables rough estimation of the amount of acrylonitrile inside each material thanks to DSC and TGA measurements.

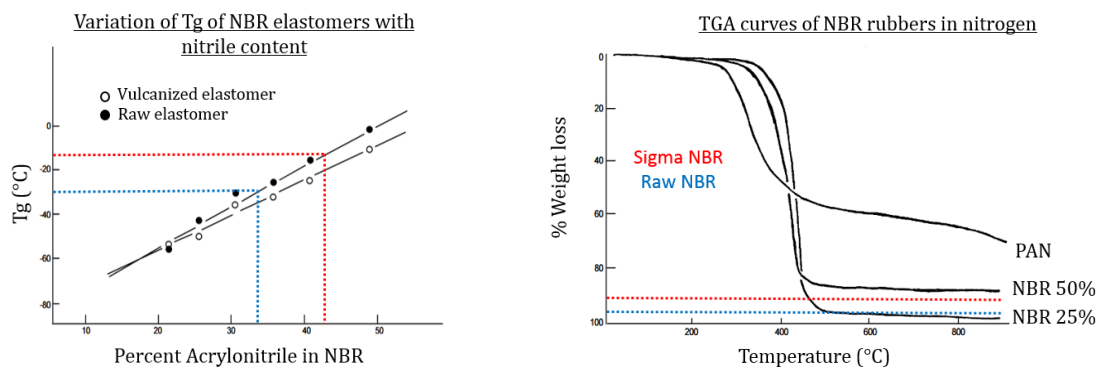


Figure 3 Comparison between our NBR and that of Sircar [1]: DSC (left) and TGA (right)

As illustrated on Figure 3 using Sircar's curves, the acrylonitrile content in raw NBR is roughly of 34% whereas that of NBR-SA is of approximately 43%. Using NMR analysis (see Annex 1.1 for NBR-SA and Chapter 3 section 2.5.2 for NBR) the acrylonitrile content of the materials were determined: NBR-SA has 44% ACN units and the industrial NBR 30wt%. Results from DSC, ATG and NMR are averaged and summarized in Table 1.

Material	Acrylonitrile content	Tg (°C)
Raw NBR	32 +/- 2%	-31
NBR-SA	43 +/- 1%	-14

Table 1 Properties of both studied NBR determined from DSC, ATG and NMR measurements

## 2. Characterization of NBR mechanical properties

Mechanical properties are of paramount importance for adhesion performances. Indeed, linear rheology is a useful tool to probe the relaxation processes, and uniaxial tensile tests give information on the large strain behavior occurring during debonding.

During this thesis, materials were shaped as follows: they were cut into small pieces, and placed into a mold. To avoid any adhesion between the samples and the plates during the molding, siliconized paper was used as liner. The assembly was placed under a molding press for one hour at 100°C under 50bars, and then during another hour at 25°C under 50bars. The samples were easy to unmold thanks to the liner.

### 2.1 Linear rheology

The mold used for the sample preparation was 2mm-thick and after unmolding, 8mm-diameter punches were cut thanks to a hammer and a punch.

#### 2.1.1. Instrumentation

Dynamic rheological measurements were performed on an Anton Paar MCR501. The device, presented on Figure 4 is made of two plates in between which the sample is put. The lower plate sets the required strain, while the force sensor on the upper plateau measures the resulting shear stress. The set-up is in a heating chamber and connected to compressed air to control the temperature. Thanks to a liquid nitrogen flow, this temperature can be brought down to -50°C and is controlled with a thermocouple connected to the lower plate.

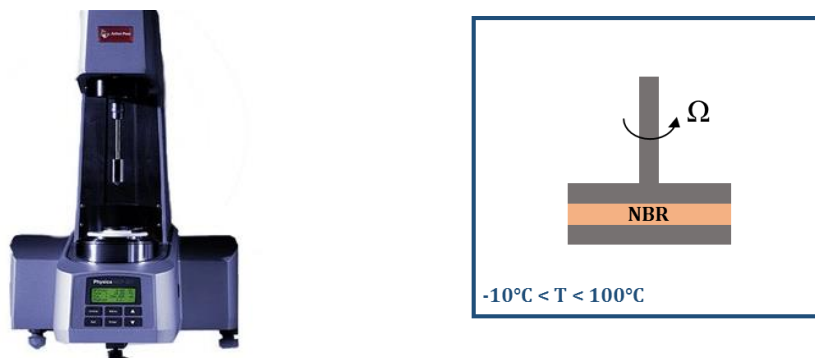


Figure 4 Anton Paar rheometer (left), and illustration of shear inside the rheometer (right)

To avoid any sliding between the plates and the sample, a “sticking step” was performed with a compressive force of -2N at 60°C during three minutes. The material was then let 20minutes to relax at room temperature before launching the test.

#### 2.1.2. Linear regime

Strain tests were run at different temperatures (25°C and 60°C) to determine the linear regime. The curves are found in Annex 2.

In the rest of the manuscript, the linear mechanical properties of NBR were probed for 0.2% deformation.

**2.1.3. Time-temperature superposition**

i. Principle

Mechanical properties of elastomers are sweep frequency- and temperature-dependent. As mentioned in Chapter 1 (1.3.4) the time-temperature superposition (TTS) principle states that the behavior of a polymer undergoing high stress at high temperature will be the same as of a polymer undergoing low stress at low temperature. This principle is available only in systems where the relaxation processes all vary with the same temperature dependency.

Rheological properties of polymers can vary over a range of frequencies going from  $10^{-3}$  to  $10^{10}$ Hz yet most rheometers only probe frequencies from  $10^{-2}$  to  $10^2$ Hz. Thanks to the TTS, it is possible to study the material's properties over a wide range of temperature, and to deduce a master curve at a single temperature with simple shifts along the frequency axis.

Williams, Landel and Ferry (WLF) proposed a model to evaluate this shift, and introduced the shift factor  $a_T$  as:

$$\log(a_T) = \frac{-C_1^\circ(T - T_o)}{C_2^\circ + (T - T_o)} \quad 2.1$$

$C_1^\circ$  and  $C_2^\circ$  depend on the material and on the temperature reference  $T_o$ ; and can be determined thanks to the  $a_T$  coefficient measured experimentally. Furthermore, a horizontal shift  $b_T$  coefficient must be applied to consider the change in density of the material with temperature and is equal to  $\rho^T / \rho_o T_o$ .

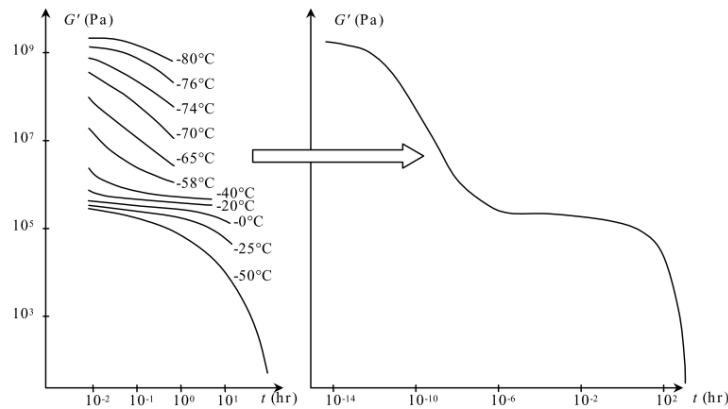


Figure 5 Illustration of the construction of a master curve with application of horizontal and vertical shifts  $a_T$  and  $b_T$  using the TTS

i Master-curves construction

The viscoelastic moduli  $G'$  and  $G''$  were measured over a range of frequencies from 0.01 to 30Hz, and for temperatures from -10 to 100°C. The measurements were done after staying during 7 minutes at the desired temperature and the temperature was then increased by 3°C, with heating at a rate of 1.5°C/min, before new measurements were performed.

Loss factors ( $\tan \delta$ ) are plotted in Figure 6 (left) for different temperatures. Horizontal shifts are applied to the curves at  $T < 25^\circ\text{C}$  and  $T > 25^\circ\text{C}$  such that they all form a single master curve at  $T_o = 25^\circ\text{C}$  in Figure 27 (right). During the experiment, due to temperature effect, the material expands and the entropic elasticity changes. In principle this cause a vertical shift factor

proportional to the change in the product  $\rho T$ , where  $\rho$  is the density. To take into account this effect an empirical vertical coefficient  $b_T$  is added to shift the moduli  $G'$  and  $G''$ , as shown in Figure 7 (before shifting) and Figure 8 (after shifting), such that all data are time-temperature shifted into one single curve.

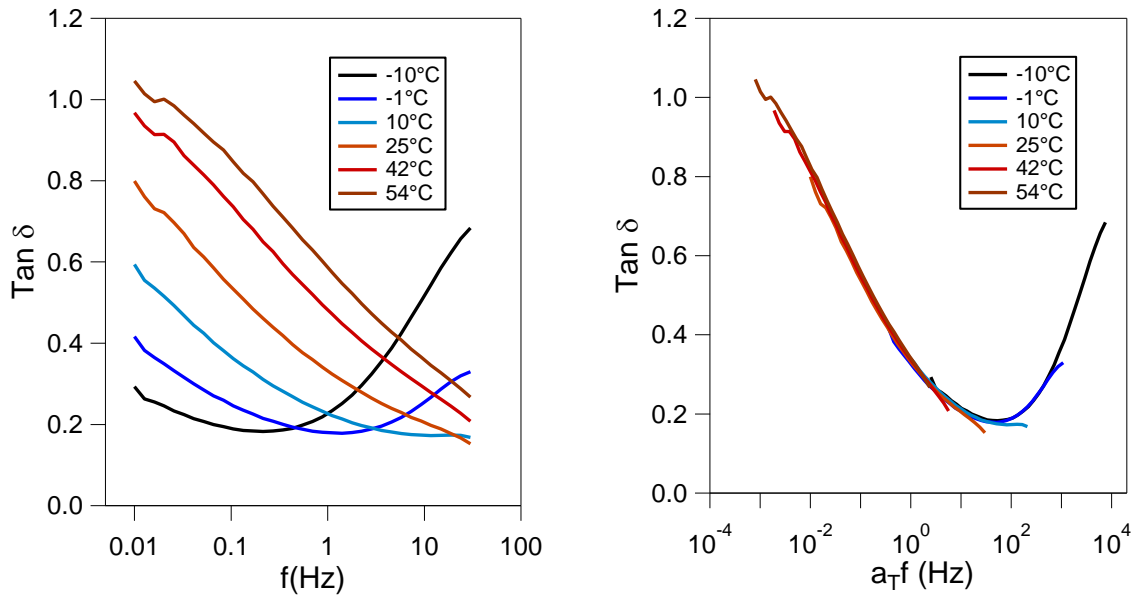


Figure 6 Loss factor at different temperatures before (left) and after (right) horizontal shifting with  $a_T$  for NBR

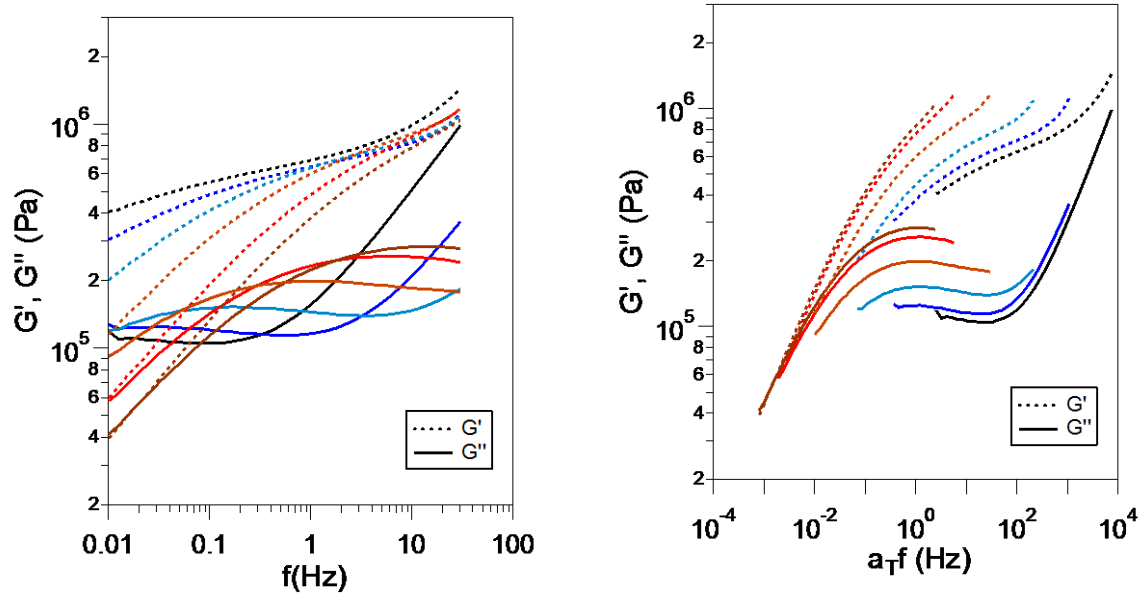


Figure 7 Moduli  $G'$  and  $G''$  as function of frequency before (left) and after (right) horizontal shifting with  $a_T$  (but without vertical shifts)

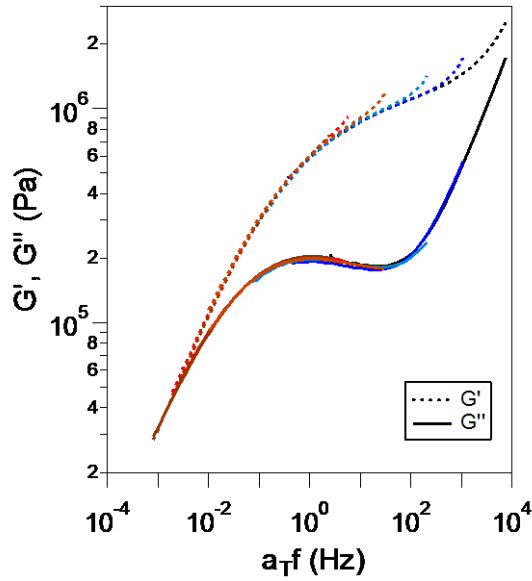


Figure 8  $G'$  and  $G''$  after applying horizontal and vertical shifting ( $a_T$  and  $b_T$ )

The vertical shifts needed to plot a single master curve for NBR are too high ( $> 1$ ) to be only due to changes in  $\rho T$ , and suggest that there is an organization causing an increase in the modulus with temperature. These effects will be commented in detail in Chapter 3.

#### 2.1.4. Result

The master curve for NBR is plotted at  $T_0=25^\circ\text{C}$  in Figure 9.

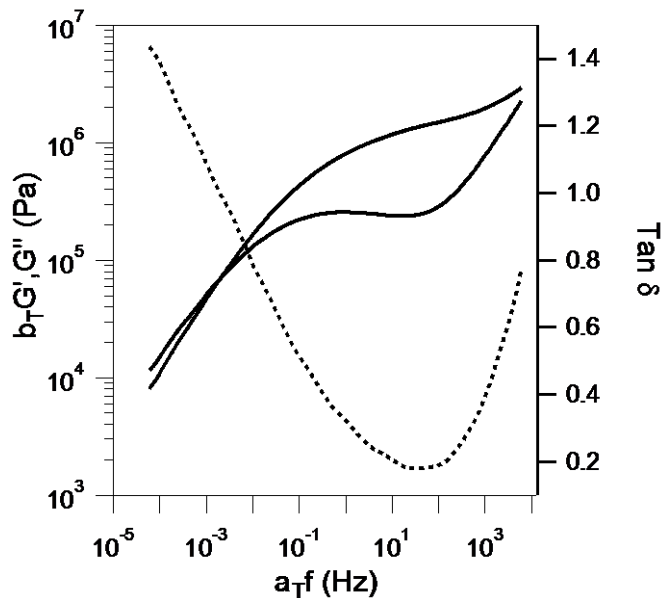


Figure 9 Master curve for NBR plotted at a reference temperature of  $25^\circ\text{C}$

There are different regimes, corresponding to the different relaxation phenomena. The average molecular weight between entanglements  $M_e$  (see equation 1.11 from Chapter 1) can be estimated using equation 2. 2 below:

$$M_e = \frac{\rho RT}{G_N^0} \quad 2.2$$

With  $\rho$  the density of the material,  $R$  the gas constant,  $T$  the temperature and  $G_N^\circ$  the plateau modulus. As the rubbery plateau is not perfectly flat, it was considered, as in [2], that this value corresponds to that of  $G'$  for the minimum value of  $G''$ . For NBR,  $M_e=2.2$  kg/mol.

The terminal relaxation regime, at very low frequencies, is of particular interest. Although the crossover of  $G'$  and  $G''$  (i.e where  $\tan \delta = 1$ ) is strictly defined as the gel point during polymerization, we will approximate in this work this point as the transition between solid-like and liquid-like behavior. As so, a reptation time is estimated from Figure 9 such that  $\tau_{REP}=500s$ .

In fact, the storage modulus  $G'$  and the loss modulus  $G''$  respectively scale as  $\omega^{0.6}$  and  $\omega^{0.5}$  with frequency, instead of scaling as  $\omega^2$  and  $\omega^1$  as expected in the Maxwell regime. This shows that even at very low frequency, the studied NBR is not in a fully relaxed state.

## 2.2 Uniaxial tensile tests

### 2.2.1. Instrument and test conditions

Uniaxial tensile tests were performed on an Instron device with a 10-Newton load cell. The mold used for the sample preparation was 0.3mm thick and after unmolding, dog bone-shape samples were cut which dimensions are shown below:

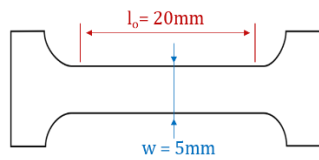


Figure 10 Dog-bone samples for uniaxial tensile tests

The traction speed was chosen as to have the same stretch rate as during the tack experiment. In tack, the debonding speed is kept constant at  $V_{deb}=10\mu m/s$  and the total thickness  $e$  of the system is of the order of 600 $\mu m$ . Therefore, the stretch rate  $\dot{\epsilon}$  is calculated as  $V_{deb}/e$  such that  $\dot{\epsilon} = 0.017s^{-1}$ . The calculated crosshead speed imposed during the uniaxial tensile test is  $V_{traction} = \dot{\epsilon} * l_0 = 0.33mm/s$ .

### 2.2.2. Results

The result for NBR is shown on Figure 11. As expected for high molecular weight rubbery materials, NBR is highly deformable. The Young's modulus is 0.5 +/- 0.1 MPa. As the material is studied in its uncrosslinked state, no strain hardening is probed and breakage occurs through flow rather than fracture propagation.

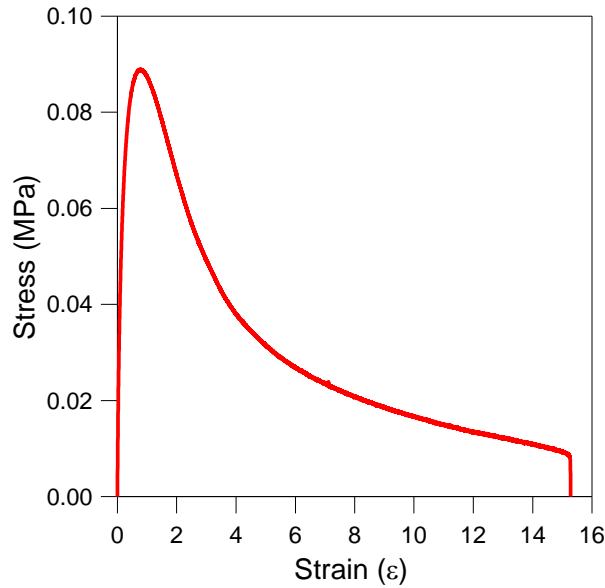


Figure 11 Uniaxial tensile test on NBR

Due to the material's incompressibility, the poisson ratio  $\nu=0.5$  and the elastic Young's modulus is linked to the storage and loss modulus  $G'$  and  $G''$  with the following relation:

$$E = 3\sqrt{G'^2 + G''^2} \quad 2.3$$

For  $\omega=0.017\text{Hz}$ , at  $T=25^\circ\text{C}$ , the rheological measurements give  $G'=0.138\text{ MPa}$  and  $G''=0.095\text{ MPa}$ . Therefore,  $3G=0.5\text{MPa}$  and equals the elastic modulus from tensile tests. Relation 2.3 is validated.

### 3. Characterization of self-adhesion properties

#### 3.1 Choice of the characterization method

Figure 12 shows the stress profiles in a  $90^\circ$  peeling front for a PSA-type adhesive [5]. Without going into details, different zones are observed: a zone with the material under compression, then an increase in stress until a maximum due to cavitation, and finally a plateau due to the traction of filaments (fibrils) until their breakage. During this experiment, one measures the force- per unit of width- needed to debond the PSA. Therefore, all the mechanisms mentioned above are evaluated with a unique value. On the contrary, during probe-tack experiments, the whole sample is stressed similarly and the analysis of a typical debonding curve (shown in Figure 13, and detailed more precisely in the following section) gives information about these successive stages.

Unlike peel tests, probe-tack experiments enable a fine control of the contact time, and short ones can be achieved. Furthermore, peeling is much better adapted for soft materials with strong adhesive properties. During this study, rigid ( $\sim\text{MPa}$ ) elastomers are studied and their self-adhesive properties are expected to be poor (from industrial's perception).

For all this reasons, all the measurements were performed on a probe-tack device.

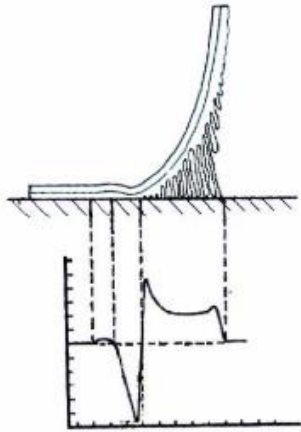


Figure 12 Schematic representation of the peel profile  
Figure from [5]

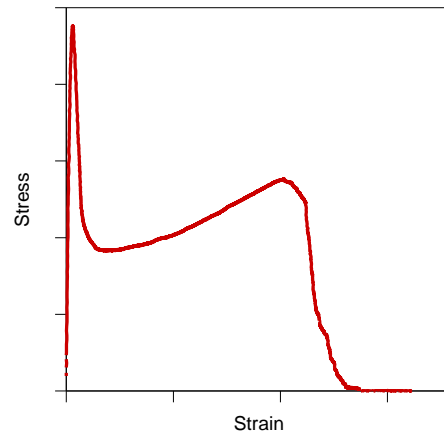


Figure 13 Probe-tack debonding curve for a PSA

## 3.2 Probe-tack tests

### 3.2.1. Instrumentation

The Probe-tack set up has been developed at ESPCI [6], on a hydraulic MTS tensile testing machine (model MTS 810) equipped with a 2kN load cell.

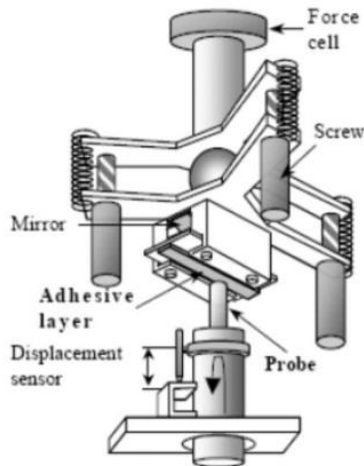


Figure 14 Probe-tack device

A 45° oriented mirror allows the observation and measurement of the effective contact area between the glass plate and the probe. In order to optimize this area, the setup has a 3-screw system to adjust the parallelism [6]. The set-up is illustrated in Figure 14.

The probe-test consists in bringing together, at an approaching speed  $V_{app}$ , the two surfaces (probe and slide) at 1MPa (70N, probe of 9.7mm diameter) during a contact time  $t_c$ , and to measure the force needed to debond the layers, at a speed  $V_{deb}$ . Three different stages can therefore be well defined: the approaching stage, the contact phase - where the sample is under compression- and the debonding one as illustrated in Figure 15.

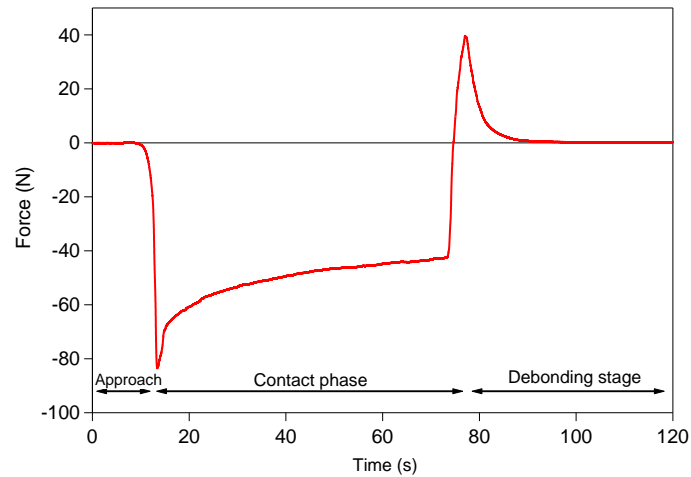


Figure 15 Typical Force-displacement curve during a Probe-tack test

During the contact phase, after reaching 1MPa the material relaxes, hence a decrease of the compression force until the debonding stage. At the end of the contact stage, the motion of the probe is reversed and the material is stretched until total debonding.

### 3.2.2. Debonding behaviors

Once the motion of the probe is reversed, debonding of the materials starts to occur, and several stages are observed and illustrated in Figure 16. First (a), the stress (or force) increases linearly with strain (or displacement): the material is elastically deformed. Before reaching its maximum, the force varies slightly non-linearly, and the nucleation of the first cavities are observed at the interface (b). This cavitation is due to the confinement of microscopic air bubbles during the contact phase. The force reaches a maximum at the end of the nucleation process (c), and the cavities then grow at the interface (d). If they propagate at the interface, the stress continues to drop to zero until debonding (e). If they are able to grow into the bulk of the materials, fibrillation [6][7] takes place (f) and different types of failure (as mentioned in Chapter 1, section 2.2) may occur.

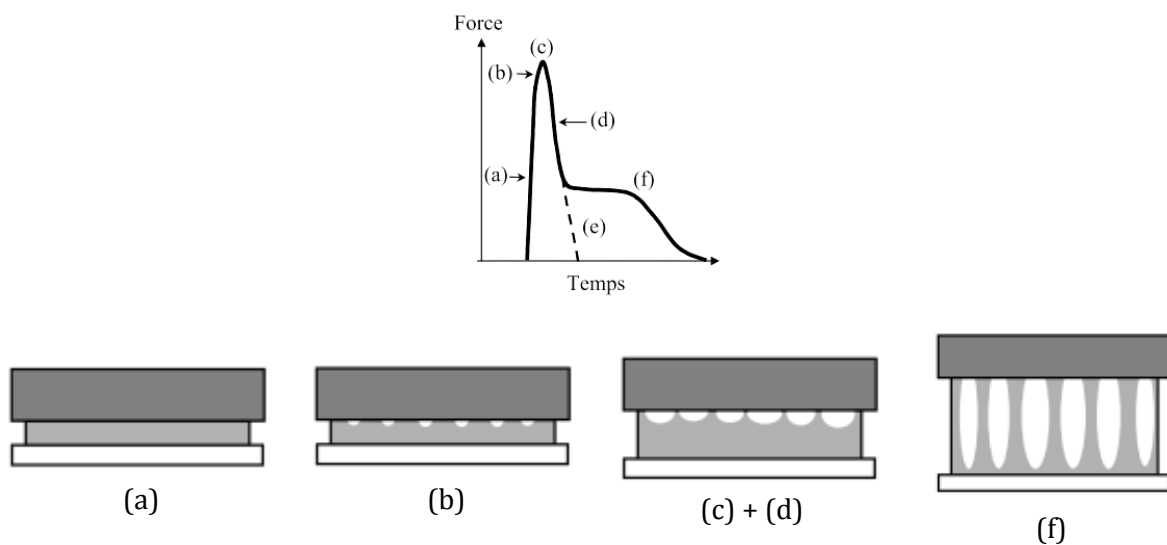


Figure 16 Typical debonding profile using Probe-Tack test. Top curve: force-time debonding profile. Below pictures: cavity growth related to such debonding profile

If the fibrils break, a cohesive debonding is measured, and residues of the material are present on both the probe and the glass slide. Adhesive failure can be of two different types, according to the material's property and its affinity for the surfaces the debonding occurs either from the slide or from the probe. If the cavities propagate at the interface (e), interfacial debonding occurs after elastic stretching of the material.

Pictures taken thanks to the 45°-oriented mirror are shown in Figure 17. The outline of the probe is shown with the dotted yellow line. In the first pictures, cavities appear in the center of the probe and some are outlined by arrows.

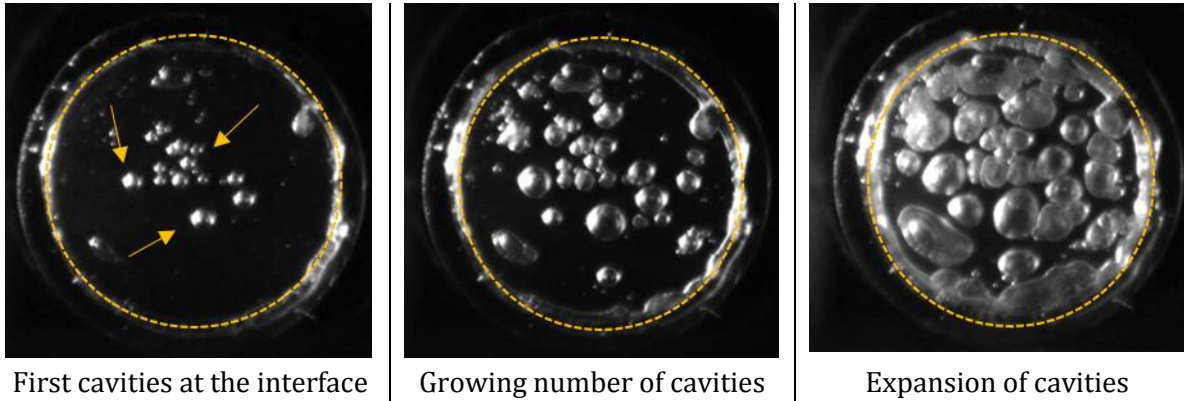


Figure 17 Illustration of three different steps during debonding process. Arrows show the appearance of cavities

The stress  $\sigma$  is calculated as the force  $F$  divided by the initial total area in contact  $A$ . The deformation  $\varepsilon$  is defined as the displacement  $l$  normalized by the displacement at  $t=0$ , i.e. the total thickness of the deformable part of the system  $h_0$ :

$$\sigma = \frac{F}{A} \quad 2.4$$

$$\varepsilon = \frac{l - h_0}{h_0} \quad 2.5$$

The adhesion energy  $W_{adh}$  corresponds to the area below the stress-strain curve (which is equal to the total dissipated energy per unit volume) multiplied by the initial thickness  $h_0$ :

$$W_{adh} = h_0 \int \sigma d\varepsilon \quad 2.6$$

$W_{adh}$  (J/m<sup>2</sup>) corresponds to the work provided to debond the layers.

This device has been used a lot [8][9][10] to study the adhesion between soft layers on glass slides (PSAs for example), and the steel probe.

### 3.2.3. Understanding debonding curves

To compare two materials or two experimental conditions, stress-strain curves are a great indicator of the shift in debonding mechanisms. The cavitation peak (maximum in stress) corresponds to the nucleation of cavities at the interface and depends on the size of initial defects (roughness), of the material's modulus, and of the strength of interfacial interactions. The total deformation is mainly due to the material's ability to dissipate energy and is therefore correlated to its mechanical properties.

Examples of two different experimental conditions are illustrated in Figure 18 below. The curve on the left (a) compares debonding processes in which both the cavitation peak and the total

deformation are doubled. If it is possible to superpose both curves with a multiplying factor  $m$  it is suggested that the effect is solely due to effective contact area, and  $m$  is the ratio between both effective contact areas.

In Figure (b), both samples cavitate at the same stress, yet show differences on the large deformation behavior. These curves suggest that although the contact areas are similar, the difference lies in the interface's ability to withstand stress. In fact, this is either due to stronger interactions at the interface (H-bonding vs Van der Waals forces for instance), or to a difference in the material's bulk properties, and especially in the capacity to dissipate energy during debonding.

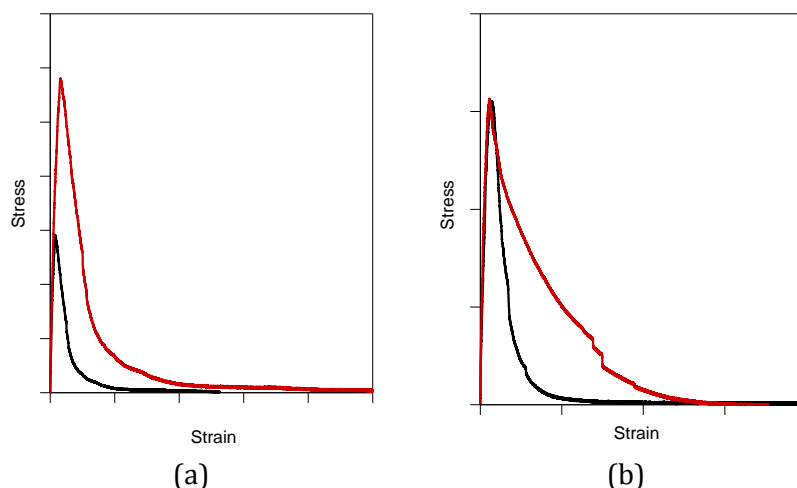


Figure 18 Stress-strain debonding curves to illustrate different contact conditions

### 3.3 Samples preparation

To be able to study self-adhesion, the same material needs to be both on the glass slide and on the steel probe. In order to visualize the debonding mechanism at the interface, a thin transparent layer is coated on the glass slide.

#### 3.3.1. Glass slides' preparation:

To avoid debonding of the coating from the glass slide during the test, both need to be chemically bonded. The glass plates were first cleaned with acetone and plasma treated to increase their surface energy. They were then introduced in a desiccator with three droplets of silanizing agent 3-(mercaptopropyl)-trimethoxysilane, and the reaction, shown in Figure 19, was carried under vacuum, at room temperature, for three hours.

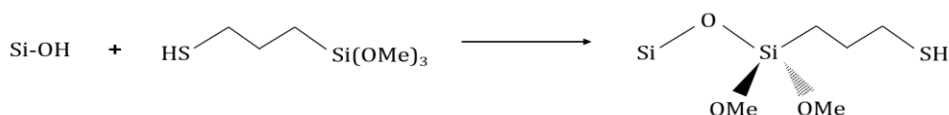


Figure 19 Silanization of the glass slides

Solutions of 2.5wt% NBR in cyclohexanone were prepared and drop coated onto the silanized glass slides. The slides were left at room temperature in the hood during 15 hours for slow evaporation and then dried in a vacuum oven at 100°C for two hours. This high temperature chemical reaction between the mercapto group of the agent and the double bonds of the elastomer

(butadiene) ensures a good adhesion between the glass slide and the elastomer, and is shown in Figure 20.

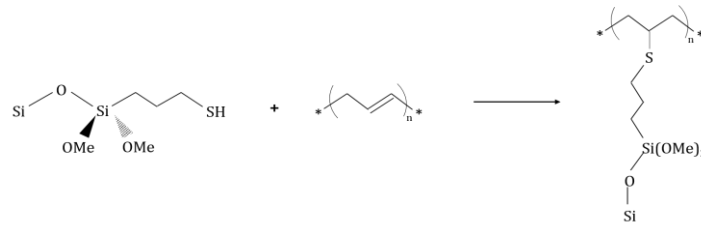


Figure 20 Chemical bonding of the elastomer on the silanized glass slide

Schematically, the glass preparation step can be illustrated as below:

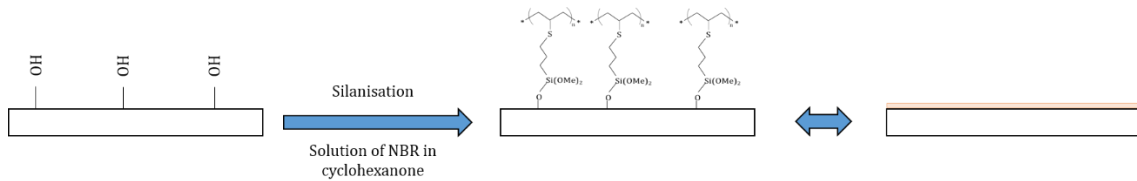


Figure 21 Illustration of the glass slide preparation process

### 3.3.2. Rubber disks' preparation:

Separately, NBR was molded in a heating press at 100°C under 50bars during one hour, and cooled down to room temperature still under 50bars during another hour. To avoid adhesion between our sample and the 500microns-thick mold, siliconized paper was using as a liner. After unmolding, 8mm-diameter cylinders were cut with a punch.

## 3.4 Self-adhesion properties

### 3.4.1. Classical Probe-tack method

The disks were then glued, using Loctite 406 glue, on steel probes. During the test, the rubber disk was brought in contact with the coated glass slide, at 1MPa, for a given contact time. When detaching the probe, debonding occurred, either by crack propagation at the interface, or by damage in the bulk of the rubber, detaching both surfaces from each other.

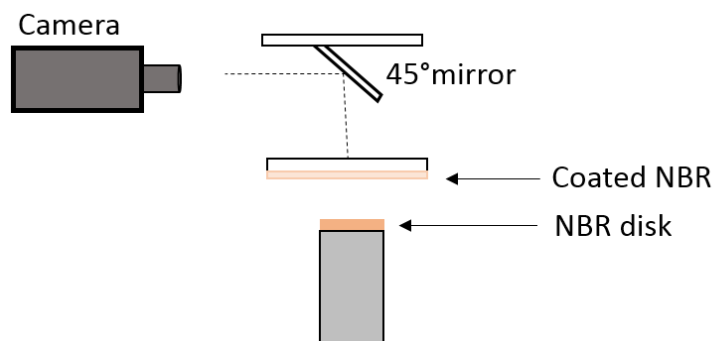


Figure 22 Illustration of Probe-tack testing for short contact times

This test was performed for different contact times, between 30 and 1000 seconds and representative stress-strain curves are shown in Figure 23.

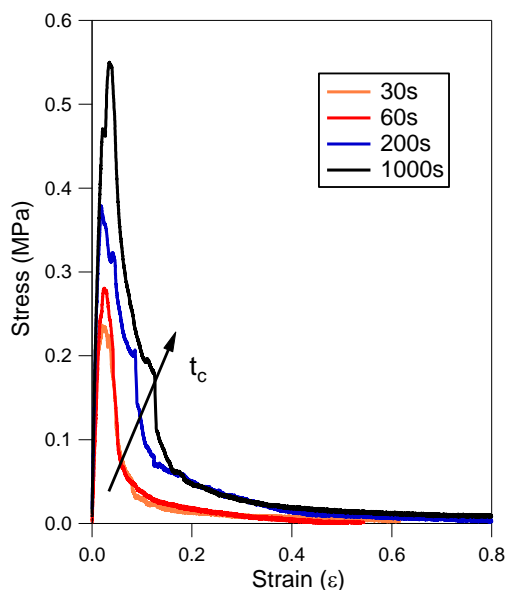


Figure 23 Self-adhesion properties of NBR for different contact times

The self-adhesion properties increase with contact time but the overall associated energy remains very small:  $W_{adh} \sim 30 \text{ J/m}^2$  for 1000 seconds of contact. Furthermore, this method enables the characterization of adhesion properties at high contact pressure (1MPa), and low contact times (typically <1000s), which is not particularly relevant regarding the industrial procedure. To be more consistent with processing, self-adhesion properties must be characterized at rather low contact pressure (pressure imposed by human's force) and for very long contact times to mimic the time between the tank's fabrication and its vulcanization. For this reason, a new method was developed where the contact between the materials is established outside the probe-tack device.

### 3.4.2. New method for tack testing

#### i. Method

The glass slides and the rubber disks were prepared as explained in the previous section (3.3).

Three punches were appended on the coated glass slides, and a load was applied to force intimate contact between the materials. The weight of the load was chosen as to be consistent with the pressure that could be applied manually by an operator. It was estimated that a thumb could apply approximately 3N, and considering a surface of  $1 \text{ cm}^2$  the applied pressure is roughly 0.3bars. Therefore, a load of 476g was prepared such that the pressure applied on each of the three 0.8mm-diameter disk was 0.3 bars. Several pressure times  $t_p$  (as in time during which load was applied) between 0.5 and 4 hours were investigated for the same contact time  $t_c$  without load. As no influence of  $t_p$  was probed, the assemblies were left for an hour under load to form the contact. After removing the loads, the samples were left for a desired contact time  $t_c$ , ranging from an hour to several days, at room temperature. This protocol is illustrated in Figure 24.

During the rest of the manuscript, "contact time"  $t_c$  will always refer to the time during which samples were in contact after load removal.

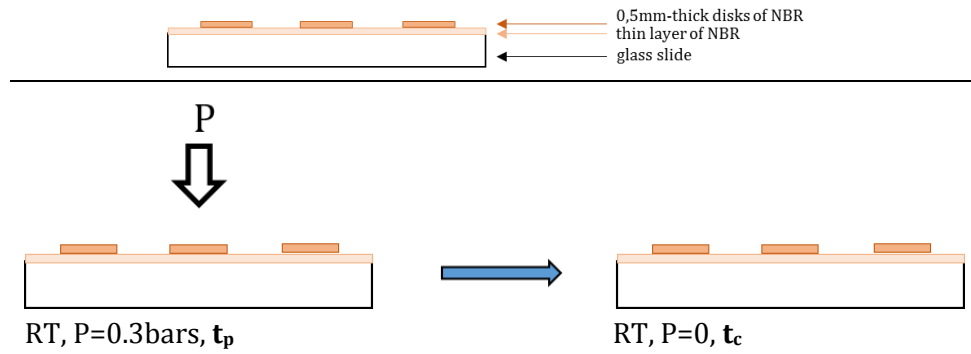


Figure 24 Illustration of the tack preparation. Top scheme: tack samples. Bottom: new protocol for contact formation

The probe-tack device was used to debond the rubber disk from the coated glass (see Figure 25). A glue (Loctite 406) drop is deposited on the steel-probe, and during the test, the steel probe glues itself to the back of the rubber disk during 500s under a light compressive force (5N).

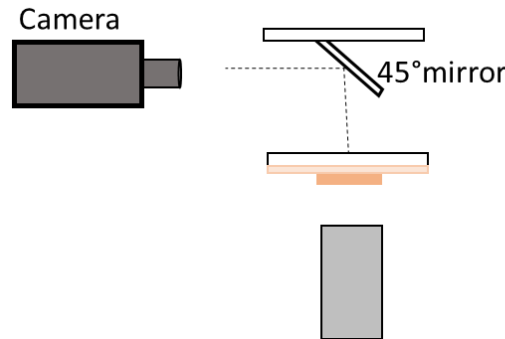


Figure 25 Illustration of the use of Probe-Tack to characterize the self-adhesion for long contact times

This method has several advantages: first, it makes it possible to probe self-adhesion properties for very long contact times under light pressure. Additionally, because the contact between the two surfaces is created by the load outside the tack device, there is no need to adjust the alignment between the two materials (which is a very tricky step). Last, this procedure separates conditions of the contact formation from the debonding step, which is of particular interest when probing the effect of temperature for example. These characteristics are summarized in Table 2.

	Typical method	New method
	Same sample preparation	
Contact pressure	1MPa = 10bar	0.3bar
Contact time	1s < contact time < 1000s	> 1hour
Alignment	Using a 3-screw system	Not needed
Bonding conditions different from debonding ones	NO	YES

Table 2 Comparison between both tack methods

ii. Results using new method

Using this technique, the self-adhesion properties of NBR were probed at long contact times (from one day to one week). As the contact time increases, Figure 26 shows that the maximum peak in force increases, as well as the total deformation. An increase in the peak stress is related to an improved contact area between the two surfaces. With time, the material is able to slightly flow at the interface, therefore increasing the contact area. Moreover, these larger contact areas can also

lead to stronger adhesion, as shown by the increase in the deformation, due to the development of new (or at least, stronger) interfacial interactions. Those can be of different types such as Van der Waals, polar, H-bonding, or inter-diffusion.

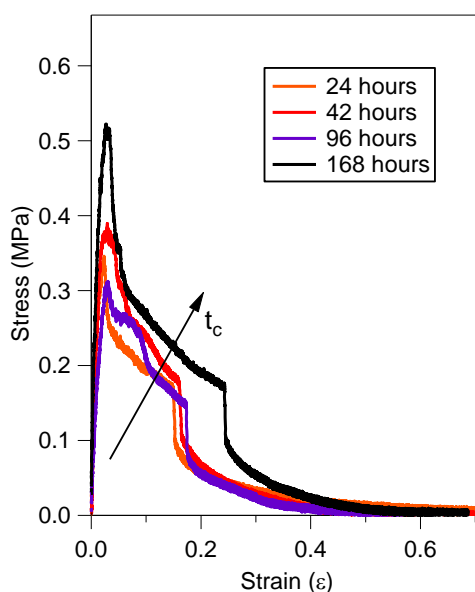


Figure 26 Stress-strain curves of self-adhesion tests for different contact times

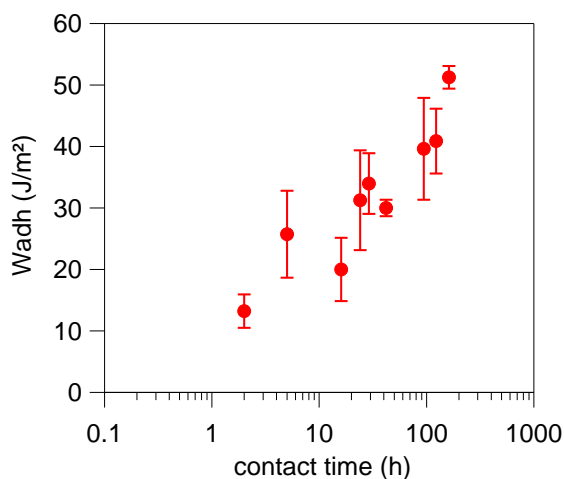


Figure 27 Evolution of the self-adhesion energy  $W_{adh}$  of NBR with time

The self-adhesion energies  $W_{adh}$  showed in Figure 27 follow a power law with contact time  $t_c$  such that  $W_{adh} \propto t_c^{0.25}$ . Yet our system is far from being a model system (in the sense that we do not finely control the interfacial properties and the fracture mechanisms) and it would thus be inappropriate to fit a model law to these data.

#### i Comments

- Due to the rubber's poor self-adhesion properties, only a thin interfacial layer of the sample is strained during the debonding experiment. The exact thickness of this layer is hard to access, and the samples were always normalized by the sample's total thickness with analogy of what is done in the study on adhesion properties of PSAs.
- The glue that was used during the debonding process is a cyanoacrylate Loctite 406 glue. It is a non-volatile, solvent free glue used in large retailers. Therefore, hardly any migration of the latter is expected in the elastomer, particularly not through the 500 $\mu$ m-thick rubber disks.

## 4. Conclusion and discussion

### 4.1 Discussion

#### 4.1.1. Comparison with SBR

An industrial Styrene-Butadiene Rubber (SBR) with a molecular weight of 2300kg/mol was used for comparison. Samples were prepared with the methodology presented in section 3.2.

Figure 28 compares the stress-strain debonding curves of both systems (NBR and SBR) after 60 and 1000 seconds of contact, and Figure 29 shows the evolution of self-adhesion energy  $W_{adh}$  with contact time. The dotted lines in Figure 29 are a guide to the eye.

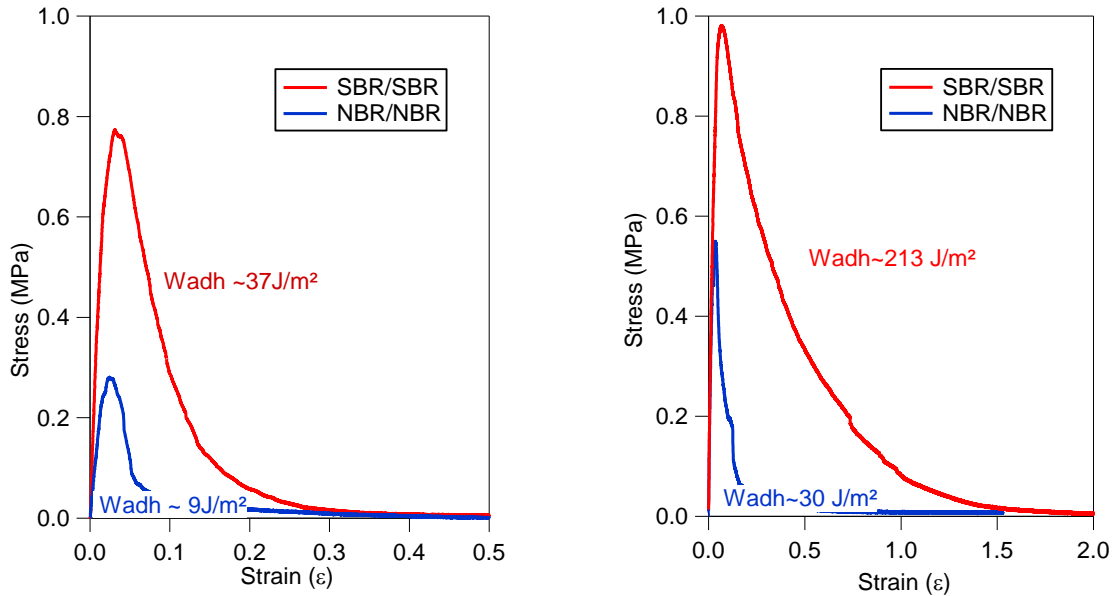


Figure 28 Comparison of the stress-strain debonding curves of SBR and NBR for 60 seconds (left) and 1000 seconds (right) of contact

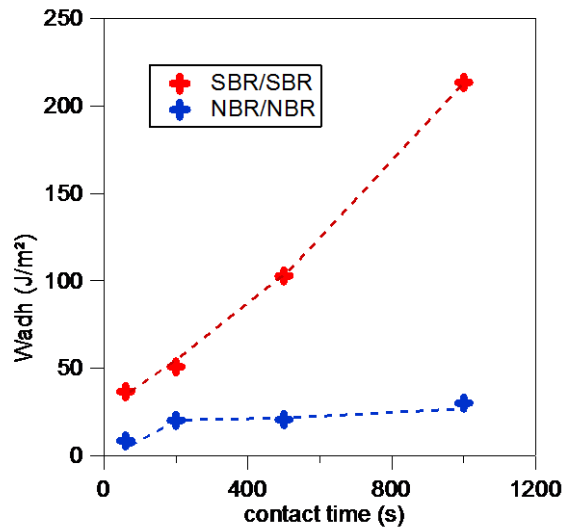


Figure 29 Evolution of the self-adhesion energy  $W_{adh}$  with contact time for NBR and SBR

The first striking observation is that the self-adhesion properties of SBR are well above those of NBR for all studied contact times. From four-fold at short contact times, to up to seven-fold at 1000s. Furthermore, the self-adhesion of NBR seems to increase very slowly with time, from  $9 \text{ J/m}^2$  after 60 seconds to  $30 \text{ J/m}^2$  for 1000 seconds; i.e. only a three-fold increase, whereas at the same time, SBR increases up to around six-fold.

#### 4.1.2. Comparison with literature

Ansarifar et al [11] used peel test to assess the self-adhesion properties of NBR. Their nitrile rubber had 38.5% acrylonitrile units, and the materials were masticated at high temperature and molded into sheets to prepare the samples. Authors claim peeling energies of the order of tens of  $\text{kJ/m}^2$ . During our study, the measured self-adhesion properties are much lower than these levels. Nevertheless, it is interesting to notice that it takes them more than a week to reach an adhesion

plateau- which is close to the cohesive strength that they estimated for NBR-, corroborating the very slow diffusion process of this material.

#### 4.1.3. Link between linear rheology and self-adhesion

As detailed in Chapter 1, Schach et al [9] studied the self-adhesion and linear rheological properties of a series of styrene-butadiene random linear monodisperse polymer melts. They showed that for contact times longer than the reptation time of the material, the diffusion of polymer chains led to a healing of the interface and hence a plateau in adhesion energy. From our rheological experiments, the terminal relaxation time of NBR was estimated to be approximately 500s. Such a long reptation time is due to the rubber's very important molecular mass as well as its wide mass distribution. For times longer than this characteristic time, the material should flow, and therefore diffuse at the interface to enhance adhesion properties. Figure 31 shows that for the studied materials, this particular time  $\tau_{\text{REP}}$  does not coincide with any change of trend in the evolution of adhesion energy with time.

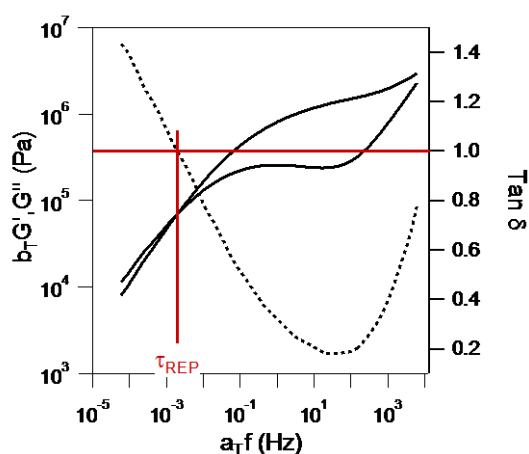


Figure 30 Determination of reptation time  $\tau_{\text{REP}}$  from linear rheology (TTS) on NBR at  $T_0=25^\circ\text{C}$

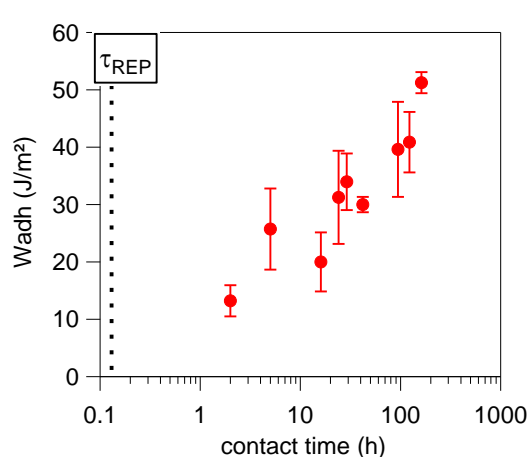


Figure 31 Comparison between reptation time  $\tau_{\text{REP}}$  and the evolution of the self-adhesion properties  $W_{\text{adh}}$  of NBR with contact time

Yet Schach's materials are well-defined monodisperse polymers whereas the studied rubber has a very important mass distribution. One can therefore wonder what is the physical meaning of the measured terminal relaxation time. The relaxation of the longer chains? Of the average size chains? And why is there no correlation between this characteristic time measured and the evolution of the self-adhesion properties? It seems that there is a discrepancy between the flow behavior measured in rheology and the molecular diffusion needed (but not observed) for the tack. Indeed, the adhesion energies reached are still very low ( $< 100\text{J}/\text{m}^2$ ) and it is therefore very unlikely that extensive inter-diffusion is occurring at the interface.

## 4.2 Conclusions

The self-adhesion properties of NBR were first characterized using the classical Probe-tack device, at short contact times (up to 1000s), and then a new method was developed to be more representative of the industrial process (long contact times, light pressure). The evolution of NBR tack energy with time were probed for contact times up to a week, and shown to be very weak ( $<100\text{J/m}^2$ ). These poor self-adhesion properties of NBR are consistent with what is noticed at the production scale. They were compared to that of SBR and cross-analyzed with rheological measurements. Whereas in the case of SBR Schach [9] measured a direct correlation between flow and diffusion, and a plateau in self-adhesion energy was reached for  $t_c > \tau_{\text{REP}}$ , such trends were not observed for NBR.

The very long relaxation times, as well as the absence of correlation between flow and diffusion for NBR could be explained by the existence of a particular organization or structure inside the material, and will be further investigated in the next chapter.

### **Take home messages :**

- **Development of a new protocol to characterize self-adhesion of elastomers at long contact times and light pressure**
- **Weak self-adhesion properties, even for long  $t_c$ , of NBR**
- **No link between diffusion and flow of the materials**

## 5. References

- [1] Sircar, "Total thermal analysis of NBR vulcanizates." 1978.
- [2] M. R. Schach, "Structure et propriétés mécaniques d' interfaces entre polymères fondus," 2006.
- [3] M. Rubinstein and A. N. Semenov, "Dynamics of entangled solutions of associating polymers," *Macromolecules*, vol. 34, no. 4, pp. 1058–1068, 2001.
- [4] Z. Zhang, Q. Chen, and R. H. Colby, "Dynamics of associative polymers," *Soft Matter*, vol. 14, no. 16, pp. 2961–2977, 2018.
- [5] D. H. Kaelble, "Peel Adhesion: Micro-Fracture Mechanics of Interfacial Unbonding of Polymers," *Trans. Soc. Rheol.*, vol. 9, no. 2, pp. 135–163, 1965.
- [6] H. Lakrout and P. Sergot, "Direct Observation of Cavitation and Fibrillation in a Probe Tack Experiment on Model Acrylic Pressure- Sensitive-Adhesives," no. 1999, pp. 37–41.
- [7] A. Zosel, "The effect of fibrillation on the tack of pressure sensitive adhesives," *Int. J. Adhes. Adhes.*, vol. 18, no. 4, pp. 265–271, 1998.
- [8] C. Creton and H. Lakrout, "Micromechanics of flat-probe adhesion tests of soft viscoelastic polymer films," *J. Polym. Sci. Part B Polym. Phys.*, vol. 38, no. 7, pp. 965–979, 2000.
- [9] C. Creton and R. Schach, "Adhesion at interfaces between highly entangled polymer melts," *J. Rheol. (N. Y. N. Y.)*, vol. 52, no. 3, pp. 749–767, 2008.
- [10] F. Tanguy, L. U. Pierre, and E. T. Marie, "Debonding mechanisms of soft adhesives : toward adhesives with a gradient in viscoelasticity Debonding Mechanisms of Soft Adhesives : Toward Adhesives with a Gradient in Viscoelasticity," 2014.
- [11] M. A. Ansarifar, K. N. G. Fuller, and G. J. Lake, "Adhesion of unvulcanized elastomers," *Int. J. Adhes. Adhes.*, vol. 13, no. 2, pp. 105–110, 1993.



# **- CHAPTER 3 -**

## **NBR AS SUPRAMOLECULAR RUBBER**

---

In the previous chapter, we have shown that the self-adhesion properties of NBR are low and not correlated to their flow properties. In this chapter, we investigate the built up of a structure inside the material itself, and observe it – at different scales- using several techniques. These observations provide an insight into nitrile rubber’s somewhat surprising behavior. Last, the self-adhesion properties at long contact times are explained with regard to the material’s structure, and a first strategy to enhance them is suggested.

To correctly apprehend the different analysis and conclusions of this chapter, it is very important that the reader realizes that the same industrial rubber will be analyzed under three different states: as-received from supplier, after extrusion, and after dissolution.

<b>1. Supramolecular behavior of NBR .....</b>	<b>73</b>
1.1. Ageing of the materials at room temperature .....	73
1.1.1. Ageing of freshly extruded NBR at room temperature.....	73
1.1.2. Comparison with as-received NBR.....	74
1.1.3. Comments and conclusion.....	77
1.2. Dissolution of NBR in a solvent to accelerate ageing process .....	77
1.2.1. Thermal measurements and linear rheology on dissolved NBR at RT.....	78
1.2.2. Frequency sweeps, at 80°C, on dissolved NBR.....	78
1.3. Conclusions .....	79
<b>2. Study of structure formation in NBR .....</b>	<b>80</b>
2.1. Literature .....	80
2.1.1. C≡N interactions .....	80
2.1.2. Structure in NBR.....	81
2.1.3. Current study .....	82
2.2. X-Ray Scattering.....	82
2.2.1. Introduction to X-Ray Scattering.....	82
2.2.2. Methodology.....	84
2.2.3. Comparison of the different materials.....	84
2.2.4. Influence of time and temperature on the microstructure of NBR.....	86
2.3. Atomic Force Microscopy.....	88
2.3.1. Instrumentation.....	88
2.3.2. Results.....	89
2.4. Transmission Electron Microscopy.....	91
2.4.1. Method .....	91
2.4.2. Results.....	91
2.5. <sup>1</sup> H NMR study .....	91
2.5.1. Method .....	91
2.5.2. Results.....	92
2.5.3. Conclusion on molecular statistics .....	93
2.6. Conclusions and discussion.....	93
<b>3. “Self”-adhesion properties .....</b>	<b>94</b>
3.1. Literature on block copolymers.....	94
3.1.1. Introduction to block copolymers.....	94
3.1.2. Diffusion and self-diffusion of block copolymers.....	95
3.1.3. Comments.....	97
3.2. Influence of NBR structure on its self-adhesion properties.....	97
3.2.1. Self-adhesion at room temperature .....	97
3.2.2. Comparison with adhesion on glass .....	98
3.2.3. Self-adhesion of NBR at higher temperatures .....	99
3.3. Self-adhesion properties of freshly extruded NBR.....	101
3.3.1. New method.....	101
3.3.2. Results.....	102
3.3.3. Discussion.....	102
<b>4. Conclusions.....</b>	<b>103</b>
<b>5. References.....</b>	<b>104</b>

## 1. Supramolecular behavior of NBR

During this section, three different states of the industrial nitrile rubber are studied. The first part (1.1.1) consists in investigating the thermal and mechanical properties of freshly extruded NBR (studied in Chapter 2) over time, and a comparison with nitrile rubber from Sigma-Aldrich (NBR-SA) is proposed. This freshly extruded NBR aged at room temperature (RT) is then compared to raw NBR, “as-received”, that has been aged for several month in the supplier’s storage room (1.1.2). A method to accelerate this ageing process is then suggested, through the dissolution of NBR (“dissolved NBR”) in a solvent and its slow drying (1.2). The behavior of NBR in these three states are compared and analyzed.

### 1.1. Ageing of the materials at room temperature

#### 1.1.1. Ageing of freshly extruded NBR at room temperature

The rubbers were systematically characterized by DSC and linear rheology measurements.

##### i. Thermal measurements

Freshly extruded NBR was characterized with DSC after remaining one month at room temperature and results are shown in in Figure 1 (left). Consistent with what was measured in Chapter 2 (1.2.1) on (un-aged) freshly extruded NBR,  $T_g$  is close to  $-30^\circ\text{C}$ . After ageing at RT for a month, the appearance of a light endothermic peak ( $\Delta=0.4\text{J/g}$ ) between  $80$  and  $85^\circ\text{C}$  is observed. This peak disappears during the second heating cycle.

To make sure that this peak was not caused by inhomogeneities of the industrial rubber, NBR received from Sigma-Aldrich (NBR-SA) was also analyzed and results are shown in Figure 1 (right). For the latter, this endothermic is more important ( $\Delta=3.6\text{J/g}$ ).

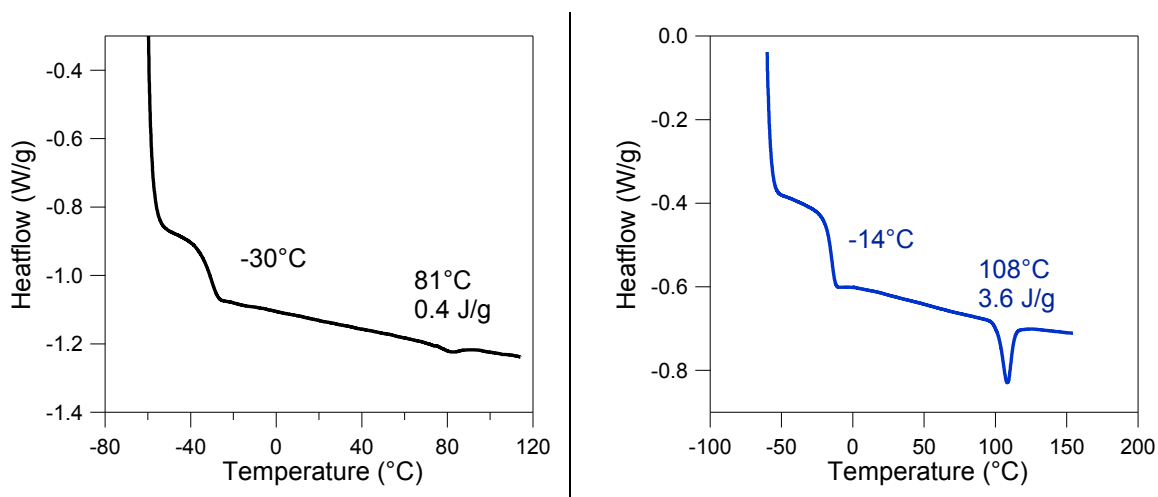


Figure 1 First heating cycle of DSC curves of extruded NBR aged a month (left) and NBR-SA (right)

The heat associated with the endothermic peaks much smaller than that of the melting of crystalline zones. Furthermore, crystallization occurs in materials with a very regular structure (as for example in cis1,4polyisoprene) and is thus not expected in the studied random copolymer. Nevertheless, it is possible that in this industrial polymer, the heat absorption might be due to specific short distances-organizations appearing with time. Geiszler and coworkers [1] have also noticed slight endothermic changes in NBR and suggested that these could be due to low-grade crystallinity of polybutadiene units along the copolymer chains. Yet such transition was observed

at temperatures between 50 to 75°C above the main glass transition temperature of the copolymer, whereas in the studied NBR, this transition occurs around 110°C above its  $T_g$ .

ii. Frequency sweeps, at 80°C, on freshly extruded NBR

Frequency sweeps were run in the linear regime ( $\gamma=0.2\%$ ) at 80°C, during four days and the evolution of the linear mechanical properties were measured. Figure 2 shows that this small amplitude shearing at 80°C leads to an evolution of the linear mechanical properties with time. The evolution is very slow and shows that the system is time and temperature-dependent. The increase in the material's stiffness, as well as the decrease in the loss factor at low frequency, is assumed to be due to an increase in physical interactions with time.

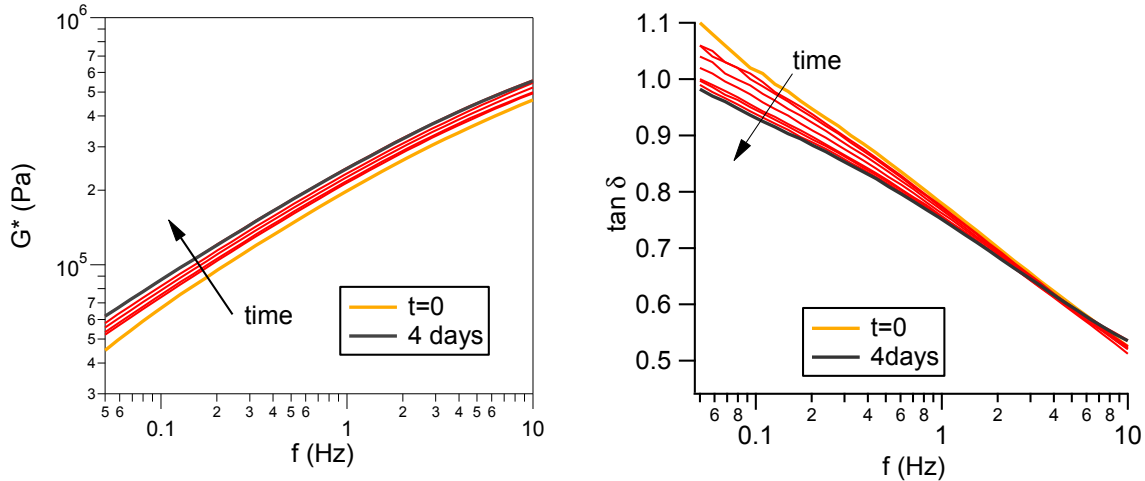


Figure 2 Frequency sweeps on freshly extruded NBR, at 0.2% and 80°C during 4 days. Red curves are for intermediate times ( $0 < t < 4$  days). Left: Complex modulus  $G^*$ . Right: Loss factor

iii. Comparison with other supramolecular materials

It is relevant to compare these results to that of Courtois et al [2] who studied bis-urea functionalized low-molecular-weight polyisobutylene (PIBUT). They showed that this material interacts through hydrogen bonds and self-organizes over time scales of days at room temperature. Samples were maintained for two hours at 80°C and frequency sweeps were then run above and below 80°C. For runs at temperatures higher than 80°C, the material behaves as a viscoelastic fluid, and a decrease in the storage modulus as well as an increase in the loss factor as a function of time are observed. At room temperature, the material self-organizes with time and  $G'$  increases while the loss factor decreases.

During our study, the endothermic peak around 80°C might be associated to some long-range order. At this temperature, thanks to enhanced mobility, the material tends to self-organize with time and favor intermolecular  $C\equiv N$  interactions. To break this physical network, frequency sweeps at higher temperature (enough to disturb these physical interactions) would have been needed.

**1.1.2. Comparison with as-received NBR**

As mentioned in the beginning of Chapter 2, to be consistent with the industrial calendaring step nitrile rubber was extruded and, from the beginning of the study, was studied after extrusion. In this section, this material (referred to as “freshly extruded”) is compared to the “as-received” (=raw, not extruded) rubber.

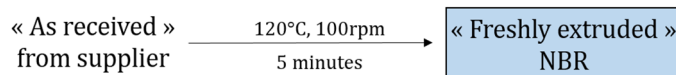


Figure 3 Extrusion during 5 min at 120°C is performed on the "as-received" (raw) NBR to reach the so-called "freshly extruded" NBR

i. Thermal measurements on as-received NBR

As-received NBR was characterized with DSC and results in Figure 4 reveal that the material also shows an endothermic peak close to 80°C. Its T<sub>g</sub> is similar to that of the freshly-extruded rubber (-30°C). The as-received rubber has remained at room temperature for several months and has had sufficient time to reach thermodynamic equilibrium. The heat associated to the long-range order (~1.2J/g) is thus higher than that of freshly extruded NBR aged a month at room temperature (~0.4J/g from Figure 1). This endothermic peak also disappears during the second heating cycle.

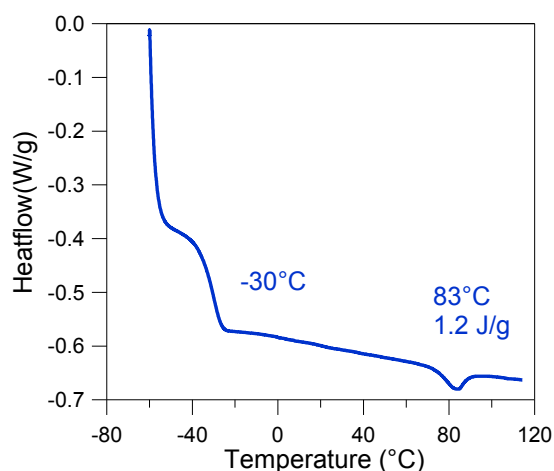


Figure 4 First heating cycle of DSC of as-received NBR

ii. Comparison of the linear rheological properties of freshly extruded and as-received NBR

Frequency sweeps, from 0.01 to 30Hz, were run at temperatures from -10°C to 90°C and the time-temperature superposition (TTS) principle was used to plot a master-curve at 22°C for both freshly extruded and as-received NBR. Figure 5 shows that  $G'$  and  $G''$  are similar over most of the frequency range, but that major differences are observed in the terminal regime (low frequencies). In fact, whereas the (freshly) extruded NBR flows ( $G' < G''$ ) at frequencies lower than  $f = 2 \cdot 10^{-3}$  Hz for the studied time-temperatures, the as-received material behaves as a physically crosslinked network ( $G' > G''$ ).

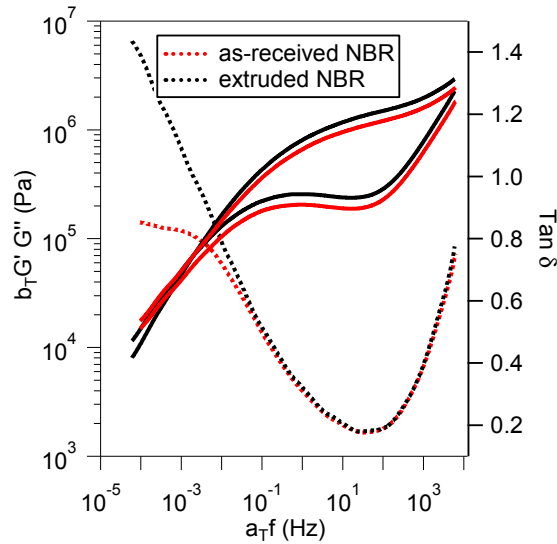


Figure 5 Master curve at  $T_0=22^\circ\text{C}$  for extruded and as-received NBR. Left axis: moduli  $G'$  and  $G''$  after  $a_T$  and  $b_T$  shifts. Right axis: Loss factor

As mentioned in Chapter 2, section 2.1.3, to plot such a master-curve, one must first determine the horizontal shift factors  $a_T$ , and then apply a vertical shift  $b_T$  to adjust the moduli. The reference temperature  $T_0$  is  $22^\circ\text{C}$  during this study.

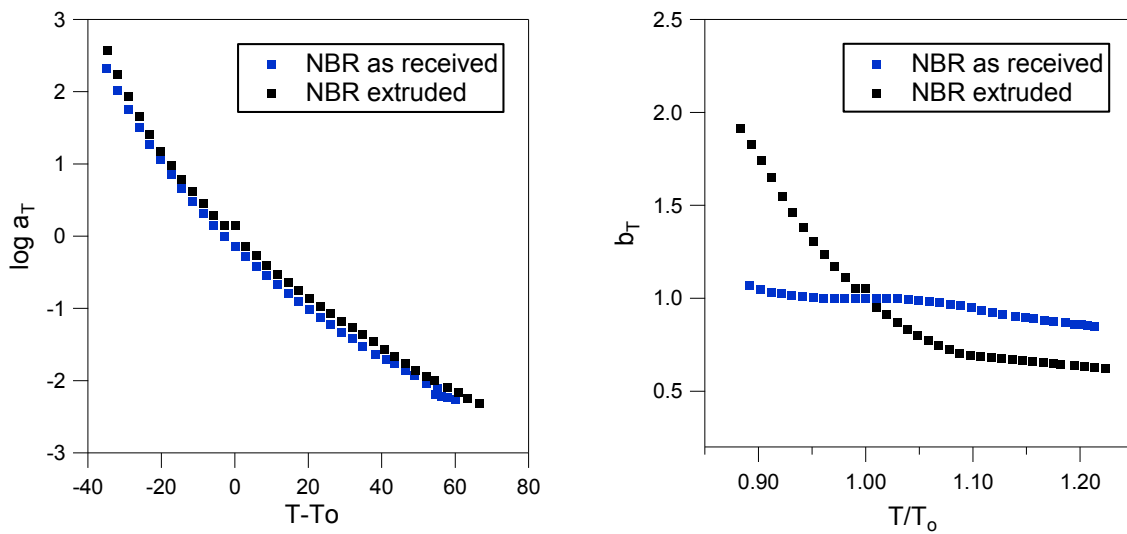


Figure 6 Evolution of the vertical (left) and horizontal (right) shift factors with temperature.  $T_0=22^\circ\text{C}$

The evolution of the horizontal and vertical shift factors needed to plot Figure 5, respectively  $a_T$  and  $b_T$ , with time are shown in Figure 6. They are plotted with regard to different horizontal axis ( $T-T_0$  and  $T/T_0$ ) in order to compare them with the WLF trends. The graphs reveals that whereas the horizontal shifts  $a_T$  of both materials are very much alike and follow a WLF trend, the evolution of their vertical factor  $b_T$  with temperature differs. In homopolymers,  $b_T$  is a measure of the change in density and entropic elasticity of the material with temperature, and scales as  $\rho^T/\rho_0 T_0$ . That of as-received NBR slowly decreases with temperature, suggesting a light expansion of the material, but remains close to unity. However, that of extruded NBR strongly decreases until  $T \sim 60^\circ\text{C}$  where it stabilizes around 0.7. This threshold temperature depends on the heating velocity as well as the duration of each temperature plateau during measurement, and the measured shift factors

are higher than mere density effects. During this study, low temperatures were probed first, and it is very likely that the trend observed for  $b_T$  in Figure 6 (right) would be modified if sweeps had been performed at high temperatures first. These results must be analyzed with regard to the work of Bartenev and coworkers [3][4]. They studied the relaxation transitions in nitrile rubbers with different acrylonitrile content, and revealed the existence of a particular relaxation process at high temperature (85°C). They revealed that this temperature matches a discontinuity in the temperature dependence of the materials' viscosity, and attributed the high-temperature behavior to a cleavage of dipole-dipole interactions leading to the material flow. As time-temperature superposition is only available if the relaxation processes all vary with the same temperature dependency, a disruption of  $C\equiv N$  interactions at high temperature could explain the specific evolution of the vertical coefficient  $b_T$  probed in Figure 6.

### 1.1.3. Comments and conclusion

SEC were performed on both states (before and after extrusion) to make sure that the change in terminal behavior between extruded and as-received NBR was not due to the breakage of chains during the extrusion process. Curves are found in Annex 1.2. The average molar mass in both cases remains similar, and very high, as well as the molecular distribution.

During this part, it was shown that the freshly extruded rubber seems to evolve with time and temperature as demonstrated by the appearance of an endothermic peak in DSC, and by frequency sweeps at 80°C. The evolution of the vertical shifts coefficient suggests the existence of a structure in nitrile rubber.

From this section, it is implied that freshly extruded samples are out-of-equilibrium whereas the as-received have reached thermodynamic equilibrium.

## 1.2. **Dissolution of NBR in a solvent to accelerate ageing process**

To study this slow ageing process, dissolution of the rubber and slow drying at room temperature was performed to reach the equilibrium state more rapidly.

Freshly extruded NBR was dissolved in butanone ( $c=3\text{wt}\%$ ) at room temperature. Once homogeneous, the solution was poured into a Teflon mold and left at room temperature for slow overnight evaporation. The sample was then dried in a vacuum oven at 100°C for two hours.

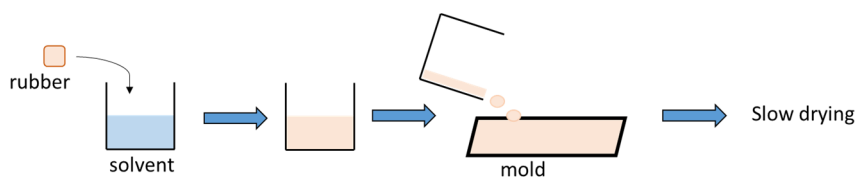


Figure 7 Preparation of "dissolved NBR": dissolution of NBR in a solvent, pouring in a Teflon mold, and slow drying

The material was analyzed using DSC, and molded under a heating press to study its linear mechanical properties. The three materials of interest are presented on the illustration in Figure 8 below.

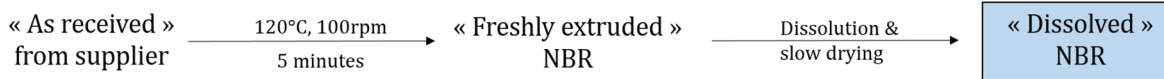


Figure 8 Illustration of the three different "states" of NBR: as-received (aged several months), "freshly extruded" after 5min extrusion at 120°C, and "dissolved" after dissolution and slow drying of NBR

**1.2.1. Thermal measurements and linear rheology on dissolved NBR at RT**

Dissolved NBR was characterized by DSC (Figure 9) and linear rheology at 0.2% deformation (Figure 10). Two temperatures, 25 and 60°C were investigated and the master curve is drawn at 25°C.

The Tg of dissolved NBR is similar to that of as-received and freshly extruded NBR (-30°C). An endothermic peak (1.3J/g) is also probed in DSC at high temperature and this peak disappears with the second heating cycle. Linear rheology reveals that after dissolution and slow drying, no terminal relaxation time is measured at very low frequencies and the rubber behaves as a physical network with  $G' > G''$ .

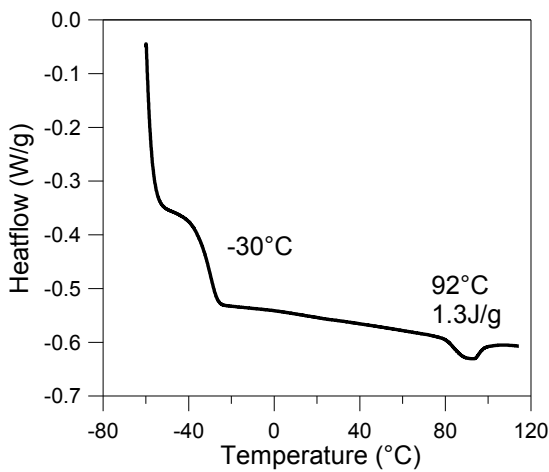


Figure 9 First heating cycle of DSC measurement on dissolved NBR

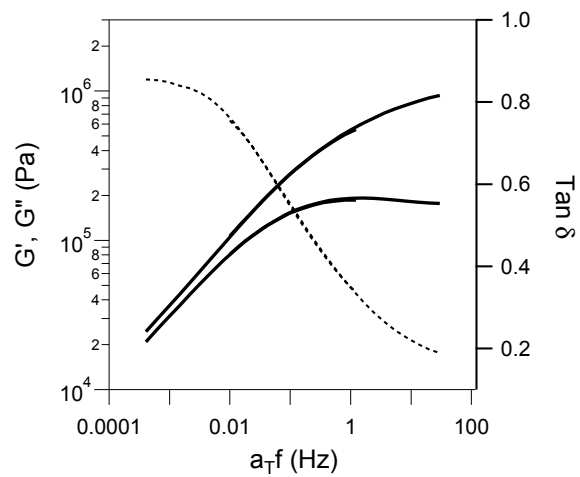


Figure 10 Linear rheological ( $\gamma=0.2\%$ ) properties of dissolved NBR plotted at 25°C

**1.2.2. Frequency sweeps, at 80°C, on dissolved NBR**

Similar frequency sweeps than that of section 1.1.1 on freshly extruded NBR were performed on dissolved NBR. The evolution of the complex modulus  $G^*$ , as well as that of the loss factor  $\tan \delta$ , at 80°C over 4 days are shown in Figure 11. No particular change is observed over the investigated time scale, suggesting that the material is already close to its equilibrium state.

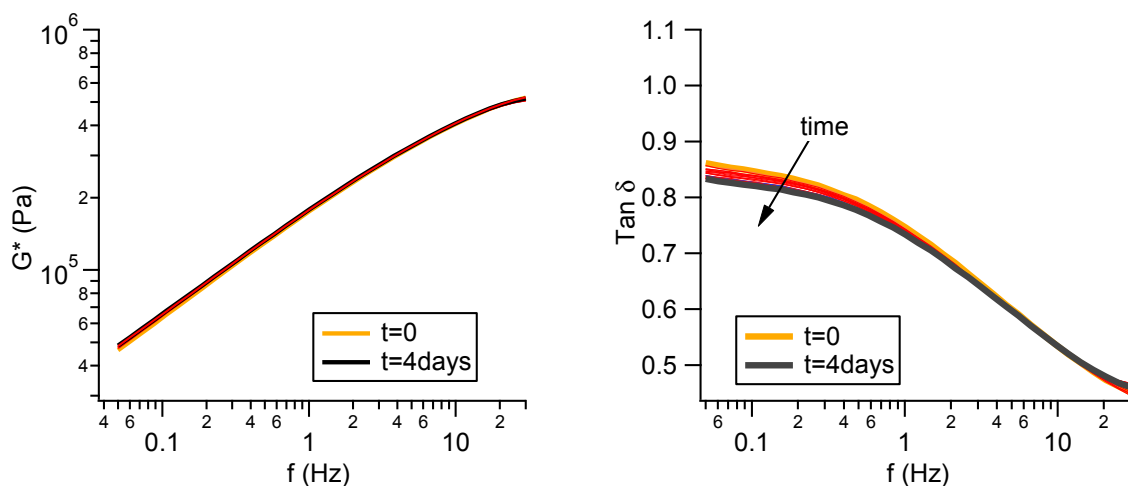
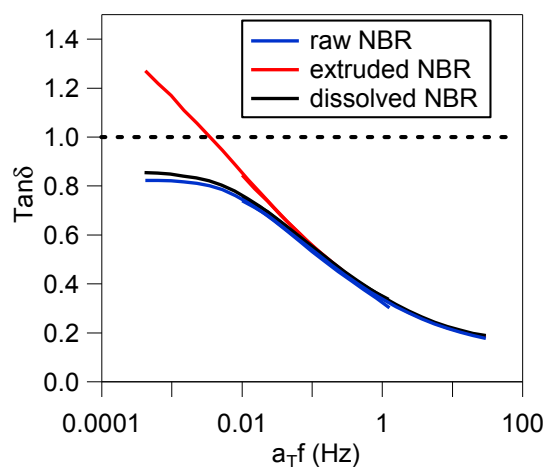
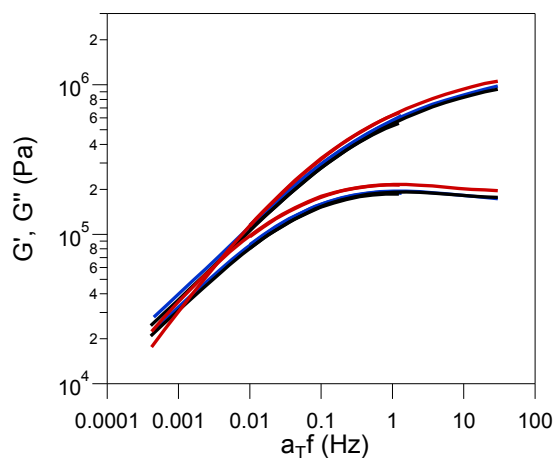


Figure 11 Frequency sweeps on dissolved NBR, at 0.2% and 80°C during 4 days. Red curves are for intermediate times ( $0 < t < 4$  days). Left: Complex modulus  $G^*$ . Right: Loss factor

### 1.3. Conclusions

During this part, DSC and linear rheological measurements - over time and temperature - were used to demonstrate the self-organizing properties of NBR. The three different stages of interest are summarized below:

- |   |  |  |
|---|--|--|
| <p>1. NBR as received<br/>Stored at RT for months</p> | <p>2. NBR extruded<br/>at 120°C during 5 minutes</p> | <p>3. NBR dissolved in butanone<br/>Dried slowly</p> |
|---|--|--|



- |   |  |  |
|---|--|--|
| <p>No terminal relaxation time<br/>Endothermic peak at high T<br/>Equilibrium state</p> | <p>Existence of <math>\tau_{REP}</math><br/>No endothermic peak<br/>Out-of-equilibrium</p> | <p>No terminal relaxation time<br/>Endothermic peak at high T<br/>Close to equilibrium</p> |
|---|--|--|

Figure 12 Linear rheological properties of the three different systems. Left: Storage and Loss modulus. Right: loss factor

Dissolved and as-received NBR show similar linear rheological behavior, and both exhibit a high temperature endothermic peak in DSC. These materials are close to NBR equilibrium state.

This change in properties between the different states is expected to be due to some self-organization of the material. What is this structure due to? Could the acrylonitrile's polarity be responsible for the absence of low frequency flow of the materials? If the material is organized, which scale is the structure at? Is the structure melted during the heating in DSC? If so, why isn't the material flowing at high temperature in rheology?

## 2. Study of structure formation in NBR

During the rest of the manuscript, the three different states of the industrial NBR and NBR-SA are compared. These materials are summarized in Table 1.

Name	Supplier	Description
NBR-raw	Safran	Raw NBR, as received. Aged months at RT
NBR-extruded		Freshly extruded NBR
NBR-dissolved		NBR dissolved in butanone and dried slowly at RT
NBR-SA	Sigma Aldrich	NBR received from Sigma-Aldrich

Table 1 Sum-up of the materials of interest

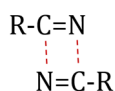
Because of the unexpected behavior of NBR probed in the previous section, we investigated the possible self-organization of the material. First, an introduction, with regard to what has been done in the literature, on the possible physical interactions responsible for such organization is presented. This structure is then probed and observed using different techniques.

### 2.1. Literature

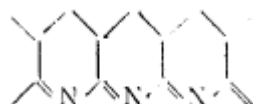
Nitrile rubber is a copolymer of two very different monomers: acrylonitrile and butadiene. The former is often used as minor comonomer in copolymers like NBR, Acrylonitrile-Butadiene-Styrene (ABS), or Styrene-Acrylonitrile (SAN). Polyacrylonitrile is a semi-crystalline polymer with a glass transition temperature between 80 and 100°C, which is frequently used as precursor for carbon fibers. The dominant characteristic of the PAN molecule is the presence of strongly polar nitrile groups. On the other side, polybutadiene is an elastomer, with a low glass transition temperature and exists in three different microstructures: 1,4-cis; 1,4-trans; and 1,2.

#### 2.1.1. C≡N interactions

The high dipole moment (3.9 Debye) of nitrile groups makes them capable of forming dimers, as illustrated below, with an energy ranging from 19 to 38 kJ/mol [5].



Polymerization of the CN groups is the first stage in the production of carbon fibers. Heating (100-200°C) polymers rich in acrylonitrile and methacrylonitrile units leads to an intramolecular reaction of neighboring nitrile groups and gives rise to a structure:



Besides, strong intermolecular interactions can lead to the appearance of a physical network in polyacrylonitrile and its copolymers. Bai et al [6] used these strong physical interactions to build an ultrahigh strength hydrogel.

Polyacrylonitrile (PAN)'s dipole-dipole interactions were studied in solution, and the polarization of solvent molecules in the vicinity of these interactions was investigated [7][8]. Figure 13 (left) shows the penetration of solvent molecules (DMF and DMSO) into PAN by breaking up the polar-

polar interactions between the nitrile groups. The effect of temperature on the competition between dipole-dipole interactions from 1. nitrile group and the solvent, and 2. nitrile groups intermolecular interactions was probed. Such competition was also studied by Climie et al [9] to explore the aggregation of block copolymers containing PAN with the addition of different solvents.

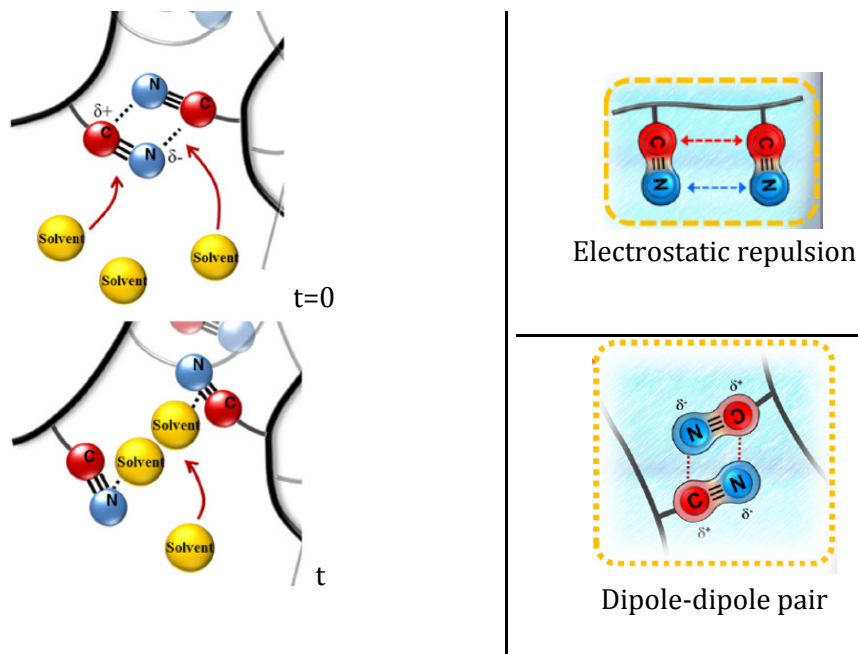


Figure 13 Left: Interactions between polyacrylonitrile and solvent molecules. Figure from [7]. Right: Evolution of electrostatic interactions with solution ageing from electrostatic repulsion (top) to dipole-dipole pairing (bottom). Figure from [8]

Furthermore, Eom et al [8] noticed a change in PAN's conformation with ageing: dipole-dipole interactions were developed at the cost of electrostatic repulsion between adjacent  $C\equiv N$  groups (see Figure 13 right).

### 2.1.2. Structure in NBR

Geiszler et al [1] used thermal analysis to study NBR and showed the existence of a mesomorphic state with a certain amount of molecular order. They suggested that this structural order could be due to partial association between adjacent nitrile groups, and that a short-range order (or "clustering") of the polybutadiene portions of the main chain could lead to the appearance of low-grade crystallinity.

Several authors have investigated the microstructure of poly(acrylonitrile-co-butadiene), at different length scales and with different techniques. Kwak et al [10] performed spin lattice relaxation time analysis of  $CH_2$  via  $^{13}C$ -NMR to show the existence of phase separation. They assume the existence of unreacted polybutadiene blocks inside the material that led to a heterogeneous phase of  $\sim 10\text{\AA}$ . This very short size presumably implies a concentration fluctuation rather than distinct domains. More recently, Ono et al [11] used pulsed  $^1H$ -NMR to look into the different molecular mobilities existing inside NBR. Two main components were identified; a low-mobility component was ascribed to alternatively copolymerized acrylonitrile-butadiene sequences, and a high-mobility one was attributed to BU block sequences. This inhomogeneity was attributed to the materials monomer sequence. In parallel, NBR was studied with Small Angle X-Ray Scattering (SAXS) measurements and a single-domain morphology, i.e.

nanodomain aggregates with a typical size of 0.1-0.4nm, was observed. In a series of articles, Sokolova et al [12][13][14][15] also argued that NBR consists of two components: microblocks of trans-1,4-butadiene units and a sequence of alternating trans-1,4-butadiene and acrylonitrile. High temperature relaxation transitions [14], Wide Angle XRay Scattering [12] and Electron Spin Resonance (ESR) spectroscopy [16] were used to compare different nitrile rubbers and to assess the impact of temperature and acrylonitrile content on the phase size. The average intermolecular distance was of the order of 5-10Å.

### 2.1.3. Current study

To the best of our knowledge, no study has been performed to examine the formation and equilibration of a structure in nitrile rubber for length scales greater than 0.4nm. Moreover, no imaging techniques have proved the existence of such organization.

During this study, X-Ray scattering experiments and Transmission Electron Microscopy were performed and sizes up to tens of nanometers were probed. Atomic Force Microscopy was used to explore the samples' surface.

## 2.2. X-Ray Scattering

### 2.2.1. Introduction to X-Ray Scattering

#### i. Technique

X-ray scattering techniques are non-destructive analytical techniques which measure the intensity of X-rays scattered by a sample as a function of the scattering angle. They are used to study the structure of a wide range of materials at different length scales, from several Angströms to hundreds of nanometers.

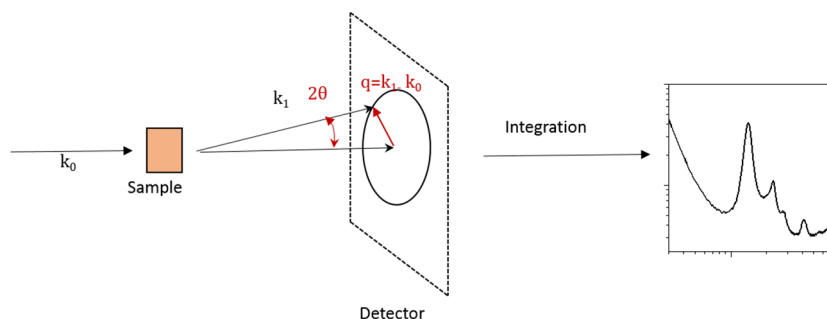


Figure 14 Illustration of a X-Ray scattering experiment

A monochromatic X-ray beam of incident wave vector  $k_0$  reaches the sample, and is deviated with a scattering angle  $\theta$  and a wave vector  $k_1$ . Photons interact with the material's electrons and the signal is scattered such that the difference  $k_1 - k_0$  is the scattering vector  $q$ . The scattered intensity  $I(q)$  is the Fourier transform of  $g(r)$ , the correlation function of the electronic density which corresponds to the probability to find a scatterer at position  $r$  in the sample if another scatterer is located at position 0. The number of photons scattered by one sample is proportional to its total volume  $V$  and to its electronic contrast. In the simple case of a binary system with  $\rho_1$  the density of the first type of scattering objects and  $\rho_2$  that of the other objects, the electronic contrast is  $(\rho_1 - \rho_2)^2$ . The higher the contrast, the greater the signal.

The choice of accessible  $q$  range is defined by the experimental set-up and usually fixed by geometric limitations. It determines the size of the objects that are observed and may be seen as an observation box of different sizes. **High  $q$**  (Wide angle X Ray Scattering (WAXS)) domains

corresponds to probing interfaces between two media, at very small scale, with a small observation box. For decreasing values of  $q$ , the box is increased such that bigger scales are investigated, and information about the structural order of the material can be obtained. For very low scattering angles, Small Angle X-Ray Scattering (SAXS) is used to study structures on the nanometer to 50nm scale. These different accessible scales are illustrated in Figure 15.

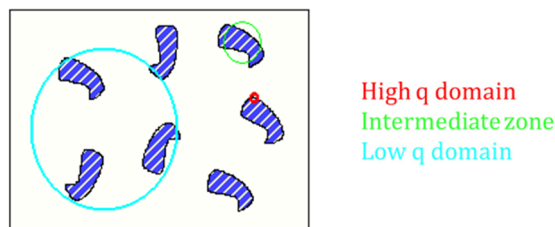


Figure 15 Illustration of the different  $q$  domains to analyze different space scales

This technique is used for any type of material showing electronic density fluctuations, from well-defined crystals to metals and polymers.

## ii. Data analysis

### Scattering 2D image

A 2D image is collected on the detector, as shown on Figure 16. The latter is composed of several (10) plates, hence the black lines (corresponding to blind detection) observed on the image.

The black dot (zoomed on the right image) corresponds to the beam stop, a piece of 3mm-thick metal cover that is set to absorb the X-Ray beam that crossed the sample without any scattering. The scattering vector  $q$  is related to the angle between each point on the detector to the middle of the transmitted beam.

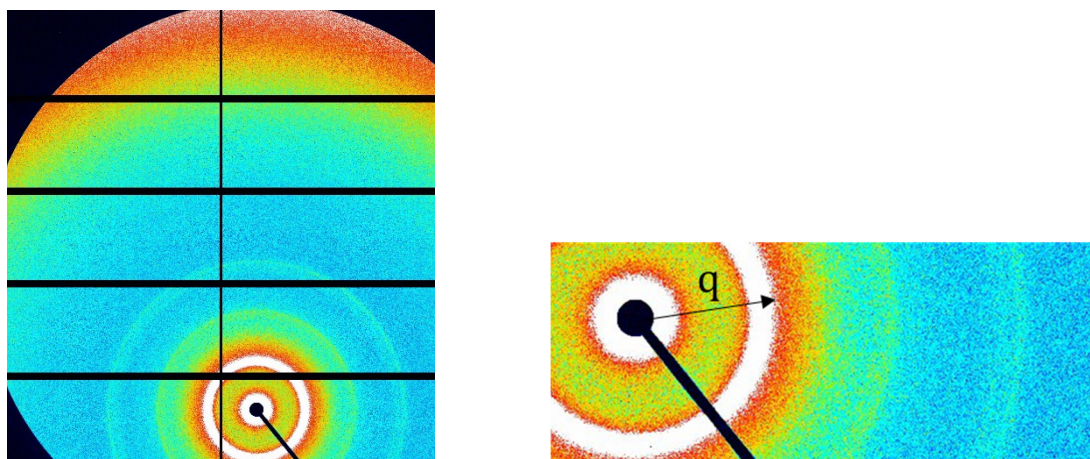


Figure 16 X-Ray scattered image of NBR. Right: Zoom on the beam stop

This is the raw scattering image of the sample.

### Processing towards 1D

If the scattering is isotropic the data can be reduced into one dimension. All the intensities of the points with the same distance to the beam center (covered by the beam stop shown as the black dot) are merged and divided by the total number of pixels at the same scattering angle  $\theta$  that have been added up. A correction removing heterogeneities coming from the detector (blind lines and aberrant pixels) must be applied simultaneously.

To be able to deduce information regarding the material, one must also process the 2D image to take into account the electronic background (all the measured signal does not come from X-Ray radiation) and the empty beam (measured on an empty container). 1D data will be corrected from the transmission (ratio between the transmitted beam through the sample and the empty beam).

The modulus of the scattering vector, simply named  $q$ , is defined as:

$$q = k_1 - k_0 = \frac{4\pi \sin \theta}{\lambda} \quad 3.1$$

Where  $2\theta$  is the scattering angle and  $\lambda$  the X-Ray wavelength.

According to Bragg's law,

$$2d \sin \theta = \lambda \quad 3.2$$

We can determine the characteristic sizes  $d$  of ordered structures (or, more specifically the interdomain spacing) by:

$$d = \frac{2\pi}{q} \quad 3.3$$

### **2.2.2. Methodology**

During this study, the tests were performed at the *Laboratoire Léon Brillouin* in the Commissariat à l'énergie atomique et aux énergies alternatives (CEA, Saclay) with Annie Brulet, on a Xenocs-Xeuss 2.0 with a Pilatus detector. The X-ray source used a copper anode  $K\alpha$  radiation of wavelength 1.54159 Å. The distance between the sample and the detector could be manually adjusted from 15cm to 2m, and a wide range of  $q$  values were thus accessible. A unique curve for all  $q$  values was concatenated.

The samples were 1mm thick and prepared in a press at room temperature to avoid any temperature effect.

### **2.2.3. Comparison of the different materials**

SAXS measurements were first performed on the three samples: as-received, extruded and dissolved NBR. Figure 17 shows the X-Ray scattering profile of dissolved NBR and confirms the development of structures inside NBR at different length scales. The different peaks are shown with arrows and explained below. Dissolved NBR is compared to freshly extruded rubber in Figure 18, and to as-received (raw) NBR in Figure 19.

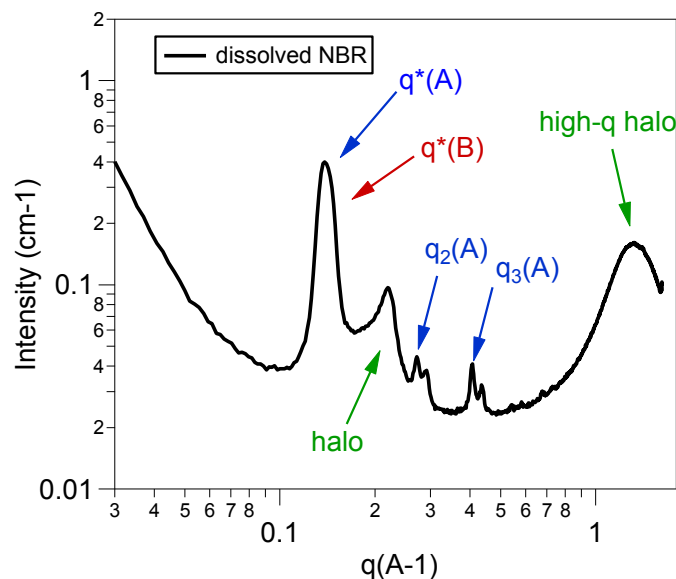


Figure 17 SAXS measurements on dissolved NBR. Arrows show the different characteristic peaks of the structure

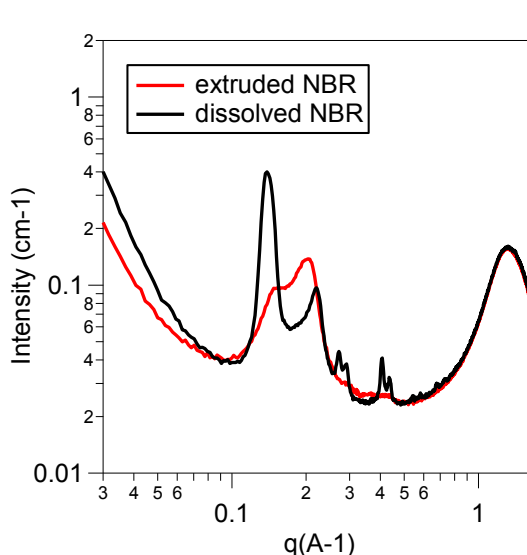


Figure 18 SAXS measurements on extruded and dissolved NBR

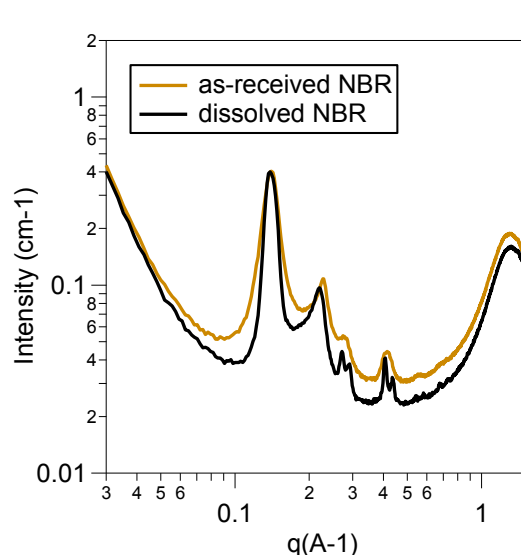


Figure 19 SAXS measurements on as received NBR and dissolved NBR

At very large  $q$ , corresponding to WAXS measurements, an amorphous halo (“high- $q$  halo”) is observed with a broad peak at  $1.348 \text{ \AA}^{-1}$ , corresponding to a characteristic distance of  $4.66 \text{ \AA}$ . Such length is attributed to few C-C bonds (typically  $1.2$  to  $1.5 \text{ \AA}$ ), or C $\equiv$ N bonds ( $1.5$  to  $2 \text{ \AA}$ ).

For intermediate values of  $q$ , from  $0.1$  to  $0.6 \text{ \AA}^{-1}$ , NBR tends to form two lamellar structures, referred to as “lamellae A” and “lamellae B”, of nanometric sizes. Indeed, three orders of organization are visible, with  $q/q^*=1, 2, 3$  and  $q^*(A)=0.1366 \text{ \AA}^{-1}$  and  $q^*(B)=0.1458 \text{ \AA}^{-1}$ . As  $d=2\pi/q$ , the characteristic sizes of these structures are respectively  $4,6$  and  $4,3 \text{ nm}$ . The first peak  $q^*(B)$  of structure B is not clear as it is included in the first major peak of structure A, but a small shouldering is observed and the existence of the structure is confirmed by the presence of  $q_2(B)$  and  $q_3(B)$  at higher scattering vectors. These lamellar structures exist in both the raw “as-

received" NBR, and the dissolved one, which is consistent with the similar mechanical properties probed in the previous section. Yet the peaks are narrower after dissolution, indicating a better defined organization. The extruded sample does not show any regular structure but still exhibits poorly defined peaks. This suggests that most of the structure was partially destroyed by the extrusion, and since it was brought from 120°C (extrusion temperature) to room temperature instantaneously it is frozen in an out-of-equilibrium state.

The results are summarized in the following table:

Materials	Characteristic distances (nm)						2.8	0.48
	4.5	2.2	1.5	none				
As-received	4.5	2.2	1.5	none			2.8	0.48
Extruded	<b>Halo at 4.2</b>			none			3.1	0.48
Dissolved	4.6	2.3	1.5	4.3	2.1	1.4	2.9	0.48
<b>Explanation</b>	Lamella A			Lamella B			Weakly defined structure	Amorphous halo Atom interaction

Table 2 Summary of the observed structure in SAXS

The rubber supplied from Sigma-Aldrich also shows a lamellar structure (but only one), with a characteristic size of 3.8nm, and its scattering profile is plotted on Figure 20. This structure is not modified by the extrusion process (within the experimental conditions studied).

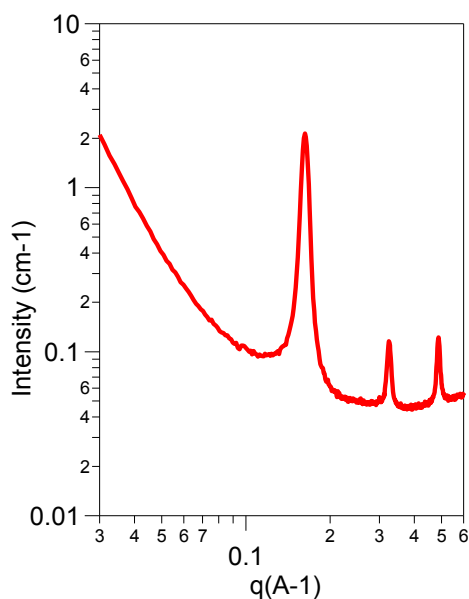


Figure 20 SAXS measurements on NBR-SA

#### 2.2.4. Influence of time and temperature on the microstructure of NBR

To correlate NBR microstructure with the materials' properties, the evolution of the X-Ray scattering profile with time and, separately, with temperature was investigated.

##### i. Effect of temperature on the SAXS profile of dissolved NBR

Fusion of specific zones were observed by DSC measurements between 80°C and 85°C. Therefore, SAXS experiments were run at 85°C to correlate the thermal measurements with the material's structure. The results are shown on Figure 21 and indicate that heating up to 85°C leads to the destruction of the first lamellar structure A, but does not influence the second one (B). The former seems to disappear for the benefit of the poorly defined peak at  $q=0.22\text{Å}^{-1}$ . These results are consistent with the loss (melting) of a structure at high temperature in DSC.

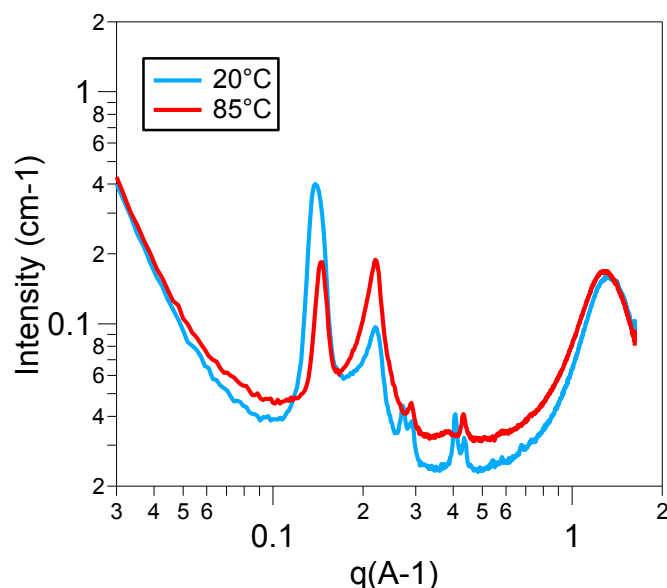


Figure 21 SAXS measurements on dissolved NBR. Blue: room temperature. Red= After heating at 85°C for 20 minutes

At high scattering vector  $q=1.3\text{\AA}^{-1}$ , the amorphous halo is slightly shifted towards bigger sizes (smaller scattering vectors), from 4.8 to 5 Å. The change in the material's structure at high temperature was suggested by Sokolova and coworkers [17]. These temperatures (80-90°C) not only correspond to the  $T_g$  of polyacrylonitrile but are also of the order of the melting temperature of 1,4-trans polybutadiene. Therefore, it is reasonable to suggest that the change in structure is possible due an increase in polyacrylonitrile's mobility and/or melting of 1,4-trans polybutadiene microblocks at this temperature(it will be shown section 2.4 that there are 58% of 1,4-trans butadiene in the studied material).

In light of the DSC measurements, the same thermal effect on the microstructure of NBR-SA was sought at 110°C. The structure of NBR-SA is not modified after remaining two hours at 110°C, and it is reasonable to assume that due to its higher (44%) acrylonitrile content, the structure of this NBR is more stable than that of raw NBR.

ii. Effect of ageing on the SAXS profile of freshly extruded NBR

As was previously shown, the structure is strongly disrupted during the extrusion process and has no time to re-organize during the fast cooling from extrusion temperature to room temperature. Figure 22 compares the scattering profile of freshly extruded NBR and that of the same sample aged during two months at room temperature. It is shown that after two months ageing at room temperature, the material self-organizes into two lamellar structures, which corresponds to its equilibrium state. The microstructure of aged and dissolved NBR are similar.

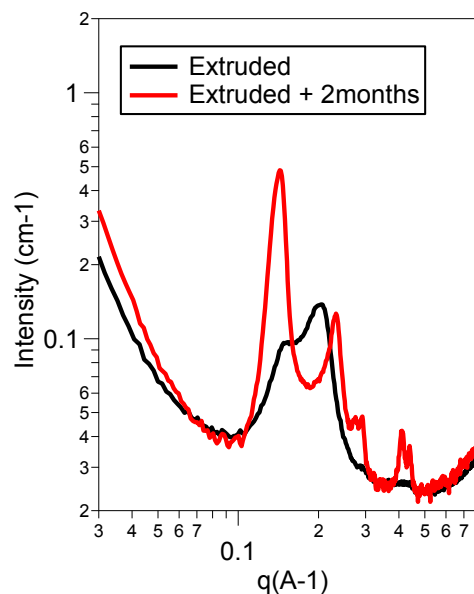


Figure 22 SAXS measurements of NBR after extrusion (black curve) and after extrusion & ageing 2 months at room temperature (red curve)

### iii. Comments

The existence of lamellar structures with two characteristic sizes can be due to the materials wide composition dispersion. Indeed, NBR is industrially synthesized using radical emulsion polymerization, and it is likely that the 33% acrylonitrile content measured is only an average. Chains with more or less acrylonitrile units coexist, and could explain their ability to form different sizes of structures. One of these structure is metastable and is annihilated with high temperature. It is fair to assume that Sigma-Aldrich samples are synthesized with more control, and that the dispersion in composition of the polymer chains is less important, hence a unique lamellar structure, stable at high temperature.

## 2.3. Atomic Force Microscopy

### 2.3.1. Instrumentation

Atomic force microscopy (AFM) is a scanning probe microscopy that gathers surface information by recording interactions between a mechanical probe –attached to a cantilever- and the aforesaid surface. Analysis were performed on an Icon device from Bruker, with a NanoScopeV controller. During this study, AFM was used in tapping mode, for which the probe oscillates at a given frequency (around 300kHz) close to, and below, resonance. When approaching the surface, the probe-surface interactions will modify the oscillations characteristics (amplitude, phase) and give information on the mechanical properties of the sample (in addition to the height profile). The phase images were analyzed to characterize the change in mechanical properties at the surface.

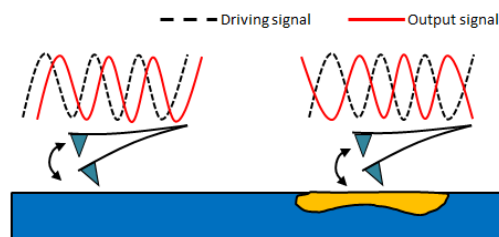


Figure 23 Illustration of AFM microscopy in tapping mode

### 2.3.2. Results

Raw aged NBR samples were molded (0.5mm-thick mold) under a heated press at 100°C, 50bars for an hour and then cooled down to room temperature still under 50 bars. Siliconized paper was used to avoid any adhesion on the press. Pictures were taken at different length scales (2, 1 and 0.5 microns) with scanning angles between 0 and 90°, with 512 points per line, and scanning frequencies between 2 and 4 Hz. Height profiles (right column) as well as phase differences (left column) are shown in Figure 24. For each length scale, it was checked that the profiles were similar at ten different locations, on different samples. The results are thus characteristics of the material. The observed structures are highly dependent on the imaging conditions. Indeed, the probed volume strongly depends on the tapping conditions.

#### i. Height profiles

Height profiles are shown at different length scales, and have been flattened to have an average height of 0. Results show that the samples hardly show any roughness, and that the surface is “clean”, i.e. that no objects are adsorbed on it.

#### ii. Phase difference

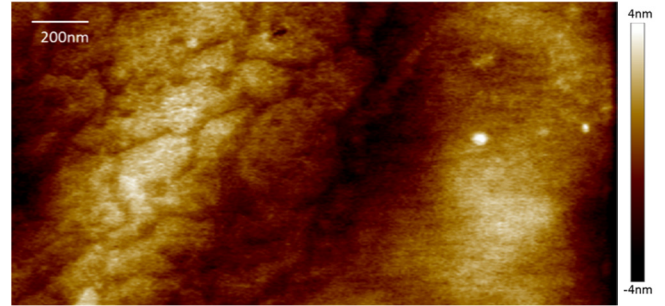
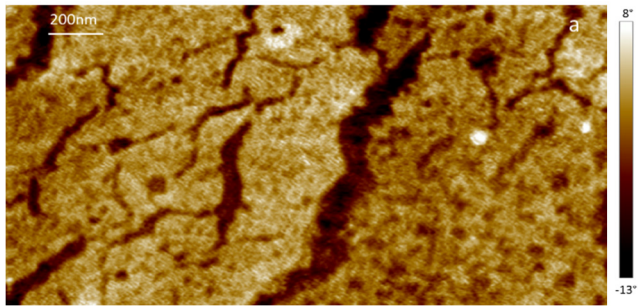
Pictures were taken in repulsive tapping conditions. They were all flattened and corrected around an average position  $\varphi_0$  (with  $\varphi_0 \sim 15^\circ$ ) and thus reveal phase differences.

The material’s anisotropy is demonstrated, and demonstrates the existence of lamellas. Thanks to profiles lines (as shown in picture b), a periodic distance between lamellas of  $6.3 \pm 1.2\text{nm}$  could be estimated. Despite the uncertainty inherent to the AFM measurements, the probed distance is consistent with that of X-Ray scattering.

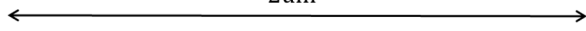
Moreover, to make sure that the observed structures are not artefacts due to oscillations of the tip of the mechanical probe, complementary measurements were done. First, scans were performed at different frequencies (1 and 2Hz) and it was checked that the lamellas’ period remained constant. Also, the bottom pictures (c and d) on Figure 24 show that when the scanning angle changes (from 50° to 80°), the lamellas orientation changes accordingly confirming that the objects are observed on the surface of the material.

**Phase differences**

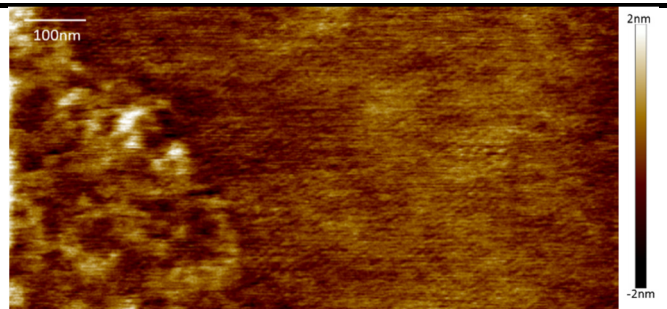
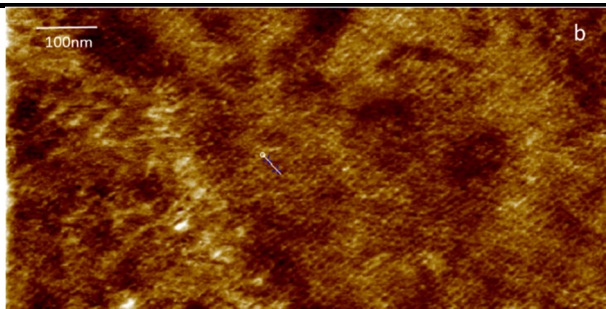
**Height profiles**



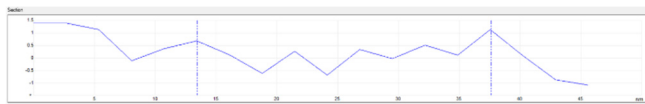
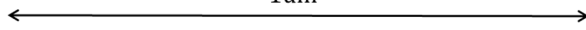
2um



(a) 2um,  $\vartheta=90^\circ$ ,  $f=4\text{Hz}$ . Left: phase difference. Right: height profile.

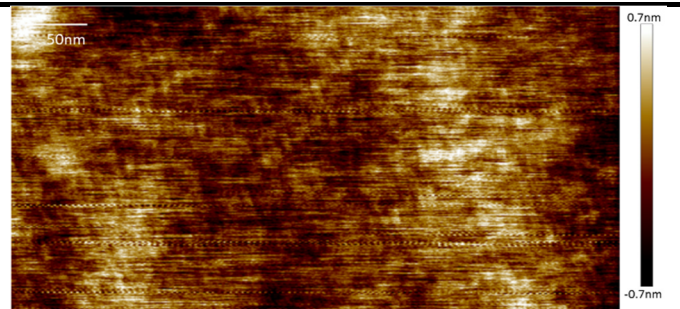
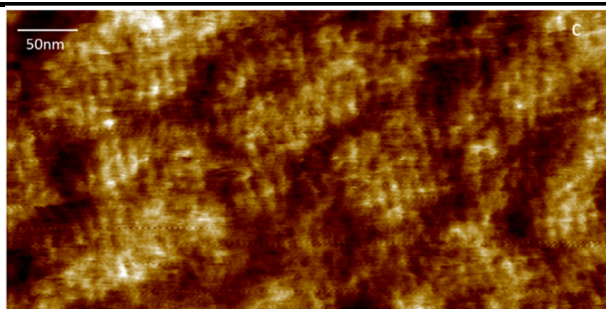


1um

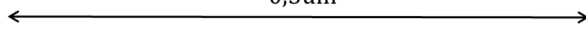


Intensity profile

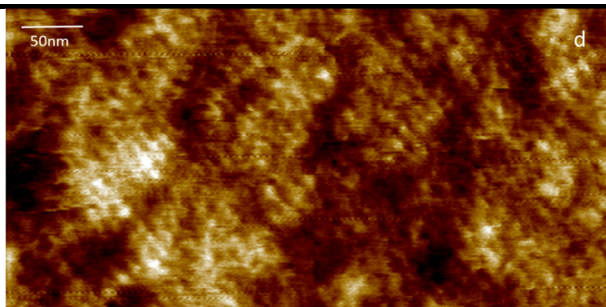
(b) 1um,  $\vartheta=50^\circ$ ,  $f=2\text{Hz}$ . Left: phase difference. Right: height profile.



0,5um



(c) 500nm,  $\vartheta=50^\circ$ ,  $f=2\text{Hz}$ . Left: phase difference. Right: height profile.



(d) 500nm,  $\vartheta=80^\circ$ ,  $f=2\text{Hz}$

Figure 24 AFM pictures of aged NBR. **a** :2um,  $\vartheta=90^\circ$ ,  $f=4\text{Hz}$ ; **b**:1um,  $\vartheta=50^\circ$ ,  $f=2\text{Hz}$  **c**: 500nm,  $\vartheta=50^\circ$ ,  $f=2\text{Hz}$  **d**:500nm,  $\vartheta=80^\circ$ ,  $f=2\text{Hz}$

## 2.4. Transmission Electron Microscopy

### 2.4.1. Method

Transmission Electron Microscopy (TEM) is a microscopy technique in which a high energy beam of electrons is transmitted through the sample to analyze. The interactions between the electrons and the sample's atoms are used to observe its structure. The TEM sample must be thin enough to transmit sufficient electrons to form an image with minimum energy loss.

During this study, the samples were prepared and analyzed by Ingrid J. Paredes from the Department of Chemical and Biomolecular Engineering of New York University, which we acknowledge for this work.

A 0.3wt% solution of NBR in toluene was prepared and coated on a TEM grid. The sample was dried during two days at room temperature, and for two days at 70°C in a vacuum oven. The analysis were performed at 120kV.

### 2.4.2. Results

Figure 25 shows the TEM picture of NBR, and reveals the presence of well-defined lamellas on the dark zones, but not in the lighter parts. It is hard to interpret the zones' contrast in terms of composition since this effect can also be due solely to thickness disparity.

The distance between the lamellas was roughly estimated with the software ImageJ. The average distance was found to be 5.2 +/- 0.9 nm, which is consistent with AFM and SAXS results despite the uncertainty inherent to the measurement method.

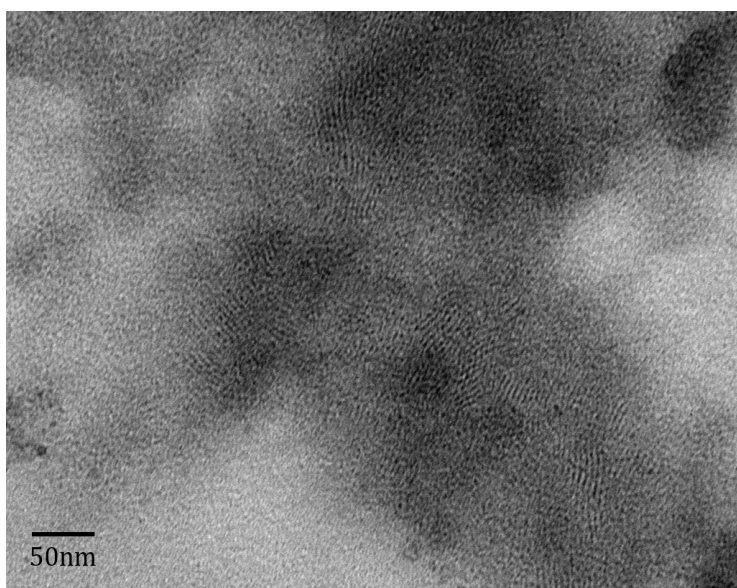


Figure 25 TEM picture of NBR coated from a 0.3% solution in toluene

## 2.5. <sup>1</sup>H NMR study

### 2.5.1. Method

Nuclear Magnetic Resonance (NMR) spectroscopy is used to observe local magnetic fields around atomic nuclei. After placing the sample in a magnetic field, the study of the resonance frequency gives details about the electronic structure and the functional groups of a molecule.

The  $^1\text{H}$  spectra were recorded at room temperature on a Bruker 400 spectrometer at 400MHz. Solutions of 1.6wt% of NBR in deuterated chloroform were prepared.

The spectra were analyzed in light of Anachkov [18] and Ono [11] in order to determine the molecular statistics of the studied NBR. The  $^1\text{H}$  signals of acrylonitrile (named "A") and of butadiene units ("B") highly depend on their neighbors and therefore enable the determination of the monomer sequence distribution. The average contents of each unit were calculated from the area of the signals.

### 2.5.2. Results

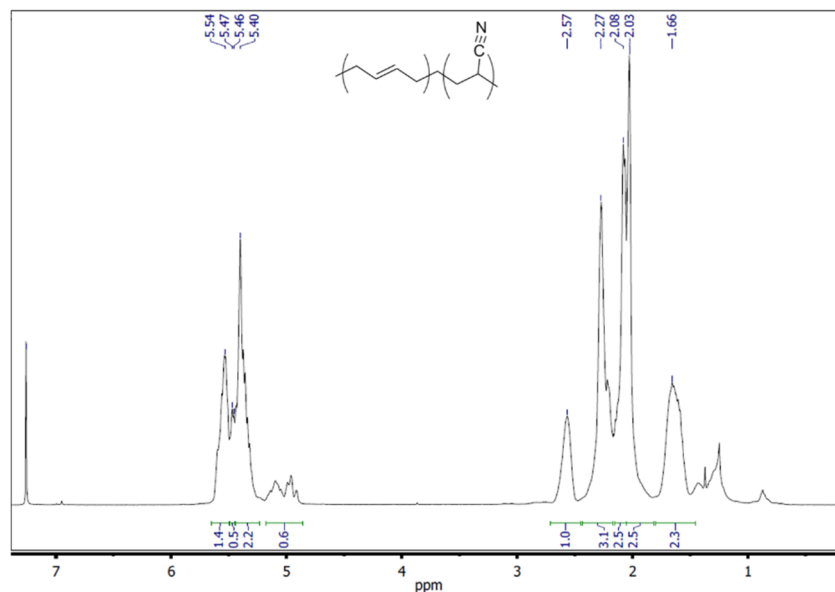


Figure 26  $^1\text{H}$  NMR of NBR in  $\text{CDCl}_3$

As observed in Ono et al [11], no methine (CH) signal of AAA at 3.1ppm, nor signal of BAA sequence at 2.85ppm, are observed. Therefore all the acrylonitrile units in the studied NBR are located between two butadiene units. The double bond methane protons of butadiene are observed in the 5.0 – 5.7ppm region. According to the literature [18], the signals between 5.20 and 5.43ppm are attributed to BBB sequences of 1,4-butadiene. The doublet at 5.46-5.48ppm correspond to a BBA sequence and that of 5.5-5.65ppm to ABA ones. According to Anachkov, the multiplet at 4.88-5.02 ppm as well as signals in the 5.02-5.20ppm region can be attributed to 1,2-butadiene. We can therefore assess that the butadiene units in our materials are for the large majority (87.2%) 1,4 units, and for a small amount (12.8%) 1,2 units.

Comparing methine protons of acrylonitrile and those of butadiene, we are able to determine that the material contains 29.9% units of acrylonitrile. The molecular statistics of NBR are summarized in Table 3.

			Acrylonitrile			1,4 butadiene			1,2 butadiene
	ACN	BU	BAB	BAA	AAA	BBB	BBA	ABA	
<b>Molar ratio %</b>	<b>29.9</b>	<b>70.1</b>	<b>29.9</b>	<b>0</b>	<b>0</b>	<b>33.2</b>	<b>7.53</b>	<b>21.16</b>	<b>9.09</b>

Table 3 Summary of the triads of acrylonitrile (A) and butadiene (B) in the studied NBR

In order to determine the ratio between *cis* and *trans* double bonds, the separate analysis of the pics at 5.37 and 5.39 (for *cis* bonds) from those at 5.41 (*trans* bonds) is necessary. This task is

quite arduous as the peaks are overlapping but it is estimated that there are 2/3 of *trans* double bonds.

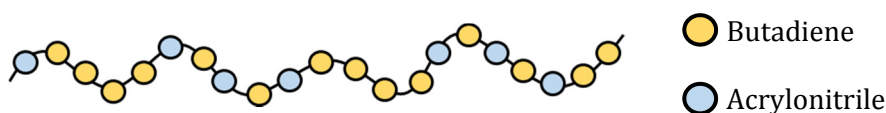
The overall composition of the industrial NBR of this study is shown in Table 4 below:

Acrylonitrile %	Structure of butadiene units		
	1,4- <i>trans</i>	1,4- <i>cis</i>	1,2
29.9	58.2	29.1	12.8

Table 4 Overall molecular composition of the studied NBR

### 2.5.3. Conclusion on molecular statistics

The studied NBR is not, as initially supposed, random. Acrylonitrile only exists in alternated sequences (BAB) whereas blocks of polybutadiene are present (BBB). Therefore, as suggested by Ono et al, a chain is very likely a succession of blocks of polybutadiene and blocks of alternated sequences. Butadiene units are for the most part (~58%) 1,4-*trans*, which is a very low level compared to that of other authors [12][16] where the studied NBR contained ~80% 1,4-*trans* butadiene units. The glass transition temperatures of this materials were not specified.



## 2.6. Conclusions and discussion

We have shown that NBR tends to form lamellar structures when reaching thermodynamic equilibrium. This equilibrium is reached either by slow ageing at room temperature, or by dissolving the rubber in a good solvent and letting it dry slowly. The effect of temperature on these organized lamellas was probed and it was shown that heating above 80°C destroys one structure. The NMR study revealed that the material is actually not a random copolymer and that there are blocks of polybutadiene in between alternating sequences of butadiene and acrylonitrile. It is suggested that due to the affinity (in particular specific polar interactions between the acrylonitrile units) of the different parts of the blocks, the chains will organize as shown in Figure 27 below:

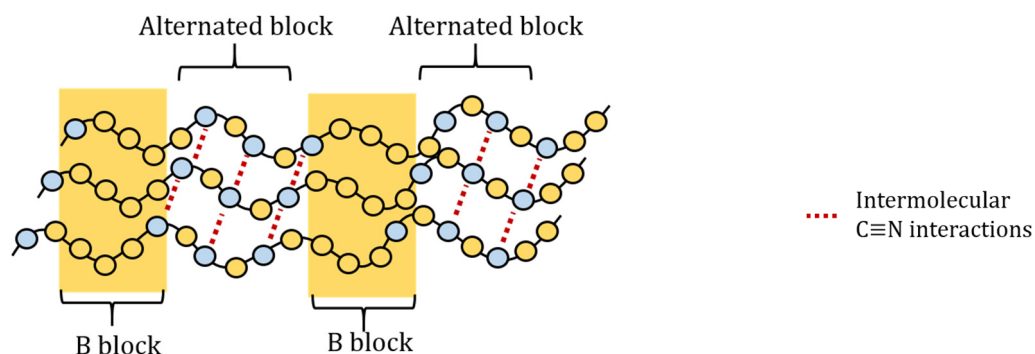


Figure 27 Schematic of the specific lamellar organization in NBR

Makhiyanov and coworkers [19] studied the dependence of polybutadienes composition (as of contents of *cis*-1,4, *trans*-1,4 and 1,2 units) on the polymer's glass transition temperature. From the composition determined with  $^1\text{H}$  NMR and with the use of their data, it could be estimated that polybutadiene blocks in the studied NBR may have a specific Tg close to -95°C. DSC measurements

were run from  $-150^{\circ}\text{C}$  to  $120^{\circ}\text{C}$  and no transition was probe below  $-30^{\circ}\text{C}$ . This lack of polybutadiene signature could be due the facts that the domains are small (nanometers), and that their motion is restricted by the polar interactions of the alternating groups.

### 3. “Self”-adhesion properties

The existence of a microstructure in NBR is of tremendous importance regarding the self-adhesion measurements. Indeed, during the sample preparation, a solution of NBR is coated on the glass slide. The previous results show that this layer has had time to self-organize during slow drying. On the other side, the extruded rubber disk has been molded and reveals no structure (at this length scale). The considered assembly during the tack experiment is therefore not symmetrical (see Figure 28) and cannot be referred to as proper “self-adhesion”.

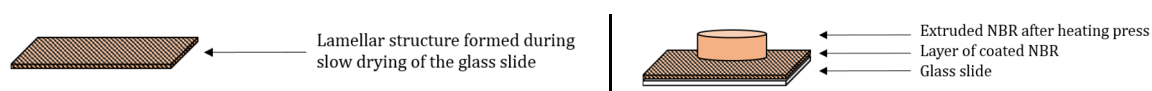


Figure 28 Illustration of a typical tack sample

Left: coated glass slide with lamellar structure. Right: disk of extruded NBR on the top of a coated layer

We showed in Chapter 2 that these self-adhesion properties were weak. The previous section (section 2) demonstrated that NBR was a multi-block copolymer and could self-organize into lamellar structures. Therefore, to understand the tack results, we first present an introduction on block copolymers and on their diffusion.

## 3.1. Literature on block copolymers

### 3.1.1. Introduction to block copolymers

Highly dependent on the protocol and the experimental conditions, the copolymerization of two (or more) monomers can lead to different statistics for the synthesized copolymer: alternating, random, or block copolymers, as illustrated on Figure 29.

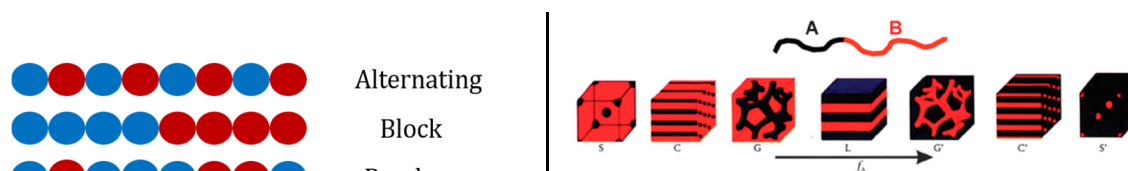


Figure 29 Different possible statistics for a copolymer

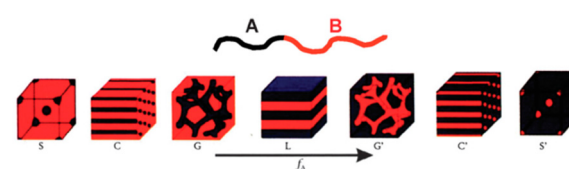


Figure 30 Illustration of different morphologies accessible with diblock copolymers. From [20]

Strong repulsion between unlike sequences occur, even when the free energy penalty of mixing unlike monomers is weak, and tends to force segregation. Yet, as the sequences are chemically bond, complete segregation of the two homopolymers at the macroscopic scale cannot occur. If the monomers are sufficiently incompatible, microphase separation takes place resulting in microdomains enriched in one of the monomers.

The Flory-Huggins interaction parameter  $\chi$  gives an indication of how two monomers A and B repel each other. From a thermodynamic standpoint, microphase separation results from the tradeoff between the enthalpy penalty associated with the creation of contacts between two monomers upon an entropy-driving mixing. As the entropy of mixing for polymers (for a given volume fraction  $\phi$ ) scales as  $N^{-1}$  (with  $N$  the polymerization index), and the enthalpy as  $\chi$ , the thermodynamic state of a block copolymer melt is governed by the product  $\chi N$ . For low values of  $\chi N$ , entropy effects are dominant and favor the formation of an isotropic phase with A and B known as the “disordered phase”. When  $\chi N$  is large, the enthalpic term in the free energy

dominates and the system microphase separates into an “ordered phase” (or mesophase). This has been extensively discussed by Leibler [21] who indeed demonstrated that  $\chi N$  and  $f$  (the volume fraction of monomers A in a chain) are the only relevant parameters to study the onset of an ordered mesophase from a homogeneous phase. Both regimes are separated by a transition known as the “order-disorder” transition (ODT).

Studies by Semenov [22] focused on the thermodynamics of block copolymers in the strong-segregation regime, where there is another trade-off between chain stretching and interfacial area. For the case of a lamellar microdomain structure, this work demonstrated that the domain size scales with  $\chi$  and  $N$  according to the following equation:

$$D = 2 \left( \frac{3}{\pi^2} \right)^{\frac{1}{3}} a N^{\frac{2}{3}} \chi^{\frac{1}{6}} \quad 3.4$$

With  $2D$  the periodicity of the structure and  $a$  the statistical length of a polymer segment.

Applying this formula the NBR structure, the number of monomers in a lamellar repeating unit of typical size 4.6nm could be estimated. Nevertheless, this expression is for block copolymers with a unique monomer composition in each block. In the studied NBR, a block is composed of alternating units of acrylonitrile and butadiene. Therefore, the calculation of the Flory parameter  $\chi$  between both monomers overestimates the enthalpic repulsion of the two blocks in our polymer as the effective  $\chi$  should be lower.

### 3.1.2. Diffusion and self-diffusion of block copolymers

#### i. Diffusion in block copolymers

##### Dependence of diffusion coefficient on $\chi$

It has been widely demonstrated in the literature [23][24][25] that the stronger the segregation between the different phases, i.e. the higher  $\chi N$ , the lower is the diffusion. Figure 31 and Figure 32 illustrate the  $\chi N$ -dependence of the diffusion coefficient  $D$  in sphere- and lamellae- forming block copolymers. The normalization by  $D_0$ , the diffusion coefficient in the disordered phase, enables evaluation of the effect of self-assembly on dynamics.

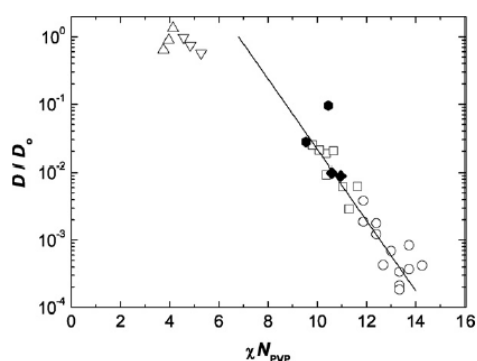


Figure 31 Dependence of the normalized diffusion coefficient on  $\chi N_{PVP}$  of polystyrene-polyvinylpyridine (PS-PVP) asymmetric block copolymers. Figure from [24]

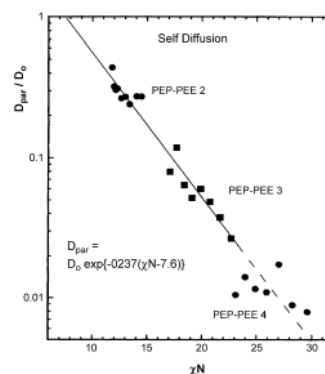


Figure 32 Dependence of the normalized diffusion (in the direction parallel to the lamellar plane) coefficient of poly(ethylene propylene)-b-poly(ethylethylene) (PEP-PEE) on the segregation strength  $\chi N$ . Figure from [23]

We will not discuss the details of the different models that predict the dependence of the diffusion coefficient with  $\chi N$ .

### Different diffusion mechanisms

In block copolymers exhibiting lamellar microstructures, the material's strong anisotropy plays a key role in its self-diffusion properties. Yokoyama and coworkers [25] have summarized the various diffusion mechanisms depending on the symmetry of the ordered phase. Two main types of mechanisms are identified for the diffusion in lamellar structures: hopping diffusion (normal to the lamellar plane), and interfacial diffusion (in plane with the lamellar plane). Hopping diffusion describes the ability of a block copolymer chain to move from one domain and to another. It is therefore strongly influenced by the incompatibility of the blocks, as one of them must be surrounded by the other block during the elementary dynamic step, while paying some energetic penalty. Interface diffusion describes the molecular motion of block copolymers along the interfaces, without disturbing the localization of joints between the blocks, as illustrated in Figure 33.

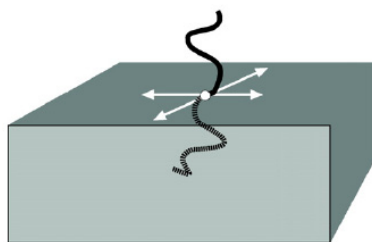


Figure 33 Schematic picture of interface diffusion in lamellar domains. Figure from [25]

While hopping diffusion of diblock copolymers is believed to be primarily controlled by the segregation strength, interfacial diffusion is dictated by entanglements. For untangled systems, interface diffusion occurs via Rouse dynamics, whereas other mechanisms (e.g. activated reptation and block retraction) are also key in the presence of entanglements.

Because of this thermodynamic cost for diffusion in direction perpendicular to the lamellar, the diffusion in this direction is much lower than in the parallel direction [23][26][27].

#### ii. Influence of temperature on diffusion

Due to enhanced molecular mobility, the self-diffusion coefficient increases with temperature. This increase in entropic contribution eventually leads to an order-disorder transition (ODT) during which the block copolymer reaches a disordered state. This transition has been probed by X-Ray and neutron scattering, as well as with linear rheology [28]. However, Shull and coworkers [27] used a model poly(ethylenepropylene)-b-(polyethyleneethylene) (PEP-PEE) to show that the overall diffusion is dominated by the fastest diffusion path in the surface, i.e. diffusion parallel to the lamellas. They compared self-diffusion of PEP-PEE films before and after annealing. Before annealing, due to the lamellas' statistical organization (see Figure 35 (a)) the self-diffusion coefficient of the material is only weakly dependent on the order-disorder transition temperature. No dramatic change in the self-diffusion coefficient is measured at this temperature (Figure 34). These results are in contrast to the temperature-dependence of the low-frequency dynamic shear moduli which is strongly influence by this ODT. Authors explain that in the case of rheological measurements, the diffusion of the bulk is considered, and is governed by the slower perpendicular diffusion coefficient, strongly dependent on the ODT.

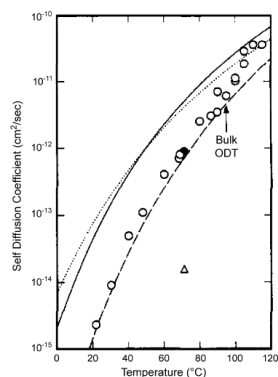


Figure 34 Diffusion coefficient of PEP-PEE block copolymers without thermal treatment (open circles). Fast (solid circle) and slow (open triangle) component of diffusion coefficients after annealing. Figure from [27]

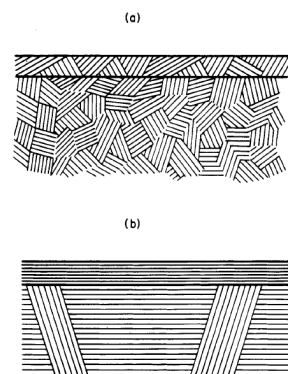


Figure 35 Schematic presentation of the block copolymer bilayer film (a) before preannealing. (b) after preannealing. From [27]

### 3.1.3. Comments

Most of the investigated materials in all the above stated studies are well-defined and monodisperse diblock copolymers. Yet to our knowledge, little has been done on the diffusion of multiblock copolymers. During this thesis, the material's architecture is not controlled, nor is its molecular weight distribution. Moreover, the block structure that has been detected is composed of blocks of polybutadiene, and blocks of alternated acrylonitrile-butadiene units. Therefore, the key parameters for segregation presented earlier does not apply here. Finally, strong physical interactions occur between the polar acrylonitrile groups, thus modifying even more the diffusion dynamics.

## 3.2. Influence of NBR structure on its self-adhesion properties

Chapter 2 showed the poor self-adhesion properties of NBR, and the beginning of this chapter revealed the buildup of a structure when reaching thermodynamic equilibrium. To investigate the influence of this organization on the tack properties of NBR, probe-tack tests were run to compare freshly extruded NBR to the as-received rubber.

The approaching speed  $V_{app}=30\mu\text{m/s}$  and the debonding speed  $V_{deb}=10\mu\text{m/s}$  were kept constant during the whole study.

### 3.2.1. Self-adhesion at room temperature

A scheme of the two compared systems is shown on Figure 36. In both cases, the glass slide was coated with the material, and is therefore structured. The main difference lies in the rubber disk on the top. In the first (red) case, NBR was freshly extruded and is therefore free of any structure. In the second (blue) case, the disk is made of as-received NBR, i.e. structured. The "self" adhesion properties were probed for contact times going from two hours to a week, and the evolution of the self-adhesion energy as a function of time is shown on Figure 37.



Figure 36 Illustration of the two self-adhesion samples. Left (red): disk of extruded NBR. Right (blue): disk of raw NBR. In both cases, the glass slides are coated and dried slowly.

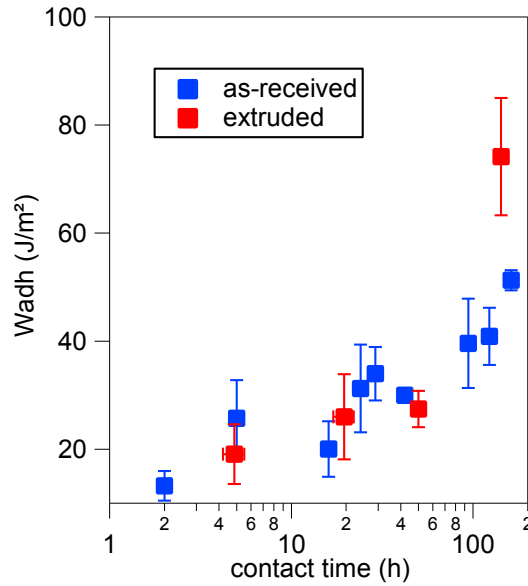


Figure 37 Comparison of the evolution of the self-adhesion energies  $W_{adh}$  of as-received and extruded NBR with contact time

For contact times lower than a week (168 hours), the two materials show similar adhesion properties. The measured adhesion energy is relatively low ( $<100\text{J/m}^2$ ) and implies that very few chains are able to diffuse at the interface. This experiment demonstrate that, in this case, the adhesion properties are limited by the structured side. For very long contact times, it seems that few chains from the extruded side are able to diffuse, slightly increasing the adhesion energy of the extruded NBR.

### 3.2.2. Comparison with adhesion on glass

The methodology is the same, but instead of coating NBR on the glass slide, it was only cleaned with acetone and dried before establishing contact with the rubber disks.



Figure 38 Illustration for the sample of NBR adhesion to glass

The effect of contact time on the adhesion properties of NBR on glass was probed and the results are shown in Figure 39. A light increase of adhesion properties with time is observed due to a strengthening of the interface, which has two possible causes. The first one is an increase in the effective contact area due to some flow of the material at the microscopic scale. Yet in Figure 39, the cavitation peak remains close to 0.4MPa, revealing no clear increase of the contact area at the macroscopic level. The second explanation lies in the rearrangement of polymer chains at the interface to maximize favorable interactions with the glass substrate. Indeed, no diffusion of polymer chains at the interface is possible, but nitrile chains can re-orient to expand the physical interactions between the polar groups of acrylonitrile and those of silica in glass.

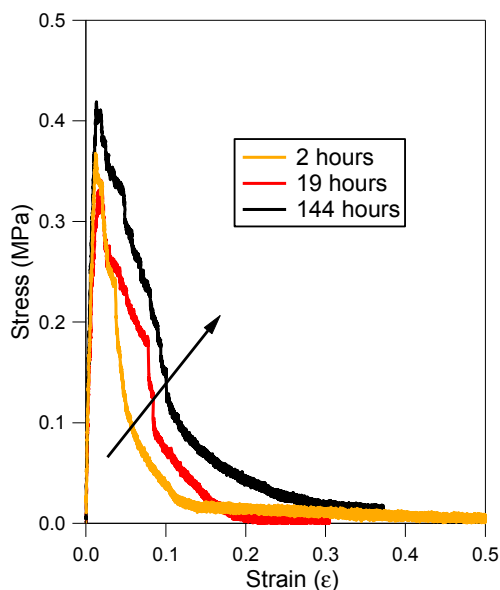


Figure 39 Effect of contact time on the adhesion properties of NBR on glass

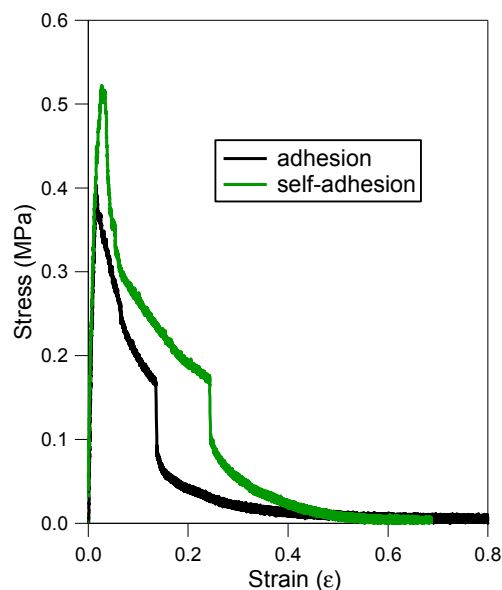


Figure 40 Comparison of adhesion on glass and self-adhesion properties of NBR, contact time=6 days

The adhesion energies measured are of the order of  $30\text{J}/\text{m}^2$  and are slightly lower than that of self-adhesion for the same contact time, as illustrated in Figure 40. Because of the structure on the coated NBR, no (or very little) diffusion of NBR chains is possible. The difference between adhesion and self-adhesion of NBR is therefore probably due to a difference in the strength of physical interactions between 1.  $\text{C}\equiv\text{N}$  and  $\text{C}\equiv\text{N}$  bonds and 2.  $\text{C}\equiv\text{N}$  and Si-O groups.

### 3.2.3. Self-adhesion of NBR at higher temperatures

In order to boost the diffusion of chains across the interface, the effect of temperature was probed. This study was performed on as-received NBR.

#### i. Method

Two strategies were considered: the contact between the two materials could either be done at room temperature and then heated to high temperatures, or made directly at the desired temperature. In order to always have the same contact conditions, and to avoid light flow of the material under pressure at high temperature, the methodology used for the sample preparation at room temperature was maintained. Hence, the contacts were formed at ambient temperature during an hour under light pressure, and the samples were then set into an oven for an hour without any load. They were let at room temperature for cooling for an extra 45 minutes and then tested at room temperature. Temperatures between  $40$  and  $120^\circ\text{C}$  were probed and the results are compared to room temperature experiments.

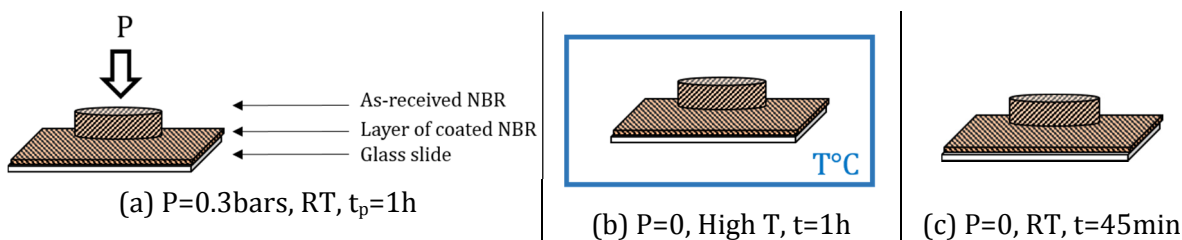


Figure 41 Protocol to characterize the effect of temperature on the self-adhesion properties of NBR: Contact with load  $P$  during 1h (a), sample in oven for 1h (b), sample let at RT for 45min

ii. Results

The stress-strain curves for the debonding stage are shown on Figure 42.

The self-adhesion properties for a 1-hour contact at 40°C are similar to those at room temperature. All the debonding curves are, for each temperature, fairly reproducible, except for 60°C. Indeed, samples that have spent an hour at this temperature show a wide range of debonding properties and the self-adhesion energies range between 70 and 270 J/m<sup>2</sup>. For contact temperatures higher than 80°C, fibrils are formed and large deformation is possible during the debonding stage. The self-adhesion energies for 1-hour contact are plotted as a function of temperature on Figure 43 and show this sharp increase around 80°C.

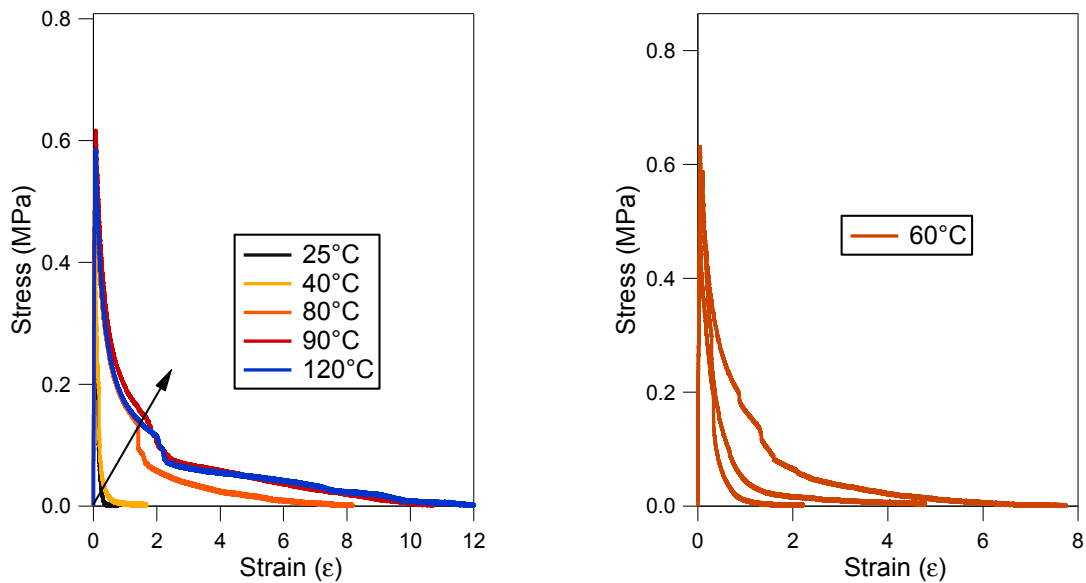


Figure 42 Stress-strain curve during the debonding of as-received NBR self-adhesion samples that have been let for an hour at high temperature. Comparison of the probed temperature (left). Reproducibility on the 60°C-heated sample (right)

These results need to be explained in light of the X-ray scattering and DSC experiments. Indeed, it was shown that an endothermic phenomena occurred close to 80°C and that heating above this temperature disturbed one of the two lamellar structures. This suggests that this structure was responsible for the slow diffusion of polymer chains at the interface. When heating above this temperature, more mobility is given to the macromolecules due to enhanced mobility of acrylonitrile groups above their glass transition temperature, and to presumed melting of 1,4-trans polybutadiene crystallites. These results are consistent with the work of Bartenev et al [3][4] on the relaxation transitions in NBR. They showed the existence of a high-temperature transition that they associated with the breakage of polar C≡N dipole-dipole interactions. In fact, the increase in self-adhesion properties at high temperature could be explained by the disruption of the physical intermolecular interactions.

The resulting self-adhesion energies  $W_{adh}$  are plotted as a function of contact temperature  $T$  for a fixed contact time, debonding velocity and debonding temperature in Figure 43. The observed trend is very similar to that of Bidaux and coworkers [29] shown in Figure 44. During their study, they used temperature to bond maleic anhydride-g-polypropylene (PPg) to polyamide 6 (PA) and showed that the strain energy release rate  $G_c$ , measured by a fracture test, increased with bonding temperature with two well defined transitions. These transitions match the melting temperatures

of PPg and PA and demonstrate that for the two materials to adhere, chain migration is needed, and therefore melting of the crystallites in both sides is necessary. The Bidaux paper describes a different system (semi-crystalline polymers) yet our material shows an analogous behavior, i.e. a well-defined structure that melts at high temperature, and its adhesion properties evolve with the same tendency.

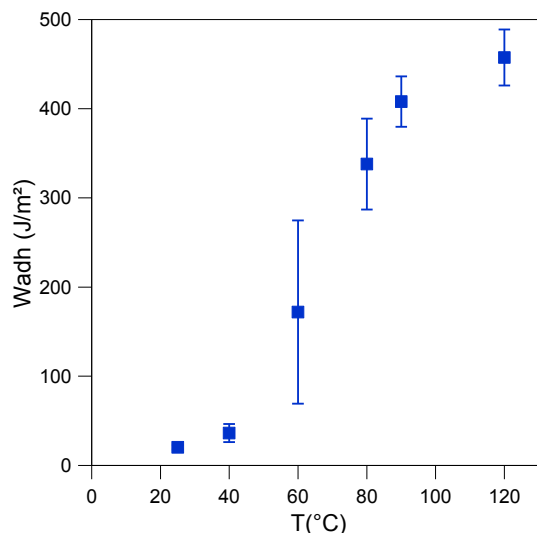


Figure 43 Influence of temperature on the self-adhesion energies of as-received NBR

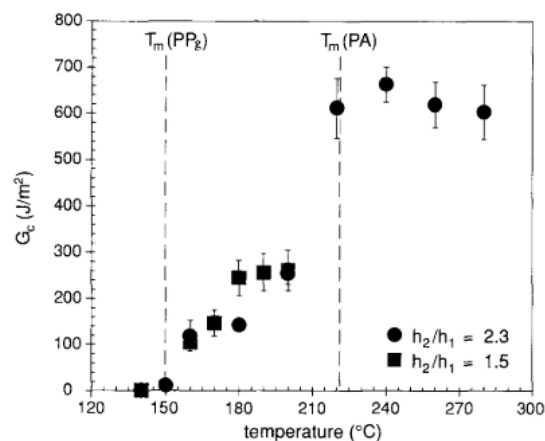


Figure 44 Evolution of the critical strain energy release rate  $G_c$  between PPg and PA as a function of bonding temperature.  $T_m$ : melting temperature. Figure from [29]

Linear rheology showed previously that the material did not flow, and that no particular shift in mechanical properties were observed at these temperatures. These results are a first insight into the non-equivalence between viscosity and diffusion for this multi-block copolymer.

### 3.3. Self-adhesion properties of freshly extruded NBR

It was concluded above that the structure on the glass slide limits the self-adhesion properties of nitrile rubber at room temperature. When this structure is disturbed, at high temperature for example, chain migration is possible at the interface. Therefore, a new method is considered in order to probe the self-adhesion properties of freshly extruded NBR on both sides, i.e. without any structure. Adhesion energies of the order of those observed for samples welded at high temperatures ( $>300\text{J/m}^2$ ) are expected.

#### 3.3.1. New method

In order to avoid any structure formation on the glass slide, dissolution and slow drying of the material must be avoided. The preparation process is described below, and the comparison between both methods is illustrated in Figure 45.

The extruded NBR was molded under a heating press for an hour at  $100^\circ\text{C}$  and 50bars, and then cooled to room temperature at 50 bars for another hour. The mold used was 0.3mm thick. A 1cm wide, 5cm long rubber layer was cut and glued (using Loctite 406) to the glass slide. Punches of 0.8mm diameter were cut and placed on the layer. The contact was, in both methods, established thanks to the same load as that of Chapter 2.

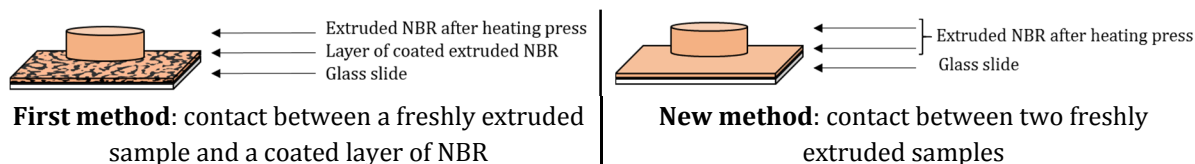


Figure 45 Comparison of the two methods to probe self-adhesion properties of extruded NBR

The overall thickness of the system was approximately 0.6mm. As a reminder, in the previous method the total thickness was close to 0.5mm. These were systematically measured before testing the materials' self-adhesion properties, and were taken into account to compute the strain and the adhesion energy.

### 3.3.2. Results

The self-adhesion properties were probed at two contact times: two and twenty-four hours. The stress-strain curves for the debonding process, for  $t_c=24$ hours are shown on Figure 46. The new system gives slightly higher self-adhesion energies, especially thanks to an increase in the contact area. This is quite surprising as the system's overall roughness is increased with this new "extruded-extruded" method, and could therefore reduce the effective contact area between both materials. Furthermore, no increase in the strength of adhesion with time is observed, and the energy associated to this debonding process is of the order of  $50\text{J}/\text{m}^2$ , well below the foreseen  $300\text{J}/\text{m}^2$ .

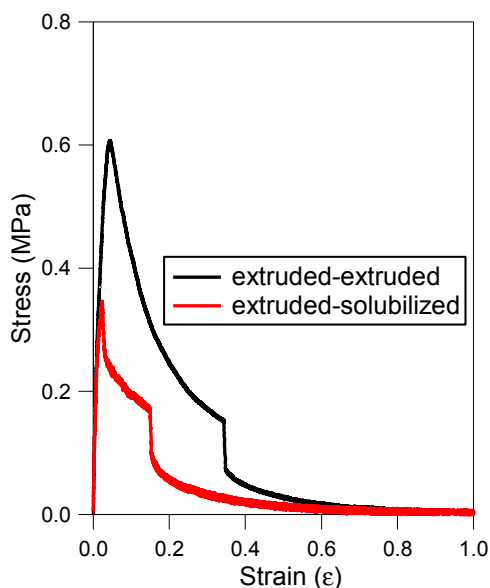


Figure 46 Debonding stress-strain curves for 24h contact time. Comparison between the two methods

### 3.3.3. Discussion

Linear rheology measurements revealed a change in behavior at low frequencies (crossing of the  $G'$  and  $G''$  curves) suggesting that a terminal relaxation time was present for extruded NBR. Additionally, X-Ray scattering experiments revealed a strong disruption of the lamellar structure with extrusion. Therefore, high self-adhesion energy levels were expected with this new method. Yet the measured energies are very low ( $<100\text{J}/\text{m}^2$ ). Several hypotheses can be discussed in order to explain these results. First, only structures of the order of tens of nanometers were probed using X-Ray scattering, and it is not excluded that some organization, that was not completely destroyed with extrusion, also exists on a larger length scale. Also, in both cases, the top disk was

prepared using a heating press at 100°C and the contact was established once the rubber had cooled down to room temperature. It is therefore possible that when heating the freshly extruded sample, some structure is recovered due to preferential rearrangement thanks to increased mobility in acrylonitrile and 1,4-trans butadiene units. This structure limits the self-adhesion of macromolecules with both methods.

#### **4. Conclusions**

Poly(acrylonitrile-co-butadiene), commonly called nitrile rubber or NBR, is a copolymer of butadiene and acrylonitrile, two very different monomers. During this chapter, two of them were compared: an “industrial” NBR, and one received from Sigma-Aldrich. Although their exact composition differs, it was shown that nitrile rubber tends to self-organize with time and that its thermodynamic equilibrium state is a complex structure with at least one lamellar structure. This supramolecular structure was studied by means of linear rheological measurements, and observed with X-Ray scattering, Atomic Force Microscopy and Transmission Electron Microscopy. <sup>1</sup>H liquid NMR revealed that, because of the difference in monomer reactivity, nitrile rubber is not a random copolymer but rather a multi-block copolymer with blocks of polybutadiene and blocks of butadiene units alternated with acrylonitrile. In between the polymer chains, specific C≡N interactions associate acrylonitrile groups and therefore prevents any flow of the polymer chains. This structure is responsible for the weak self-adhesion properties of NBR at room temperature, but it is shown that heating above the melting temperature of the first lamellae causes a significant enhancement of the tack properties.

##### **Take home messages:**

- Ageing of NBR with time : self-organization in lamellar structure(s)
- NBR is a multi-block copolymer with blocks of PB and blocks of alternating PB-ACN
- This microstructure prevents flow of the chains at the interface and explains the weak self-adhesion properties of NBR
- Heating above 80°C disturbs a lamellar structure and greatly enhances self-adhesion properties

## 5. References

- [1] W. A. Geiszler, J. A. Koutsky, and A. T. Dibenedetto, "Amorphous state transitions in butadiene-acrylonitrile copolymers," *J. Appl. Polym. Sci.*, vol. 14, no. 1, pp. 89–102, 1970.
- [2] J. Courtois *et al.*, "Supramolecular Soft Adhesive Materials," pp. 1803–1811, 2010.
- [3] G. M. Bartenev, V. V. Tulinova, and I. V. Razumovskaya, "Relaxational transitions in butadiene-nitrile copolymers according to the data from mechanical relaxation," *Polym. Sci. U.S.S.R.*, vol. 27, no. 9, pp. 2147–2155, 1985.
- [4] G. M. Bartenev, S. V. Baglyuk, and V. V. Tulinova, "Relaxational transitions of poly(butadiene-acrylonitrile) above the glass transition temperature," *Polym. Sci. U.S.S.R.*, vol. 30, no. 4, pp. 834–843, 1988.
- [5] G. Henrici-Olivé and S. Olivé, "Molecular interactions and macroscopic properties of polyacrylonitrile and model substances," pp. 123–152, 1979.
- [6] T. Bai *et al.*, "Construction of an ultrahigh strength hydrogel with excellent fatigue resistance based on strong dipole-dipole interaction," *Soft Matter*, vol. 7, no. 6, pp. 2825–2831, 2011.
- [7] Y. Eom and B. C. Kim, "Solubility parameter-based analysis of polyacrylonitrile solutions in N,N-dimethyl formamide and dimethyl sulfoxide," *Polymer (Guildf)*, vol. 55, no. 10, pp. 2570–2577, 2014.
- [8] Y. Eom and B. C. Kim, "Effects of chain conformation on the viscoelastic properties of polyacrylonitrile gels under large amplitude oscillatory shear," *Eur. Polym. J.*, vol. 85, pp. 341–353, 2016.
- [9] I. E. Climie and E. F. T. White, "The Aggregation of Random and Block Copolymers Containing Acrylonitrile in Mixed Solvents," vol. XLVII, pp. 149–156, 1960.
- [10] S.-Y. Kwak and S. Y. Kim, "Microphase structures of polymers containing structural heterogeneity as probed by nmr spin lattice relaxation analysis.pdf." 1998.
- [11] H. Ono, H. Fujiwara, and S. Nishimura, "Nanoscale heterogeneous structure of polyacrylonitrile-co-butadiene with different molecular mobilities analyzed by spin-spin relaxation time," *Polym. J.*, vol. 45, no. 10, pp. 1027–1032, 2013.
- [12] L. V Sokolova and N. A. Kichaev, "The influence of the structural organisation of nitrile butadiene rubbers on their vulcanisation," no. 6, p. 12535, 2016.
- [13] L. V. Sokolova, A. F. Nepomnyashchiy, and G. A. Tatarinov, "Rotational mobility of the radical probe in butadiene-nitrile rubbers," *Polym. Sci. - Ser. A*, vol. 59, no. 1, pp. 27–32, 2017.
- [14] L. V. Sokolova and A. V. Danchenko, "On the high temperature relaxation transitions in butadiene-nitrile elastomers," *Polym. Sci. U.S.S.R.*, vol. 23, no. 12, pp. 2941–2951, 1981.
- [15] L. . Sokolov, O. . Chesnokova, O. . Nikolayeva, and V. . Shershnev, "On the nature of high-temperature structural transitions in polymers and copolymers of butadiene," *Polym. Sci. U.S.S.R.*, vol. 27, no. 2, pp. 392–403, Jan. 1985.

- [16] N. M. Livanova, S. G. Karpova, and A. A. Popov, "Microstructures and supramolecular structures of butadiene-nitrile rubbers: Paramagnetic-probe study," *Polym. Sci. Ser. A*, vol. 53, no. 12, pp. 1128–1134, 2011.
- [17] L. V. Sokolova and E. V. Matukhina, "Effect of an anionic emulsifier on the structure of butadiene-nitrile elastomers," *Polym. Sci. Ser. A*, vol. 52, no. 4, pp. 383–391, 2010.
- [18] M. P. Anachkov, R. V. Stefanovab, and S. K. Rakovskya, "I H NMR Study of Monomer Sequence Distributions in some Commercial Acrylonitrile-butadiene copolymers," vol. 21, pp. 429–432, 1989.
- [19] N. Makhiyanov and E. V. Temnikova, "Glass-transition temperature and microstructure of polybutadienes," *Polym. Sci. - Ser. A*, vol. 52, no. 12, pp. 1292–1300, 2010.
- [20] H. Feng, X. Lu, W. Wang, N. G. Kang, and J. W. Mays, "Block copolymers: Synthesis, self-assembly, and applications," *Polymers (Basel)*, vol. 9, no. 10, 2017.
- [21] L. Leibler, "Theory of Microphase Separation in Block Copolymers," *Macromolecules*, vol. 13, no. 6, pp. 1602–1617, 1980.
- [22] A. N. Semenov, "Theory of Block-Copolymer Interfaces in the Strong Segregation Limit," *Macromolecules*, vol. 26, no. 24, pp. 6617–6621, 1993.
- [23] T. P. Lodge and M. C. Dalvi, "Mechanisms of chain diffusion in lamellar block copolymers," *Polymer (Guildf)*, vol. 75, no. 4, pp. 657–660, 1995.
- [24] H. Yokoyama and E. J. Kramer, "Self-diffusion of asymmetric diblock copolymers with a spherical domain structure," *Macromolecules*, vol. 31, no. 22, pp. 7871–7876, 1998.
- [25] H. Yokoyama, "Diffusion of block copolymers," *Mater. Sci. Eng. R Reports*, vol. 53, no. 5–6, pp. 199–248, 2006.
- [26] J. L. Barrat and G. H. Fredrickson, "Diffusion of a Symmetric Block Copolymer in a Periodic Potential," *Macromolecules*, vol. 24, no. 24, pp. 6378–6383, 1991.
- [27] K. R. Shull, E. J. Kramer, F. S. Bates, and J. H. Rosedale, "Self-Diffusion of Symmetric Diblock Copolymer Melts near the Ordering Transition," *Macromolecules*, vol. 24, no. 6, pp. 1383–1386, 1991.
- [28] G. H. Fredrickson and F. S. Bates, "Dynamics of block copolymers: Theory and experiment," *Annu. Rev. Mater. Sci.*, vol. 26, no. 1, pp. 501–550, 1996.
- [29] J. E. Bidaux, G. D. Smith, N. Bernet, J. A. E. Månson, and J. Hilborn, "Fusion bonding of maleic anhydride grafted polypropylene to polyamide 6 via in situ block copolymer formation at the interface," *Polymer (Guildf)*, vol. 37, no. 7, pp. 1129–1136, 1996.



# **- CHAPTER 4 -**

## **INFLUENCE OF TACKIFIERS ON THE SELF-ADHESION OF NITRILE RUBBER**

---

Tackifiers are often used to enhance the adhesion and self-adhesion properties of soft materials, yet few investigations have focused on their effects on structured block-copolymers with strong physical interactions. During this chapter, a general introduction on the role of tackifiers in rubbers and phase-separated block copolymers is first presented. The effect of two types of tackifiers on the self-adhesion properties of NBR are then studied at low (3%) and high (>10%) concentrations. These results are explained in the context of both mechanical (in the linear and non-linear regime) and structural (SAXS) analysis.

<b>1. Literature on the blending of tackifiers .....</b>	<b>109</b>
1.1. General picture .....	109
1.2. Influence of the nature and the amount of tackifier.....	109
1.2.1 Influence of the amount of tackifier .....	109
1.2.2 Influence of the nature of the tackifier.....	110
1.3. Additives in phase-separated materials.....	111
1.3.1 Tackifiers in rubbery block copolymers.....	111
1.3.2 Tackifiers in nitrile rubber .....	112
1.4. Conclusion and discussion.....	112
<b>2. Introduction .....</b>	<b>113</b>
2.1. Materials.....	113
2.2. Sample preparation .....	114
2.2.1 Instrumentation .....	114
2.2.2 Extruding conditions.....	114
2.3. Objectives.....	115
<b>3. Blending of 3% tackifier in NBR.....</b>	<b>115</b>
3.1. Self-adhesion properties.....	116
3.1.1 Reproducibility of tack measurements.....	116
3.1.2 Effect of contact time on the adhesion properties .....	117
3.1.3 Comparison between both tackifiers.....	117
3.2. Bulk properties and structure.....	118
3.2.1 Linear mechanical properties of freshly extruded blends .....	118
3.2.2 Uniaxial tensile tests.....	119
3.2.3 X-Ray Scattering .....	120
3.3. Conclusion and discussion.....	120
<b>4. Blending of a high tackifier content in NBR .....</b>	<b>122</b>
4.1. Self-adhesion properties.....	122
4.1.1 At 10 and 20% resin content.....	122
4.1.2 At 40% resin content.....	124
4.1.3 Conclusions.....	125
4.2. Properties of the high concentration blends.....	126
4.2.1 Thermal properties.....	126
4.2.2 Linear mechanical properties .....	127
4.2.3 X-Ray scattering .....	128
4.2.4 Conclusions.....	130
<b>5. Conclusion.....</b>	<b>132</b>
<b>6. References.....</b>	<b>134</b>

## 1. Literature on the blending of tackifiers

Tackifiers are low molar mass additives (between 500 and 2000g/mol), of high glass transition temperature, designed to enhance the adhesive properties of the material in which they are incorporated. They are added at low concentration (~10phr) in rubbers, and at high concentration (>30phr) in Pressure Sensitive Adhesives (PSAs). The most common tackifiers used in rubber compounding are resins based on alkyl modified phenol-formaldehyde (PFR), coumarone indene (CIR), and hydrocarbonated (HCR).

### 1.1. General picture

Tackifiers have been widely studied in the PSA and in the rubber industry, with special focus on their effect on the rheological properties of materials. Tackifiers both dilute entanglements and increase the Tg. Therefore at low frequencies, or high temperature [1][2], the storage modulus  $G'$  decreases; whereas it increases at high frequency. A tackifier thus acts as a plasticizer at low frequencies, and as a filler at high frequencies. This behavior is illustrated in Figure 1.

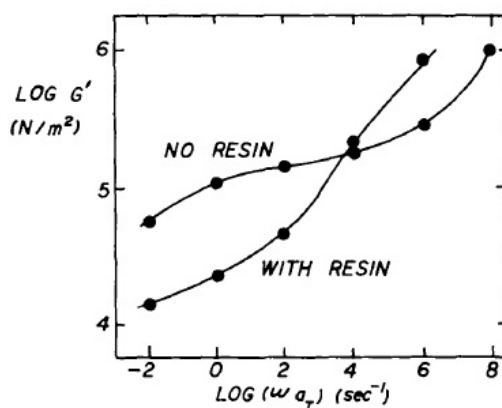


Figure 1 Influence of the addition of tackifier on the storage modulus of NR as a function of reduced frequency. Figure from [1]

Hamed rationalized these observations with adhesion properties, and suggested [1] that the decrease of  $G'$  at low frequencies promotes the flow of the material at the interface and therefore faster interfacial bonds' formation; whereas the increase of  $G'$  at high frequencies improves the bond strength when debonding at higher rates. Tackifiers also favor energy dissipation at high strain rates, and hence fracture energy increases. Kumar et al [3] demonstrated that a tackifier having a good miscibility with the elastomer induces an increase in the  $T_g$  – thus increasing energy dissipation- as well as a decrease and broadening of the plateau modulus.

A poor miscibility between the resin and the matrix may be observed due to the nature of the tackifier, and/or to the amount of tackifier.

### 1.2. Influence of the nature and the amount of tackifier

#### 1.2.1 Influence of the amount of tackifier

Kumar and coworkers [4][5] studied the influence of a hydrocarbon resin on the peeling energy of a brominated isobutylene-co-p-methylstyrene (BIMS) rubber. By evaluating the so-called compatibility of the resin and the rubber via DMA, they suggested that when the blend exhibits ideal mixing properties (i.e. an increase in the rubber's  $T_g$  and a decrease in its plateau modulus), the matrix and the resin are compatible, by which they mean miscible. Blends of BIMS and

hydrocarbon resin are an example of such compatibility. For concentrations up to 10phr, the addition of tackifier lowers the materials modulus and this increase in chain mobility leads to enhanced adhesion. Nevertheless, for higher concentrations, this dynamic effect is counterbalanced by a decrease in the bulk mechanical properties (probed with uniaxial tensile tests). This loss in green strength led to easier debonding of the blends. The tack strength, measured with a 180° peel test, of BIMS-tackifier blends is plotted in Figure 2 with respect to the resin content. It reveals the existence of an optimum in tackifier concentration for tack properties, presumably due to the competing effects aforementioned.

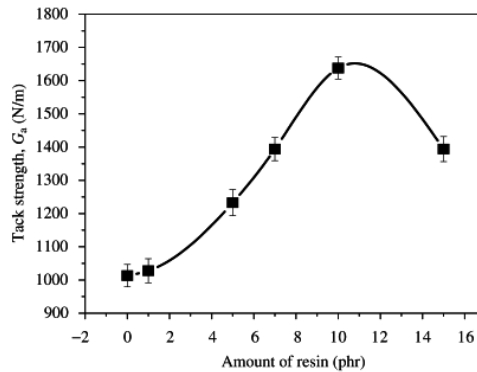


Figure 2 Influence of tackifier amount on tack strength of BIMS-hydrocarbon tackifier system. Figure from [5]

### 1.2.2 Influence of the nature of the tackifier

If the resin and the matrix are poorly miscible, the increase of tackifier concentration leads to a decrease in adhesion energy, even at low concentrations. Some authors [6][7] attributed this effect to a reduction in true contact area, caused by resin surface migration, and to an increase in the plateau modulus due to phase separation. In fact, Basak and coworkers [6] compared the influence of two tackifiers with different chemical nature, a coumarene-indene (CI) and a hydrocarbon (HC) resin, on the self-adhesion properties of EPDM. The tack strength of the blends is plotted in Figure 3 as a function of resin content. The CI resin phase-separates in EPDM due to its poor miscibility, and an increase in its concentration leads to a decrease in the material tack strength. Conversely, HC resin is miscible with EPDM for the studied concentrations and an increase in its content leads to enhanced adhesion.

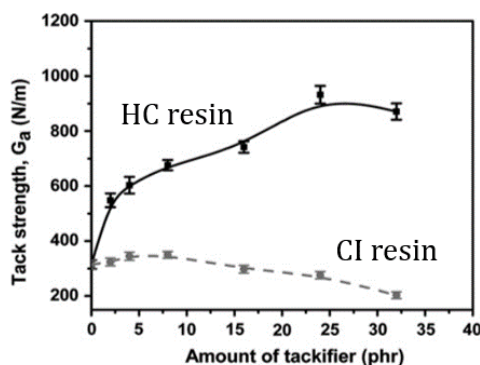


Figure 3 Influence of the nature of the tackifier on tack strength of EPDM. Figure from [6]

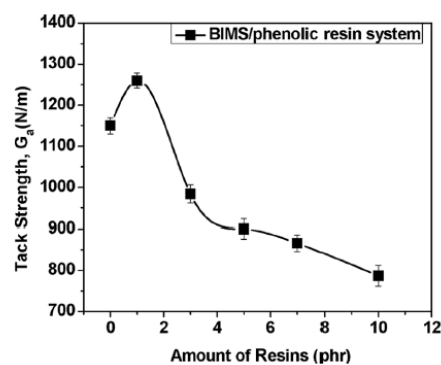


Figure 4 Existence of an optimum in tackifier concentration. Figure from [7]

Figure 4 from Kumar [7] also shows that due to the poor BIMS-phenolic resin compatibility, increase in the concentration of the tackifier leads to further decrease in the tack strength.

Rhee et al [8] compared the influence of a phenolic and a hydrocarbon resin, at a concentration of 2phr, on the self-adhesion of natural rubber. Considering that the viscoelastic properties of the rubber were not influenced by such tackifier content, this study suggested that the difference in polarity, and the ability of the phenolic tackifier to form hydrogen bonds at the interface explained its higher tack strength.

### 1.3. Additives in phase-separated materials

#### 1.3.1 Tackifiers in rubbery block copolymers

Block copolymers composed of one or two glassy blocks and one elastomeric block (typically polyisoprene or polybutadiene) are widely used to prepare Pressure Sensitive Adhesives (PSA) and are generally blended with tackifiers to ensure good adhesive performance. One of the most used PSAs is composed of polystyrene (PS) and polyisoprene (PI) units, and is a mix between a triblock and a diblock of PS-PI-PS and PS-PI. It is well documented [9][10][11] that these block copolymers can self-assemble into microstructures with glassy domains of polystyrene embedded in a rubbery polyisoprene matrix, as illustrated in Figure 5.

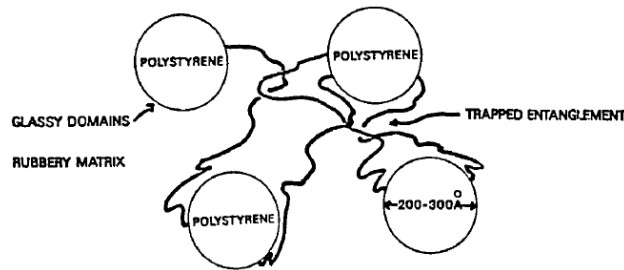


Figure 5 Self-organization of SIS systems. Figure from [10]

Nakamura and coworkers [11] compared the influence of hydrogenated (HC) and phenolic (PH) resins on the adhesion properties of SIS/SI block copolymers. Whereas the phenolic resin is soluble in both PS and PI, the hydrogenated one is insoluble in the PS phase and segregates into the PI rubbery matrix. In both cases, the overall molecular mobility is increased by the presence of the tackifier in the PI phase and a better contact with the substrate is achieved. However, the swelling of the PS with the phenolic resin yields an enhanced adhesion at low concentrations, though an optimum is eventually observed due to a decrease in bulk strength with higher tackifier content (Figure 6 left).

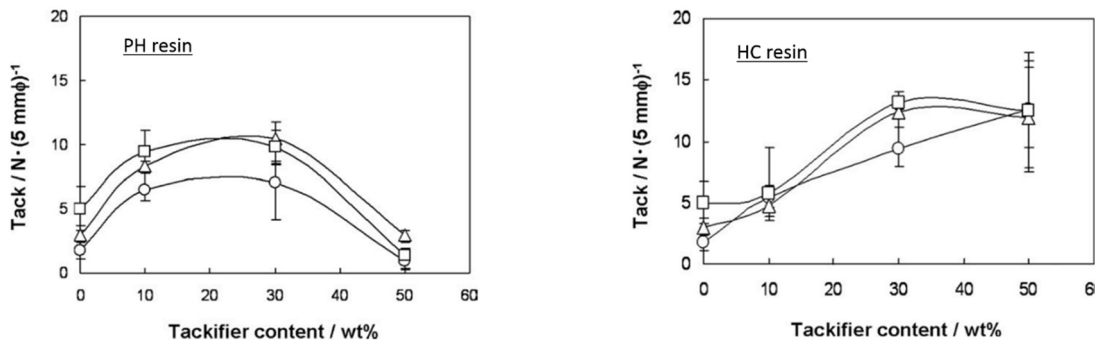


Figure 6 Effect of tackifier content on the tack of SIS/SI blends. Left= Effect of HC resin. Right: Effect of PH resin. Different curves show different SI contents

The HC resin reaches its solubility limit in the PI phase more easily (as it is not soluble in PS), and tends to form aggregates. It was found that the peel strength increases with increase in the agglomerates' size, and therefore keeps increasing with resin content (Figure 6 left). Both tackifiers have different effects on the structure of SIS/SI block copolymers and therefore show dissimilar adhesion properties. Their properties are highly dependent on the resin nature and concentration.

### **1.3.2 Tackifiers in nitrile rubber**

Sokolova et al [12] studied the diffusion and solubility of two low molecular weight substances (diphenyl-guanidine- DPG, and sulphur) into nitrile rubber. They showed that when the solubility of DPG in the copolymer is high enough (through increased temperature for example), complexation may occur between the molecule and the nitrile groups of NBR, weakening the intermolecular  $C\equiv N$  interactions. The adhesion properties of such systems were not probed during these studies.

## **1.4. Conclusion and discussion**

Tackifiers have been used to enhance the adhesion properties of rubbers and PSAs, and rely on two main features: the decrease in the modulus and the increase in the glass transition temperature. The former facilitates material deformation while enhancing contact with rough substrates [13] as well as stretchability of the material during the debonding stage. Moreover, given that entanglements impose topological constraints on chain dynamics, their reduction with tackifiers not only decreases the modulus but also enables faster relaxation times and better contact. The increase in  $T_g$  ensures higher energy dissipation (higher  $G''$ ), and thus also favors adhesion.

Good miscibility (i.e. no demixing)- with regard to chemical nature and concentration - between the resin and the matrix is needed. If not, the opposite effect, i.e a reduction in the adhesion properties, might be observed.

To the best of our knowledge, there are only few investigations on the role of tackifiers in the adhesion of structured polar elastomers. Sokolova and coworkers [12] have initiated work on the effect of additives on the polar interactions in nitrile rubber, and Henrici [14] has discussed the plasticizing effect of polar additives on the inter and intramolecular  $C\equiv N$  bonds of polyacrylonitrile.

## 2. Introduction to the blending of tackifiers in NBR

### 2.1. Materials

Two different tackifiers are considered during this study: a terpene phenolic resin, and a hydrocarbon one. The latter, like most tackifiers, create weak ( $E_{\text{dissociation}} < 3\text{kcal/mol}$ ) Van der Waals interactions with the rubber, whereas phenolic tackifiers possibly build strong specific hydrogen bonds ( $E_{\text{dissociation}} > 12\text{kcal/mol}$ ).

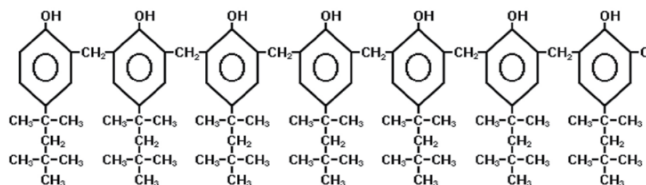


Figure 7 Typical phenolic resin

Tackifiers were stored under ambient conditions. They were analyzed by DSC and their Tg are listed in Table 1.

Name		Chemical nature	Interactions	Tg(°C)
Polar	POL	Terpene phenolic	Hydrogen bonding	46.8
Non polar	NP	C9- Hydrocarbon	Van der Waals	48.8

Table 1 Presentation of the tackifiers

For industrial applications, tackifiers are typically added at weight percentages going from 0 to 15. During this study, and for instructive purposes, four different compositions for each tackifier were studied: 3, 10, 20 and 40wt%. The nitrile rubber blended with x% polar tackifier will be referred to as NBR-POL<sub>x</sub> and those blended with x% nonpolar tackifier: NBR-NP<sub>x</sub>. All concentration are expressed in % and are in weight percentages.

## 2.2. Sample preparation

### 2.2.1 Instrumentation

A DSM Xplore Micro15cc laboratory twin screw extruder (see Figure 8) was used to blend the tackifiers and the rubber. Temperature can be monitored independently on 6 locations of the extruding chamber. The material is introduced in pellet form, and the imposed high-temperature enables its fusion and processing through the chamber. Shear is imposed by two co-rotating conical screws. The recirculation channel permits a continuous mixing of the material for the desired time. The exit channel is then opened to collect the material at room temperature.

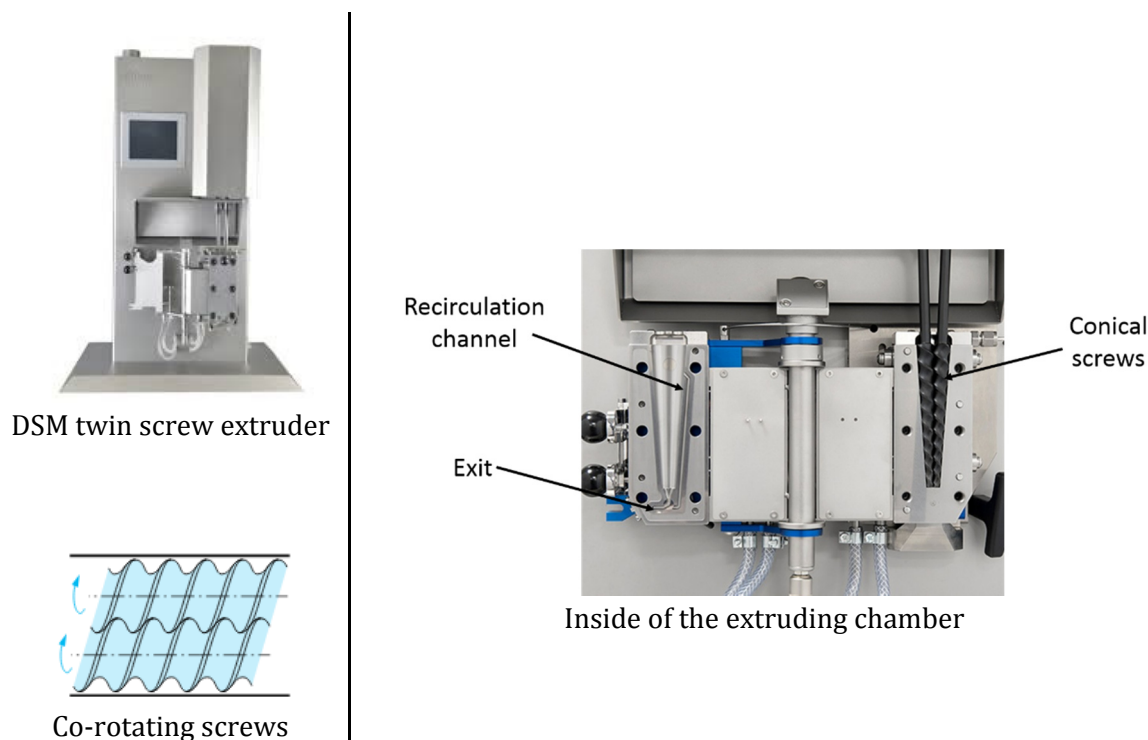


Figure 8 DSM X-Plore twin screw extruder

### 2.2.2 Extruding conditions

In this study, the materials were extruded at 120°C, with a rotating speed of 100rpm during 5min. This temperature was high enough to decrease the material's modulus, but low enough to avoid any degradation. The extruding conditions were kept constant during this study.

After extruding, the materials were first allowed to cool from 120°C to room temperature, and further stored in a freezer until use. The temperature of the freezer (~ -25°C) was above the materials T<sub>g</sub> but close enough to expect no evolution on the considered timescales.

### 2.3. Objectives

The main objective of this chapter is to understand how the studied tackifiers influence the self-adhesion properties of the segmented block copolymer NBR.

The previous chapter demonstrated that poly(acrylonitrile-co-butadiene) tends to self-organize and form complex structures, including well-defined lamellas. Specific polar  $C\equiv N$  interactions occur between acrylonitrile monomers, resulting in a dense physical network. To achieve high adhesion levels, the polymer chains need to be able to move at the interface. Interfacial diffusion, i.e. diffusion along the joints between the blocks, is hindered by physical interaction between chains. For a chain to relax from its initial state and migrate through hopping diffusion, it needs to overcome polar intermolecular interactions either by thermal or mechanical energy. Although a unique  $T_g$  was probed in DSC, it is likely that high glass transition temperature zones (i.e. slow dynamics) exist where the acrylonitrile content is high. Figure 9 sketches a 2D illustration of this process.

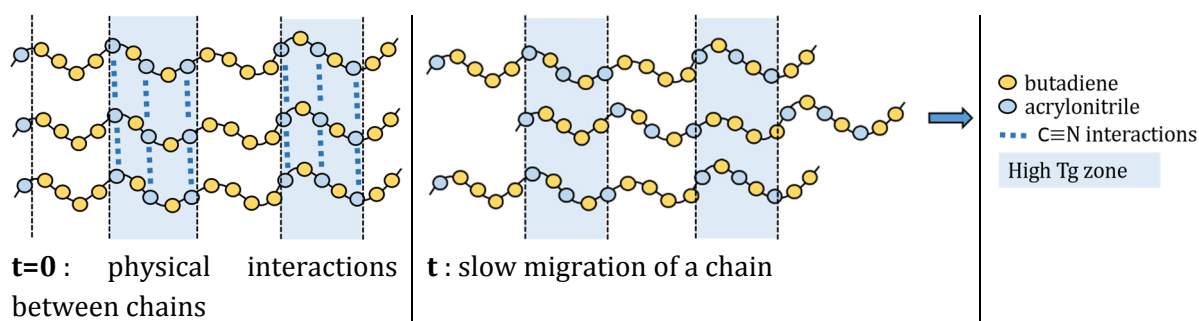


Figure 9 Illustration of the studied NBR and the slow diffusion of one polymer chain with time

The goal of tackifiers is to improve the adhesion strength through enhanced chain mobility. Due to their dissimilar polarities, both tackifiers are expected to interact with the matrix with both different physical bonds (Van der Waals, or hydrogen bonds), and number of interaction with each phase of the ordered block copolymer (butadiene zones, or alternated sequences area). The comparison between both tackifiers will provide information on the role of the physical processes triggering the self-diffusion of this structured nitrile rubber on the polymer self-adhesion.

The adhesion tests will be complemented with mechanical tests (linear rheology and uniaxial tension), DSC measurements, and X-ray scattering profiles in order to rationalize the results.

### 3. Blending of 3% tackifier in NBR

The blended samples (NBR-POL3 and NBR-NP3) were first thermally analyzed by DSC. *Fresh* samples (in the sense that they were kept in the freezer right after extrusion) were compared to samples left at room temperature for some time (called “aged samples”).

For both blends, and for all ageing times (up to a month), a unique  $T_g$  was observed suggesting a good solubility of the resin in the matrix at such tackifier content. The  $T_g$  increased from  $-31.2^\circ\text{C}$  for pure extruded NBR, to  $-30^\circ\text{C}$  for NBR blended with polar tackifier, and to  $-28.5^\circ\text{C}$  for the nonpolar one. Moreover, an endothermic peak appeared close to  $75^\circ\text{C}$  for all materials after ageing several days at room temperature. This temperature rose for approximately  $1^\circ\text{C}$  over the first month outside the freezer.

Sample	T <sub>g</sub> (°C)
NBR extruded	-31.2
NBR-POL3	-30
NBR-NP3	-28.5

Table 2 Evolution of glass transition temperature with the addition of 3% tackifier

These measurements suggest that the polar tackifier provides slightly more local mobility to the NBR chains than the nonpolar one. Nevertheless, the difference is small and the adhesion measurements are performed at room temperature, i.e. more than 55°C above T<sub>g</sub> such that the viscoelastic effects are expected to be negligible.

### 3.1. Self-adhesion properties

The “self”-adhesion properties of the 3% blend were studied over time and at room temperature. Tack samples are schematically illustrated on Figure 10, and reminds that the contacting surfaces are dissimilar: the rubber disk is freshly extruded whereas the coated layer is in a close-to-equilibrium state.

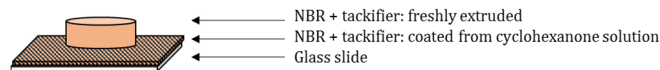


Figure 10 Illustration of tack samples for NBR + tackifier

#### 3.1.1 Reproducibility of tack measurements

Figure 11 shows representative stress-strain curves of NBR+3% tackifier for both resins, for short (5h) and long (7days) contact times. Several curves of each samples are plotted to demonstrate the reproducibility of each measurement.

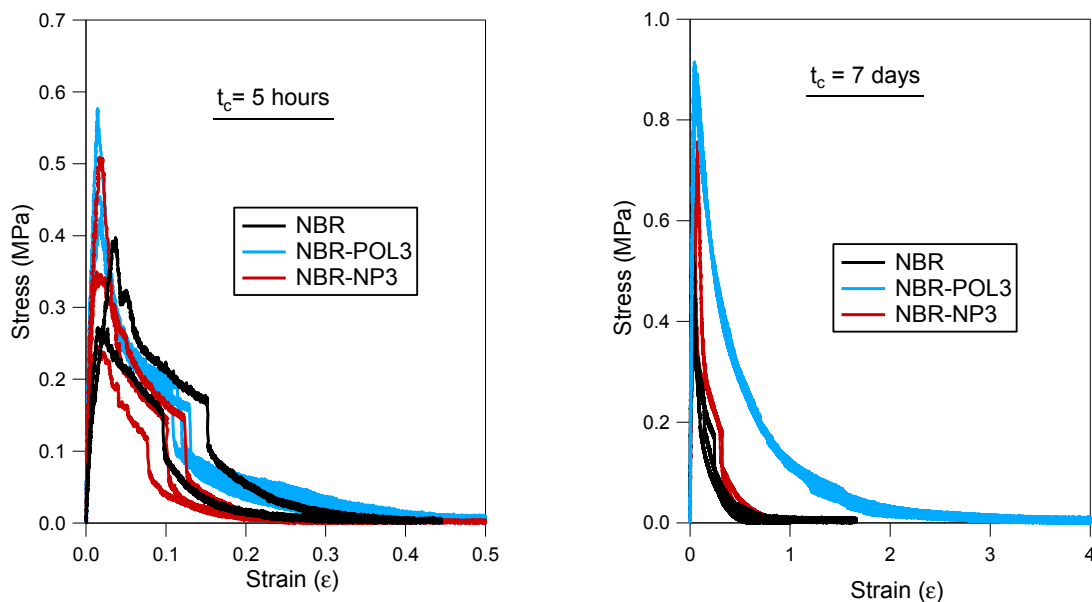


Figure 11 Stress-strain curves of tack measurements for NBR, NBR+3% polar tackifier and NBR+3% nonpolar tackifier. Left: contact time=5h. Right: contact time=7days

At short contact times, results do not enable to discriminate the different samples, and the self-adhesion levels are low (<50J/m<sup>2</sup>). At long contact times, a clear difference is observed between the blends and reproducibility is good enough to establish comparisons.

### 3.1.2 Effect of contact time on the adhesion properties

The influence of contact time on the stress-strain curves is shown in Figure 12 for the three samples: (a) pure extruded NBR; (b) NBR-NP3 and (c) NBR-POL3. The three samples behave differently. For pure NBR, as was previously shown in Chapter 3 section 3.4, the self-adhesion properties evolve slowly with time through a slight increase of both the cavitation peak and the deformation. With 3% non-polar tackifier (NBR-NP3), the maximum deformation increases, and higher stresses are needed for cavitation, likely due to better microscopic contact at the interface. Yet, for contact time longer than 3 days, a small decrease in both, contact quality and deformation is observed. With the addition of 3% polar tackifier (NBR-POL3), microscopic contact seems better because of the higher peak stress, and there is a significant enhancement of the deformability ( $\epsilon=400\%$  for the polar blend after  $t_c=7$  days). As such, the interface is strong enough to withstand the overall stresses, and the final rupture of the assembly is cohesive.

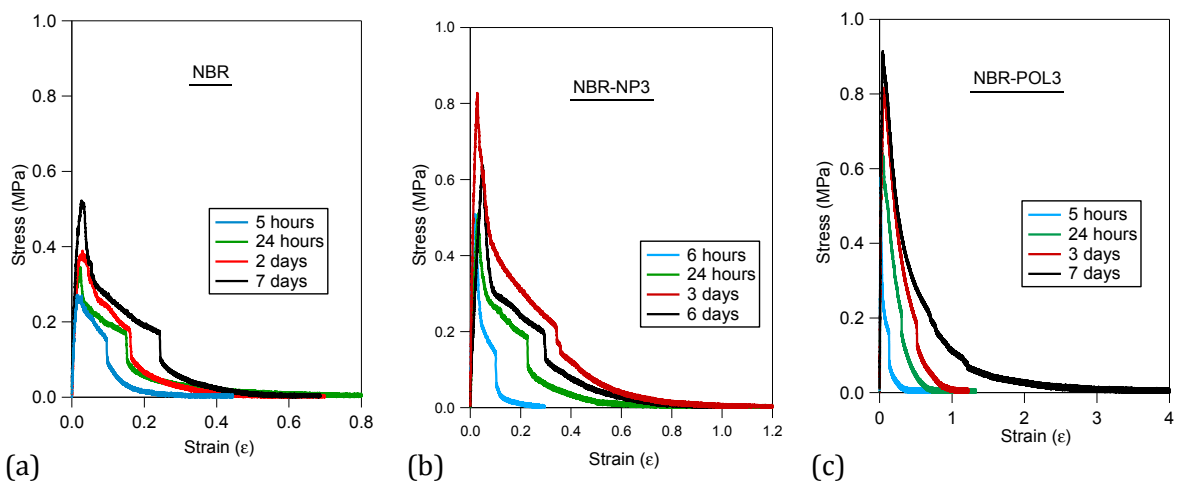


Figure 12 Influence of contact time on the self-adhesion properties of (a) pure NBR (b) NBR-NP3 (c) NBR-POL3

### 3.1.3 Comparison between both tackifiers

From Figure 11 in section 3.1.1 it is clear that the main difference between samples appears at very long contact times ( $> 6$  days) and is due to the NBR ability to dissipate energy in large strain through the formation of fibrils prior failure. The corresponding self-adhesion energies  $W_{adh}$  are plotted on Figure 13 as a function of contact time.

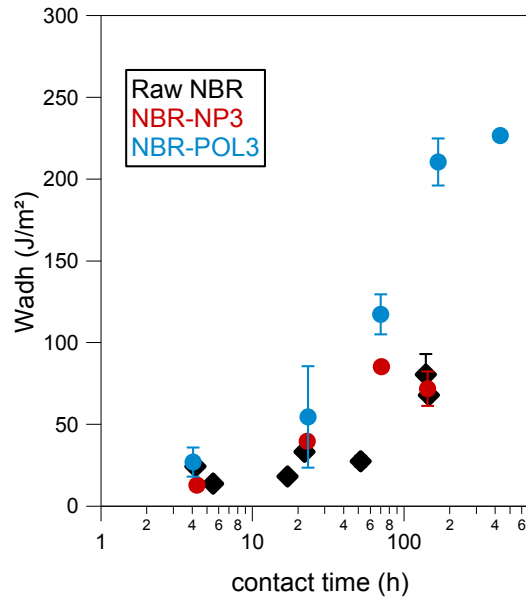


Figure 13 Self-adhesion energy as a function of contact time for NBR and NBR +3% tackifier for polar resin (NBR-POL3) and non-polar one (NBR-NP3)

To explain such differences in self-adhesion levels, the mechanical properties as well as the microstructure were probed.

## 3.2. Bulk properties and structure

The main difference in tack between both samples appears at long contact times. It is reasonable to assume that this change in self-adhesion is due to an evolution of the mechanical properties with time, thus modifying the ability of the material to dissipate energy in the bulk during debonding. As such, it is therefore interesting to compare the materials behavior first without ageing, and then after 7 days ageing at room temperature (corresponding to long contact times where the difference between both tackifiers is probed).

During this section the mechanical properties as well as the X-ray scattering profiles will be analyzed, for freshly extruded (un-aged) and aged samples.

### 3.2.1 Linear mechanical properties of freshly extruded blends

The linear mechanical properties of NBR, NBR-POL3 and NBR-NP3 were investigated. Frequency sweeps were performed at 25 and 60°C and a master curve, presented on Figure 14, was plotted at the chosen reference temperature (25°C). In the plateau regime, the moduli are similar suggesting that the molecular weight between entanglements remains constant with the addition of 3% tackifier. The terminal relaxation time are similar and close to 750 seconds, suggesting that the tackifiers do not increase the chain dynamics at low frequencies and scaling of the moduli  $G' \propto \omega^{0.6}$  and  $G'' \propto \omega^{0.5}$  are probed.

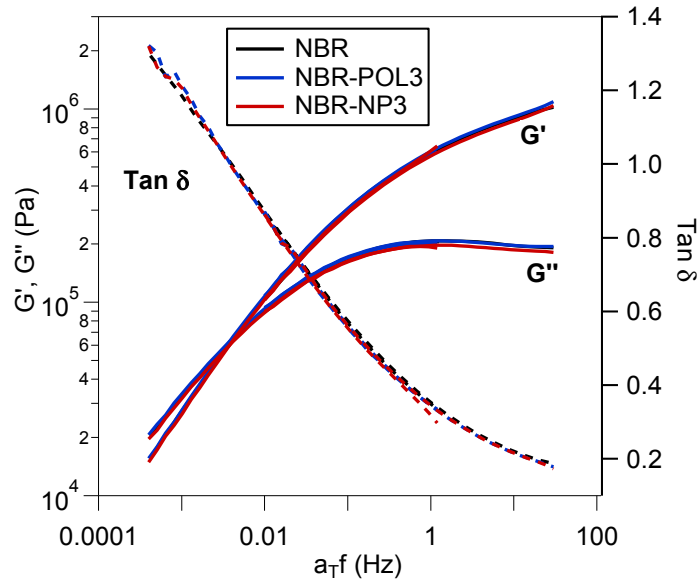


Figure 14 Master curves for the moduli  $G'$  and  $G''$  (left), and the loss factor (right) as a function of reduced frequency, at the reference temperature  $T_0=25^\circ\text{C}$  for NBR, NBR-NP3 and NBR-POL3

It seems that these short relaxation processes cannot account for the difference in tack properties appearing for very long contacts, and creep tests would have enabled access to such time scales, yet were not performed during this work.

### 3.2.2 Uniaxial tensile tests

To investigate potential changes in the ability of NBR to dissipate energy at large strains, uniaxial tensile tests were performed. Sample preparation and testing conditions are detailed in Chapter 2 (section 2.1). Figure 15 shows the result for fresh samples tested after unmolding and for samples aged 7 days at room temperature.

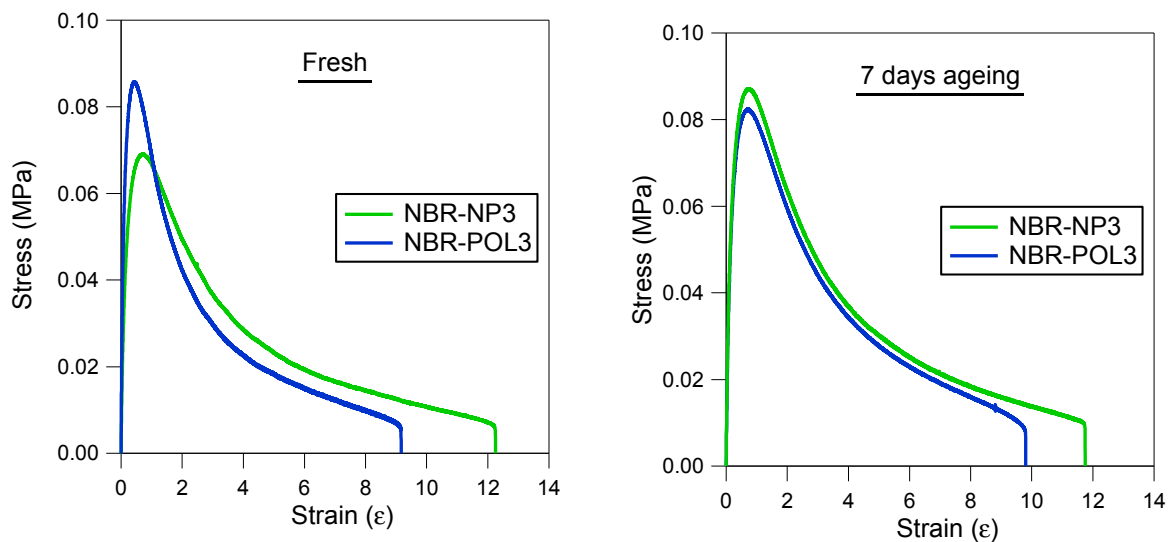


Figure 15 Uniaxial tensile tests for NBR-NP3 and NBR-POL3. Left: fresh sample tested after molding. Right: Samples tested 7 days after molding (ageing at RT)

The large strain behaviors (in terms of maximum stress, maximum extensibility, shape of the curves) of both materials are very similar, regardless of the ageing time, and do not explain the difference probed in self-adhesion.

### 3.2.3 X-Ray Scattering

The small angle X-ray scattering (SAXS) patterns of 1-mm thick samples were analyzed with the method described in Chapter 3. The tack samples being asymmetrical due to the slow drying on the glass slide (see Figure 10), measurements were performed on both aged bulk samples, and solvent-casted ones. No difference between the blends is observed (see curves in Annex 3.1) suggesting that for such resin content the bulk structures are similar.

## 3.3. Conclusion and discussion

The self-adhesion properties of NBR and NBR-NP3 are very similar for the range of contact times studied. However, the addition of polar tackifier (NBR-POL3) significantly increases the self-adhesion properties for long contact times. The results were analyzed in light of Hamed's three criteria [1] to reach a good adhesion. As both materials have similar bulks properties and the contact conditions were identical, no difference in microscopic contact (due to roughness) is expected. Indeed, the stress peak corresponding to cavitation in the tack experiment is very similar for all materials. The observed difference cannot be explained neither by bulk mechanical properties changes nor by a change in bulk structure detectable by small angle X-ray scattering. Therefore, one can hypothesize that it must be due to a change in interfacial interactions. The pie-chart in Figure 16 illustrates Hamed criterias:

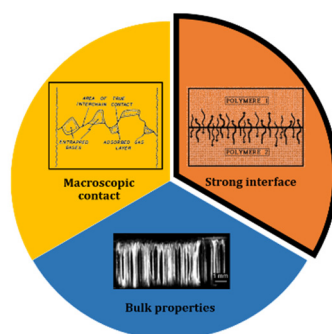


Figure 16 Illustration of Hamed's three criteria. In this part, difference in interface strength explains the difference in self-adhesion properties

An explanation for such behavior is suggested in light of the different polarities (both of tackifiers and of the rubber matrix). The phenolic resin may have more affinity for polar groups and therefore could migrate towards the acrylonitrile-concentrated areas. There is thus a competition between  $C\equiv N$  intermolecular interactions, and coupling between  $C\equiv N$  and the phenolic resin. The dipolar moment associated with the O-H bond being stronger than that of  $C\equiv N$ , the physical association of the resin with the elastomer is likely to happen. On the other side, the hydrocarbon tackifier is hardly polar,  $C\equiv N$  intermolecular bonds are thus favorable, and the resin concentrates in the polybutadiene-rich zones. Due to the low concentration regime, it is suggested that entropy-driven forces can be neglected such that these enthalpic arguments are valid.

Physical links between polymer chains are thus disturbed by the polar tackifier, and the overall network is disrupted. In fact it is likely that the addition of phenolic resin weakens the association

energy of intermolecular  $C\equiv N$  interactions. Such effects are not probed by linear rheology as the accessible experimental timescale is not long enough. The polar interactions between acrylonitrile moieties and the tackifier are dynamic, and reversible association-dissociation processes may occur thus leading to a slow diffusion of the polymer chain despite unchanged mechanical properties. This process is illustrated in Figure 17, and is comparable to the supramolecular networks previously reported by Liu et al [15]. During their study, authors were able to synthesize a dynamic, self-healable network exhibiting high energy dissipation and fracture toughness thanks to these association-dissociation processes. The trade-off between self-healing efficiency and mechanical robustness has been thoroughly addressed for the development of self-healing polymers, and vitrimers are an attractive type of self-healing polymers exhibiting both high bulk modulus and important dynamic properties.

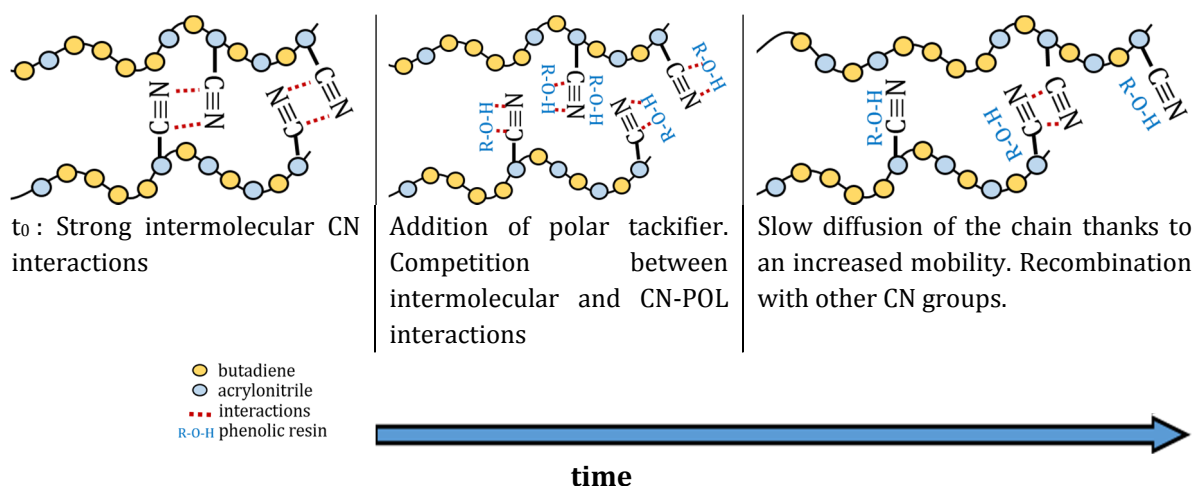


Figure 17 Illustration of a possible time-dependent mechanism for chain diffusion with 3% phenolic tackifier

On the other hand, the non-polar resin migrates to, and swells, the PB domains. This process should in principle not disturb the physical associations holding the network together. An illustration is presented in Figure 18.

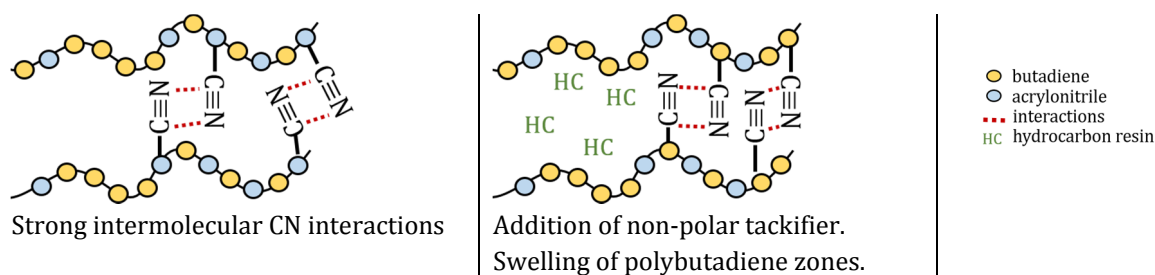


Figure 18 Illustration of a possible scheme for the addition of non-polar tackifier

Therefore, despite their similar effect on the overall  $T_g$  of NBR, it is likely that the phenolic tackifier locally reduces that of the high- $T_g$  alternated blocks whereas the hydrocarbon resin reduces the entanglement density of the low- $T_g$  butadiene domains. These two transitions are just a “hypothetical-picture” and could not be measured experimentally.

Nevertheless, the diffusion is slow and long contact times are needed to reach significant self-adhesion properties. In order to accelerate this process, higher amounts of tackifier were added and further investigated.

## 4. Blending of a high tackifier content in NBR

10, 20 and 40% tackifier were blended into the rubber, and the self-adhesion properties probed over contact times ranging from two hours to several days. The self-adhesion properties of the different blends are first compared, and results then interpreted in light of mechanical and X-ray scattering experiments.

### 4.1. Self-adhesion properties

#### 4.1.1 At 10 and 20% resin content

##### i Evolution with contact time

The influence of contact time on the self-adhesion properties of blends with 10 and 20% tackifier are shown on Figure 19. For both resins at 10% (top pictures), the self-adhesion energy increases with time primarily because of higher bulk deformation. When blended at 20% (bottom pictures), the effect of contact time on the self-adhesion properties is less pronounced with only a mild increase in tack strength.

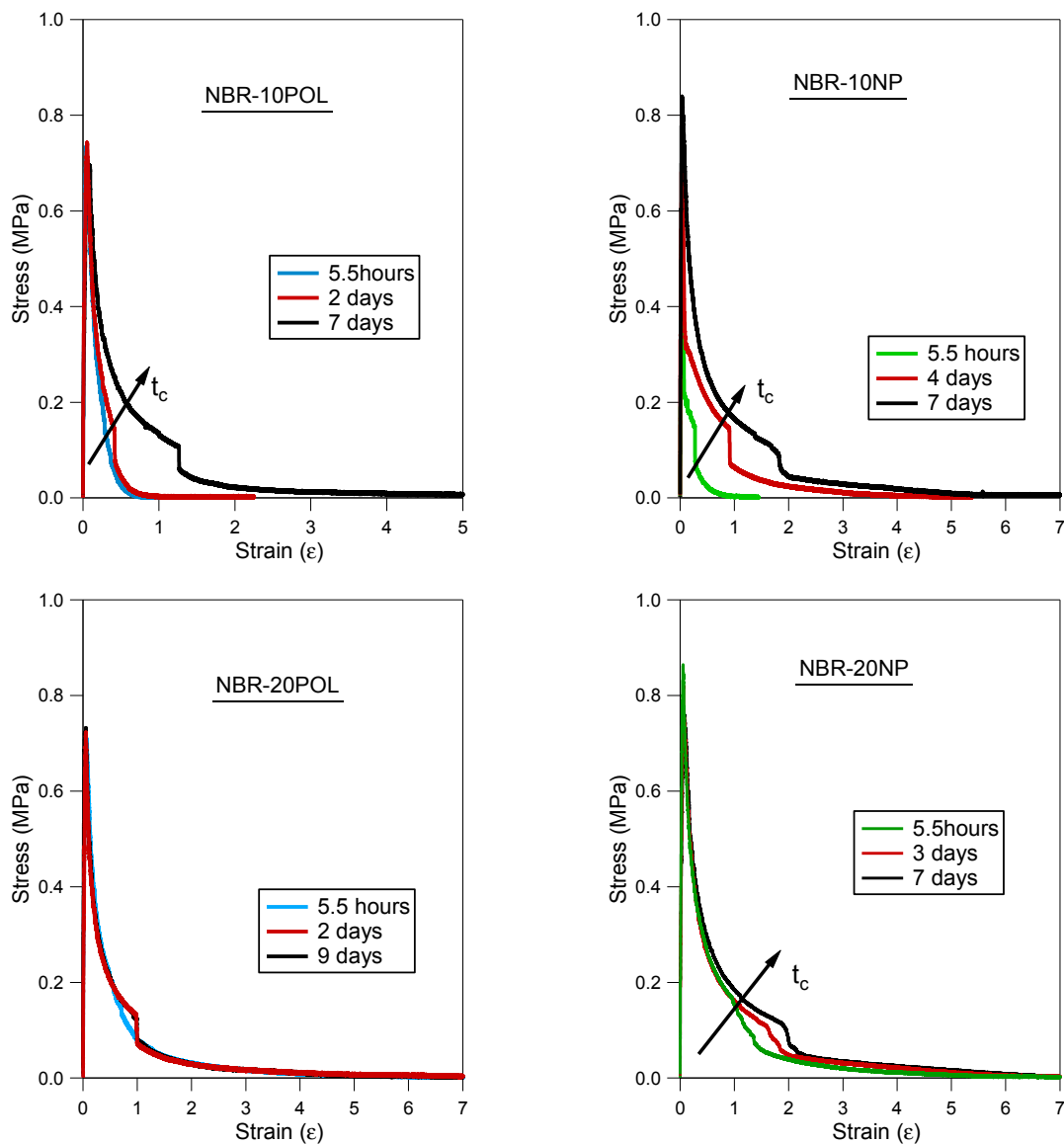


Figure 19 Influence of contact time on the stress-strain curves of blends with 10 and 20% resin

ii Comparison between 10 and 20% blends

Figure 20 shows the influence of tackifier concentration (0, 10 and 20%) on the self-adhesion of nitrile rubber, at short (5.5 hours) and long (7 days) contact times. The corresponding self-adhesion energies are shown in Figure 21.

At short contact times (top graphs), an increase in the cavitation peak and in the extensibility lead to a significant enhancement of the self-adhesion energy when the tackifier content is increased from 10 to 20%. The self-adhesion energies of blends with 10% tackifier keep increasing with time whereas those of the blends with 20% resin hardly evolves (see Figure 21) such that for long contact times, no difference in self-adhesion properties is probed between the blends with 10% and those with 20% resin (see bottom graphs in Figure 20).

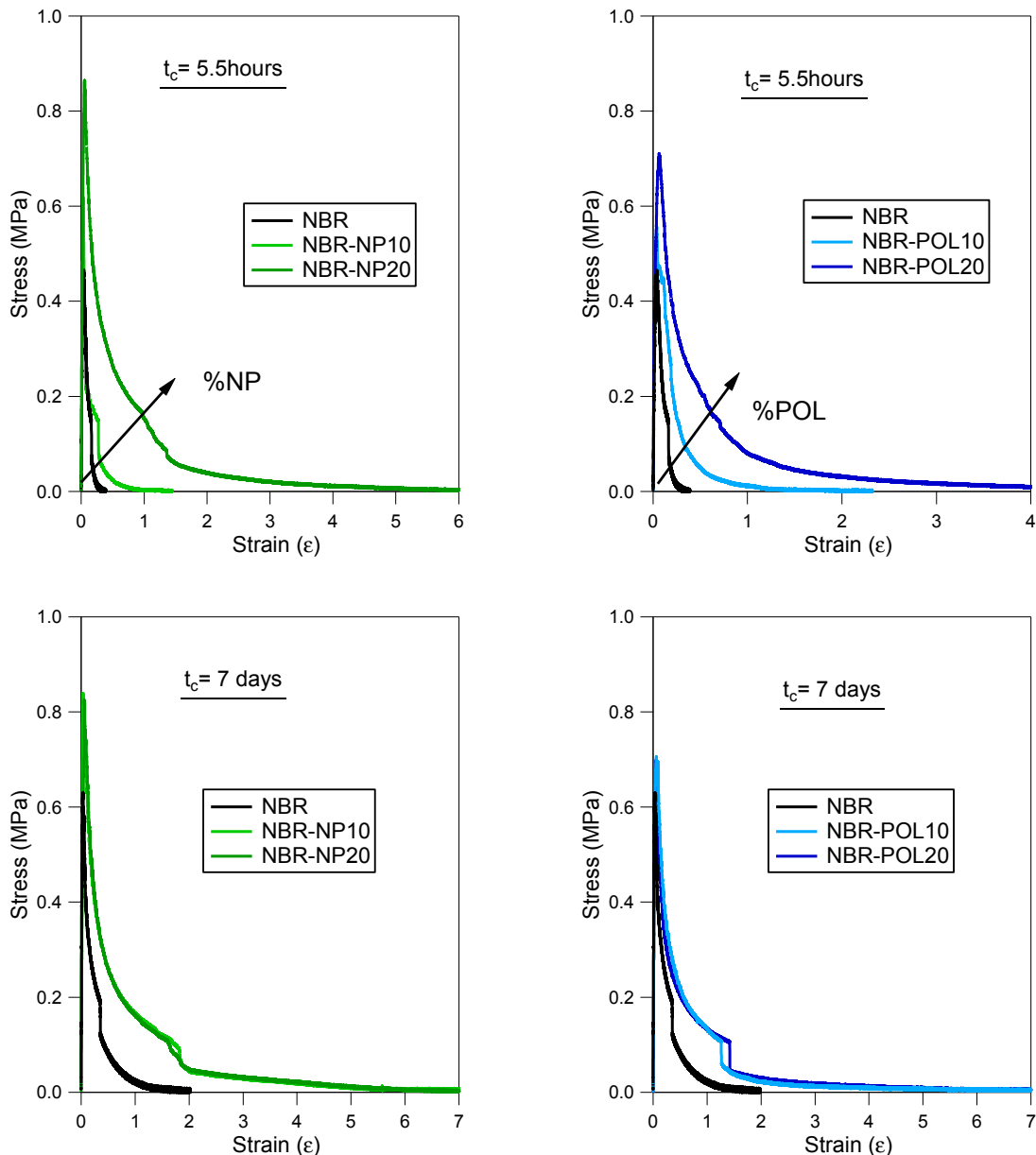


Figure 20 Self-adhesion properties of blends of NBR. Top left: contact time 5.5hours, nonpolar tackifier. Top right: contact time 5.5hours, polar tackifier. Bottom left: contact time 7days, nonpolar tackifier. Bottom right: contact time 7days, polar tackifier.

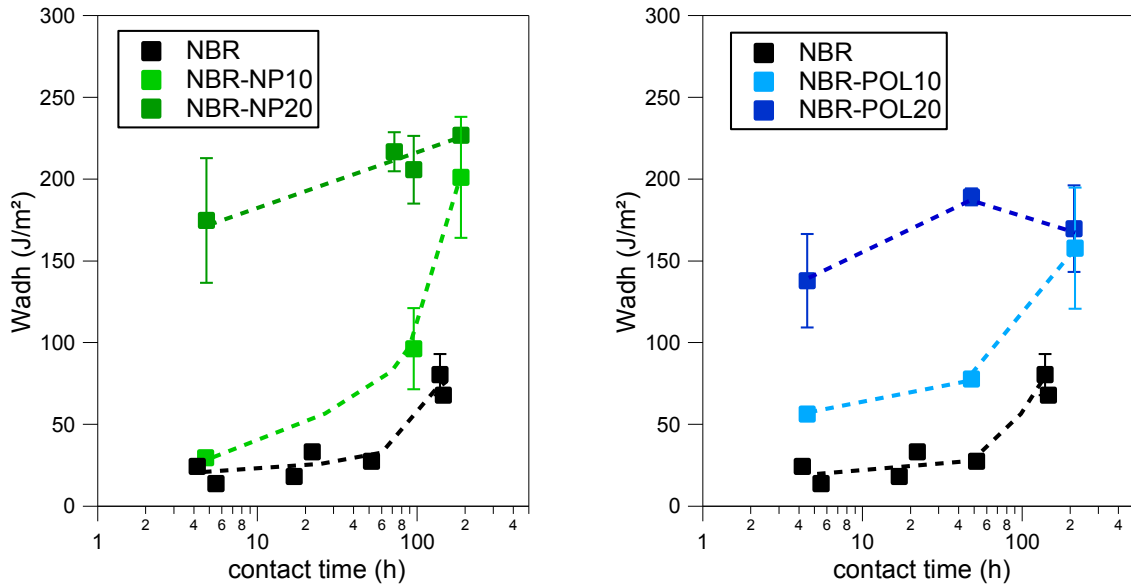


Figure 21 Adhesion energy as a function of time and of the amount of nonpolar (left) and polar (right) tackified NBR blends

The dotted lines are to guide the eye.

No significant difference between both tackifiers are measured.

#### 4.1.2 At 40% resin content

When the amount of tackifier is increased even more (40%), the effective contact area- estimated by the peak stress- is slightly impacted, and the main difference in adhesion comes from the material's ability to dissipate energy in large deformation (Figure 22). A decrease in the self-adhesion properties at such high concentration is observed for all contact times considered and the corresponding energies are plotted in Figure 23.

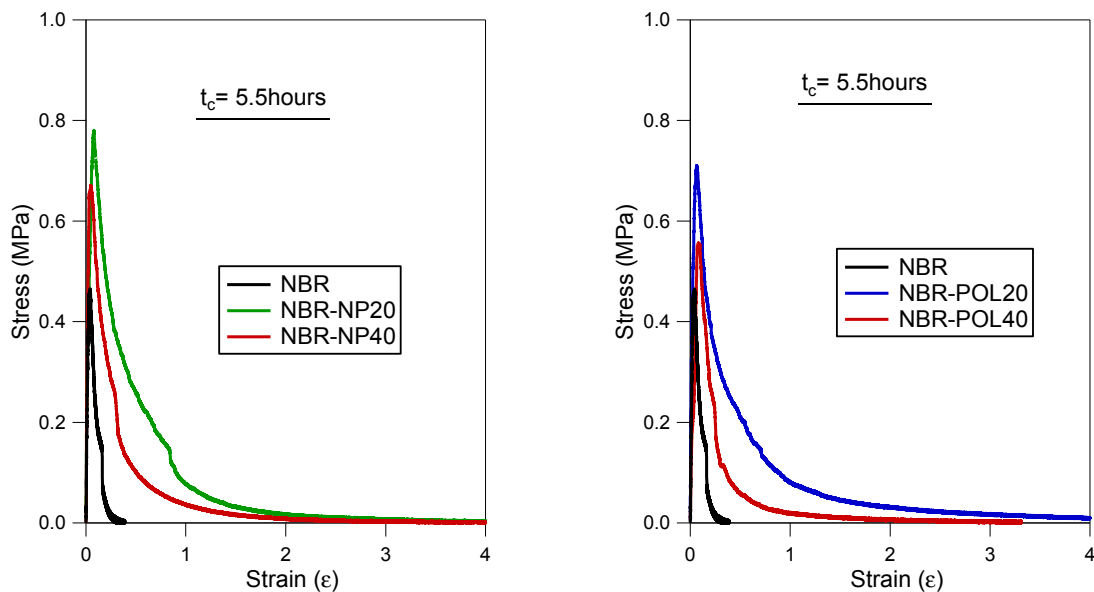


Figure 22 Self-adhesion properties of blends of NBR + tackifier for 6 hours of contact time.

Left: non-polar tackifier. Right: polar tackifier

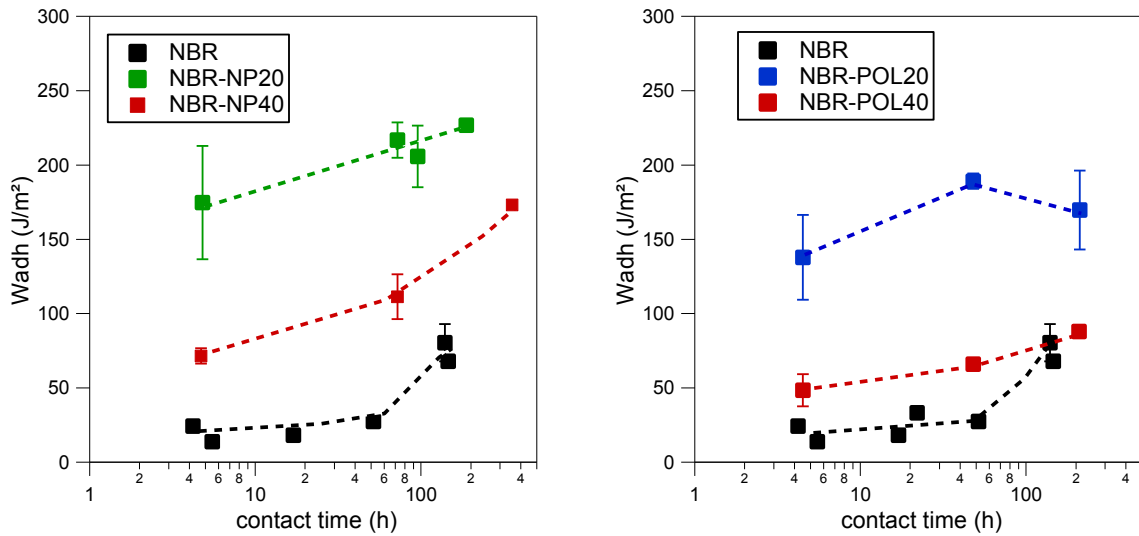


Figure 23 Self-adhesion energies of NBR with non-polar (left) and polar (right) tackifier at high concentrations

The dotted lines are to guide to eye.

### 4.1.3 Conclusions

At short contact times, Figure 24 (left) reveals a great enhancement of the self-adhesion properties for an increase in resin content from 10 to 20%. This boost is measured for both resins (increase of a factor of 2.4 for the polar resin, and of more than 6.5 for the nonpolar one). After reaching such levels, the self-adhesion energy of the 20%-systems hardly evolves whereas that of the 10% blends keep increasing with contact time such that after 7 days of contact (see Figure 24 right), samples with 10 and 20% tackifiers show similar self-adhesion energies, close to 200J/m<sup>2</sup>. For blends with 40% resin, the self-adhesion properties of NBR decreases, at both short (5.5 hours) and long (7 days) contact times.

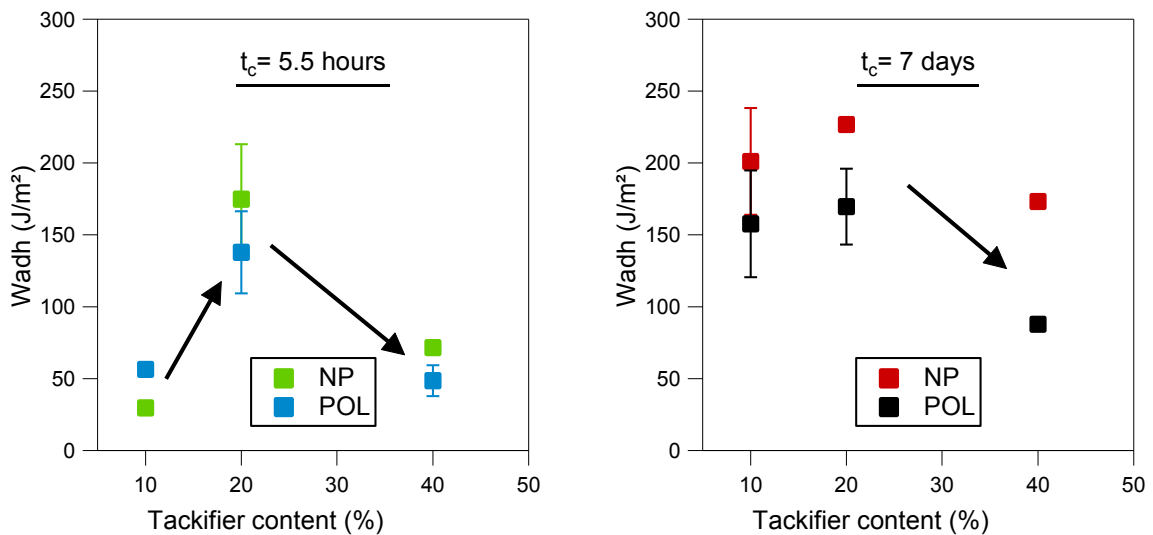


Figure 24 Self-adhesion energy of NBR + tackifier as a function of tackifier content, for both polar (POL) and non-polar (NP) one. Left= short contact times (5.5hours). Right=long contact times (7 days)

Unlike for the blends with 3% tackifier, no significant difference in self-adhesion properties between both types of resins is observed at high concentrations.

In order to properly interpret these results it is essential to complement them with the characterization of the mechanical properties and structures of the different blends.

## 4.2. Properties of the high concentration blends

### 4.2.1 Thermal properties

Figure 25 shows the first heating cycle from DSC measurements of NBR blended with 40% tackifiers. For both highly concentrated blends, a high-temperature transition is probed even for freshly extruded samples. For NBR-POL40, the endothermic peak is observed close to 60°C, whereas it is near 80°C for NBR-NP40. Both transitions are not present on the second heating cycle. It is important to discuss the origin of these peaks to have a better insight on the structure inside each blends.

The 80°C-transition in [NBR-NP40](#) is similar to that observed for aged samples of pure NBR (see Chapter 3). Furthermore, no lower temperature transition that could be related to the demixion of the hydrocarbon resin Tg appears. In the case of [NBR-POL40](#), the measured peak is close to the resin's Tg (50°C) and is presumably due to a lack of miscibility between the tackifier and the rubber matrix. In fact, Kumar and coworkers [4] suggest that phenolic tackifiers are capable of forming stiff resin aggregates due to their polarity. It is noteworthy that unlike for aged NBR samples, no 80°C-endothermic peak appear after ageing of NBR-POL40.

It is suggested that due to the elastomer composition (70% of butadiene units), the non-polar resin has a higher solubility limit in the matrix than the phenolic one, and is thus still miscible at high (40%) concentrations. In agreement with Sokolova [16], it was suggested in Chapter 3 that this 80°C-peak was either due to the melting of 1,4-trans polybutadiene microblocks or to a thermal transition associated with polyacrylonitrile's glass transition temperature. These DSC measurements suggest that the 80°C-peak is only influenced by the addition of phenolic tackifier, and it is therefore likely that this transition is associated with the rubber's polar zones.

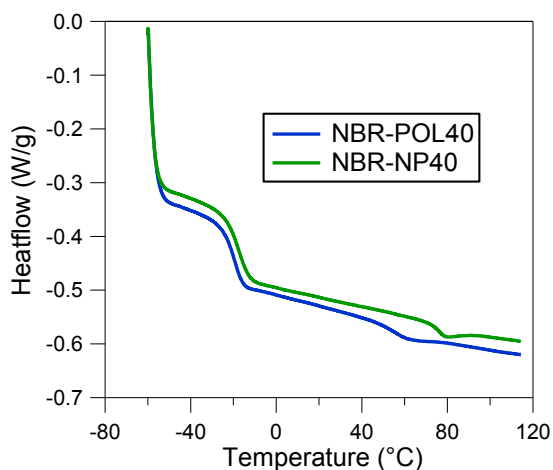


Figure 25 First heating cycle of DSC measurements on freshly extruded 40%-resin blends

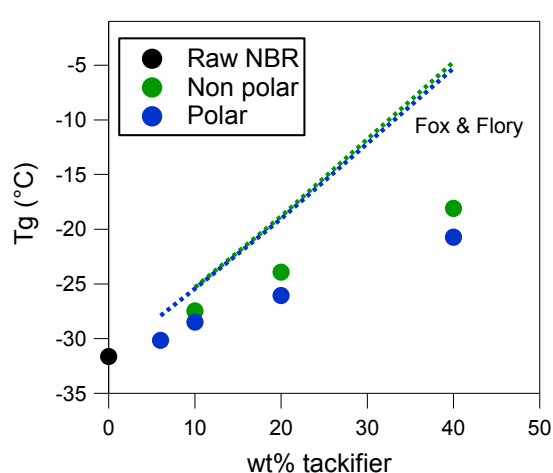


Figure 26 Evolution of Tg with the amount of tackifier. Comparison with Fox & Flory's prediction

For concentrations up to 40%, only one Tg is measured, confirming that blends are homogeneous on the micrometer scale.

As the material is a complex structured block copolymer, it is not surprising that the blends do not match Fox and Flory’s experimental relationship (see Figure 26):

$$1/T_g = w_1/T_{g1} + w_2/T_{g2} \quad 5.1$$

with  $w_1$  and  $w_2$  the weight fractions of components 1 and 2 having respectively  $T_{g1}$  and  $T_{g2}$ . In this study, component 1 is the nitrile rubber and component 2 each tackifier.

**4.2.2 Linear mechanical properties**

Preparation of the samples are detailed in Chapter 2 (2.1). The linear mechanical properties of the different samples were probed at 25°C and 60°C, and the master curves are plotted at 25°C in Figure 27. A zoom on the low frequency behavior is shown on the right.

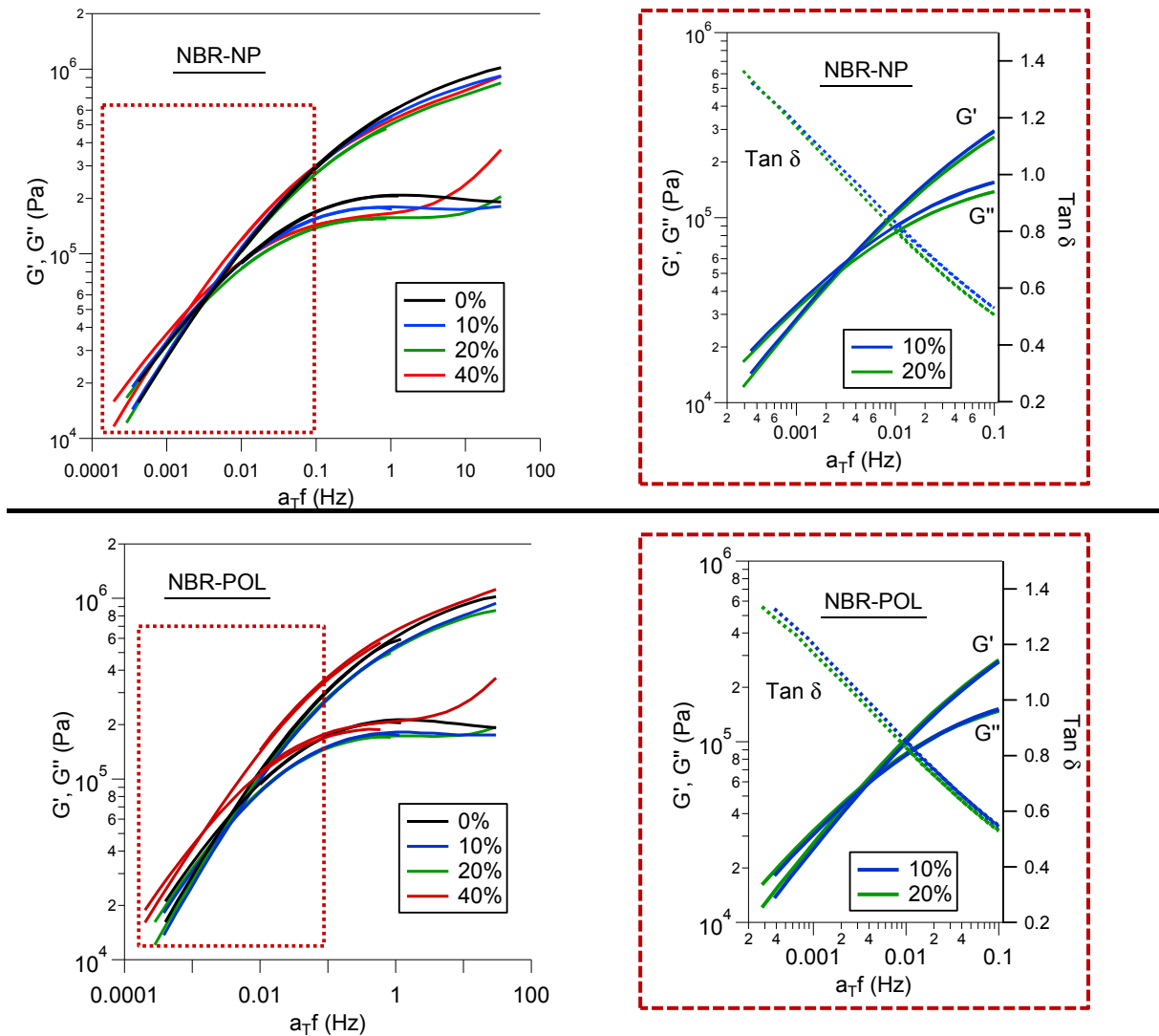


Figure 27 Linear mechanical properties of NBR blends with non-polar (top) and polar (bottom) tackifier. Right: Zoom on the low-frequency behavior

With increasing tackifier content from 0 to 20%, a light decrease in the plateau modulus and a reduction in the plateau length (range of frequencies), is observed. A decrease in the length of the plateau suggests the existence of fewer relaxation processes in the material, and is opposite to the work of Kumar and coworkers [3] who suggested an increase in the plateau length with the addition of tackifiers. The softening of the material is responsible for the increase in the effective contact area for a given surface roughness, and hence for an increase in the cavitation peak in the

tack measurements in Figure 20. Low frequency behaviors (see zooms on the graphs in Figure 27) were analyzed to investigate the great difference in self-adhesion properties of blends with 10% and 20% resins, yet not difference are observed.

Furthermore, all curves have a  $G' \propto \omega^{0.6}$  scaling at low frequencies, except for NBR-POL40. Indeed, as expected from the DSC measurements, the excess of resin in NBR-POL40 presumably segregates inside the rubber matrix acting as a filler and increasing the modulus. For NBR-NP40, the value of the plateau modulus is similar to that of NBR-NP20, but its frequency span is reduced due to an increase in  $T_g$ . The decrease in self-adhesion properties for such high concentration of resin (Figure 24) is assumed to be due to a loss in the material's green strength. These two blends (with 40% resin) will not be studied further.

Tensile tests were run on blends with 10 and 20% tackifiers, and show similar large deformation properties.

Therefore, both linear rheology and tensile test do not seem to explain the large increase in the self-adhesion properties at short contact times for 20% tackifier.

### 4.2.3 X-Ray scattering

X-ray scattering experiments were performed on 1-mm thick samples of NBR-POL10, NBR-POL20; NBR-NP10 and NBR-NP20. The experimental procedure is detailed in Chapter 3 (section 2.2). Freshly extruded samples, and samples aged at room temperature are compared.

#### i Close-to-equilibrium structures

Samples were kept at room temperature for two months, and the aged blends were compared to aged NBR (data from Chapter 3). Figure 28 plots the X-Ray scattering profiles of these close-to-equilibrium blends, and show that both tackifiers modify NBR structure differently. **NBR-NP10** seems to prevent the lamella's formation (no clear formation of the  $q_2$  and  $q_3$  peaks, important peaks width), whereas **NBR-POL10** exhibit a clear ( $q^*$ ,  $q_2$ ,  $q_3$  peaks narrow and well defined) lamellar structure and has completely annihilated the structure associated with  $q=0.2A^{-1}$ .

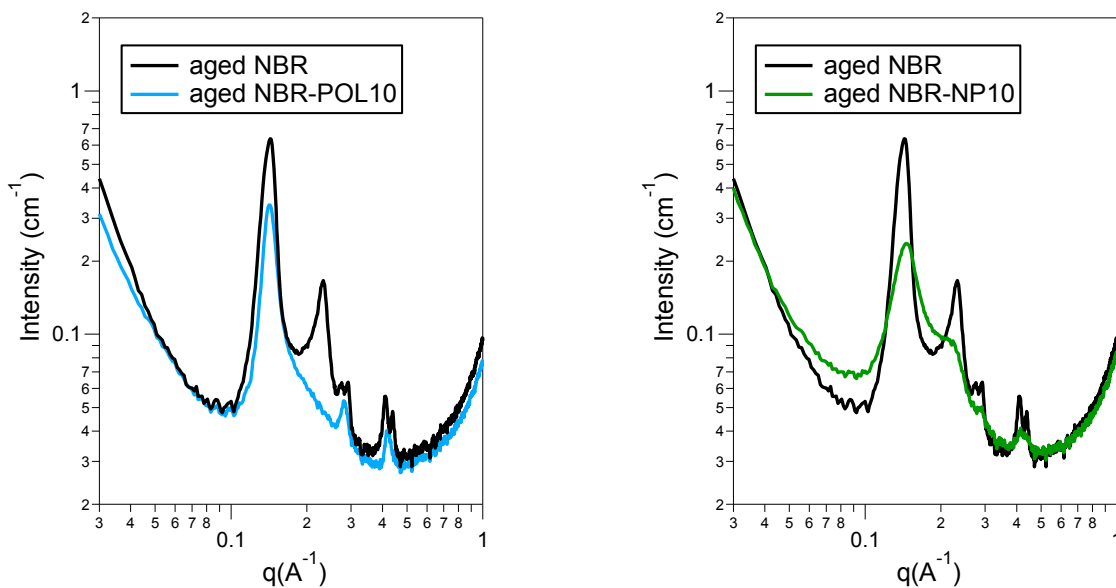


Figure 28 SAXS scattering profiles of aged samples. Comparison between aged NBR (black curve) and NBR-POL10 (left, blue curve), and between aged NBR and NBR-NP10 (right, green curve)

The unique lamellar structure in the blend with the polar tackifier has a characteristic size ( $d=4.5\text{nm}$ ) intermediate between both lamellar structures of aged NBR ( $d_1=4.6\text{nm}$  and  $d_2=4.3\text{nm}$ ). The thermodynamic equilibrium structure of samples with 20% tackifier were not characterized.

ii Out-of-equilibrium structures

The samples were stored in the freezer after extrusion until structural characterization. They are compared to freshly extruded pure NBR, and the results are presented in Figure 29. It was shown in Chapter 3 that extrusion strongly disrupts the lamellar structures of NBR (see black curve). With the addition of 10% polar tackifier (Figure 29 left) the lamellar structure is restored even for freshly extruded samples. This structure hardly evolves with time (see Figure 30 left). This fast kinetic is presumably due to an increase in the chains' mobility thanks to the disruption of intermolecular  $C\equiv N$  bonds. With 20% polar tackifier the microstructure is strongly disrupted and no lamellar peaks are observed on freshly extruded samples. With such an important amount of resin, the system is unable to self-organize on short time scales. The addition of 10 and 20% non-polar tackifier (see Figure 29 right) does not enable the re-built of the lamellar structure shortly after extrusion. The amorphous halo ( $q=0.2\text{\AA}^{-1}$ ) is decreased with increasing resin content. In Figure 30 it is shown that the microstructure of NBR-NP10 tends to evolve with time but with a slower kinetic than NBR-POL10.

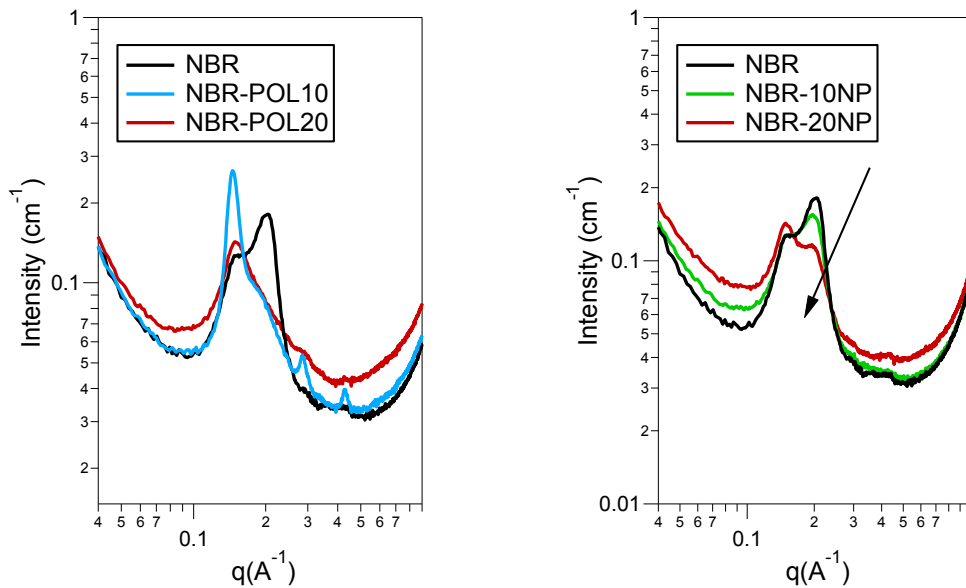


Figure 29 SAXS scattering profiles of fresh samples: Addition of tackifier on the structure of NBR. Left: polar Right: non-polar

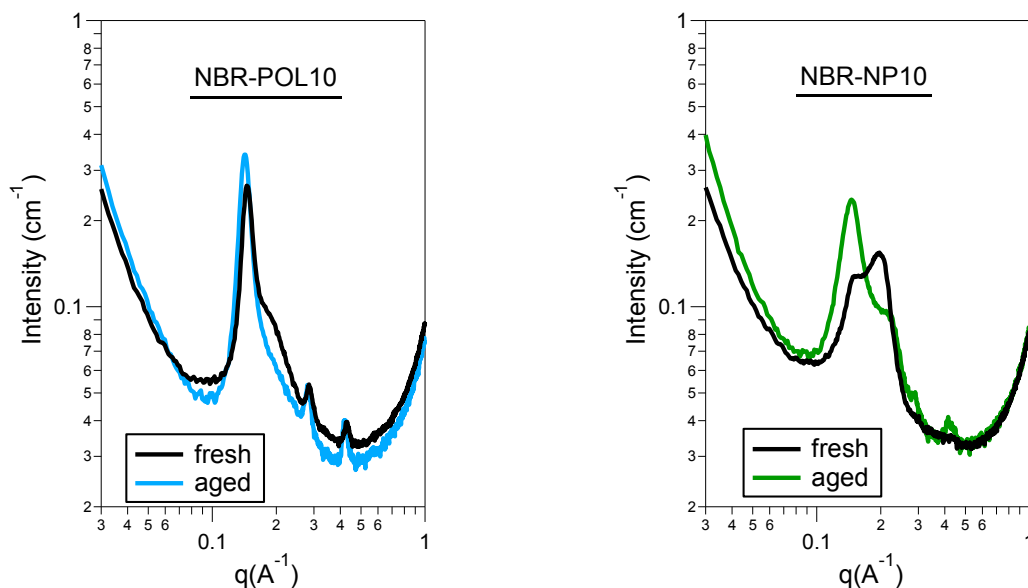


Figure 30 Effect of ageing on the SAXS scattering profiles of NBR-POL10 (left) and NBR-NP10 (right)

### iii Comment

To investigate the structure of the coated glass slide (in the tack samples) the microstructure of the dissolved NBR-POL20 was measured and was similar to that of dissolved NBR-POL10.

## 4.2.4 Conclusions

Two different tackifiers were blended at three concentrations (10, 20 and 40%) into NBR to investigate their influence on self-adhesion.

For each concentration, hardly any difference was probed between both types of tackifiers in terms of self-adhesion energy and linear mechanical properties. For both resins, a significant increase in the short-contact time tack strength was observed when the resin content was increased from 10 to 20%. SAXS profiles reveal, through the disappearance of the amorphous peak or that of the lamellar structure, that the material's microstructure is modified with the addition of resins. It is suggested that whereas the phenolic tackifier disturbs the physical network by directly disrupting  $C\equiv N$  intermolecular interactions, the hydrocarbon resin swells the polybutadiene blocks and, at adequate concentrations (20% in this study), enables sufficient spacing between the polymer chains to disturb the overall structure. In fact, at such concentrations, it is plausible that due to entropic penalty the resin also migrates in the less enthalpically-favorable areas, i.e. polar zones and thus disturb intermolecular interactions. These mechanisms are illustrated in Figure 31 and Figure 32. Even if differences in the X-Ray scattering profile between blends with 10 and 20% are weak, structural analysis does not provide any information on the strength of the intermolecular dipole-dipole interactions. It is thus possible that with 20% tackifier, in addition to the light structure modification observed in Figure 29, the physical bonds are weakened by this elevated resin content and diffusion of polymer chains occurs faster.

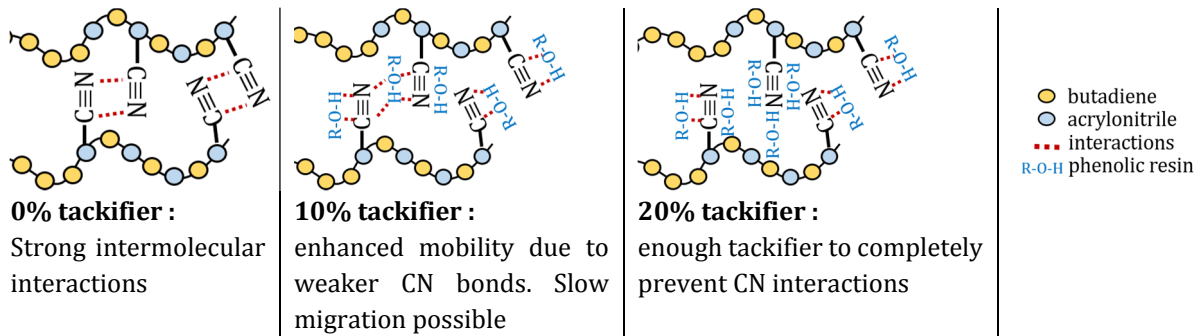


Figure 31 Suggestion for mechanism with increasing polar resin content

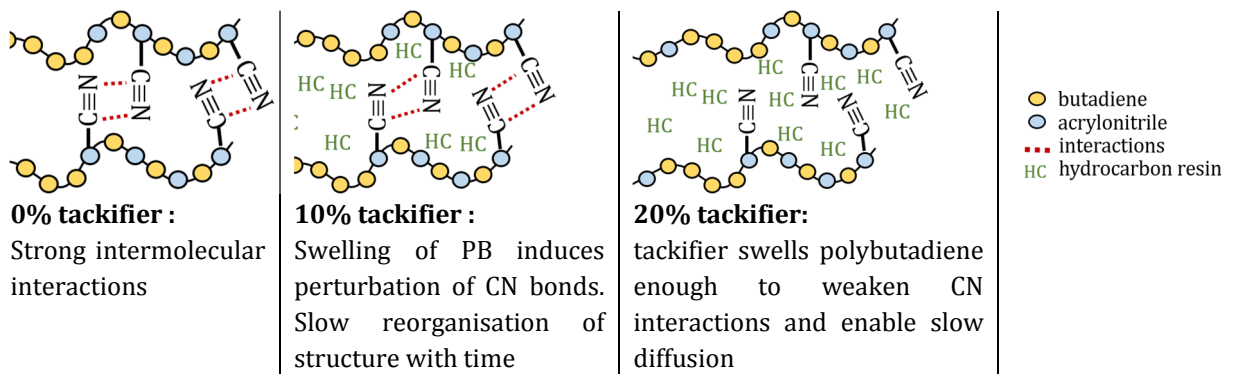


Figure 32 Suggestion for mechanism with increasing non-polar resin content

Moreover, the evolution -with time- of the self-adhesion properties of blends with 10% resin (see Figure 20 and Figure 21) are assumed to be due to two different mechanisms depending on the tackifier's chemical nature. Whereas in the case of polar tackifier association-dissociation processes enable slow diffusion of the polymer chains despite unchanged X-Ray structure and mechanical properties; in the case of hydrocarbon resin it is likely that the increase of tack properties with time is caused by a slow rearrangement of the material's structure leading to changes of the bulk mechanical properties.

## 5. Conclusion

Two types of tackifiers, a phenolic and a hydrocarbon one, were blended in nitrile rubber to enhance its self-adhesion properties. They were introduced at concentration ranging from 3 to 40%; and the tack properties were interpreted in light of mechanical and X-ray scattering measurements.

It is shown that for low resin contents, the addition of non-polar tackifier is ineffective but that of a polar one considerably increases adhesion energies for long contact times. For increasing amounts of tackifiers (10 and 20%), there is hardly any difference in self-adhesion properties between both resins despite their different effect on the microstructure of NBR at short and long times. A step-increase in the tack properties at short contact times is observed from 10 to 20% resin and is assumed to be due to a disruption of the rubber's physical interactions enabling faster diffusion of the chains at the interface.

This study gives a better understanding of the structure and the dynamics of tackified NBR, and gives an insight on how to accelerate the dynamics of the physical bonds of the structure to increase the self-adhesion levels. It is shown that there is not a unique strategy to accelerate chain diffusion in the material, and that the choice of resin, as well as its amount, are application-dependent. Indeed, if long contact between both materials is acceptable from a process standpoint, low amounts of tackifiers are sufficient, and polar ones are needed (see Figure 33 right). Yet if tack properties are needed for short contact times, it seems that the addition of 20% tackifier (of any type) is necessary (see Figure 33 left). These conclusions are supported by Figure 33. The existence of an optimum resin content between 10 and 40% might exist but was not explored.

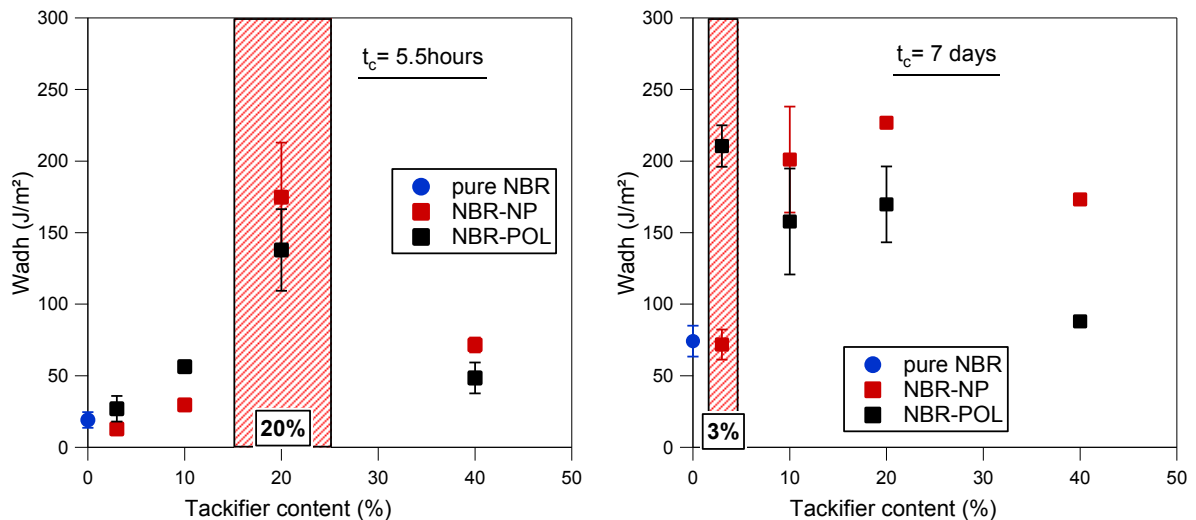


Figure 33 Self-adhesion energies  $W_{adh}$  as a function of tackifier content for short (left) and long (right) contact times

**Take home messages :**

- At low concentration:
  - addition of non-polar tackifier does not improve self-adhesion properties of NBR ( $W_{adh}$ )
  - addition of polar tackifier significantly increases  $W_{adh}$  for long contact times
- At high concentration:
  - chemical nature of the tackifier does not influence the  $W_{adh}$  of the blends
  - drastic improvement of  $W_{adh}$  at short contact times for 20% resin
- Polar tackifier directly disturb intermolecular  $C\equiv N$  interactions and thus enables slow migration of the chains through association-dissociation processes
- Hydrocarbon tackifier swells polybutadiene blocks and intermolecular  $C\equiv N$  interactions are weakened with increasing resin content

## 6. References

- [1] G. R. Hamed, "Tack and Green Strength of Elastomeric Materials," *Rubber Chem. Technol.*, vol. 54, no. 3, pp. 576–595, 1981.
- [2] D. W. Aubrey, M. Sherriff, and N. College, "Viscoelasticity of Rubber-Resin Mixtures," vol. 16, pp. 2631–2643, 1978.
- [3] K. D. Kumar, A. H. Tsou, and A. K. Bhowmick, "Interplay between bulk viscoelasticity and surface energy in autohesive tack of rubber-tackifier blends," *J. Polym. Sci. Part B Polym. Phys.*, vol. 48, no. 9, pp. 972–982, 2010.
- [4] K. D. Kumar, S. Gupta, B. B. Sharma, A. H. Tsou, and A. K. Bhowmick, "Probing the viscoelastic properties of BIMS rubber/tackifier blends using a rubber process analyzer," *Engineering*, vol. 47, pp. 21–25, 2008.
- [5] D. K. Kumar, A. H. Tsou, and A. K. Bhowmick, "Unique behavior of hydrocarbon resin tackifier on unaged and aged tack of brominated isobutylene-co-p-methylstyrene (BIMS) rubber," *J. Adhes. Sci. Technol.*, vol. 22, no. 16, pp. 2039–2058, 2008.
- [6] G. C. Basak, A. Bandyopadhyay, and A. K. Bhowmick, "The role of tackifiers on the auto-adhesion behavior of EPDM rubber," *J. Mater. Sci.*, vol. 47, no. 7, pp. 3166–3176, 2012.
- [7] K. D. Kumar, A. K. Bhowmick, and A. H. Tsou, "Influence of aging on autohesive tack of brominated isobutylene-co-p-methylstyrene (BIMS) rubber in the presence of phenolic resin tackifier," *J. Adhes.*, vol. 84, no. 9, pp. 764–787, 2008.
- [8] Rhee C.K. and Andries J.C., "Factors which influence autohesion of elastomers." 1981.
- [9] C. D. Han, D. M. Baek, and J. K. Kim, "Effect of Microdomain Structure on the Order-Disorder Transition Temperature of Polystyrene-block-Polyisoprene-block-Polystyrene Copolymers," *Macromolecules*, vol. 23, no. 2, pp. 561–570, 1990.
- [10] M. F. Tse, "Studies of triblock copolymer-tackifying resin interactions by viscoelasticity and adhesive performance," *J. Adhes. Sci. Technol.*, vol. 3, no. 1, pp. 551–570, 1989.
- [11] Y. Nakamura and M. Adachi, "Effects of Compatibility Between Tackifier and Polymer on Adhesion Property and Phase Structure ...," *J. Appl. Polym. Sci.*, vol. 116, no. 5, pp. 2658–2667, 2010.
- [12] L. V Sokolova, O. A. Chesnokova, and V. A. Shershnev, "Features of dissolution of crystalline low molecular weight compounds in butadiene-nitrile elastomers," vol. 0, no. 2, pp. 314–321, 1984.
- [13] C. Creton and L. Leibler, "How does tack depend on time of contact and contact pressure?," *J. Polym. Sci. Part B Polym. Phys.*, vol. 34, no. 3, pp. 545–554, 1996.
- [14] G. Henrici-Olivé and S. Olivé, "Molecular interactions and macroscopic properties of polyacrylonitrile and model substances," pp. 123–152, 1979.
- [15] J. Liu, C. S. Y. Tan, Z. Yu, N. Li, C. Abell, and O. A. Scherman, "Tough Supramolecular Polymer Networks with Extreme Stretchability and Fast Room-Temperature Self-Healing," *Adv. Mater.*, vol. 29, no. 22, pp. 1–7, 2017.
- [16] L. V. Sokolova and E. V. Matukhina, "Effect of an anionic emulsifier on the structure of butadiene-nitrile elastomers," *Polym. Sci. Ser. A*, vol. 52, no. 4, pp. 383–391, 2010.

# - CHAPTER 5 -

## SURFACE EFFECTS ON THE SELF-ADHESION OF NITRILE RUBBER

---

It was shown in the previous chapters that for two polymer melts to adhere, migration of chains across the interface must occur. In this chapter, a well-known industrial strategy, called “solvent welding”, is used to favor this interdiffusion and the key physical mechanisms triggering it will be discussed. Once polymer interdiffusion has reinforced the interface, strong mechanical properties are needed to dissipate energy during the debonding stage. We will thus show how the bulk’s structure influences the self-adhesion properties of welded uncrosslinked rubbers. Last, unwelded systems with identical bulk properties but difference surface preparation (through the glass slide drying step) are compared.

“Surface effects” is a generic term to refer to these different interface-related aspects of adhesion.

<b>1. Introduction to solvent welding</b> .....	<b>137</b>
1.1. Literature .....	137
1.2. Methods .....	138
1.2.1 Solvent welding .....	138
1.2.2 Swelling measurements.....	139
<b>2. Influence of solvent welding on the adhesion and self-adhesion of NBR</b> .....	<b>140</b>
2.1. Effect of welding on the adhesion of NBR to glass .....	140
2.2. Self-adhesion of welded NBR.....	140
2.2.1 Influence of welding on the self-adhesion of NBR .....	141
2.2.2 Welded samples: Comparison between adhesion and self-adhesion.....	141
2.2.3 Influence of contact time .....	142
2.2.4 Conclusion.....	143
<b>3. Influence of the solvent</b> .....	<b>144</b>
3.1. Presentation of the different solvents.....	144
3.2. Influence of solvent's quality for the polymer .....	144
3.3. Importance of solvents' vapor pressure .....	147
3.4. Site-specific swelling for welding .....	148
3.5. Influence of the dipole moment.....	149
3.6. Conclusions .....	150
<b>4. Effect of microstructure on solvent-welded NBR</b> .....	<b>151</b>
4.1. Introduction .....	151
4.2. Influence of microstructure on self-adhesion of NBR .....	151
4.3. Conclusion .....	153
<b>5. Influence of drying conditions</b> .....	<b>154</b>
5.1. Effect on the self-adhesion properties .....	154
5.2. Investigations.....	155
5.2.1 Assess of chain's mobility via residual solvent.....	155
5.2.2 Influence of the drying condition on the structure of NBR.....	155
5.2.3 Surface observation .....	157
5.3. Conclusion and discussion .....	158
<b>6. Conclusions</b> .....	<b>159</b>
<b>7. References</b> .....	<b>160</b>

## 1. Introduction to solvent welding

### 1.1. Literature

In order to enhance adhesion - and self-adhesion - properties of uncrosslinked elastomers, companies commonly wipe out the surfaces to be welded with a cloth imbued in solvent. The first objective is to remove any contaminants or pollution that might prevent good surface contact. Although the process is well known and widespread, the mechanisms by which a solvent promotes adhesion is not well understood.

In the literature, the subject is tackled for mainly two purposes: coating solvents and self-healing materials, and is usually referred to as “solvent wiping”, “solvent welding” or “solvent cementing”.

The first explanation lies in the capacity of the solvent to swell the polymer chains and to improve their mobility, thus helping the diffusion of the macromolecules across the interface [1]. Solubility parameters are very often addressed when comparing different solvents' quality for adhesion [2][3][4]. The Hildebrand solubility parameter  $\delta$  is defined as the square root of the cohesive energy density of a compound, which is related to the enthalpy of vaporization (per unit volume) and is thus a measure of the strength of the intermolecular forces in solution. Authors have found different effects of  $\delta$  on adhesion properties. On the one hand, Nadkarni et al [5] showed that the difference in solubility parameters between the polymer and the solvent, which can be used as a quantitative measure of the polymer solvation, plays a key role in achieving good film adhesion. On the other hand, Schuman and coworkers [4] studied the adhesion of coatings to PP and ethylene-styrene copolymers and concluded that adhesion properties were poorly predicted by solvent miscibility. They found out that an improved adhesion was linked to changes in surface topography and moderate swelling, and explained that this swelling might be due to a specific localized swelling (due to composition or morphology) rather than a homogeneous one. Chang [3] and Lin [2] have also observed a correlation between the solvent used for welding and its influence on the surface microstructure of the materials. Caruso and coworkers [6] studied various solvents for the healing of fractured epoxy-based thermosets materials and probed the effect of what they called the “empirical solubility parameter”  $E_T$  of the solvents. Although no information is given on how such parameter has been measured,  $E_T$  of the studied solvents seem to follow a similar trend than the Hildebrand solubility parameter  $\delta$ . Figure 1 shows that the fracture load seems to be maximize for intermediate  $E_T$ . Polar aprotic solvents work well as healing agents whereas protic ones do not. The hydrogen bond acceptor ability of the five most effective solvents is mentioned as another possibility to explain such results.

Remaining solvent in the material acts also as a plasticizer and therefore weakens the mechanical strength of the material. The solvent volatilization is thus necessary after welding [8], and Lin [2] suggested heating to decrease the remaining solvent content. Schuman [4] showed that peel adhesion strength developed faster for higher vapor pressure solvents due to faster volatilization and de-swelling, but that the largest coating adhesion strength were obtained for the less volatile solvents after volatilization of the solvent. For crystallisable polymers, there is an optimum solvent content to develop high adhesive strength, and Figure 2 shows the adhesion strength of highly crystallisable polychlorobutadiene as a function of residual chloroform content [7]. With increasing solvent content at the interface, the autohesion first sharply increases and then diminishes. A low solvent content provides solvation of the contact planes and thus enables a faster diffusion of the polymer chains. Yet if the solvent content is increased even more, its plasticization effect on the mechanical properties of the contact zone affects the bond strength.

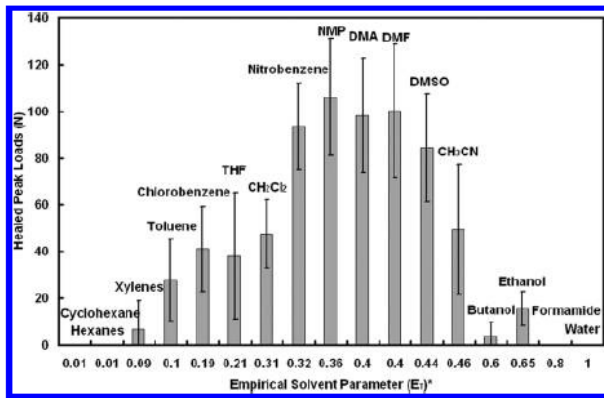


Figure 1 Healed fracture load as a function of empirical solvent parameter. Figure from [6]

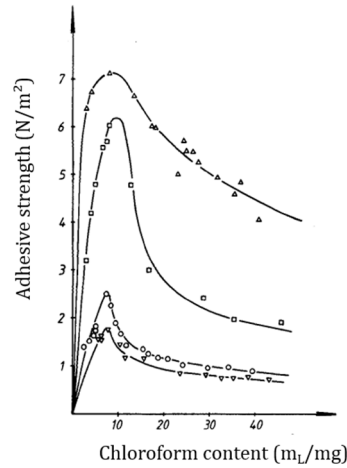


Figure 2 Adhesive strength of highly crystallisable polychlorobutadiene as a function of chloroform content for various contact times. Figure from [7]

The penetration depth of the solvent in the material is correlated to the affinity between the solvent and the polymer, and to the solvent’s vapor pressure, and was found to be a key parameter for effective solvent welding [2]. Other authors [9][5] have investigated the link between solvent wiping and the material’s surface energy and showed that the better the wetting, i.e. the lower the contact angle between the solvent and the polymer, the better was the adhesion.

All the articles stated for this introduction focus on a wide variety of systems, from adhesion of solvent-based coating to self-healing epoxy materials. Substrates are different, as well as application techniques and adhesive strength measurement methods. This short review is thus just an insight into solvent welding and a starting point for our study. Moreover, most of the mentioned articles consider the surface welding of polymers with a solvent, or co-solvent, for a single homogeneous material. Few studies have focused on understanding the welding process for the self-adhesion, or self-healing, of a copolymer with a heterogeneous structure. How does each monomer influence the diffusion? Should the solvent be good for the copolymer as a whole, or mainly for one of the comonomers?

## 1.2. Methods

### 1.2.1 Solvent welding

This strategy is inspired by the industrial process in which the material’s surface is wiped with a rag full of solvent prior to bringing the two elastomer layers into contact. To mimic this process at the laboratory scale, 3uL of solvent were dropped on the glass slide before placing the rubber disk on top, as illustrated on Figure 3 below:

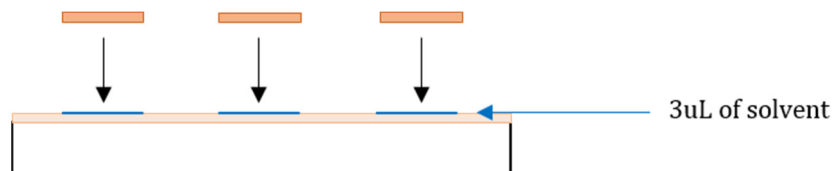


Figure 3 Illustration of solvent welding at the laboratory scale

Unlike what is done in the industrial process, this method does not enable removal of surface pollutant from the surface. Yet the samples are prepared as to avoid any dust deposition, and this method enables a perfect control of the wetting condition, especially the deposit volume.

### 1.2.2 Swelling measurements

To determine solvents' quality for the used NBR, swelling experiments were run on crosslinked samples.

#### i. Crosslinking of NBR

In the literature, the vulcanization of nitrile rubber with either sulfur or peroxides is well documented [10][11][12][13]. During this study, dicumyl peroxide (DCP) was used for crosslinking. DCP first decomposes to form free radicals, and then reacts with the elastomer by abstraction of hydrogen from the elastomer chains, or by the addition to a double bond of unsaturated rubbers [12][11]. The elastomer radicals that are formed during these reactions then mutually recombine to form crosslinks (see Figure 4).

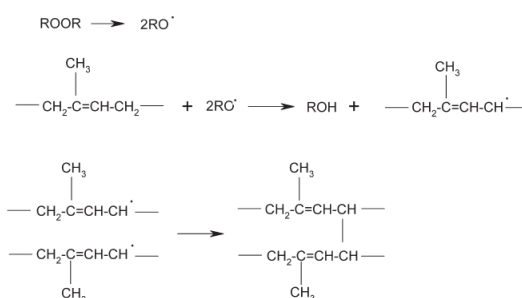


Figure 4 Peroxide crosslinking of natural rubber. From [11]

Authors have used DCP between 1 [12] and 2.5 [13][10] phr and used different time-temperature pairs to ensure total curing.

In this work, as received NBR was blended with 2.4phr DCP in the twin screw extruder. To ensure homogeneous mixing, the blend was masticated during 20 minutes at 85°C. The material was then set in a heating press, with a 2mm-thick mold, at 150°C during 2 hours to achieve complete crosslinking. The same method was used to vulcanize polybutadiene.

#### ii. Swelling measurements

A punch was used to cut 8mm-diameter cylinders in the 2mm-thick layer of crosslinked NBR. These were weighed and placed into vials full of solvents. After a desired swelling time, the samples were taken out of the vials and weighed after removal of solvent excess using a KimTech paper wiper. The swelling ratio  $Q$  (%) is computed as:

$$Q = \frac{m - m_i}{m_i} * 100 \quad 5.1$$

With  $m_i$  the sample initial mass (mg) and  $m$ (mg) its mass at the time of measurement.

## 2. Influence of solvent welding on the adhesion and self-adhesion of NBR

### 2.1. Effect of welding on the adhesion of NBR to glass

Butanone (also called methylethylketone, “MEK”) was first used as a welding solvent. The effect of solvent (MEK) welding on the adhesion of NBR to glass is investigated and the samples illustrated in Figure 5 are compared after 24 hours of contact at room temperature.

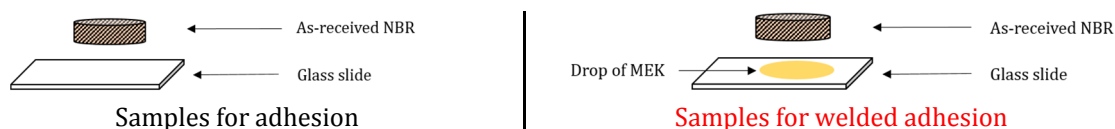


Figure 5 Tack samples for adhesion on glass with (right) and without (left) welding

From Figure 6, it is clear that the use of solvent increases the quality of the contact between the rubber and the glass surface (increase in the cavitation peak) and also reinforces interfacial interactions (increase in the total deformation).

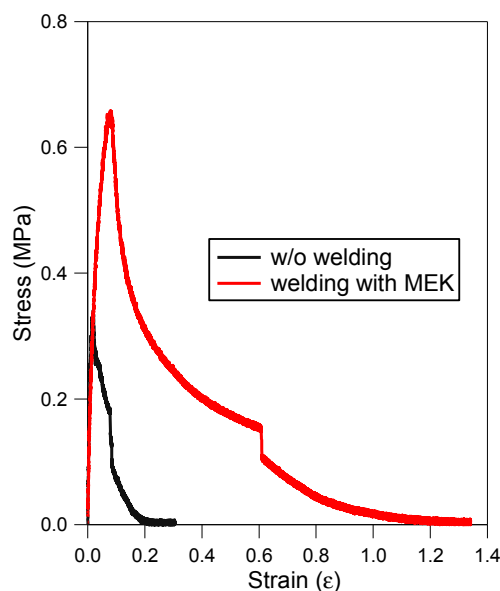


Figure 6 Effect of welding on the adhesion properties of NBR on glass. Contact time=24h

Indeed, in the presence of solvent, more mobility is given to the polymer chains from NBR, which can re-orient to favor C≡N polar interactions with glass' silanols.

### 2.2. Self-adhesion of welded NBR

Butanone was used as a welding solvent, and the influence of contact time on the self-adhesion properties of NBR was probed.

NB: For strains  $\epsilon$  higher than 800% the limit of the extensometer is reached, hence a final stress different than zero.

**2.2.1 Influence of welding on the self-adhesion of NBR**

Welded and un-welded NBR interfaces are compared, and samples are illustrated in Figure 7. The comparison of their stress-strain debonding curves after 24 hours of contact are shown in Figure 8.

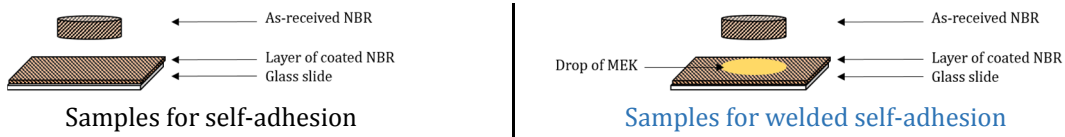


Figure 7 Tack samples for self-adhesion with (right) and without (left) MEK welding

Consistent with what has been probed for adhesion on glass in paragraph 2.1, the cavitation peak as well as the overall deformation are significantly increased compared to non-welded samples. Welding with a solvent ensures intimate contact between both surfaces, hence a higher stress needed for cavities to appear. Furthermore, solvent gives mobility to the interfacial layers of NBR and thus enable migration of polymer chains at the interface. High energy dissipation is possible through fibrils formation in the bulk hence the plateau in stress at around 0.04MPa. Debonding occurs via cohesive failure inside the fibrils. With MEK welding the self-adhesion energy of NBR is increased from 30J/m<sup>2</sup> to 470J/m

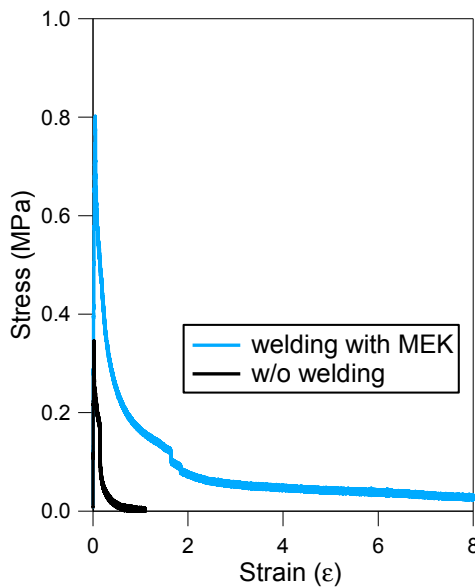


Figure 8 Effect of solvent welding on the self-adhesion properties of raw NBR. Contact time=24h

**2.2.2 Welded samples: Comparison between adhesion and self-adhesion**

The effect of welding on the self-adhesion of NBR, and on its adhesion on glass are compared. Samples are illustrated in Figure 9 below.



Figure 9 Tack samples for NBR adhesion on glass (left) and for NBR self-adhesion (right), both with MEK welding

Figure 10 compares their behavior during the debonding stage. The contact area is, as expected, the same. The difference comes from the nature of the interfacial interactions, i.e. its mechanical reinforcement. In the case of self-adhesion, not only is there chain re-arrangement at the interface to favor polar interactions, but also chain migration across the interface to heal it.

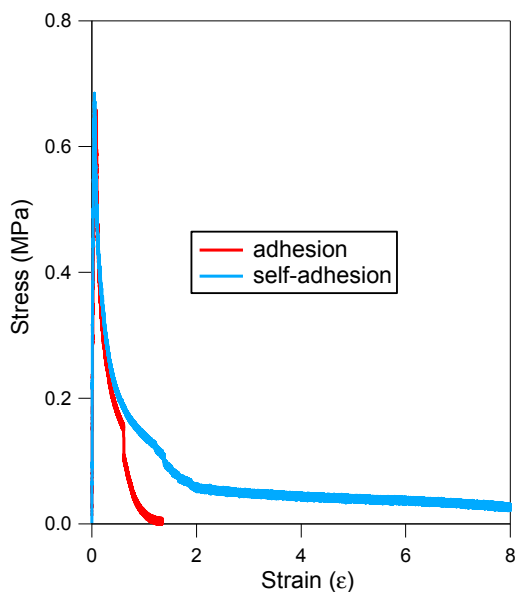


Figure 10 Comparison of adhesion on glass and self-adhesion of NBR, welded with butanone. Contact time = 24h

Table 1 summarizes the different energies for adhesion and self-adhesion, with and without solvent welding for 24 hours of contact:

System	Welding?	Average Wadh (J/m <sup>2</sup> )
Adhesion	No	30
Adhesion	Yes	170
Self-adhesion	No	30
Self-adhesion	Yes	470

Table 1 Effect of welding with MEK on the adhesion and self-adhesion properties of NBR

### 2.2.3 Influence of contact time

The effect of contact time on MEK-welded self-adhesion samples is shown in Figure 11. The self-adhesion energies of NBR with and without welding with MEK are compared in Figure 12, and reveal that the use of solvent boosts the energy by more than 10-fold for any contact time.

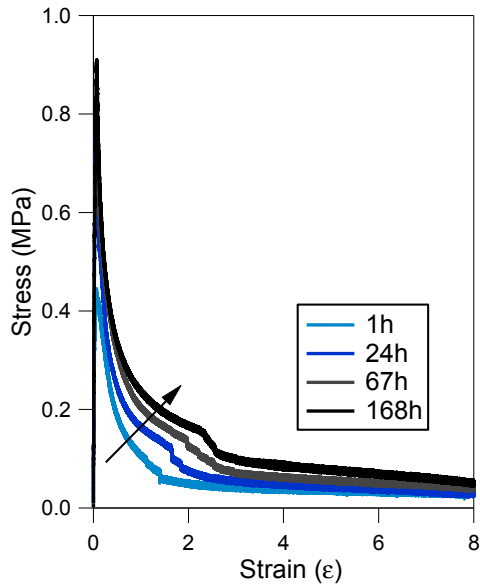


Figure 11 Effect of contact time on the self-adhesion properties of as-received NBR welded with MEK

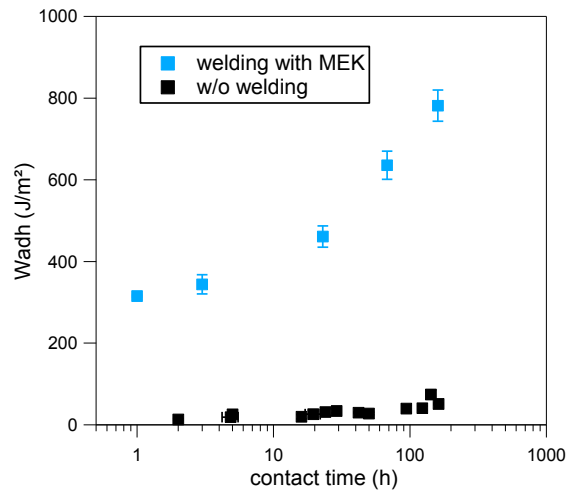


Figure 12 Influence of solvent welding with MEK for the self-adhesion of as-received NBR, for various contact times

We can hypothesize that the use of solvent disturbs the lamellar structures in the bulk and on the coated glass slide, and therefore permits flow of the chains. Even for contact times of the order of a week the self-adhesion energy keeps increasing, even though most of the solvent has disappeared from the interface. It is possible that during this slow drying process, the solvent-affected layer (called “interfacial layer” in Figure 13) self-organizes into a structure different from that of the bulk. This structure is likely to evolve and re-arrange over time and can lead to a strengthening of the bulk mechanical properties. The effect of solvent welding is therefore suggested to happen in two stages: first an interdiffusion step, followed by a strengthening of the interface through a change in mechanical properties. It is also possible that the structure of the interfacial layer (unlike that of as-received NBR) enables chains migration at the interface hence the increase of  $W_{adh}$  with  $t_c$  even for long contact times.

These different phases are illustrated on Figure 13.

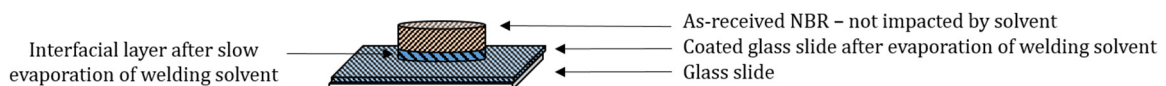


Figure 13 Illustration of tack contact after drying of solvent welding

To gain a better insight on the parameters controlling the efficiency of solvent welding, several solvents were tried and compared for a given contact time.

### 2.2.4 Conclusion

In this section, two key conditions for self-adhesion performance were illustrated, the effective contact area and the interfacial interactions. These can be triggered by modifying one of the materials, or by the use of solvent to weld the interfaces. When one of these two, or both, is increased, the adhesion and self-adhesion properties of uncrosslinked elastomer is enhanced. During this part, the bulk properties remained constant as the same NBR was used all along.

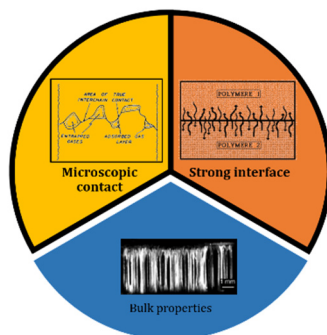


Figure 14 Microscopic contact and interfacial interactions are key to explain the difference unwelded and welded samples

### 3. Influence of the solvent

Different solvents were probed using the same methodology, and debonding was performed after three hours of contact.

#### 3.1. Presentation of the different solvents

Thirteen solvents, with various characteristics in terms of physical and chemical behavior, have been tried for welding.

Solvent	Type	Teb (°C)	$\delta$ (MPa <sup>1/2</sup> )
Butanone (MEK)	Polar aprotic	77	18.7
Acetone		56	20.3
Ethyl acetate		77	18.6
DMF		153	24.9
Cyclohexanone		156	20.3
Toluene	Nonpolar aprotic	111	18.2
Dichloromethane		40	20.2
Chloroform		61	18.7
Tetrahydrofuran		66	18.6
Pentane		36	14.3
Isopropanol	Protic	83	13.7
Methanol		65	29.7
Industrial	NA	>190	NA

Table 2 Characteristics of the solvent used for welding

The goal is to have an increased comprehension of the key criteria determining solvent welding's efficiency. Several hypothesis will be made and their relevance discussed.

#### 3.2. Influence of solvent's quality for the polymer

As mentioned in section 1.1, one of the most examined parameter is the role of the solvent's quality for the polymer. Indeed, some argue that the higher the affinity between the polymer and the solvent, the better overall swelling, and therefore the enhanced chains' mobility. To probe this affinity, the Hildebrand solubility parameter  $\delta$  is used. Materials with similar solubility parameters are able to interact with one another, resulting in solvation, miscibility or swelling. Yet for nitrile rubber, copolymer of acrylonitrile and butadiene, the solubility parameter highly

depends on the ratio between the two monomers [14][15] and differs for each material. In the literature, parameters between 19.2 and 21.1 MPa<sup>1/2</sup> are found for NBR [14]. To better probe the solvents' quality for the studied NBR, swelling measurements (see method in 1.2) were performed and the influence of the swelling ratio on the self-adhesion energies of the welded system is probed.

Solvent	Teb (°C)	Swelling (%)	W <sub>adh</sub> (J/m <sup>2</sup> )
Butanone (MEK)	77	250	370
Acetone	56	170	354
Ethyl acetate	77	200	322
Toluene	111	250	301
Dichloromethane	40	760	269
Industrial	>190	180	267
Cyclohexanone	156	410	252
Chloroform	61	900	241
Tetrahydrofuran	66	380	237
Isopropanol	83	20	160
Methanol	65	20	129
Pentane	36	20	31

Table 3 Solvents capacity to swell NBR, and to weld NBR interfaces

Table 3 summarizes the results for the studied solvent (with decreasing values of W<sub>adh</sub>), and Figure 15 plots the self-adhesion energy W<sub>adh</sub> of welded NBR samples as a function of swelling ratio. Unfortunately DMF was introduced lately in the study and the rubber's swelling properties were not measured in this solvent.

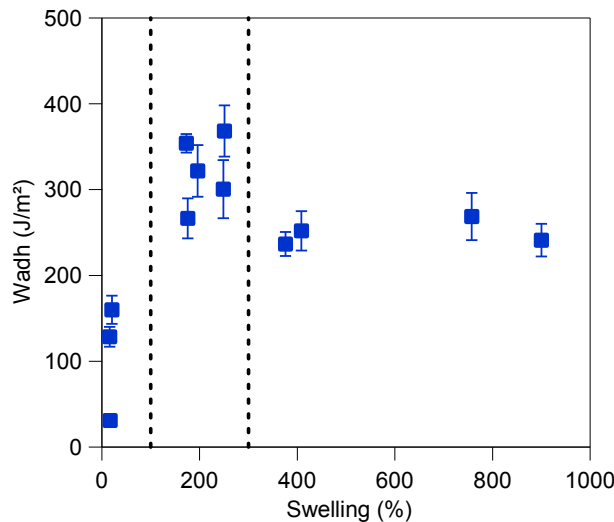


Figure 15 Influence of solvent quality (probed by swelling) on the self-adhesion energy of raw-NBR. Contact time=3h

As expected, bad solvents for the polymer [Q<100%] are the least efficient in welding polymer interfaces. Yet except for Pentane [Q=20%; W<sub>adh</sub>~31]/m<sup>2</sup>] which will be commented later, all adhesion energies are higher than 100]/m<sup>2</sup>, meaning that even for some relatively poor solvents, the self-adhesion properties are enhanced compared to unwelded samples. Figure 16 compares the stress-strain curves of raw NBR without welding, and that with welding with methanol [Q=20%], both for a contact time of three hours.

Welding with a bad solvent still may soften the surface and enhances the effective contact area (increase in cavitation peak), thus increasing the number of interfacial interactions and the self-adhesion properties. Yet they are unable to give enough mobility to the polymer chains, hence a limited effect.

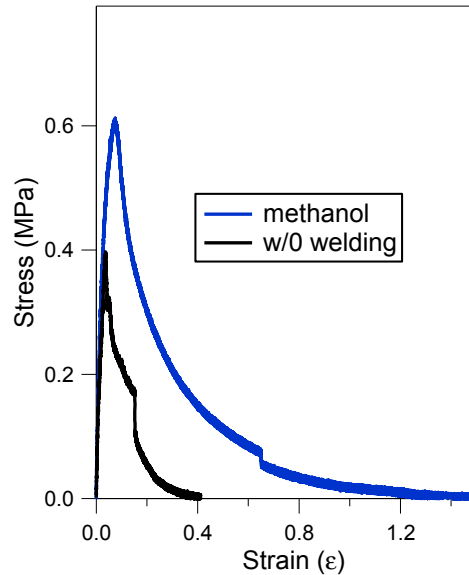


Figure 16 Effect of methanol [Q=20%] welding on the self-adhesion properties of NBR

In Figure 15, it is clear that the best solvents for welding are not necessarily the best solvents in terms of swelling properties. For swellings greater than 300%, the self-adhesion properties are reduced. Figure 17 compares the stress-strain curves during debonding for samples welded with butanone [Q=250%] and with cyclohexanone [Q=410%], and for butanone and chloroform [Q=900%]. The curves are similar at low strains, and the main difference comes for strains higher than 100%. Butanone has an intermediate boiling temperature between cyclohexanone and chloroform such that the effect probed is not due to mere difference in solvent vapor pressure.

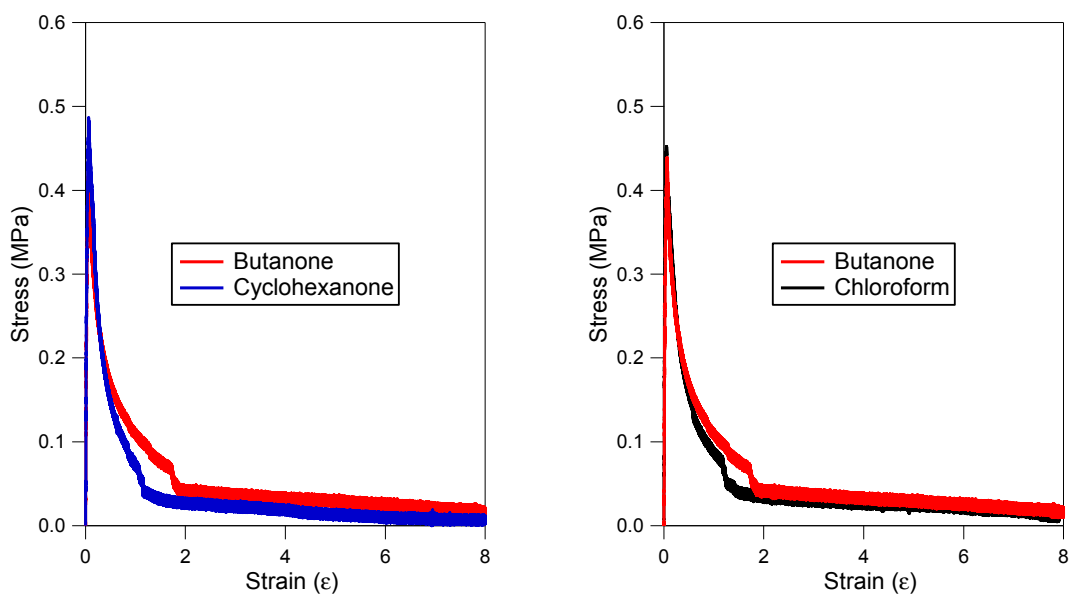


Figure 17 Comparison of several welding solvents' effect on the self-adhesion properties of NBR. Contact time=3h

When the solvent-polymer affinity is high, solvent-polymer interactions delay the solvent removal, and increases the penetration depth. Therefore, as suggested by Ryntz [8] and Lin [2], solvent residues after three hours of contact may swell the material in the bulk near the interface and alter its mechanical properties. This influence on the material bulk's behavior induces a difference in the large deformation regime.

Moreover, the time during which the solvent is present determines the time during which migration of the polymer chains across the interface is possible, and is therefore another key parameter. There is thus a tradeoff between the solvent's ability to enhance chain migration, and its influence on the bulk's mechanical properties.

### 3.3. Importance of solvents' vapor pressure

Methanol and pentane give nitrile rubber similar swelling properties [ $Q=20\%$ ]; yet for a contact of three hours, methanol is a much better welding solvent than pentane [ $W_{adh}(\text{MeOH})=129\text{J}/\text{m}^2$  whereas  $W_{adh}(\text{pentane})=31\text{J}/\text{m}^2$ ]. The corresponding stress-strain curves are plotted in Figure 18 and compared to that of un-welded NBR samples.

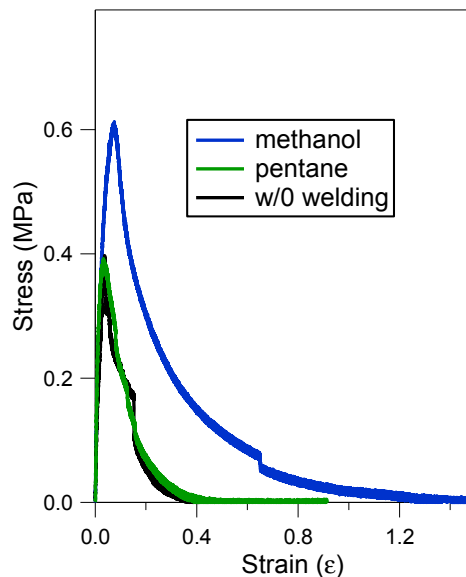


Figure 18 Effect of methanol and pentane as welding solvent for NBR. Comparison with un-welded sample.

Pentane has a boiling temperature of  $36^{\circ}\text{C}$  and has presumably evaporated before the contact between both materials is performed. Therefore, its effect on the self-adhesion property of NBR is negligible and the debonding is similar to that of raw un-welded NBR.

One can thus fix a boiling temperature-related criteria stating that solvents for which the characteristic temperature is lower than  $50^{\circ}\text{C}$  are inappropriate for welding. On the other side of the spectra, if the boiling temperature is too high, the mechanical properties are impacted by residual solvent. This upper limit criteria depends on the desired process, i.e. on the time available before testing the assembly.

### 3.4. Site-specific swelling for welding

As seen in Chapter 3, the material is a multi-block copolymer with blocks of polybutadiene and sequences of alternating butadiene-acrylonitrile units. The whole polymer is physically crosslinked thanks to intermolecular polar interactions between the CN groups of the chains. To enable chain diffusion, these interactions need to be broken or at least weakened. Therefore, similar to what was shown in Chapter 4 with two tackifiers having a different affinity for each block, one can picture that solvents can either specifically swell butadiene blocks, or specifically disturb acrylonitrile interactions, regardless of their global interaction parameter for the copolymer.

We have thus decided to compare the effect of four different solvents (butanone, cyclohexanone, toluene and an industrial solvent) on the self-adhesion properties of NBR, with regard to their affinity for polybutadiene and acrylonitrile separately. To assess that of polybutadiene, it was swelled in the studied solvents and the maximum swelling ratios are shown in Table 4. On the other side, as acrylonitrile (ACN) is not soluble in these solvents and that swelling measurements are arduous due to its complicated shaping, their relative affinity was estimated by comparing the solvents ability to swell NBR and PB. It was estimated that the difference in swelling of NBR and PB [Q(NBR)-Q(PB)] gives an indication of the solvents affinity with ACN and is calculated in column 5 ("estimated ACN"). This value is qualitative and can only be an indicator of the solvent's affinity for acrylonitrile. A solvent with high affinity for ACN will disturb  $C\equiv N$  physical interactions [17][18] and could therefore explain enhanced mobility of the polymer chains, as illustrated in Figure 19. As toluene is the best known solvent for polybutadiene [16][14], all PB swellings are normalized by that in toluene to make the data more clear (column 4).

Solvent	Swelling NBR (%)	Swelling PB (%)	Swelling PB/toluene	Estimated ACN (%)	$W_{adh}^*$ (J/m <sup>2</sup> )
Butanone	450	50	0.25	400	370
Toluene	220	200	1	20	300
Industrial solvent	200	7	0.035	163	270
Cyclohexanone	630	160	0.8	470	250

\*values +/-20J/m<sup>2</sup>

Table 4 Swelling properties and self-adhesion energies of solvents used for welding of NBR

From Table 4 it is suggested that toluene hardly swells acrylonitrile parts (~20%) yet its effect on self-adhesion properties are at least as good as that of other solvents with better affinity for acrylonitrile.

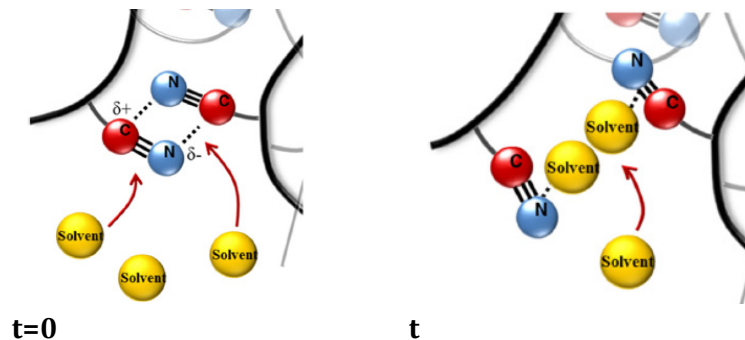


Figure 19 Interactions between polyacrylonitrile and solvent molecules [17]

Following the same logic, the self-adhesion properties of toluene (best solvent for polybutadiene) are compared to those of DMF which is assumed [19][17] to be the best solvent for polyacrylonitrile. Results are shown in Annex 4 and show that both solvents enhance in a similar manner the tack performance of NBR. Therefore, there is no unique way to enhance self-adhesion of the studied NBR block copolymer and two completely different solvent, one preferential for polybutadiene and the other preferential for polyacrylonitrile, can give the same result. These results go along with the site-specific swelling mechanisms proposed by Schuman and coworkers [4], and are relevant to compare with the proposed mechanisms for the polar and non-polar tackifier mentioned in Chapter 4.

### 3.5. Influence of the dipole moment

For the previously mentioned reasons (3.3), only solvents with boiling temperatures between 50 and 150°C have been compared in this section. They are listed in Table 5, and ranked with decreasing self-adhesion energy  $W_{adh}$ .

Solvent	$W_{adh}$ (J/m <sup>2</sup> )	Dipolar moment $\mu$ (D)	Dielectric constant
Butanone	370	5.22	18.5
Acetone	350	2.86	20.7
Ethyl acetate	320	1.78	6.02
Toluene	300	0.43	2.38
THF	240	1.75	7.58
Chloroform	240	1.15	4.8
Isopropanol	160	1.65	19.9
Methanol	130	1.71	32.7

Table 5 Description of the studied solvents, with 50°C <  $T_{eb}$  < 150°C

A dipole moment  $\mu$  is present in any molecule in which the average positive charge and the average negative charge are not over imposed. Rosenbaum and co-workers [20] studied the plasticizing effect of different solvents for poly-acrylonitrile. They suggested that the dipole moment  $\mu$  is the best single measure of the plasticization effectiveness. They performed uniaxial tensile tests on fibers immersed in solvents, and considered plasticizing as the decrease of the fiber's resistance to an imposed stress. The influence of the dipole moment  $\mu$  on the self-adhesion energy of NBR  $W_{adh}$  is plotted on Figure 20 for these eight solvents.

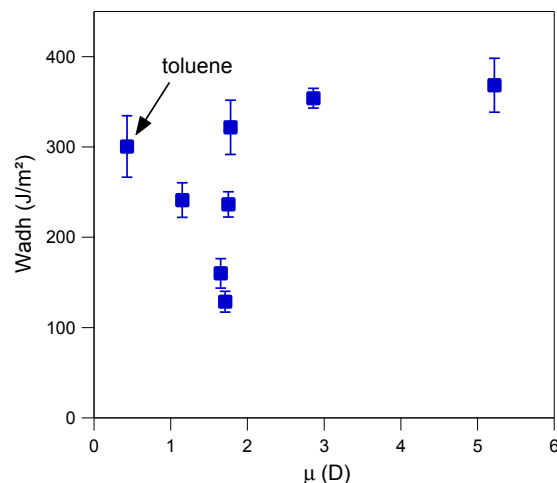


Figure 20 Self-adhesion energy  $W_{adh}$  as a function of dipolar moment  $\mu$ .  
Contact time=3h

It is shown that in the case of solvents with a strong ( $\mu > 2D$ ) dipolar moment, the self-adhesion property of NBR are increased. The trend is not so clear for lower dipolar moments. Toluene has the lowest dipolar moment (of the studied solvents) and yet is very effective for welding. This is likely due to its great affinity for polybutadiene, which permits important swelling of the PB segments, thus disrupting the physical network.

Let us comment that no clear trend was observed regarding the effect of dielectric constant.

### 3.6. Conclusions

Thirteen solvents were used as welding agents for NBR. Their effect on the self-adhesion properties of nitrile rubber were investigated for three hours of contact, and the results analyzed in light of the solvents physical parameters. From the above study, there is no unique parameter predicting the efficiency of a solvent for welding but a combination of several ones are needed to explain the behaviors probed. A first criteria is the affinity between the solvent and the material, which was probed thanks to swelling measurements. There seems to exist an optimum in affinity for welding properties, as was previously suggested by Caruso and coworkers [6]. Indeed, when the affinity is too high, the penetration depth is increased, which impacts the polymer's mechanical properties by plasticization. To limit the long diffusion of solvent molecules into the polymer, the solvent's vapor pressure must not be too low.

Solvents with high dipolar moment seem to be the most efficient for solvent welding of NBR. More generally speaking, polar aprotic solvents with reasonable (between 50°C and 150°C in this study, but depends on the practical application considered) boiling temperature appear to be the best choice. Yet as several solvents are shown to be efficient, other criterias can be chosen for industrial applications, such as environmental impact, price and toxicity.

Moreover, this study was performed for a contact time of three hours but it was shown in section 2.2 that the self-adhesion properties continue to evolve for long contact times. As different drying solvents lead to different microstructures (see X-Ray scattering profiles in Annex 3.2) it is very likely that the self-adhesion properties of NBR evolve differently with time, with respect to the solvent used for welding.

## 4. Effect of microstructure on solvent-welded NBR

So far, apart from a comparison in Chapter 3, part 3.2, all the self-adhesion properties were measured with a rubber disk molded from as-received NBR. We now investigate the effect of this disk's microstructure on the self-adhesion of NBR.

### 4.1. Introduction

During this section, cyclohexanone was used as welding solvent, and the self-adhesion properties of as-received NBR and extruded NBR, as well as their evolution with time, were compared. Both systems are illustrated in Figure 21 below. The colors of the rubber disk (red for the **extruded** NBR, blue for the **as-received** one) on the top is used to make the graphs in the next paragraph clearer.



Figure 21 Illustration of the two systems: self-adhesion of welded as-received (blue) and freshly extruded (red) NBR

### 4.2. Influence of microstructure on self-adhesion of NBR

Samples in Figure 21 were debonded after several contact times  $t_c$  and the evolution, with time, of the self-adhesion properties of freshly extruded NBR, welded with cyclohexanone, are plotted in Figure 22. As expected, an increase of the overall deformation with time is measured thanks to the reinforcement of the interface with polymer chain diffusion. In fact, for both systems (freshly extruded and as-received), the structure at the interface is disrupted thanks to the welding with cyclohexanone, thus enhancing the mobility of polymer chains and favoring healing of the interface.

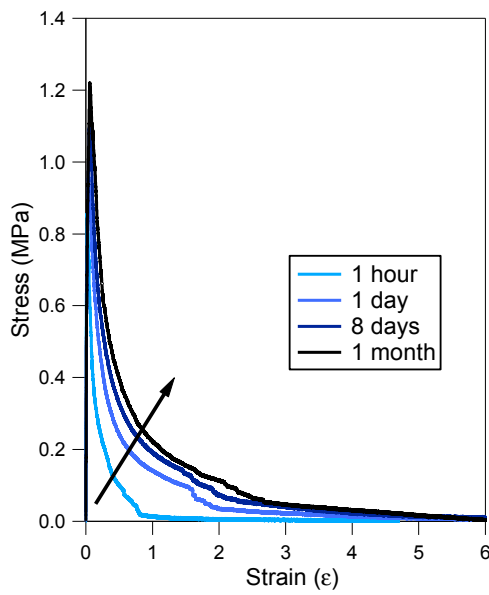


Figure 22 Influence of contact time on the stress-strain debonding curves of freshly extruded NBR, welded with cyclohexanone

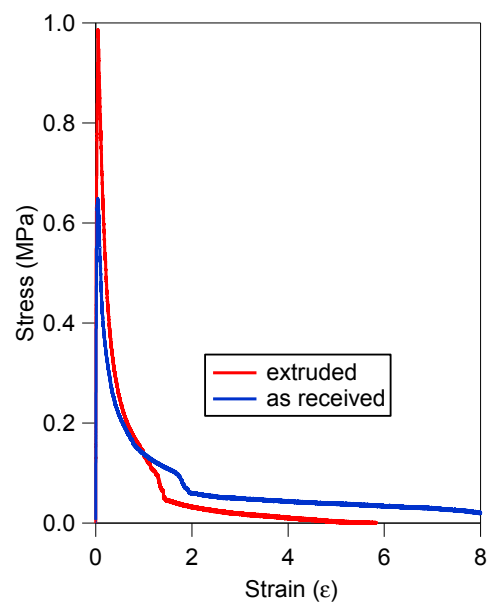


Figure 23 Comparison between the stress-strain debonding curves of freshly extruded and as-received NBR. Contact time=24h

Figure 23 compares the self-adhesion properties of as-received and extruded NBR, welded with cyclohexanone, for a contact time of 24 hours. The corresponding self-adhesion energies are respectively 350 and 200J/m<sup>2</sup>, and the difference is mainly due to the overall deformation, and more specifically to the stress plateau during the debonding stage. This plateau is due to the materials' ability to dissipate energy and to form fibrils, and is a direct sensor of its mechanical properties. Therefore, uniaxial tensile tests were run on both samples, with the same strain rate as that in the tack experiment, and the results are plotted on Figure 24. Thanks to the structure of the as-received sample, the material is strengthened and much more energy is needed to deform it compared to the extruded sample in which the organization has been disrupted.

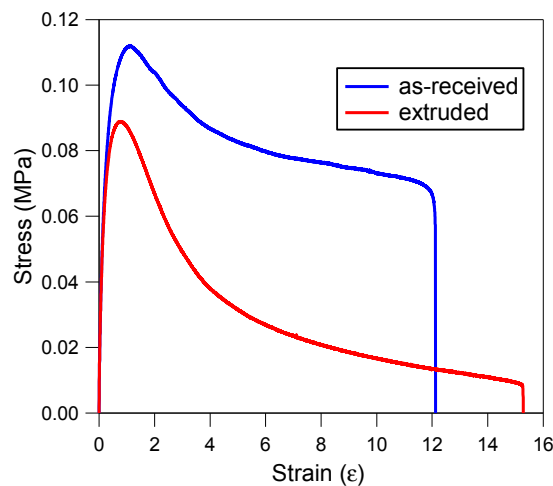


Figure 24 Uniaxial tensile test. Comparison between freshly extruded and as-received NBR

The self-adhesion energies for different contact times are plotted in Figure 25 and show the importance of cohesive strength to reach high adhesion levels. It is estimated, from the uniaxial tensile curves, that the energy dissipated during uniaxial traction is close to two times higher for the as-received sample than that for the extruded one (respectively 1.0 and 0.47MPa). The same difference is measured in self-adhesion energies between both welded systems.

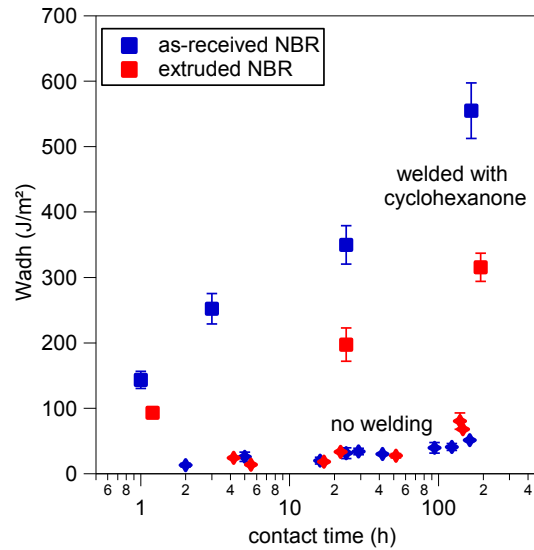


Figure 25 Self-adhesion energy  $W_{adh}$  as a function of contact time  $t_c$  for freshly extruded and as-received NBR. Effect of cyclohexanone welding

### 4.3. Conclusion

During this part, the contacts quality (both the effective area, and the interfacial properties) were insured thanks to solvent welding such that the difference between both samples was solely due to a change in mechanical properties of the bulk. The as-received sample is at thermodynamic equilibrium and behaves as a strong physical network. During the debonding stage, its fibrils are more stable than that of the out-of-equilibrium extruded NBR, leading to enhanced energy dissipation and high overall self-adhesion energy. For both systems, welding is necessary to disturb the microstructure on the glass slide and enable diffusion of the polymer chains at the interface.

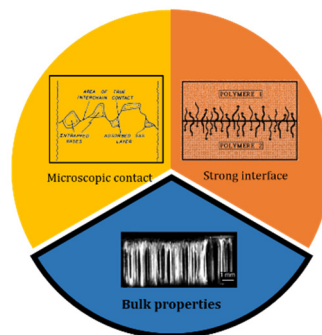


Figure 26 A shift in green strength considerably modifies the self-adhesion properties

## 5. Influence of drying conditions

Since the beginning of the study, the glass slides were dried overnight at room temperature and then in a vacuum oven at 100°C for 2 hours. During this section, another drying condition was investigated, and the impact on the self-adhesion properties was probed. The rubber disk remained as-received NBR in both cases. Contact was established similarly (see methodology in Chapter 2) and the influence of contact time on self-adhesion properties was investigated. The two drying conditions were:

- 1- Overnight at room temperature + 2 hours at 100°C in a vacuum oven
- 2- 2 days at room temperature + 2 days at 70°C in a vacuum oven

They will be referred to as DRY100 and DRY70.

Note: During this section, the two surfaces were not solvent welded.

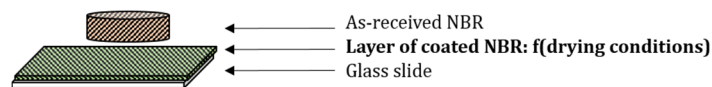


Figure 27 Illustration of the tack samples with modification of the glass slide drying conditions

### 5.1. Effect on the self-adhesion properties

The stress-strain curves during the debonding after 1. five hours and 2. five days of contact are shown in Figure 28. The self-adhesion properties are similar at short (5 hours) contact times ( $W_{adh} \sim 20\text{J/m}^2$ ), but whereas that of DRY100 hardly evolve with time, that of DRY70 tremendously increase. An increase in both the cavitation peak and the overall deformation with contact time is probed. The resulting self-adhesion energies  $W_{adh}$  are plotted as a function of contact time in Figure 29.

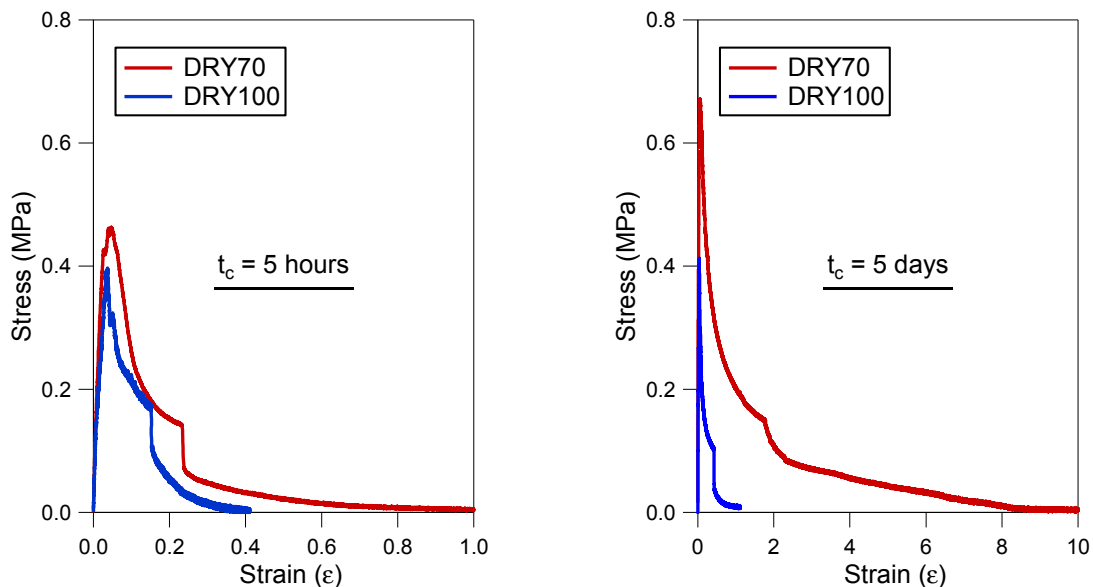


Figure 28 Stress-strain curves during debonding of NBR for both drying conditions, for contact times of 5 hours (left) and 5 days (right)

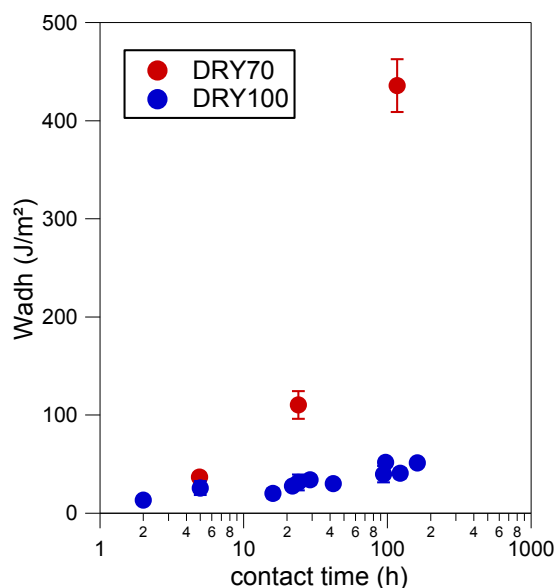


Figure 29 NBR self-adhesion energy for the two drying conditions

These observations tend to show that one system (DRY70) enables the diffusion of NBR chains, whereas the other (DRY100) does not. The only difference between the two tests being the coated glass slides, the coating was scrapped using a razor blade and analyzed by means of TGA and DSC.

## 5.2. Investigations

### 5.2.1 Assess of chain's mobility via residual solvent

TGA was used to compare the residual solvent (cyclohexanone) in each samples between 50 and 300°C. As there was no significant difference between both samples, the difference in self-adhesion properties is not due to remaining solvent. To assess the difference in the chains' mobility between the two samples, DSC measurements were run from -60°C to 120°C at 20°C/min. For both materials, the measured T<sub>g</sub> is identical (~ -31°C). This result first confirms that there are no impact of residual solvent, but also points out that the overall chain mobility should be the same in both samples.

### 5.2.2 Influence of the drying condition on the structure of NBR

It was hypothesized that the change in self-adhesion properties was due to a change in the structure on the coated glass. Sokolova and coworkers [21] used WAXS experiments to show a slight change in the scattering vector of small structures (<2.4Å) of nitrile rubbers after annealing at 100°C. Authors suggest that annealing at such temperature leads to an increase in the size and/or amount of ordered structures due to an increase in the local mobility of acrylonitrile sequences (T<sub>g</sub> (PAN) ~ 85°C) and partial decomposition of microblocks of trans-1.4-butadiene units. To examine if this annealing at 100°C has similar effects on the structure of the studied NBR, the structure of the material after both drying conditions was investigated. X-ray scattering experiments were therefore performed on samples that had been prepared with the same methodology as the glass slides, and the results are shown on Figure 30.

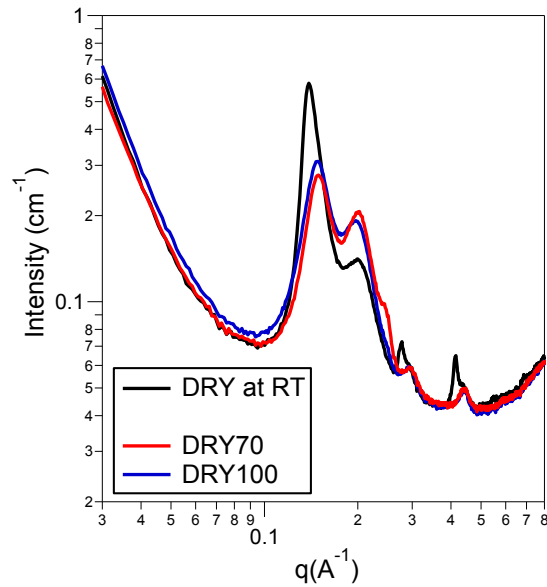


Figure 30 Influence of drying conditions on the structure of solubilized NBR (SAXS data). Black curve shows the sample that has only dried at room temperature during one day

It is shown that, as already exposed in Chapter 3, when drying, be it at 70°C or 100°C, the first lamellar structure is disrupted. The resulting microstructure is the same, at least at the investigated length scale, for both drying conditions (DRY70 and DRY100). Yet the SAXS experiments are run on 1mm thick samples and the measured intensity is an average of the probed thickness. It is likely that there are surface effects and that the structure is not similar at the air-interface and in the bulk. Moreover, only the nanometer scale is probed with these experiments.

To be more consistent with the tack experiments, AFM observations were also performed, and surface was analyzed over several square micrometers.

### 5.2.3 Surface observation

Atomic Force Microscopy was used to probe the surface structure of the coated glass slides after annealing at 70°C and 100°C. Shull and coworkers [22] demonstrated that annealing of lamellae-forming block copolymers may lead to the orientation of the domains parallel to the surface, preventing any diffusion of polymer chains. This effect was investigated in the studied NBR system.

Solutions of 2.5wt% NBR in cyclohexanone were filtered with 0.2µm cellulose acetate membranes prior to coating. Samples were analyzed with AFM after drying at 70°C and 100°C. Pictures were taken at 20 and 1 microns and are compared in Figure 31.

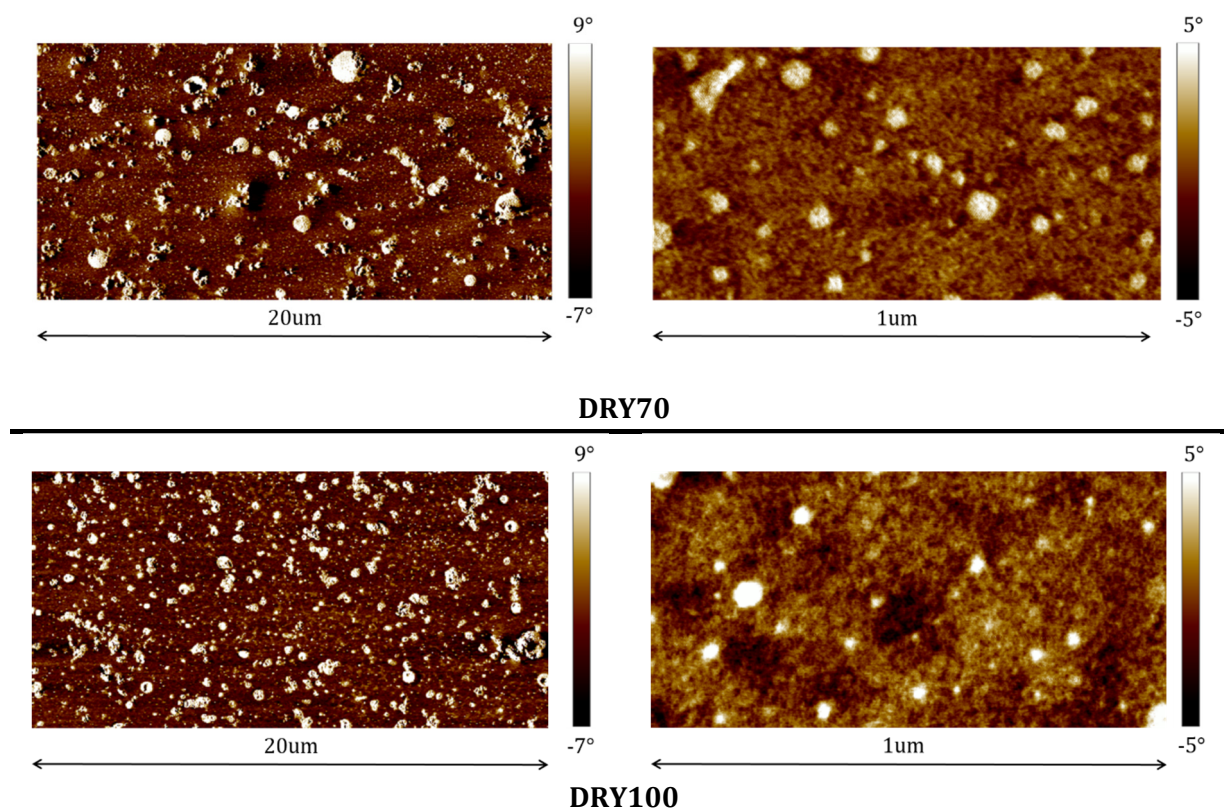


Figure 31 AFM pictures of NBR layers annealed at different temperatures: DRY70 (top) and DRY100(bottom)  
Left: 20µm. Right: 1µm

For both drying conditions, the coated layer is composed of two major phases. Careful analysis of the 1- µm pictures show lamellas yet it is difficult, at first sight, to find differences between the two drying conditions. A more extensive study on the structure of each phase would be needed to conclude on a possible link between surface structure and self-adhesion.

### 5.3. Conclusion and discussion

To understand the intriguing difference in self-adhesion properties of NBR with drying conditions, several complementary experiments were done. The only difference between both series being the preparation of the glass slide, the shift in properties is assumed to be due to distinct interfacial properties.

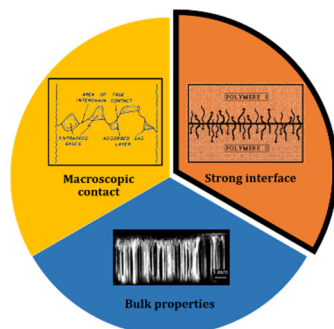


Figure 32 The difference in self-adhesion properties is due to a difference in interfacial properties

Molecular mobility was probed with DSC, and both materials exhibit similar  $T_g$ . Yet as the material is a multiblock structured copolymer, it is possible that the average  $T_g$  is the same while that of the different components (i.e. polar and nonpolar blocks) are dissimilar. A decrease in the  $T_g$  of the alternated ACN-PB block is assumed to be more efficient than one in polybutadiene block in which the mobility is already high.

X-Ray scattering experiments reveal no difference, at the nanometer length scale between both 1-mm bulk systems. Grazing Incidence X-Ray Scattering (Gi-SAXS) experiments would have been useful to assess the difference between the surface and bulk structure at this scale. AFM experiments show that the surface on the glass slide is much more complex than just two lamella structures and the composition of each phase is not clear. Moreover, AFM gives images of the structure of the coated layer but no measurements of the mobility of the chain. In fact, it seems reasonable to assume that the strength of the  $C\equiv N$  intermolecular interactions are dissimilar in both drying conditions, despite similar observable lamellas, leading to different diffusion dynamics.

Previously mentioned articles [21][22] suggest that annealing at high temperature may lead to a change in the material's organization. Maes et al also [23] showed that the self-healing properties of samples that had been annealed and equilibrated at high temperature prior to contact, have had enough time to equilibrate and rearrange on a molecular scale. These evolution are said to be responsible for the weak self-healing properties (called "deactivation") of the material after annealing.

## **6. Conclusions**

During this chapter two ways of enhancing the self-adhesion properties of nitrile rubber were discussed. The first one consists in welding the surfaces with a solvent to bond them. Such strategy leads to an increase in the contact quality between the materials, as well as a strengthening of interfacial interactions due to enhanced polymer mobility and presumably interdiffusion across the interface. The influence of several solvents were probed and key parameters were identified to maximize the welding efficiency. Polar aprotic solvents with an intermediate boiling temperature ( $50 < T < 150^{\circ}\text{C}$ ) seem to be the best option for solvent welding of NBR. Once the surface is welded, and therefore reinforced, it was shown that the bulk properties of the rubber are essential to reach high self-adhesion levels. In the case of NBR, these bulk properties are ensured by the supramolecular structure present at different length scales, forming a physical network. Last, it was shown that a change in the drying conditions considerably modifies the self-adhesion properties. Several analysis have been performed to investigate the cause of this surface effect, but a specific in-depth study is needed to completely apprehend this effect.

### **Take home messages:**

- **Solvent welding is a very efficient method to enhance self-adhesion properties of uncrosslinked rubbers**
- **Polar aprotic solvents, with a moderate boiling temperature, are the best option to weld NBR interfaces**
- **For efficiently welded surfaces, bulk mechanical properties are the limiting criteria**
- **Surface effects can drastically modify self-adhesion properties**

## 7. References

- [1] E. Odrobina and M. A. Winnik, "Influence of Entanglements on the Time Dependence of Mixing in Nonradiative Energy Transfer Studies of Polymer Diffusion in Latex Films," pp. 6029–6038, 2001.
- [2] C. B. Lin, S. Lee, and K. S. Liu, "The Microstructure of Solvent-Welding of PMMA," *J. Adhes.*, vol. 34, no. 1–4, pp. 221–240, 1991.
- [3] K. C. Chang, S. Lee, and C. B. Lin, "Strength and microstructure of solvent welded joints of polycarbonate," *J. Adhes.*, vol. 56, no. 1–4, pp. 135–155, 1996.
- [4] T. Schuman and S. F. Thames, "Coating solvent effects producing adhesion to molded plastic parts," *J. Adhes. Sci. Technol.*, vol. 19, no. 13–14, pp. 1207–1235, 2005.
- [5] P. D. Nadkarni, P. A. Kramer, G. S. Banker, and D. O. Kildsig, "Effect of Surface Roughness and Coating Solvent on Film Adhesion to Tablets," *J. Pharm. Sci.*, vol. 64, no. 9, pp. 1554–1557, Sep. 1975.
- [6] M. M. Caruso, D. A. Delafuente, V. Ho, N. R. Sottos, J. S. Moore, and S. R. White, "Solvent-promoted self-healing epoxy materials," *Macromolecules*, vol. 40, no. 25, pp. 8830–8832, 2007.
- [7] L. Bothe and G. Rehage, "Autohesion of Elastomers," *Rubber Chem. Technol.*, vol. 55, no. 5, pp. 1308–1327, Nov. 1982.
- [8] R. A. Ryntz, D. Britz, D. M. Mihora, and R. Pierce, "Measuring adhesion to poly(olefins): The role of adhesion promoter and substrate," *J. Coatings Technol.*, vol. 73, no. 921, pp. 107–115, 2001.
- [9] M. M. Pastor-Blas, M. S. Sánchez-Adsuar, and J. M. Martín-Martínez, "Surface Modification of Synthetic Vulcanized Rubber," *J. Adhes. Sci. Technol.*, vol. 8, no. 10, pp. 1093–1114, 1994.
- [10] P. R. Dluzneski, "Peroxide Vulcanization of Elastomers," *Rubber Chem. Technol.*, vol. 74, no. 3, pp. 451–492, 2001.
- [11] J. Kruželák, R. Sýkora, and I. Hudec, "Sulphur and peroxide vulcanisation of rubber compounds-overview," *Chem. Pap.*, vol. 70, no. 12, pp. 1533–1555, 2016.
- [12] J. L. Valentín, A. Rodríguez, A. Marcos-Fernández, and L. González, "Dicumyl peroxide cross-linking of nitrile rubbers with different content in acrylonitrile," *J. Appl. Polym. Sci.*, vol. 96, no. 1, pp. 1–5, 2005.
- [13] L. Gonzales, A. Rodrigues, A. Marcos, and C. Chamorro, "Crosslink reaction mechanisms of diene rubber with dicumyl peroxide." 1996.
- [14] J. Brandrup, E. H. Immergut, and E. A. Grulk, *Polymer Handbook- Fourth edition*. 1999.
- [15] G. Salomon, "Influence of structure on polymer-liquid interaction. Influence of nitrile groups," *Salomon*, vol. 355, no. 75, pp. 173–180, 1948.
- [16] M. S. Seehra, M. Yalamanchi, and V. Singh, "Structural characteristics and swelling mechanism of two commercial nitrile-butadiene elastomers in various fluids," *Polym. Test.*, vol. 31, no. 4, pp. 564–572, 2012.

- [17] Y. Eom and B. C. Kim, "Solubility parameter-based analysis of polyacrylonitrile solutions in N,N-dimethyl formamide and dimethyl sulfoxide," *Polymer (Guildf)*, vol. 55, no. 10, pp. 2570–2577, 2014.
- [18] Y. Eom and B. C. Kim, "Effects of chain conformation on the viscoelastic properties of polyacrylonitrile gels under large amplitude oscillatory shear," *Eur. Polym. J.*, vol. 85, pp. 341–353, 2016.
- [19] B. G. Min, T. W. Son, B. C. Kim, C. J. Lee, and W. H. Jo, "Effect of solvent or hydrophilic polymer on the hydration melting behavior of polyacrylonitrile," *J. Appl. Polym. Sci.*, pp. 457–462, 1994.
- [20] S. Rosenbaum, "Polyacrylonitrile fiber behavior. I. Mechanisms of tensile response," *J. Appl. Polym. Sci.*, vol. 9, no. 6, pp. 2071–2084, 1965.
- [21] L. V. Sokolova and E. V. Matukhina, "Effect of an anionic emulsifier on the structure of butadiene-nitrile elastomers," *Polym. Sci. Ser. A*, vol. 52, no. 4, pp. 383–391, 2010.
- [22] K. R. Shull, E. J. Kramer, F. S. Bates, and J. H. Rosedale, "Self-Diffusion of Symmetric Diblock Copolymer Melts near the Ordering Transition," *Macromolecules*, vol. 24, no. 6, pp. 1383–1386, 1991.
- [23] F. Maes, D. Montarnal, S. Cantournet, F. Tournilhac, L. Corté, and L. Leibler, "Activation and deactivation of self-healing in supramolecular rubbers," *Soft Matter*, vol. 8, no. 5, pp. 1681–1687, 2012.



# **- CHAPTER 6 -**

## **FIRST INSIGHTS INTO PVC-BLENDED NITRILE RUBBERS (NBR/PVC)**

---

Polyvinylchloride (PVC) particles are often blended into NBR to enhance its mechanical properties, yet the influence of those polar particles on the adhesion behavior of NBR has not been studied. This chapter intends to give a first insight on the impact of PVC particles on the self-adhesion properties of NBR. Results will be enlightened with mechanical testing and X-Ray scattering measurements.

<b>1. Literature: Blending of PVC in NBR.....</b>	<b>165</b>
1.1. Introduction to NBR/PVC.....	165
1.1.1. Presentation of polyvinyl chloride .....	165
1.1.2. Preparation step .....	165
1.2. Composition-dependent properties.....	165
1.2.1. Influence of PVC amount.....	165
1.2.2. Influence of acrylonitrile content (ACN).....	166
1.3. Nanoscale heterogeneity .....	166
<b>2. Samples preparation and characterization .....</b>	<b>167</b>
2.1. Blends preparation .....	167
2.1.1. Polyvinyl Chloride .....	167
2.1.2. Blending of PVC into NBR .....	167
2.1.3. Thermal analysis.....	167
2.2. Mechanical properties of NBR/PVC blends .....	168
2.2.1. Linear rheology of NBR/PVC.....	168
2.2.2. Large strains .....	169
2.3. Structural organization .....	170
2.3.1. SAXS.....	170
2.3.2. Atomic Force Microscopy .....	171
<b>3. Self-adhesion properties of NBR/PVC .....</b>	<b>173</b>
3.1. Samples' preparation .....	173
3.2. Influence of contact time on the self-adhesion properties of NBR/PVC.....	173
3.2.1. Self-adhesion of the NBR/PVC blend .....	173
3.2.2. Comparison with the self-adhesion of NBR.....	174
3.3. Solvent welding to enhance self-adhesion properties .....	175
3.3.1. Influence of contact time.....	175
3.3.2. Comparison with NBR.....	176
3.4. Conclusion and discussion.....	177
<b>4. Addition of tackifiers to NBR/PVC.....</b>	<b>178</b>
4.1. Self-adhesion properties of NBR/PVC with tackifiers.....	179
4.1.1. Without welding .....	179
4.1.2. Welding of the interface of NBR/PVC + resin with MEK.....	180
4.2. Mechanical properties of NBR/PVC with tackifiers .....	181
4.2.1. Linear regime .....	182
4.2.2. Uniaxial tensile tests .....	182
4.2.3. Comment .....	183
4.3. Discussion .....	183
<b>5. Conclusion and discussion .....</b>	<b>184</b>
<b>6. References.....</b>	<b>185</b>

## 1. Literature: Blending of PVC in NBR

Blending of two or more polymers is of considerable importance in the field of polymer science, and its major interest is that the resulting properties are, in some cases, better than those exhibited by either of the single component. Composites of polyvinyl chloride (PVC) and nitrile butadiene rubber (NBR) have been widely studied and used in practical applications such as wires, cable insulation, food containers etc. NBR acts as a permanent plasticizer for PVC and the latter improves, among others, nitrile rubbers' ozone and chemical resistance, its thermal ageing, abrasion resistance, tear resistance and tensile properties [1][2].

### 1.1. Introduction to NBR/PVC

#### 1.1.1. Presentation of polyvinyl chloride

PVC is a thermoplastic polymer synthesized from radical polymerization of vinyl chloride and has a glass transition temperature close to 80°C. Prior to using it as a finite product, PVC is often blended with additives, among which heat stabilizers that increase its poor thermal stability.

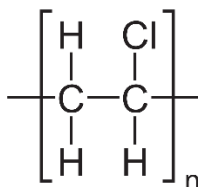


Figure 1 Polyvinylchloride (PVC)

#### 1.1.2. Preparation step

PVC has frequently been blended into nitrile rubbers and their compatibility as well as the mechanical properties of the blend have been studied. Authors [3][4][5][6] used high temperatures (>100°C) and shear to blend both materials. For example, Zakrewski [5] mixed both components on a rubber mill at 175°C, but the mixing time is not clarified. George and coworkers [6] first introduced the NBR in the hot (115°C<T<175°C) mixer, waited for one minute and then added PVC and its stabilizer for five extra minutes.

The mechanical properties of NBR/PVC were studied and shown to be highly dependent on the composition of the blend.

### 1.2. Composition-dependent properties

#### 1.2.1. Influence of PVC amount

Blends of NBR and PVC have been studied in the literature. Sen et al [1] and Zakrewski et al [5] showed that their experimental data match Fox and Flory's expression for compatible polymer-polymer systems, implying a certain degree of compatibility. Ougizawa [7] and Wang [8] examined the influence of PVC content on the blend's mechanical properties and concluded that an increase in the PVC content leads to a reduction in the elongation at failure as well as boost in the Young's modulus (see Figure 2 and Figure 3). In fact, Wang [9] measured an increase from 2.27MPa for pure NBR to 9.75MPa for NBR+ 40wt% PVC. Huang at al [10] blended NBR with contents from 0 to 50wt% PVC and evaluated their mechanical properties in terms of tensile strength, elongation at break, friction and shore hardness. Composites with 30% PVC seemed to have the best 'compromise' in mechanical properties and, indeed, this ratio is often [11] used when studying NBR/PVC.

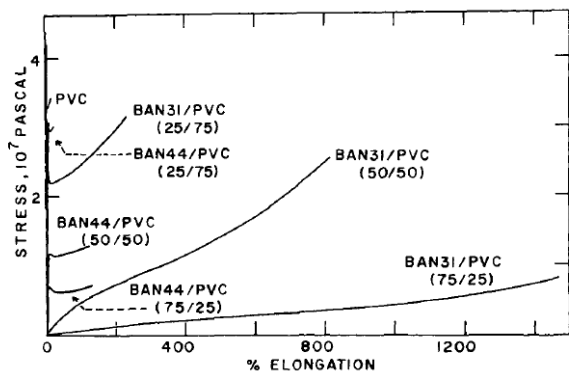


Figure 2 Stress-strain curves of NBR/PVC samples for acrylonitrile content of 31 and 44%. Figure from [8]

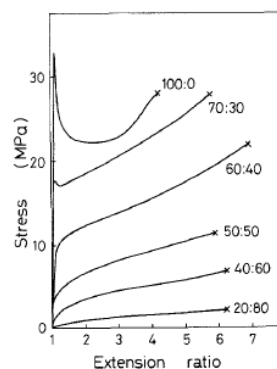


Figure 3 Stress-strain curves of NBR/PVC with various compositions. Figure from [7]

### 1.2.2. Influence of acrylonitrile content (ACN)

Several authors studied the influence of the ACN content on the overall NBR/PVC compatibility and structure. An increase in the ACN content results in a rise in the blend's compatibility [1][12] thanks to specific dipole-dipole interactions. In light of FT-IR measurements, Xiaojiang et al [13] suggested that the principal force of interaction between PVC and NBR molecules is the formation of a hydrogen bond between the PVC's  $\alpha$ H atom and the nitrogen atom from the NBR molecule. Zakrewski et al [5] found that PVC and nitrile rubber were compatible for 23-45% ACN, which is consistent with Sen et al [1] who used interaction parameters and glass transition temperature measurements to assess compatibility up to 34% ACN. Ranby et al [12] confirmed homogeneity with 30-35% ACN; and Wang et al [8] used both DSC and DMA to show that blending of high ACN content (44%) leads to a heterogeneous system containing PVC microdomains.

### 1.3. Nanoscale heterogeneity

However, calorimetric methods do not give information about the mixing of the polymers on the molecular scale, and for domain sizes smaller than 150Å a single  $T_g$  is observed. From pulsed  $^1\text{H}$  nuclear magnetic resonance (NMR) [14], to solid state  $^{13}\text{C}$ -NMR [15], DMA [16] and small angle light scattering [7], several methods have investigated the heterogeneity of "compatible" PVC/NBR blends. According to the composition of the blends and the used techniques, authors either find three distinct phases [9][15] or only two [14]. The different phases are a mixed PVC/NBR phase, an unmixed NBR phase and/or an unmixed PVC one, and are illustrated in Figure 4 and Figure 5.

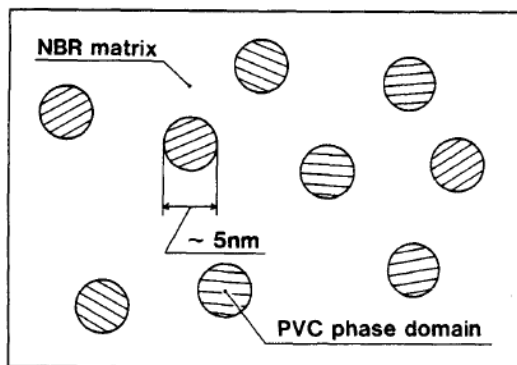


Figure 4 Schematic of the microheterogeneous structure in NBR/PVC blends. PVC phase domains are finely dispersed in the NBR Matrix. Figure from [14]

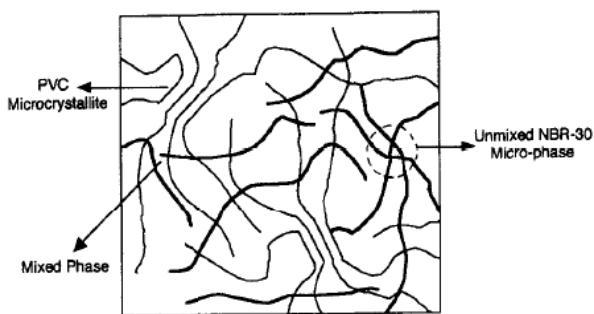


Figure 5 Schematic of structure in NBR/PVC blends with PVC microcrystallites, unmixed NBR phase, and a mixed phase. Figure from [15]

These inhomogeneities are approximately evaluated to be of the order of 10nm or less [14][15][17][18]. If the ACN content is increased up to a level where the material is incompatible [8], the PVC-rich phase will lead to an increase in the Young modulus and a sharp decrease in the elongation at break.

## **2. Samples preparation and characterization**

### **2.1. Blends preparation**

#### **2.1.1. Polyvinyl Chloride**

Polyvinyl chloride (PVC) is provided by the supplier without any specific information.

DSC measurements show that its glass transition occurs at 86°C. Granulometry shows an average particle size of 150 microns. Also, 3mg/mL solution of PVC in THF+Et<sub>3</sub>N was prepared and analyzed by gas phase chromatography (GPC). An average weight molar mass of 112 kg/mol was measured.

Nitrile Butadiene Rubber is similar to that used in the previous chapters.

#### **2.1.2. Blending of PVC into NBR**

To be consistent with industrial interests, PVC was blended at 30wt% in nitrile rubber. As no specific information was given regarding PVC, it is not clear whether it was already mixed with heat stabilizers. Therefore, to limit degradation hazards, and also to maintain the same extruding temperature as that of previously studied NBR, the blending was performed at 120°C, 100rpm, during 15minutes on the twin-screw extruder of Chapter 4 (2.2.1).

During the mixing process, few PVC grains remain on the inside of the extruder, slightly modifying the overall composition. The composition of each blend was controlled with TGAs analysis. Method is detailed in Annex 1.3. The desired 30% PVC was accurate with an error of 1%.

Samples for rheology and tensile testing were prepared as presented in Chapter 2 for raw NBR: heat molded at 100°C under 50bars for an hour and cooled down to 25°C at 50bars for an extra hour.

#### **2.1.3. Thermal analysis**

DSC measurement was performed on a freshly extruded blend, between -60 and 120°C, with a heating speed of 20°C/min. The curve is shown on Figure 6 (left) and reveals a unique Tg at -30 +/- 1°C, which is far from that estimated with the Fox and Flory's equation (-5°C). Yet due to the complex structure of NBR as a multiblock copolymer, and to possible polar interactions with PVC it is not surprising that this empirical law is not applicable.

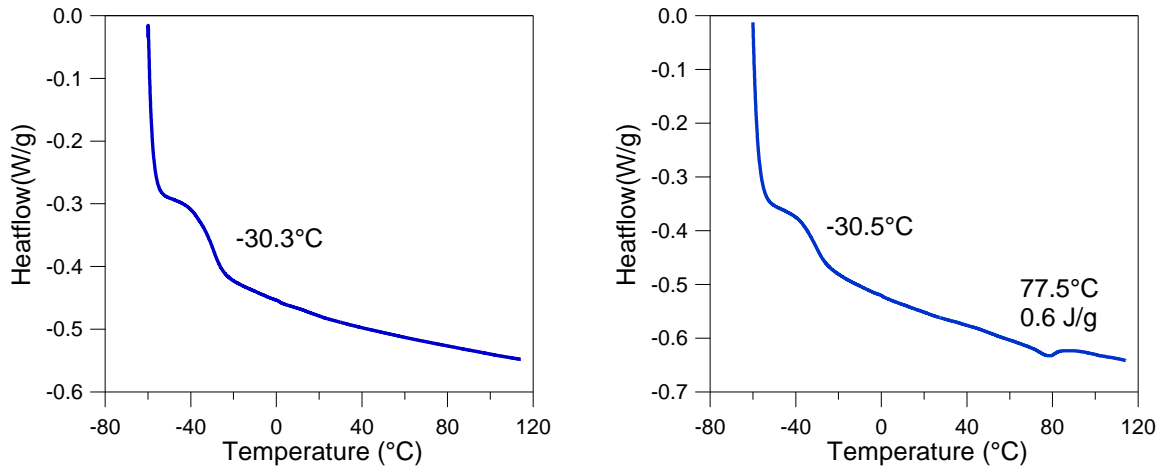


Figure 6 DSC measurement of freshly extruded (left) and aged one year (right) NBR/PVC

After several days at room temperature (Figure 6 right), an endothermic peak is observed at high temperature (close to 80°C). The origin of such a peak is hard to assess as this temperature is close to that of the T<sub>g</sub> of polyacrylonitrile, of that of the melting temperature of 1,4-trans polybutadiene, and of the T<sub>g</sub> of PVC.

## 2.2. Mechanical properties of NBR/PVC blends

The mechanical properties in the linear regime as well as at large strains were probed using rheology and uniaxial tensile tests.

### 2.2.1. Linear rheology of NBR/PVC

2,5mm-thick and 8mm-diameter disks were prepared using the heating press. To avoid slippage between the sample and the plates of the rheometer, a cyanoacrylate glue (Loctite 406) was used. The mechanical properties were probed at 25 and 60°C, between 0.01 and 30Hz. The loss factor  $\tan \delta$  is plotted in Figure 7 after applying a horizontal shift  $a_T$  to the 60°C-curve. After an additional vertical shift with  $b_T$  moduli  $G'$  and  $G''$  are plotted as a function of reduced frequency in Figure 8 at  $T_0=25^\circ\text{C}$ . For this NBR/PVC it was found that the shifting coefficients are  $a_T=0.03$  and  $b_T=1.2$ .

Such vertical shift factor  $b_T$  indicates an increase in the material's stiffness with temperature. This linear rheological properties are compared to those of extruded NBR in Figure 9. As a reminder, the horizontal and vertical shift factor for NBR in the same conditions are respectively  $a_T=0.04$  and  $b_T=0.9$ . These results suggest that the addition of PVC leads to a structural modification of the blend with increasing temperature that increases its modulus. It may be that the miscibility between the NBR and PVC is temperature dependent.

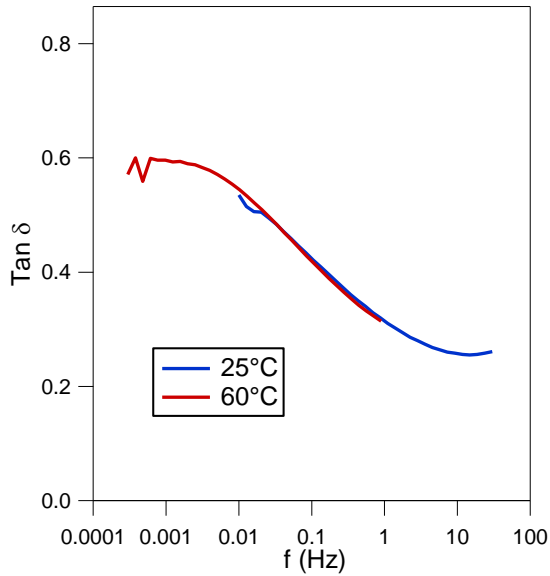


Figure 7 Loss factor of NBR/PVC at  $T_0=25^\circ\text{C}$  after applying the horizontal shift  $a_T$  on the  $60^\circ\text{C}$ -data

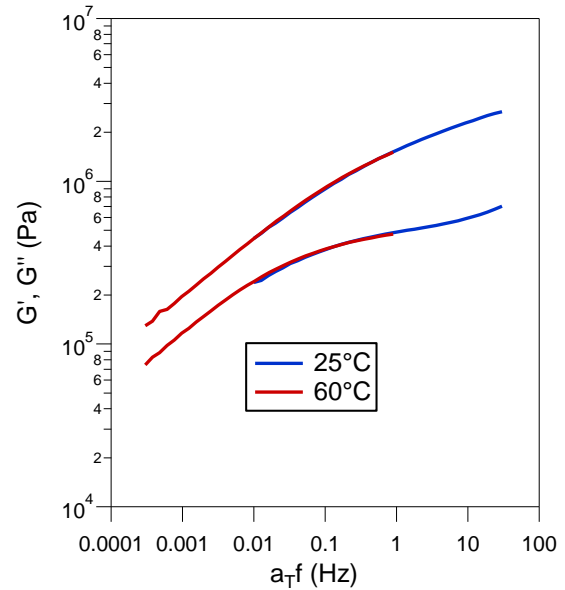


Figure 8 Master curve of NBR/PVC at  $25^\circ\text{C}$  after horizontal and vertical shifts

Despite the change in the plateau moduli, NBR and NBR/PVC show very different low-frequency behavior. In fact, NBR/PVC behaves like a physical gel and does not flow at low frequency ( $\tan \delta < 1$ ).

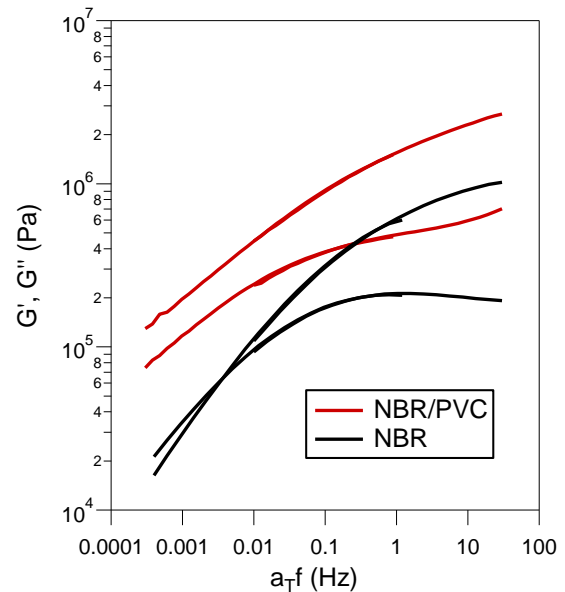
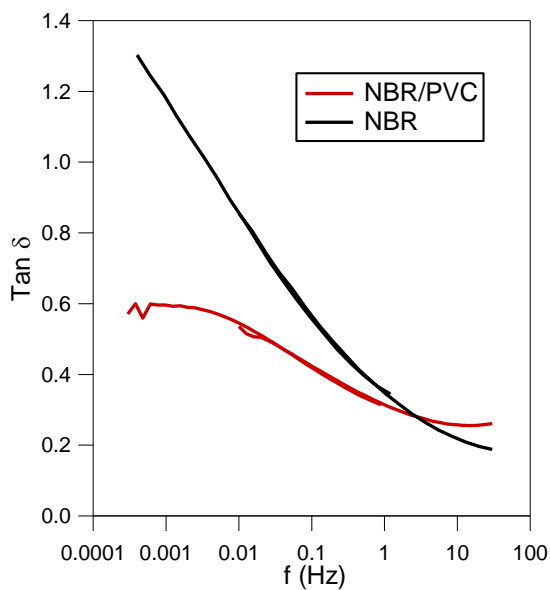


Figure 9 Comparison of the linear rheology of NBR/PVC and NBR. Left: loss factor Right: modulus

### 2.2.2. Large strains

The results are shown on Figure 10 and compared to the large deformation behavior of NBR under the same conditions. Blending with 30% PVC leads to an increase in the Young's modulus from 0.5 MPa to 2.2 (+/- 0.5) MPa, to an increase in the maximum stress (from 0.09 to 0.6MPa) and to a sharp decrease in the maximum deformation (from 1500 to 250%).

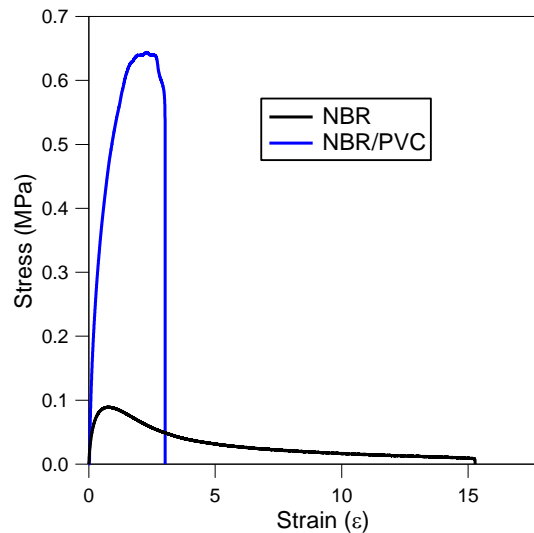


Figure 10 Comparison of the large strain behavior of NBR/PVC and NBR for similar strain rate

Let us briefly comment that unlike the Young's modulus which is reproducible, the maximum deformation and maximum stress of NBR/PVC are strongly dependent on defects due the molding step.

## 2.3. Structural organization

### 2.3.1. SAXS

X-ray Scattering measurements were performed on freshly extruded NBR/PVC, and influence of room temperature ageing was probed. Similarly to what was observed with NBR, the thermoplastic elastomer NBR/PVC self organizes with time, as shown in Figure 11 and Figure 12. The lamellar structure, shown with the three orders  $q^*$ ,  $q_2$  and  $q_3$ , is less pronounced than for the aged NBR sample yet the peaks of both materials appear for the same scattering length. The characteristic size is of the order of 4.5nm and is consistent with that from Fukumori and coworkers [14]. After extrusion, the structure is strongly annihilated, and amorphous halos at  $q = 0.14$  and  $0.2 \text{ \AA}^{-1}$  are measured. At very small scattering factors, the curves follow a power law with a slope  $\propto 1/q^{-4}$ . This behavior is consistent with Porod's law [19] for ideal two-phases systems with sharp boundaries, yet as raw NBR does not show the same trend (presumably due to rougher interfaces) no comparison of the structural parameters is possible. Therefore, the larger scale behavior will be compared from AFM experiments and this small- $q$  trend will not be commented further.

The lamellar peak is wider in NBR/PVC, meaning that the structure is not as well-defined as for raw NBR. Moreover, the levels of scattered intensity are higher for all scattering vectors, suggesting that the electronic contrast is stronger, probably due to PVC particles (and particularly chlorine atoms).

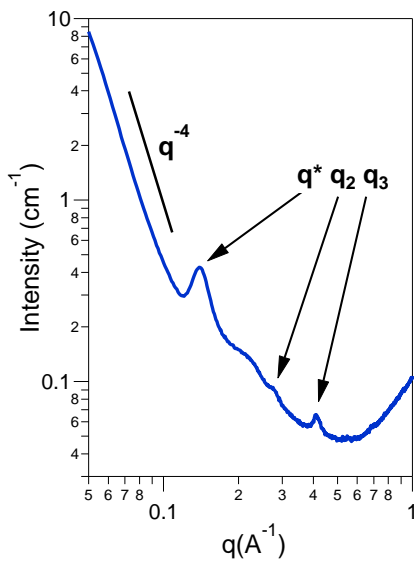


Figure 11 SAXS of NBR/PVC aged for a month at room temperature

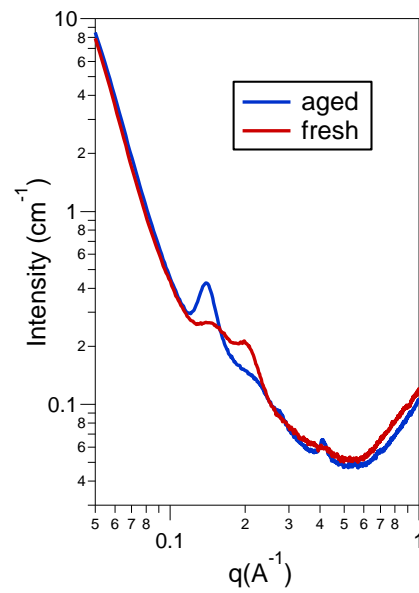


Figure 12 SAXS: Comparison of fresh and aged NBR/PVC sample

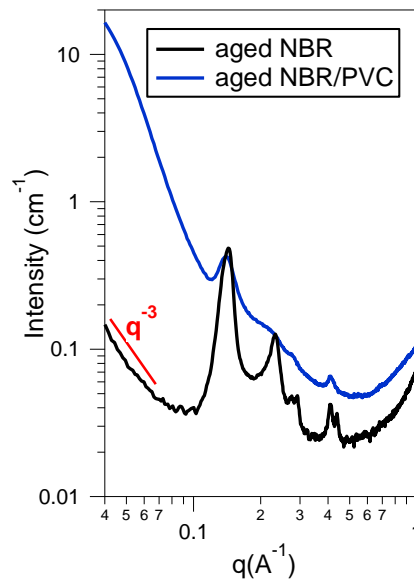


Figure 13 SAXS: Comparison of aged NBR and aged NBR/PVC

### 2.3.2. Atomic Force Microscopy

AFM was used in tapping mode, in the same conditions as for raw NBR in Chapter 3, to visualize the structure of aged NBR/PVC. The methodology and the sample preparation is similar to that detailed in Chapter 3 (2.3) for NBR samples.

Pictures shown in Figure 14 are taken at two length scales: 20 and 1 microns. Height profiles (right column) reveal that there are some large scale (microns) variations in height, likely due to the material's relaxation after demolding. Nevertheless, at shorter length-scale, samples are quite flat (variation between -2 and +2nm).

The upper phase picture, at 20 $\mu$ m, shows a strong anisotropy of the material and a coexistence of two phases. In the bottom picture, at 1 $\mu$ m, two zones are distinguished and separated by a dotted white line. The upper part (zone "2") reveals the presence of well-defined lamellas. With profile lines (illustrated in Figure 14 (b)) a period distance of 8+/- 1.3nm could be estimated. Despite the uncertainty inherent to the AFM measurements, the probed distance is consistent with that of X-Ray scattering. The bottom part (zone "1") of the pictures shows a worm-like organization rather than lamellas. Both structures (lamellas and worm-like) are found statistically on the samples and their ratio was not studied.

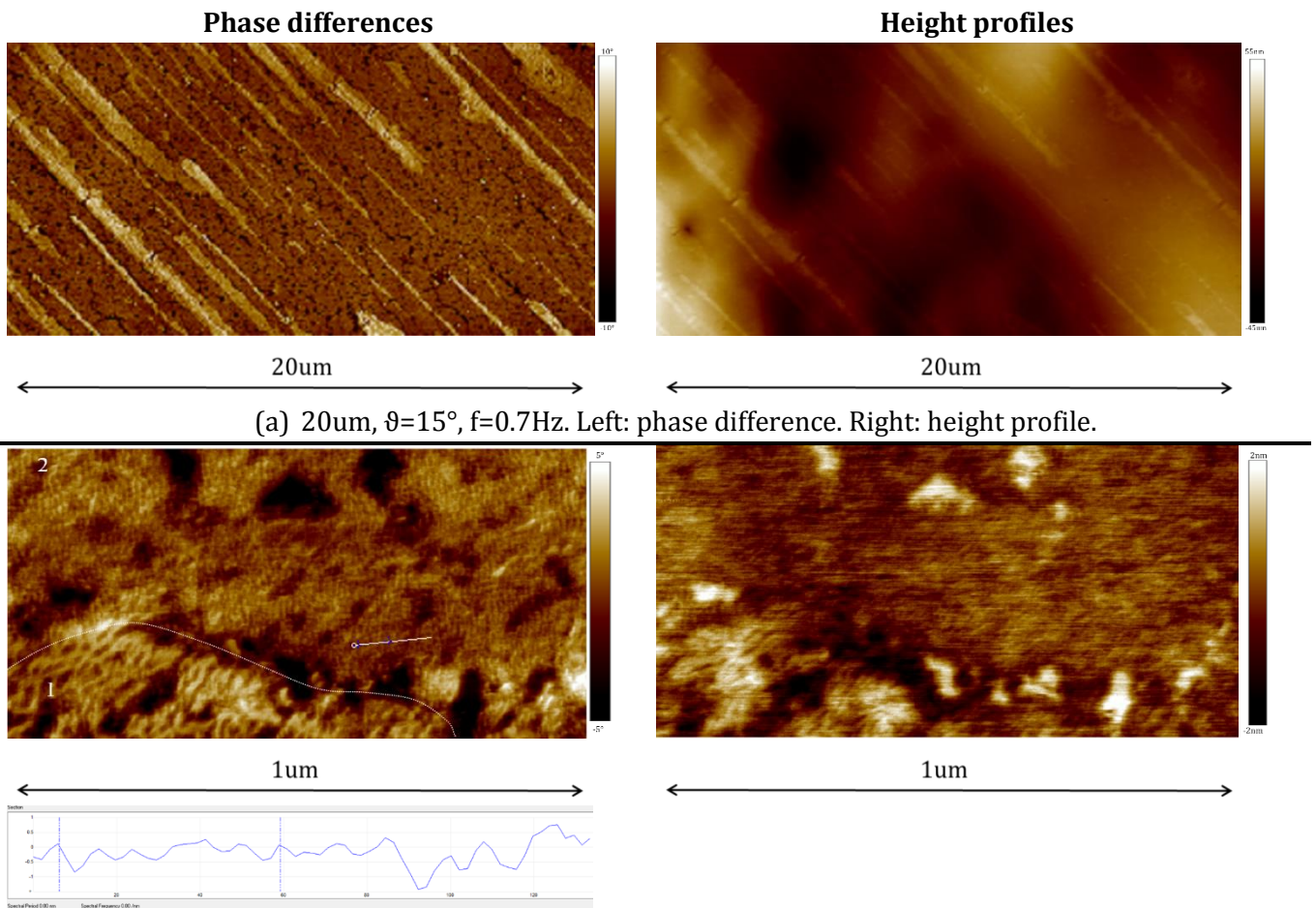


Figure 14 AFM (phase differences and height profiles) of aged NBR/PVC at 20 and 1 microns

### 3. Self-adhesion properties of NBR/PVC

#### 3.1. Samples' preparation

In order to characterize the self-adhesion properties of NBR blended with PVC, it is important to make sure that the adhesion between the glass slide and the coated layer is strong enough to prevent any debonding during the probe-tack test. NBR/PVC was first directly coated on the silanized glass (similar to the preparation process in Chapter 2, 3.3), but it was observed that the polymer layer detaches from the glass slide during the debonding step. The chemical reaction between the mercapto group of the silanisation agent and the double bond of the butadiene is presumably disturbed by PVC. To overcome this issue, the slides' preparation process was adapted.

The very first steps remained the plasma treatment of the glass slides and their silanization in gas phase using 3-(mercaptopropyl)-trimethoxysilane (see Chapter 2). A 6.6wt% solution of NBR in toluene was then spincoated, at a rotating speed of 2000rpm during 1 minute, in order to have a thin layer of 0.9 +/- 0.1microns. The slides were dried first at room temperature overnight and then during two hours in a vacuum oven at 100°C. 1mL of a 2.5wt% solution of NBR/PVC in cyclohexanone was then drop-coated on the glass slides, and left at room temperature during two days for slow drying. Finally, they were placed in a 70°C vacuum oven for another two days. These drying conditions were chosen with regard to Chapter 5 section 5.

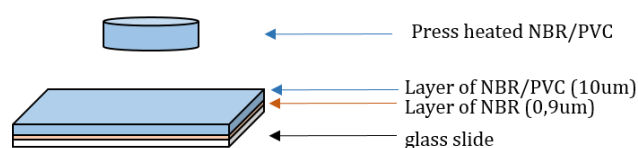


Figure 15 Illustration of tack samples for NBR/PVC

The rubber disks were prepared using a heating press as in Chapter 3 for NBR. They were brought into contact with the glass slide under a load of 1.7 kg during an hour and then removed. Indeed, as the Young's modulus of NBR/PVC is approximately four times greater than that of NBR, the load was also around four times higher (such that  $P_{\text{contact}}=1\text{bar}$ ), in order to impose approximately the same deformation as that during the NBR self-adhesion measurements.

The effect of tackifiers and solvent welding, on the self-adhesion properties of NBR/PVC were also studied as a function of contact time.

#### 3.2. Influence of contact time on the self-adhesion properties of NBR/PVC

##### 3.2.1. Self-adhesion of the NBR/PVC blend

The self-adhesion properties of NBR/PVC samples were probed as a function of time (from 2 hours to 8 days) and are shown on Figure 16. Cavitation peak and maximum deformation hardly increase with time, and the resulting self-adhesion energies are low ( $\sim 40\text{J/m}^2$  after a week).

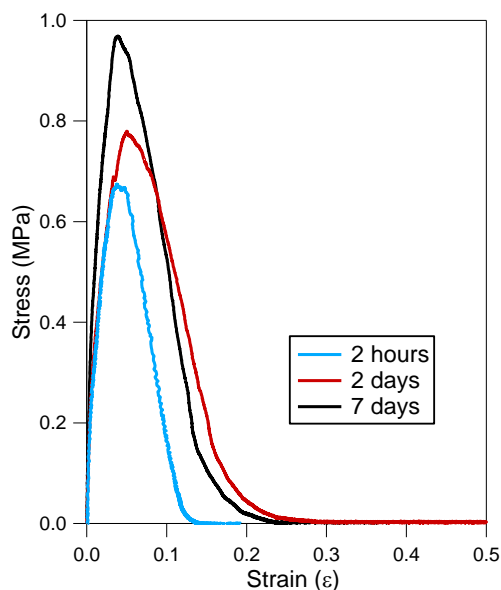


Figure 16 Influence of contact time on the self-adhesion properties of PVC/NBR

### 3.2.2. Comparison with the self-adhesion of NBR

Figure 17 compares stress-strain debonding curves for NBR (for coated slides dried at 100°C) and NBR/PVC self-adhesion tests, after two and seven days of contact. Cavitation occurs at a higher stress for PVC/NBR but is, unlike raw NBR, hardly deformable. Indeed, once cavities appear, they immediately propagate at the interface (adhesive failure) and bulk deformation is negligible. Figure 18 shows the evolution of the self-adhesion energies  $W_{adh}$  as a function of contact time for both systems, and reveal that they are of the same order of magnitude ( $<50\text{J}/\text{m}^2$ ).

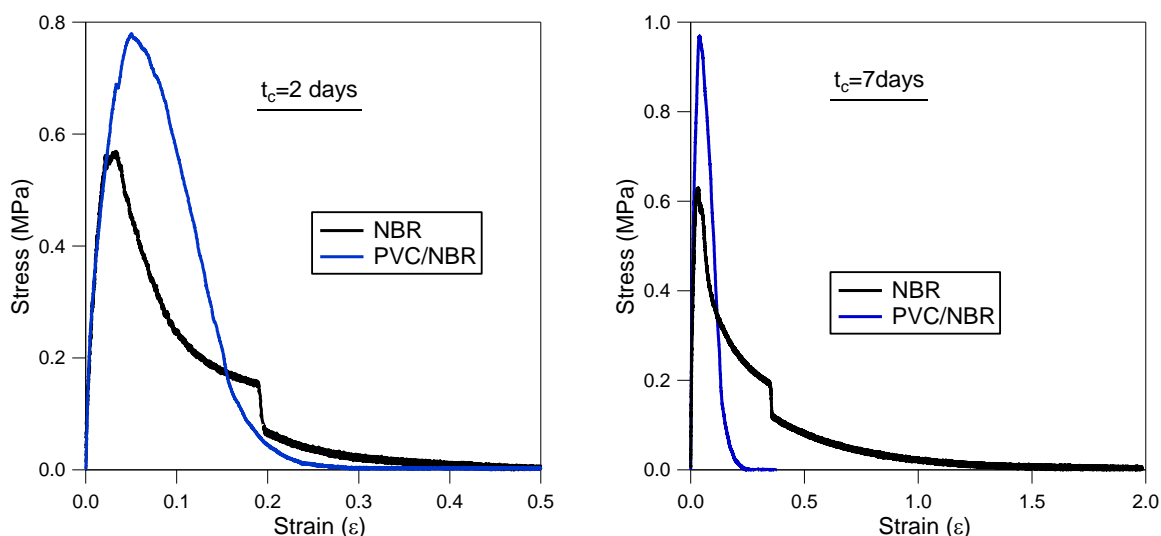


Figure 17 Stress-strain curves during debonding of tack samples: Comparison of the self-adhesion properties of PVC/NBR and NBR for 48h (left) and 7days (right) of contact

Due to the very poor self-adhesion energies of NBR/PVC blends, the system was not even compared to the much more adherent NBR interfaces dried at 70°C.

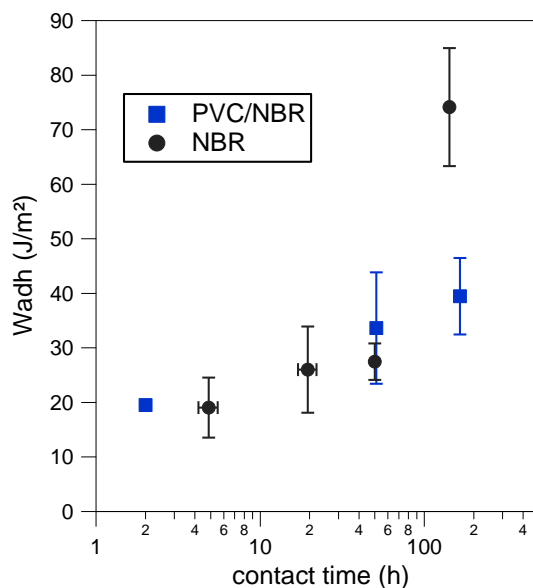


Figure 18 Evolution of the self-adhesion energies  $W_{adh}$  of PVC/NBR and NBR with contact time

### 3.3. Solvent welding to enhance self-adhesion properties

With regard to Chapter 5, a 3 $\mu$ L drop of solvent was used to weld both surfaces and its impact on the self-adhesion properties of PVC/NBR was probed. During this study, only butanone (methyl ethyl ketone, referred to as “MEK”) was used as welding solvent.

#### 3.3.1. Influence of contact time

The self-adhesion properties of welded samples were studied as a function of contact time.

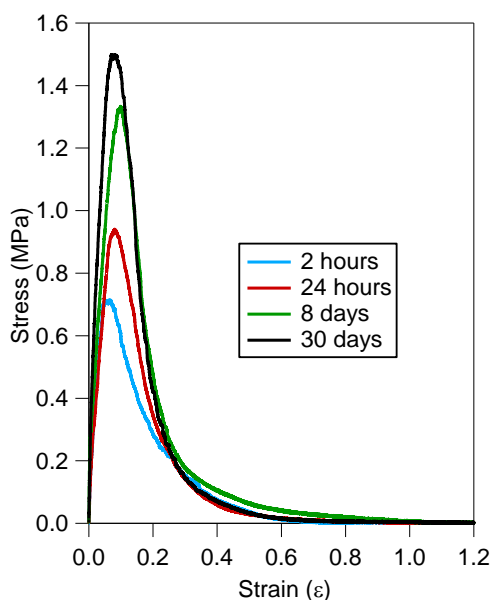


Figure 19 Influence of contact time on the self-adhesion properties of NBR/PVC. Welding with MEK.

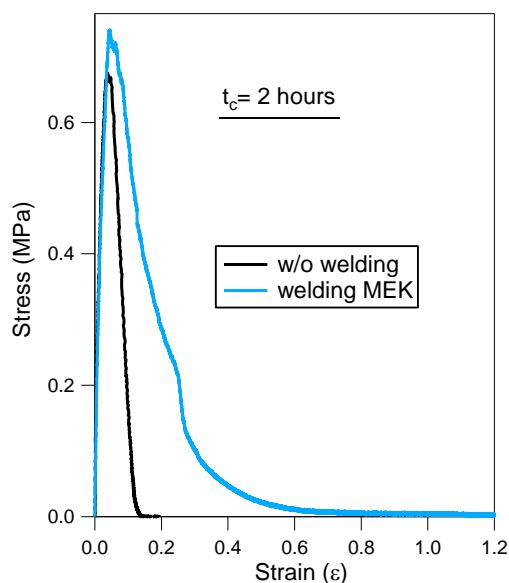


Figure 20 Influence of welding with MEK on the self-adhesion properties of NBR/PVC for 2 hours of contact

With increasing contact time, Figure 19 shows that the maximum deformation remains constant, but the maximum peak for cavitation increases, leading to increased self-adhesion energies. This increase in cavitation peak is assumed to be due to a rise in the number of interfacial interactions

and can be explained by increasing polar interactions between both surfaces. Yet poor volume deformation is observed and sample fail through crack propagation, suggesting that the interface is much weaker than the bulk properties of the material. It is likely that hardly any diffusion of polymer chain has occurred.

Figure 20 shows that welding with butanone increases the material's deformation during debonding due to a strengthened interface. Without welding, limited mobility of the material prevents any migration of polymer chains at the interface. Due to the material's high green strength, the achieved maximum deformations remain small (<100%) compared to that of welded NBR samples. It is interesting to note that the cavitation peak for welded and unwelded samples are identical, suggesting that the effective contact areas are similar and that the contact conditions without welding are good. The corresponding self-adhesion energies of welded NBR/PVC seem to reach a plateau close to  $150\text{J/m}^2$ , and are compared to that of unwelded samples in Figure 21.

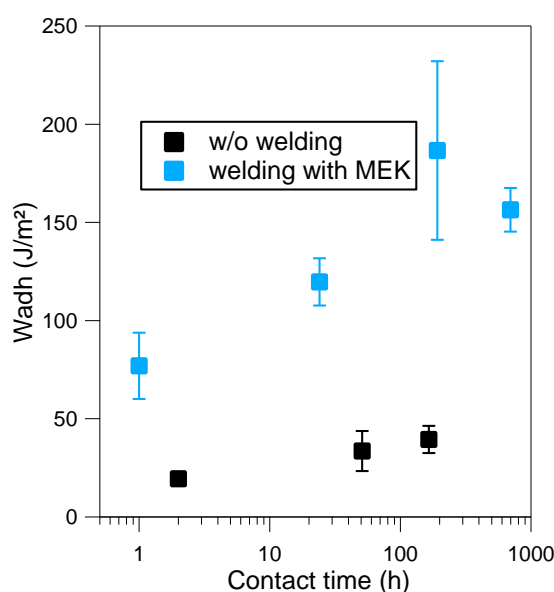


Figure 21 Self-adhesion energies of NBR/PVC with and without welding with MEK, as a function of contact time

### 3.3.2. Comparison with NBR

NBR/PVC and NBR samples, both welded with butanone, are compared. Figure 22 plots the stress-strain debonding curves after twenty four hours of contact, and Figure 23 the corresponding self-adhesion energies as a function of contact time. NBR welded samples show up to four-time higher energies, due to their ability to dissipate energy during debonding, leading to very high strains. Whereas NBR samples fail through fibrils rupture (cohesive failure), NBR/PVC ones fail through crack propagation at the weak interface.

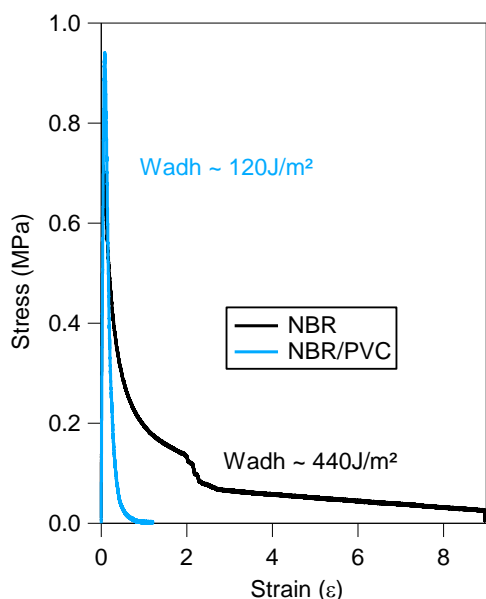


Figure 22 Comparison of NBR/PVC and NBR welded samples, for 24h of contact

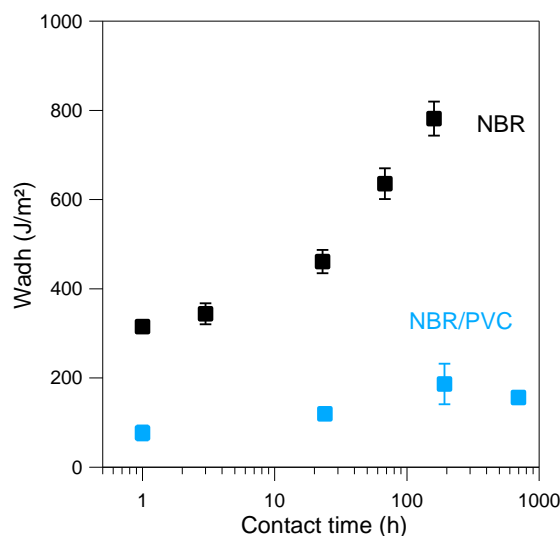


Figure 23 Self-adhesion energies of NBR/PVC and NBR welding with MEK, as a function of time

### 3.4. Conclusion and discussion

PVC is a polar molecule and it could have been hypothesized that its effect on the self-adhesion of NBR was to be similar to that of the phenolic tackifier presented in Chapter 4. Indeed, the C-Cl bond is more polarized than  $\text{C}\equiv\text{N}$  and it is therefore likely that PVC disturbs intermolecular CN interactions.

Yet tack measurements reveal that its blending considerably reduces the self-adhesion properties of NBR, due to very limited deformation. Because of its high molar mass (in comparison to that of a tackifier), and the strong physical network it creates with NBR, diffusion of polymer chains is hindered. Fracture occurs through crack propagation at the interface, and no energy is dissipated through fibril formation. The association-dissociation process of NBR with polar tackifier is strongly impeded. Suggestions for both mechanisms are illustrated in Figure 24.

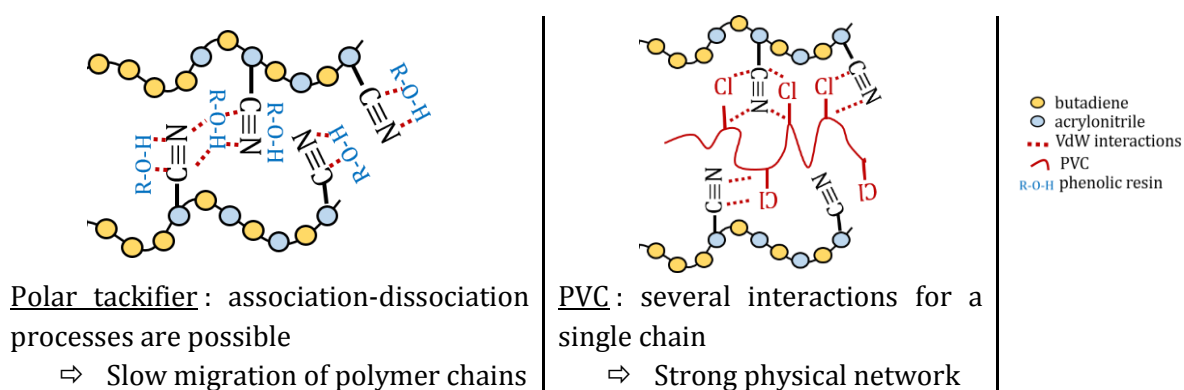


Figure 24 Comparison of polar tackifier and polar polymer (PVC) Van der Waals (VdW) interactions with NBR

Xiaojiang and coworkers [13] suggested that the main force of interaction between PVC and NBR is the formation of a hydrogen bond between the hydrogen atom in alpha position of chlorine in PVC, and the nitrogen atom of the rubber matrix. This mechanism is illustrated in Figure 25 below:

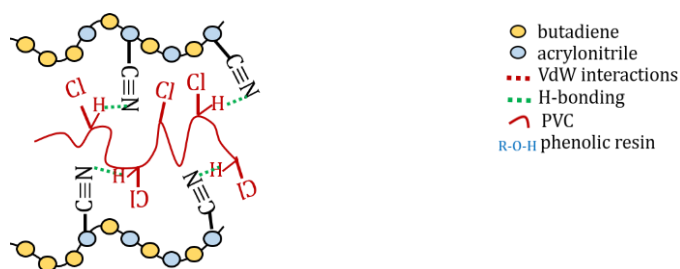


Figure 25 Suggested mechanism from Xiaojiang [13]: H-bonds between  $C\equiv N$  nitrogen and PVC's hydrogen

Also, the fact that PVC can crystallize [20] and therefore form additional small but hard crystals might also explain this stiffening of NBR/PVC blends relative to pure NBR. Furthermore, Bergman et al [21] observed an anti-plasticization effect for PVC blended with NBR ( $\sim 7\text{wt}\%$ , AN content  $>40\%$ ). In fact, due to nitrile rubber's high polarity, it is suggested that mutual interactions between NBR and PVC occurs, and that physical crosslinks between chains are responsible for the stiffening of the material. These polar interactions are assumed to prevent the flow of polymer chains at the interface and to be responsible for the material's poor self-adhesion properties. Welding with butanone is very effective but the reached energies are still much lower than that of NBR. Moreover, for the contact times studied, the self-adhesion levels seems to be limited to  $\sim 200\text{J}/\text{m}^2$ .

#### 4. Addition of tackifiers to NBR/PVC

Two tackifiers, a phenolic and a hydrocarbon resin, were blended at 3% into NBR/PVC samples. The rubbers blended with polar tackifier will be referred to as NBR/PVC-POL3 and those blended with nonpolar tackifier: NBR/PVC-NP3.

DSC measurements were run and samples show a unique  $T_g$  shortly after extrusion. Yet after ageing for a week at room temperature, an endothermic peak is probed at high temperature, similar to that observed for raw NBR/PVC.

Sample	Tackifier	$T_g(^{\circ}\text{C})$	$T_{\text{endo}}(^{\circ}\text{C})^*$
NBR/PVC	/	-28.7	80.5
NBR/PVC-3POL	Polar	-27.2	80.1
NBR/PVC-3NP	Non-polar	-27.1	80.0

\*after a week at room temperature

Table 1 Influence of tackifiers on the thermal properties of NBR/PVC

The addition of 3% tackifier slightly increases the  $T_g$  of NBR/PVC. This effect is opposite to that observed on NBR blended with tackifier (see Chapter 4) but is consistent with the impact of tackifier on rubbers from the literature [22]. Yet the samples are tested at room temperature and it is unlikely that this change in  $T_g$  will impact the energy dissipation at  $25^{\circ}\text{C}$ .

During this part, results for blends with **polar** tackifier will be represented in **blue**, and that for **non-polar** resin in **green**.

## 4.1. Self-adhesion properties of NBR/PVC with tackifiers

### 4.1.1. Without welding

Tack samples were prepared using the method detailed in section 3.1. The evolution of their self-adhesion properties with time were measured, and the stress-strain curves of the debonding stage are shown in Figure 26 and Figure 27. For both materials, an increase in contact time leads to a slow increase in self-adhesion energy due to a higher cavitation peak. The corresponding self-adhesion energies are plotted in Figure 28.

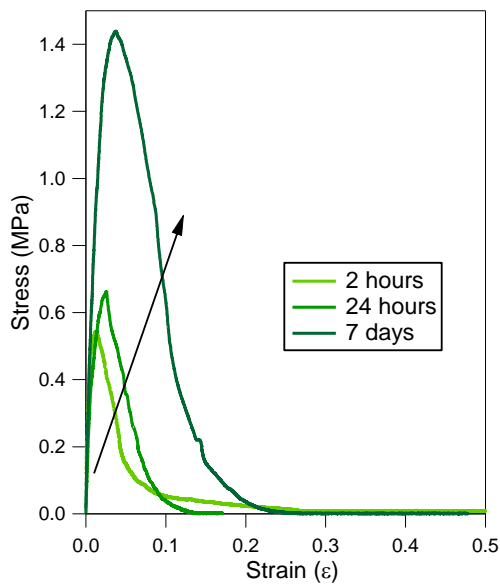


Figure 26 Influence of contact time on the self-adhesion properties of NBR/PVC-3NP

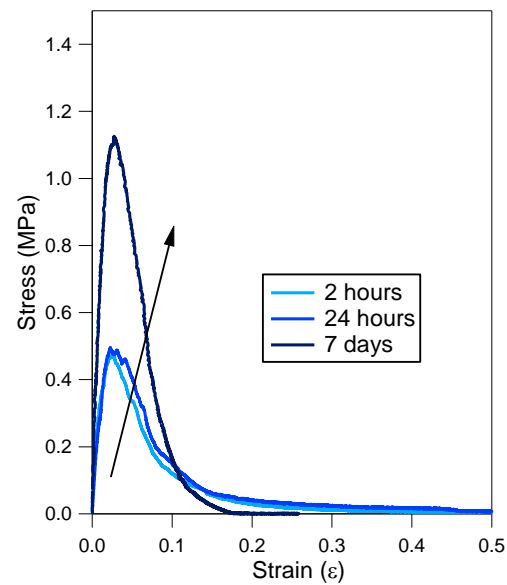


Figure 27 Influence of contact time on the self-adhesion properties of NBR/PVC-3POL

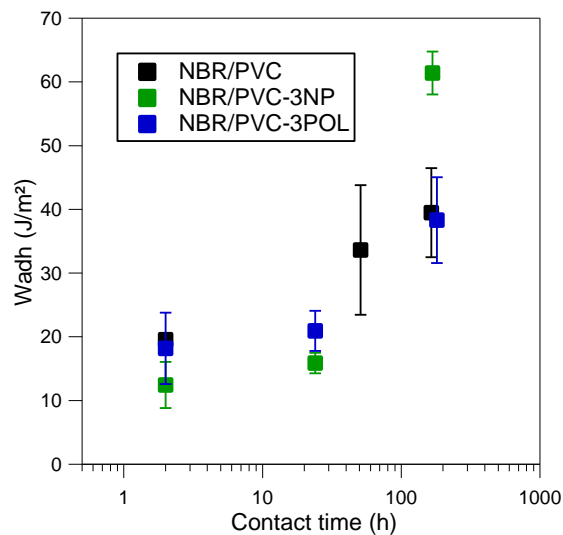


Figure 28 Self-adhesion energy as a function of contact time for the NBR/PVC and the blend with 3% resin (NBR/PVC-3NP and NBR/PVC-3POL)

Both tackifiers have similar effects and only slightly increase the self- properties of NBR/PVC. For long contact times (>100 hours), a slight increase is measured for blends with non-polar tackifier yet the self-adhesion energies are still low (<100J/m<sup>2</sup>).

Butanone was therefore used to weld both surfaces.

#### 4.1.2. Welding of the interface of NBR/PVC + resin with MEK

Samples were welded with 3uL of butanone and the evolution of their self-adhesion properties with time were probed.

##### i Influence of contact time on the self-adhesion of welded NBR/PVC + resin blends

Figure 29 and Figure 30 respectively show the debonding curves of NBR/PVC-3POL and NBR/PVC-3NP. In both cases an increase of the self-adhesion energy with time is probed, yet both materials behave completely differently. For NBR/PVC-3POL an increase in the cavitation peak is observed with time, suggesting a reinforcement of the interface with time. Yet crack propagates at the interface and the maximum deformation remains very low. This poor interfacial reinforcement can be due to some reorientation of chains to favor polar interactions rather than extensive chain migration. In the case of NBR/PVC-3NP, fibril are formed and bulk dissipation is observed. The cavitation peak first increases but remains constant after a contact of one day.

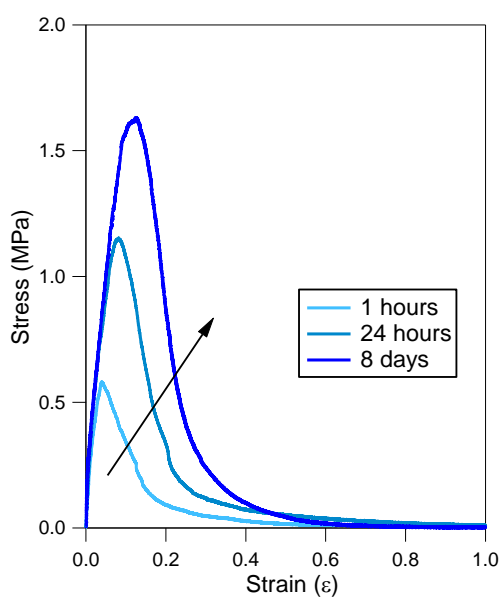


Figure 29 Self-adhesion properties of NBR/PVC-3POL. Influence of contact time. MEK welding

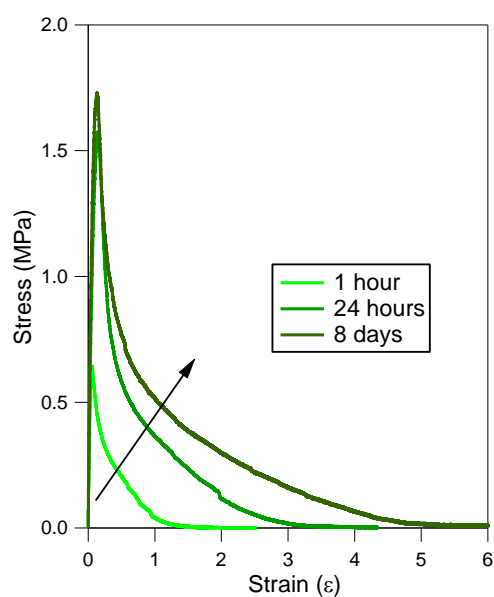


Figure 30 Self-adhesion properties of NBR/PVC-3NP. Influence of contact time. MEK welding

##### ii Comparison of the effects of both tackifiers

Both blends (NBR/PVC-3POL and NBR/PVC-3NP) are compared for contact times of one and twenty four hours in Figure 31 and Figure 32. It is very clear that, with welding, the addition of non-polar tackifier is much more efficient to enhance the self-adhesion properties of NBR/PVC, and Figure 33 shows the corresponding self-adhesion energies as a function of contact time.

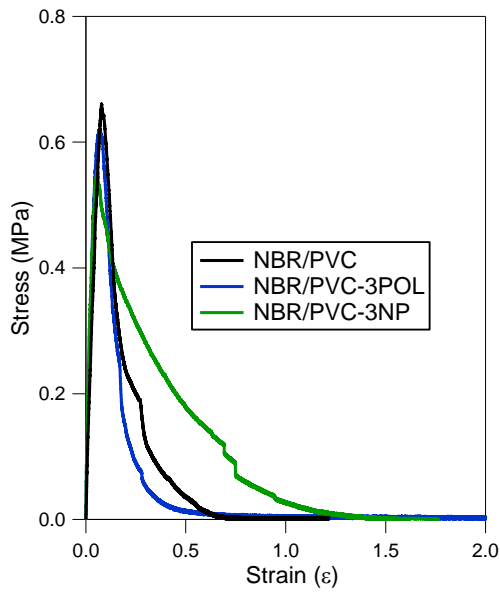


Figure 31 Comparison of the self-adhesion properties of blended samples. Contact time:1h. MEK welding

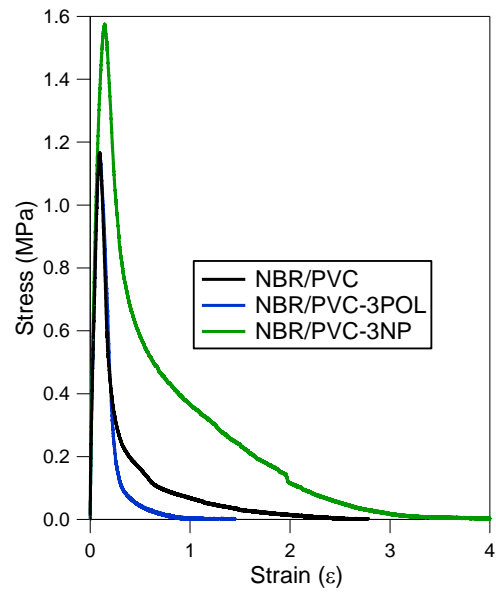


Figure 32 Comparison of the self-adhesion properties of blended samples. Contact time:24h. MEK welding

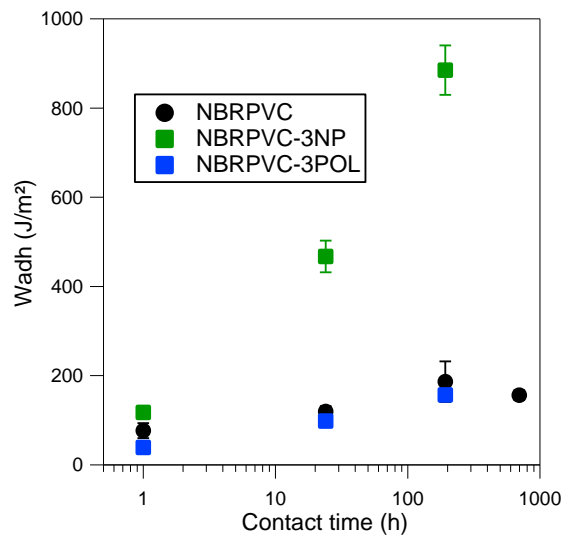


Figure 33 Self-adhesion energy as a function of contact time for NBR/PVC and blended samples, welded with MEK.

To understand such differences between the blends, their mechanical properties were investigated.

#### 4.2. Mechanical properties of NBR/PVC with tackifiers

X-Ray scattering experiments were run on the blends. No significant difference with raw PVC/NBR samples was probed. A time-dependent self-organization (similar to that in Figure 12) was also observed. To understand the different self-adhesion properties, the mechanical behavior of the samples were probed, in the linear regime as well as in large deformation.

### 4.2.1. Linear regime

Frequency sweeps were performed at 25 and 60°C and a master curve, shown in Figure 34, was plotted at 25°C. The three materials show similar trends over the investigated frequency range.

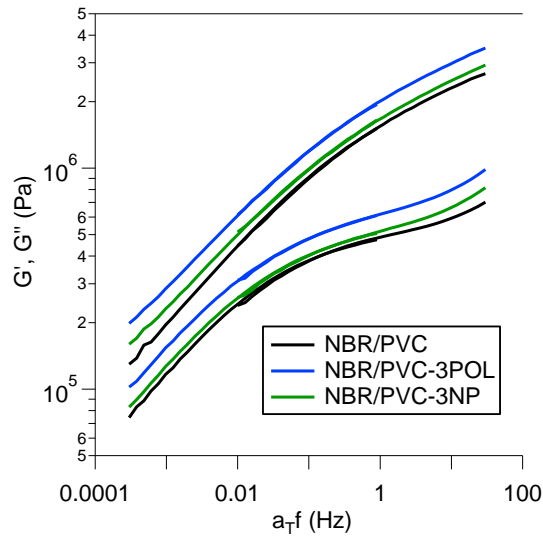


Figure 34 Linear rheology of NBR/PVC and blended samples. Curve plotted at 25°C.

Whereas the addition of non-polar resin hardly affects the linear mechanical properties of NBR/PVC, a strengthening of the material is observed (increase of the modulus by 20%) with the addition of polar tackifier.

### 4.2.2. Uniaxial tensile tests

Uniaxial tensile tests were run on the samples, at  $V_t=0.333\text{mm/s}$  ( $\dot{\epsilon} = 0.017\text{s}^{-1}$ ). All the samples broke with fast crack propagation and the results are strongly defects-driven. Therefore, curves are hardly reproducible at large strains. Comparison of the two blended samples is shown on Figure 35.

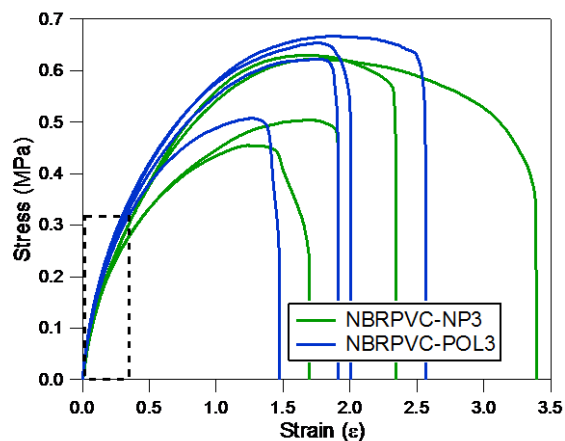


Figure 35 Uniaxial tensile test of blended samples.

It is hard to conclude any difference in large strains with such curves. Nevertheless, the tendency observed for the linear regime is similar to that probed by rheological experiments, and the modulus are compared in Table 2.

Sample	Young's Modulus (MPa)	$3\sqrt{(G'^2 + G''^2)}$ (MPa)
NBR/PVC	1.7	1.6
NBR/PVC-3NP	1.7	1.4
NBR/PVC-3POL	2.1	2.1

Table 2 Comparison of the Young's modulus (from uniaxial tensile test) and the elastic modulus calculated from linear rheology at the same frequency  $f=0.017\text{Hz}$

#### 4.2.3. **Comment**

This strengthening of NBR/PVC blend with the addition of polar tackifier can be explained by the anti-plasticization effect developed by Bergman and coworkers [21]. Indeed, due to the blends high polar content, it is likely that specific interactions (i.e physical crosslinks) occurs between the chains (both PVC and NBR), and the phenolic tackifier. As no particular heat transition corresponding to the phenolic tackifier was probed with DSC, it is unlikely that this mechanical reinforcement is due to the phase separation of the polar resin from the material.

### 4.3. Discussion

The addition of tackifiers in NBR/PVC, without welding, does not seem to be effective for the range of contact times investigated. Due to a low mobility inside the strong NBR/PVC physical network, it is plausible that tackifiers cannot migrate to specific favorable zones inside the matrix. This effect was mentioned by Sokolova and coworkers [23] who blended low molecular mass diphenylguanidine (DPG) into NBR. They showed that heating above  $85^\circ\text{C}$  was needed to have diffusion of the DPG molecules inside the micro-regions formed by acrylonitrile units. Below this temperature, limited mobility of ACN prevented any migration inside these regions.

Welding enhances the self-adhesion properties of the three blends. The use of butanone gives mobility to surface layers of NBR/PVC + tackifiers, and resins are able to migrate to the desired regions. Whereas the addition of 3% nonpolar tackifier, is very effective through increased bulk dissipation; that of phenolic resin does not modify the self-adhesion properties of welded NBR/PVC. In fact, the study of the blends' mechanical properties reveal that the addition of only 3% phenolic tackifier stiffens the material. The most likely explanation lies in the anti-plasticization effect of Bergman [21] and on the stronger physical interactions between the chains with the addition of phenolic tackifier. It is therefore suggested that the strong physical crosslinking in NBR/PVC and in NBR/PVC-3POL are hardly disrupted with MEK welding. On the other side, the addition of 3% nonpolar tackifier, soluble, is very effective and likely swells the polybutadiene portions.

Yet it is hard to explain such significant increase in the self-adhesion properties with solely swelling effects and this justification seems to contradict the results from Chapter 4 on the effects of tackifiers on the self-adhesion properties of NBR. Indeed, we had shown that the addition of polar tackifier disturbed the intermolecular  $\text{C}\equiv\text{N}$  interactions and thus enabled a slow diffusion process, and that the addition of non-polar tackifier was ineffective due to limited swelling. It is therefore very surprising that in the case of MEK-welded NBR/PVC, blending of only 3% non-polar resin is responsible for such high adhesion levels. Nevertheless, let us quickly comment that the combined effects of tackifier AND welding were not tested simultaneously for NBR and we cannot thus affirm that such surprising behavior would not have happened for NBR welded blends with non-polar tackifier.

## 5. Conclusion and discussion

PVC particles were blended into NBR and their influence on the self-adhesion properties of NBR/PVC were studied. To avoid debonding from the glass slide, the method developed in Chapter 2 was adapted, and a thin NBR layer was spincoated prior to the drop-casting NBR/PVC. The self-adhesion properties of NBR/PVC were measured for contact times up to two weeks and are shown to be very weak compared to that of NBR due to low deformation. No fibrils are formed and crack propagation occurs at the interface. In light of the results of Chapter 4, phenolic and hydrocarbon tackifiers were added at a concentration of 3% to enhance these self-adhesion properties. Nevertheless, the observed effects are weak, and very limited- if any - diffusion of polymer chains occurs. Welding with butanone strongly increases self-adhesion properties of NBR/PVC but the achieved energies are still relatively low compared to that of NBR. Both welding and tackifiers effects were probed simultaneously. Whereas the addition of polar tackifier is ineffective, that of hydrocarbon has a tremendous effect on the tack properties of MEK-welded NBR/PVC.

This study constitutes a preliminary study on the self-adhesion properties of NBR/PVC. Extensive investigations need to be launched to fully understand the blends structure and to correlate it to its mechanical behavior. Several leads are discussed. First, the acrylonitrile units' low mobility prevents diffusion of tackifiers in the matrix, and therefore limits their effect. Also, it was shown that for pure NBR, heating above 80°C drastically increased self-adhesion properties thanks to the disruption of a lamellar structure. For both reasons, tests at higher temperature could enhance the self-adhesion properties of NBR/PVC blends. Furthermore, only butanone was used as welding solvent and it would be interesting to try other solvents to deduce optimal criteria for solvent welding. Use of solvents with higher dipolar moment to disturb the strong polar network in NBR/PVC-3POL could be considered. Moreover, experimental procedures such as drying process or extruding conditions could be modified and their influence on structure, mechanical and self-adhesion properties investigated.

### Take home messages :

- Blending of PVC leads to a stiffening of nitrile rubber
- Similar to raw nitrile rubber, NBR/PVC blends tends to self-organize with time
- The self-adhesion properties of NBR/PVC are weak, and blending with tackifiers is not effective for the studied contact time
- Blending of a phenolic tackifier in NBR/PVC stiffens the materials due to strong polar interactions between the chains (anti-plasticization effect)
- Welding with MEK enhances the self-adhesion properties of the blend
- The combined effect of MEK welding and blending with non-polar tackifier is very effective for enhancing the self-adhesion of NBR/PVC. Yet the mechanism by which it operates remains poorly understood

## 6. References

- [1] A. K. Sen and G. S. Mukherjee, "Studies on the thermodynamic compatibility of blends of poly(vinyl chloride) and nitrile rubber," *Polymer (Guildf)*, vol. 34, no. 11, pp. 2386–2391, 1993.
- [2] H. H. Bertram, "Developments in Acrylonitrile—Butadiene Rubber (NBR) and Future Prospects," in *Developments in Rubber Technology—2*, Dordrecht: Springer Netherlands, 1981, pp. 51–85.
- [3] Z. H. Liu *et al.*, "Effect of morphology on the brittle ductile transition of polymer blends: 4. Influence of the rubber particle spatial distribution in poly(vinyl chloride)/nitrile rubber blends," *Polymer (Guildf)*, vol. 39, no. 21, pp. 5035–5045, 1998.
- [4] A. Mousa, U. S. Ishiaku, and Z. A. Mohd Ishak, "Rheological and mechanical properties of dynamically cured poly(vinyl chloride)/nitrile butadiene rubber thermoplastic elastomers," *Polym. Int.*, vol. 52, no. 1, pp. 120–125, 2003.
- [5] G. A. Zakrzewski, "Investigation of the compatibility of butadiene-acrylonitrile copolymers with poly ( vinyl chloride )," vol. 14, pp. 347–351, 1973.
- [6] K. E. George, R. Joseph, and D. J. Francis, "Studies on NBR / PVC Blends," vol. 32, pp. 2867–2873, 1986.
- [7] O. T. and I. T., "Mechanical properties of poly ( vinyl chloride ) - poly (acrylonitrile- co-butadiene ) blends with modulated structure," vol. 23, pp. 718–722, 1988.
- [8] C. B. Wang and S. L. Cooper, "Morphology and properties of poly(vinyl chloride)–poly(butadiene-co-acrylonitrile) blends," *J. Polym. Sci. Polym. Phys. Ed.*, vol. 21, no. 1, pp. 11–27, 1983.
- [9] W. Wang, Q. Yao, J. Song, B. Yao, H. Wang, and Z. Li, "Direct visualization of the nanoscopic three-phase structure and stiffness of NBR/PVC blends by AFM nanomechanical mapping," *J. Polym. Sci. Part B Polym. Phys.*, vol. 57, no. 11, pp. 662–669, 2019.
- [10] X. Huang, N. Tian, T. Wang, K. Wang, and Q. Xue, "Friction and wear properties of NBR/PVC composites," vol. 21, no. 7, pp. 449–456, 2007.
- [11] A. H. Jorgensen, L. A. Chandler, and E. A. Collins, "Multiple glass transitions in butadiene-acrylonitrile copolymers. II. Formation of incompatible phases during copolymerization." 1973.
- [12] B. G. Rånby, "Two-component polymer systems: Physical properties as related to compatibility and interaction," *J. Polym. Sci. Polym. Symp.*, vol. 51, no. 1, pp. 89–104, 1975.
- [13] Z. Xiaojiang, H. H. Pu, Y. Yanheng, and L. Junfeng, "A FT-IR study on NBR / PVC, BR / PVC, and BR / PVC / NBR blends," *J. Polym. Sci. Part C Polym. Lett.*, vol. 27, no. 7, pp. 223–227, 1989.
- [14] Fukumori K., S. N., and K. T., "Pulsed NMR Study of Motional Heterogeneity in Acrylonitrile-Butadiene Poly(Vinyl Chloride) Blends." 1990.
- [15] S.-Y. Kwak and N. Nakajima, "CP/MAS <sup>13</sup>C NMR analysis of micromorphology in a thermoplastic elastomer prepared from nitrile rubber and poly(vinyl chloride)," vol. 37, no. 2, pp. 195–199, 1996.
- [16] M. C. Senake Perera, U. S. Ishiaku, and Z. A. Mohd. Ishak, "Characterization of PVC/NBR and PVC/ENR50 binary blends and PVC/ENR50/NBR ternary blends by DMA and solid state NMR," *Eur. Polym. J.*, vol. 37, no. 1, pp. 167–178, 2001.

- [17] S. Kwak and N. Nakajima, "Monitoring of Homogenization and Analysis of Nanoscale Structure in a Butadiene - Acrylonitrile Copolymer / Poly ( vinyl," pp. 5446–5452, 1996.
- [18] M. Matsuo and C. Nozaki, "Fine Structures and Fracture Processes in Plastic / Rubber Two-Phase Polymer Systems . 1 . Observation of Fine Structures Under the Electron Microscope," 1968.
- [19] G. Porod, "Die Röntgenkleinwinkelstreuung von dichtgepackten kolloiden Systemen - I. Teil," *Kolloid-Zeitschrift*, vol. 124, no. 2, pp. 83–114, 1951.
- [20] D. G. . Ballard, A. . Burgess, J. . Dekoninck, and E. . Roberts, "The 'crystallinity' of PVC," *Polymer (Guildf)*., vol. 28, no. 1, pp. 3–9, Jan. 1987.
- [21] G. Bergman, H. Bertilsson, and Y. J. Shur, "Antiplasticization and transition to marked nonlinear viscoelasticity in poly(vinyl chloride)/acrylonitrile–butadiene copolymer blends," *J. Appl. Polym. Sci.*, vol. 21, no. 11, pp. 2953–2961, Nov. 1977.
- [22] K. D. Kumar, A. H. Tsou, and A. K. Bhowmick, "Interplay between bulk viscoelasticity and surface energy in autohesive tack of rubber-tackifier blends," *J. Polym. Sci. Part B Polym. Phys.*, vol. 48, no. 9, pp. 972–982, 2010.
- [23] L. V Sokolova, O. A. Chesnokova, and V. A. Shershnev, "Features of dissolution of crystalline low molecular weight compounds in butadiene-nitrile elastomers," vol. 0, no. 2, pp. 314–321, 1984.

# - CONCLUSIONS AND PERSPECTIVES -

---

A general conclusion is now presented in which we first show that the thesis' main objectives have been addressed during the different chapters of the manuscript. Perspectives and future works on these simplified NBR and PVC/NBR systems are then discussed. It is then shown how this work can be relevant for other materials. Last, the industrial relevance of the results is highlighted.

\*\*\*\*\*

## Review of the thesis conclusions

This thesis had three main objectives:

- Development of a method to characterize the self-adhesion properties of rubbers. The method had to be consistent with the industrial process (long contact times, low contact pressure) and show results in agreement with the industrial operators' impression of the quality of the adhesion.
- Understanding the poor self-adhesion properties of NBR.
- Exploring strategies to overcome these poor tack properties.

An adaptation of the well-known probe-tack method was developed and enabled the testing of self-adhesion properties for contact times ranging from an hour to several weeks. The contact was made thanks to a load and a corresponding pressure of 0.3bars. During this work, the self-adhesion properties were first probed at room temperature. They were then compared to that of a nonpolar SBR elastomer and revealed the much poorer adhesion performance of nitrile rubber relative to SBR. Furthermore, it was shown that contrary to linear monodisperse SBR elastomers, no link could be established between the flow probed at low frequencies in linear rheology and the diffusion time at the interface during the tack experiments.

DSC measurements as well as frequency sweeps at 80°C showed that the macromolecules tend to progressively self-organize with time and temperature. Dissolution in a solvent and slow drying was used to accelerate the slow self-structuring process. X-Ray scattering, Atomic Force Microscopy and Transmission Electron Microscopy revealed the existence of a complex organization, with a clear lamellar structure. Liquid <sup>1</sup>H NMR gave a strong indication that this lamellar structure was composed of blocks of polybutadiene, and blocks of alternating polybutadiene-acrylonitrile sequences. Due to the strong polarity of the C≡N bond, it was assumed that the material was physically crosslinked through intermolecular interactions. The self-adhesion properties of this multi-block copolymer were studied at higher temperatures and it was shown that beyond a threshold temperature, 80°C, the self-adhesion properties of NBR were significantly enhanced. We concluded that this increase was due to the disruption of a lamellar structure, as revealed by X-Ray measurements.

To boost the tack performance of NBR, a first strategy consisted in the addition of tackifiers with an extruder. The influence of two types of tackifiers was investigated, a polar –phenolic- resin and a nonpolar–hydrocarbon- one. At low concentration it was shown that the polar tackifier is very effective in increasing the self-adhesion properties of NBR for long contact times. This effect was attributed to the ability of polar resins to interact with the intermolecular C≡N interactions and thus to disturb the physical network. Indeed, despite similar mechanical properties (linear rheology, tensile tests) and a similar structure (SAXS) as the blend with a non-polar resin, the addition of polar tackifier favors a slow migration of the macromolecules through association-dissociation processes.

At high concentrations, the self-adhesion properties were independent of the resin's chemical nature but we assumed that this similarity was due to different mechanisms. The increase in self-adhesion properties over time for blends with 10% tackifier are due to slow chain migration in the blend with polar tackifier, whereas it is assumed to be due to slow structural changes for the blend with the hydrocarbon resin. Furthermore, a jump in self-adhesion properties of NBR at short contact times for blends with 20% tackifier is measured. This effect is attributed to a dilution outcome and the disruption of the material's structure through weakened intermolecular dipole-dipole interactions at such high resin content, thus increasing diffusion dynamics.

The second strategy to enhance the self-adhesion performance of NBR was the use of solvents to weld the interface between both elastomer surfaces. It was shown that the use of solvent at the interface drastically boosts the self-adhesion (more than 10-fold for any contact time) thanks to the enhancement of contact area, and to the increase in interfacial interactions (be they just physical, or due to the diffusion of chains) between the two welded materials. Among twelve tested solvents, it was shown that polar aprotic ones are the most efficient in enhancing self-adhesion, and the role of the boiling temperature of the solvent was also highlighted. Once the contact has been sufficiently reinforced thanks to solvent-enhanced polymer interdiffusion, the bulk strength of the material becomes the limiting factor for strong tack performance. This mechanical resistance of the bulk is highly dependent on the material's structure.

Finally, polyvinylchloride (PVC) particles were blended into NBR and their impact on the self-adhesion and mechanical properties of the rubber was probed. Poor tack performance was measured due to the existence of a structure, probed by X-Ray and AFM measurements. The two previously mentioned strategies, i.e. the addition of tackifiers and solvent welding were used to boost the self-adhesion performance. The combined effect of non-polar tackifier and MEK welding was shown to be very effective yet the characterizations performed are not sufficient to conclude on the diffusion mechanism of such system.

### Future work

This thesis has opened routes for future works on the self-adhesion of uncrosslinked polar materials. Further investigations could enable a better understanding of molecular dynamics in block-structured rubbers with strong intermolecular interactions. In fact, several experimental results could not be completely explained with the proposed mechanisms and in-depth studies would be needed to provide answers to the remaining questions marks. Indeed, the jump in NBR self-adhesion properties at short contact times when the tackifier content was increased from 10 to 20% was assumed to be due to chain mobility through weakened intermolecular bonds. Similar explanation was provided to justify the influence of the glass slide's drying condition on the self-adhesion of NBR. To confirm – or reject- these hypothesis neutron reflectivity could be considered to assess chain dynamics. Such study might also provide explanation for the more general role of polar bonds (C≡N, C-Cl and RO-H) on the diffusion dynamics of polar blends such as NBR/PVC.

Besides, cyclic tensile tests could be considered to estimate the rate at which the associative-dissociative mechanisms of intermolecular polar interactions occur.

What's more, to decouple each effect, the different strategies (temperature, tackifier, solvent welding) were not combined to increase the self-adhesion properties of NBR during this thesis. It would not be surprising that the role of temperature or solvent welding changes for tackified rubber. In addition, it would be interesting to see if the choice of solvent for welding is dependent of the tackifiers' chemical nature. Other investigations could also be launched on the use of blends of solvents (rather than pure ones) to weld surfaces.

Furthermore, the studied systems were simplified compared to industrial formulations, and it would be interesting to blend other additives (such as plasticizers or fillers) in the rubber and probe their impact on the structure and properties of the material. The role of their chemical composition (and particularly their polarity) will presumably also be a determining factor.

\*\*\*\*\*

### Fundamental interest

It is interesting to put these results into perspective and to discuss their relevance for other systems. The interesting behavior of NBR presented in this study was primarily due to the combination of three effects: the intrinsic polarity of acrylonitrile units, the polymerization process which resulted in a block copolymer rather than a statistical one, and the immiscibility of both blocks. The strong intermolecular polar interactions considerably slowed (if not completely annihilated) the diffusion dynamics of chains.

Based on these results, one could expect a similar behavior with other copolymers containing acrylonitrile as co-monomer, and with polymers with strong polarities such as polychloroprene. The microphase separation into a lamellar structure is caused by the immiscibility between both blocks, and, associated with strong intermolecular bonds, is responsible for the absence of correlation between flow properties and diffusion dynamics. Knowing that additives and solvent tend to interact with a specific part of this self-assembled structure, a better choice of the blended molecules could lead to a significant change in mechanical and adhesive properties without a need to use high concentrations. This highlights the possible synergistic effect between additives and microphase separated structures.

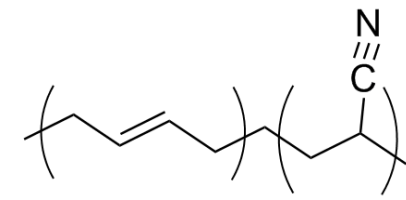
### Industrial interest

Our work provides a fundamental picture of the structure in nitrile rubber and its influence on the material's mechanical and self-adhesion properties. Several results are of practical interest for Safran as they are strongly related to their fabrication process.

In fact, the method developed already lead to the purchase of a new testing device that will be implemented on-site to control the tack performance of new rubbers and blends. Moreover, the role of the tackifiers' chemistry on the self-adhesion properties of NBR permits a finer control of the raw materials and their specifications. Now that several key parameters for solvent welding have been identified, several others –meeting the industrial requirements in terms of price and environmental and security requirements- may be tested using the method developed.

Furthermore, this work gives a more general picture of the impact of each fabrication step on the materials properties. Indeed, as it is shown that with time and temperature the material ages and forms a physical network, it is strongly suggested that the storing conditions mentioned in the Introduction (time, temperature) be controlled. After reception from suppliers, the materials' 'quality' (Mooney viscosity) are controlled at high temperature and high strains, and therefore probe the materials' properties without structure. In fact, two nitrile rubbers can exhibit similar properties under such conditions and yet show different structural organizations after cooling to room temperature. This ambient temperature properties not only depends on the processing conditions, but also on the polymerization strategy as well as on the amount of acrylonitrile units.

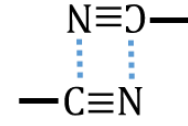
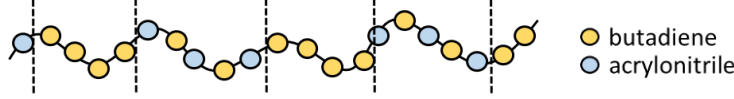
# Self-adhesion properties of uncrosslinked nitrile rubber



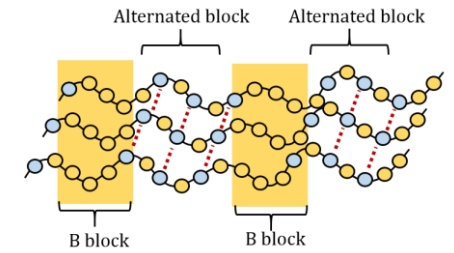
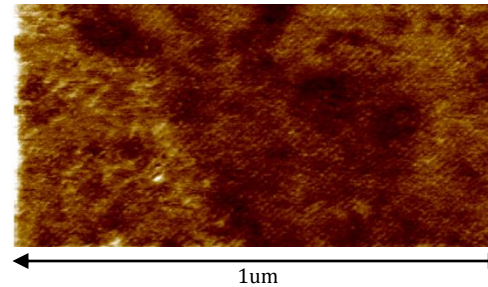
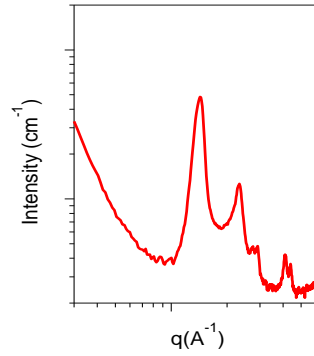
NBR = block copolymer with 1. blocks of polybutadiene  
2. blocks with alternated acrylonitrile-butadiene sequences

+

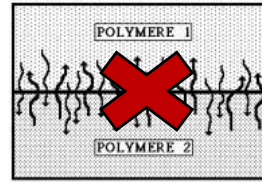
Polar C≡N interactions



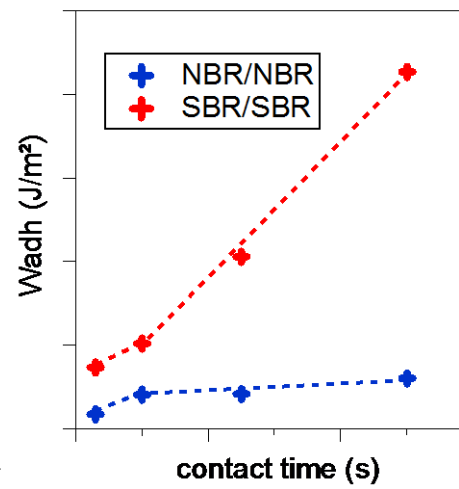
Material self-organizes with time to form lamellar structures  
↔ Physical network



Intermolecular C≡N interactions and lamellar structures prevent diffusion of chains at the interface



Weak self-adhesion energies



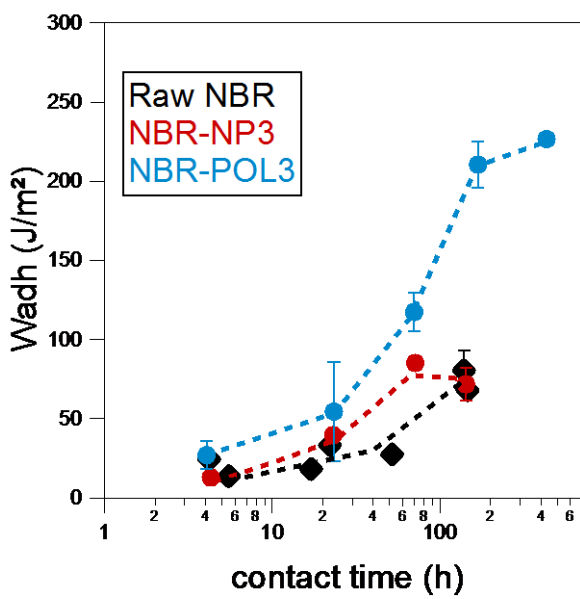
Two strategies to boost them:

**Addition of tackifiers**

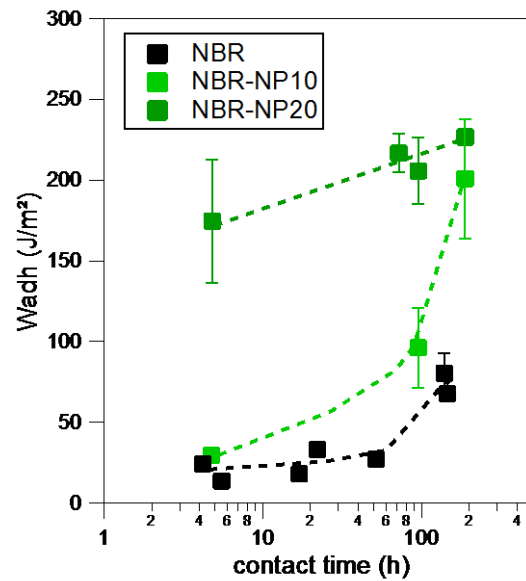
Polar phenolic resin = POL | Hydrocarbon resin = NP

**Welding with a solvent**

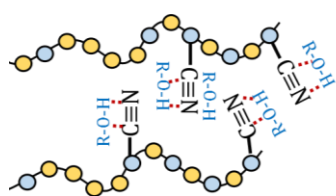
At low concentration



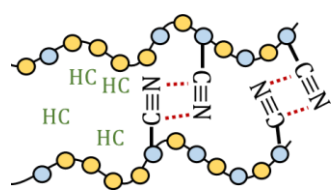
At high concentrations



Dissimilar effects due to tackifiers' different ability to interact with intermolecular C≡N bonds

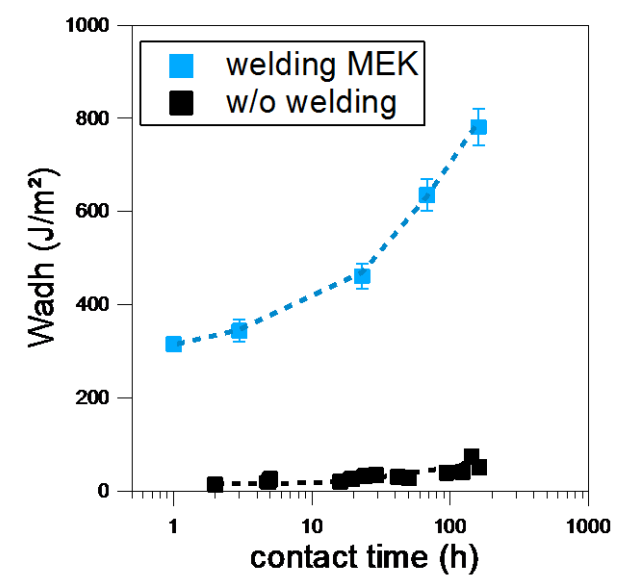


Association-dissociation processes with POL

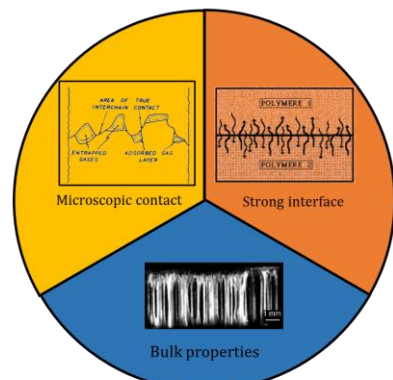


Swelling of PB blocks with NP

12 solvents tried  
Best option for NBR welding: Polar aprotic solvents with moderate boiling temperature



All the results are explained in lights of Hamed three criteria for self-adhesion energies





# ANNEXES

## 1. Characterizations of the materials

### 1.1 NMR of NBR-SA

A solution of 2wt% of NBR-SA in d8-toluene was prepared and <sup>1</sup>H NMR were recorded at 400MHz.

The double bond methine protons of butadiene are observed between 5 and 5.7ppm. With comparison to the peak at 0.4 ppm corresponding to the alpha protons of acrylonitrile, it is possible to deduce the amount of acrylonitrile units in the studied NBR. With this graph, it is calculated that NBR-SA has 44% acrylonitrile units.

Yet some parts of the material were not soluble and could therefore not be analyzed. Due to emulsion polymerization, the composition in ACN is possibly different from one polymer chain to the other, this number might not be representative of the whole polymer. The technical data sheet of Sigma-Aldrich stipulates a 37-39% acrylonitrile content. This suggests that only high-ACN content chains were soluble whereas the other one are physically crosslinks. Indeed, high-CAN chains very likely show a statistical organization with butadiene, whereas for low-ACN chains, alternated sequences and blocks of PB are present.

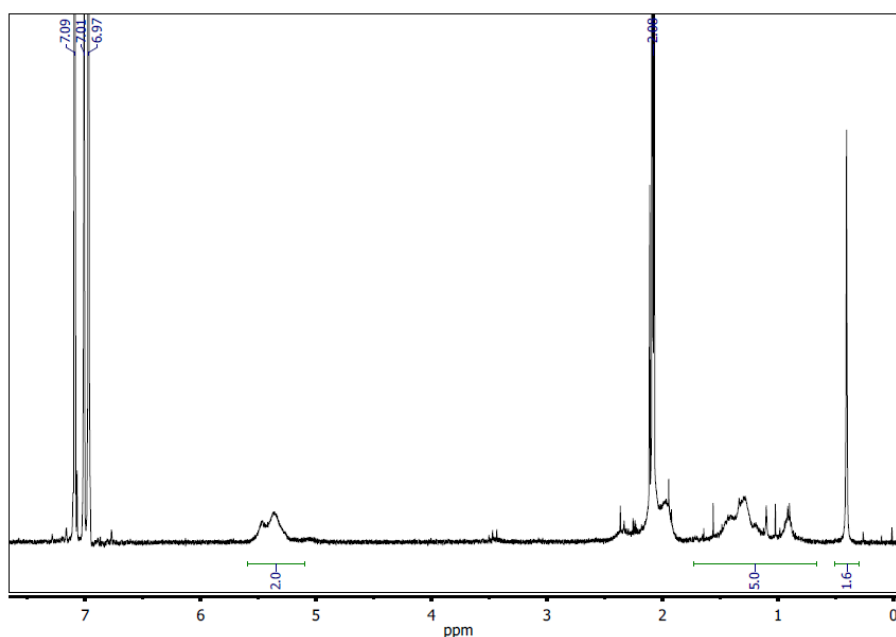


Figure 1 NBR-SA in toluene d8

## 1.2 SEC curve of raw NBR in toluene

The SEC experiments were performed by the Institut Charles Sadron (Strasbourg, France). The device was calibrated with polystyrene, using nine Polymer Lab standards with molar masses between 2400 and 370 000g/mol. The materials were solubilized during 48h in toluene at concentrations around 4mg/mL and filtrated on a PP filter (Dynagard) of 0.2microns before injecting it into the column. During the analysis, approximately 20wt% of the material could not be analyzed because the chains were too large (>400kDa) to go through the column. Therefore, the molar mass (as well as the polydispersity index) considered are under-estimated.

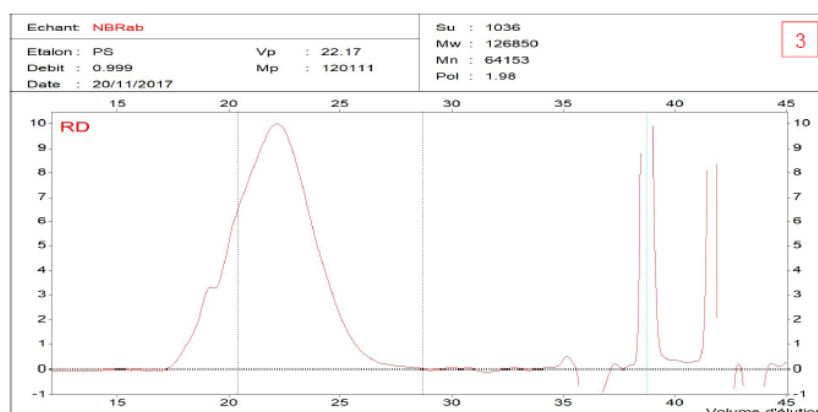


Figure 2 SEC of raw NBR

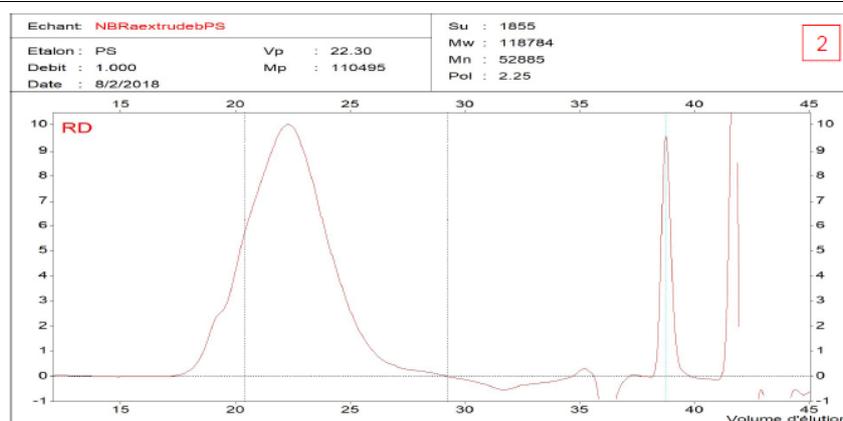


Figure 3 SEC of extruded NBR

The raw material (the 80wt% that could be analyzed), has a weight average molar mass  $M_w = 126\,850$  g/mol and a polydispersity index of 1.98. The extruded material (the 86wt% that could be analyzed), has a weight average molar mass  $M_w = 118\,744$  g/mol and a polydispersity index of 2.25.

## 1.3 Method to check concentration of PVC in blends

In order to make sure that the different blends of PVC/NBR had similar compositions in PVC, samples of 10-20mg were analyzed with TGA and a typical curve is shown in Figure 4. From the data presented in Chapter 2 on raw NBR, it is suggested that any mass loss before a threshold temperature (close to 400°C) is due to the presence of PVC particles. This threshold temperature is determined thanks to the analysis of the derivative of the weight (see Figure 5). Therefore, by

determining the amount of weight associated to this mass change (from  $\sim 400^{\circ}\text{C}$  to  $\sim 600^{\circ}\text{C}$ ) the exact composition of NBR/PVC blends could be determined.

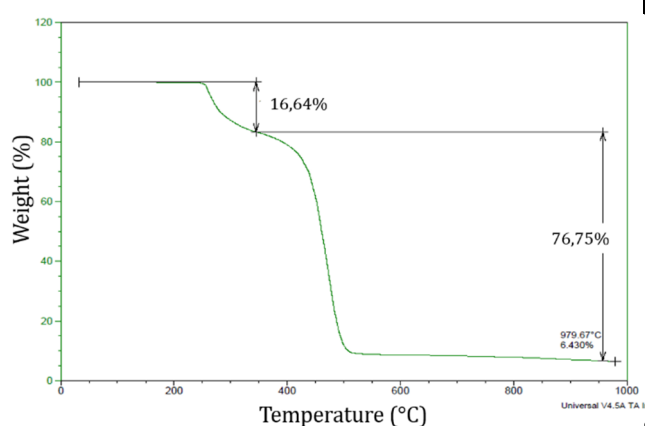


Figure 4 TGA of NBR/PVC

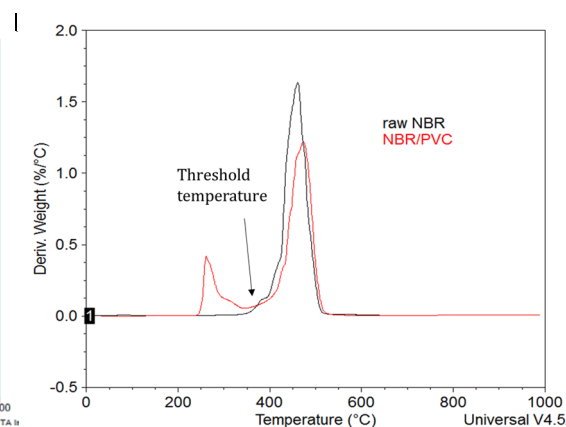


Figure 5 TGA: weight derivative as a function of temperature for NBR and NBR/PVC

## 2. Determination of NBR linear regime

Raw NBR was molded under a heating press ( $100^{\circ}\text{C}$ , 50 bars, 1 hour +  $25^{\circ}\text{C}$ , 50 bars, 1 hour), and a 8mm-diameter punch was cut.

Strain sweeps were performed at 1Hz, at 25 and  $60^{\circ}\text{C}$ . Figure 6 shows that from  $\gamma=0.01\%$  to  $\gamma=1\%$ , the linear regime of NBR is probed.

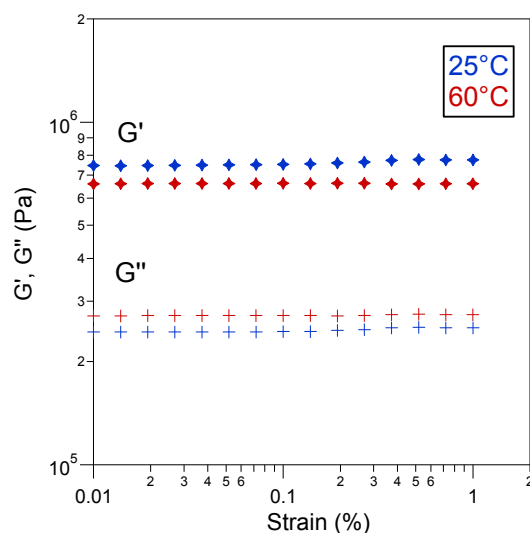


Figure 6 Determination of linear regime- strain sweeps on NBR

### 3. Structure observation

#### 3.1 SAXS of Tackifier + 3%: solubilized and aged

The X-Ray scattering profiles of aged samples of NBR-NP3 and NBR-POL3 is shown on Figure 7, and that of blends solubilized in cyclohexanone and dried slowly (RT + 100°C 2h) are shown on Figure 8.

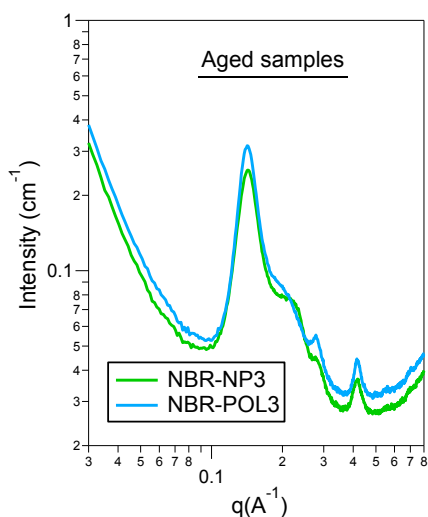


Figure 7 X-Ray scattering of aged NBR + 3% tackifier blends

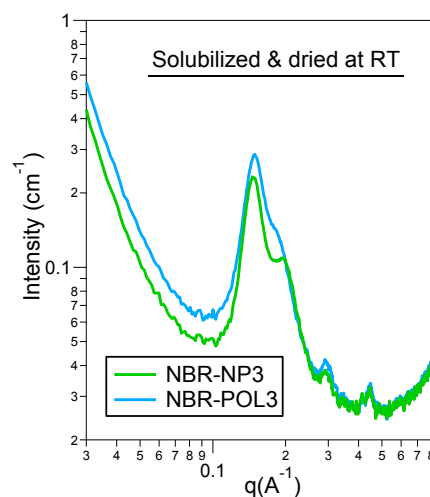


Figure 8 X-Ray scattering of samples solubilized and dried slowly

#### 3.2 SAXS- Drying conditions

After dissolution, NBR was drying at 2 days at room temperature followed by 2 days in a vacuum oven at 70°C. The influence of the solvent used (toluene vs chloroform) for dissolution is shown on Figure 9.

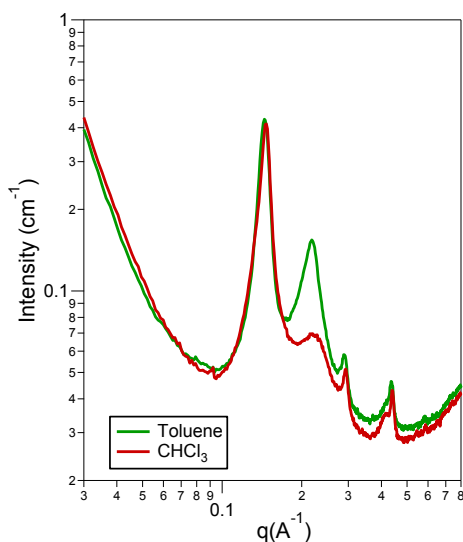


Figure 9 Influence of the solvent used on the SAXS profile of dissolved-NBR

#### 4. Influence of welding solvent on the self-adhesion of NBR

The stress-strain curve of the debonding between two raw NBR surfaces welded with DMF and toluene are compared in Figure 10. Despite their dissimilar properties regarding acrylonitrile and butadiene (DMF being a good solvent for acrylonitrile and toluene a good one for butadiene), their effect on the self-adhesion properties of NBR are similar after 3 hours of contact.

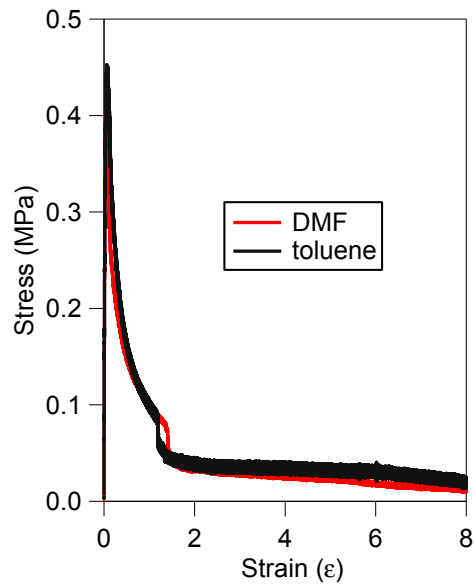


Figure 10 Comparison of welding with DMF and with toluene on raw NBR. Contact time = 3hours

## RÉSUMÉ

---

De nombreux procédés de mise en œuvre des élastomères impliquent la superposition de pièces de caoutchoucs non-vulcanisés. Une adhérence suffisante entre les différentes couches est nécessaire afin d'empêcher le décollement spontané et l'apparition de défauts.

Pour caractériser les propriétés autohésives (d'un matériau sur lui-même), à faible pression et longs temps de contact, nous avons adapté la méthode du Probe-Tack. Si le mécanisme d'interdiffusion des chaînes polymères à l'interface lors d'une mise en contact au-dessus de  $T_g$  est connu et a fait l'objet de différentes études, toutes ces études ont porté sur des polymères non polaires linéaires. Les propriétés autohésives d'un matériau polaire, le caoutchouc nitrile, sont étudiées et se révèlent être très faible en comparaison à celles d'élastomères non polaires type SBR. Nous montrons que le caoutchouc nitrile est en réalité un copolymère à blocs composé d'enchaînements d'unités butadiène (blocks de polybutadiène), ainsi que de parties où les monomères butadiène et acrylonitrile sont alternés. Cette composition conduit à la formation de structures lamellaires auto-organisées, et les fortes interactions polaires intermoléculaires créent un réseau physique limitant la diffusion des macromolécules. Cette organisation est responsable des faibles propriétés autohésives du caoutchouc nitrile même pour de longs temps de contact. Deux stratégies sont proposées pour les améliorer. L'ajout de résine tackifiante polaire se révèle très efficace même à faible concentration si le temps de contact est suffisamment long. L'avivage de la surface par différents solvants est étudiée, et paraît fondamentale afin d'atteindre de très hauts niveaux d'adhésion.

## MOTS CLÉS

---

Autohésion, Elastomère polaire, résine tackifiante, Probe-Tack, avivage

## ABSTRACT

---

Many industrial processes rely on the superposition of unvulcanized rubber pieces to shape their product. Sufficient adherence between the overlapping layers is necessary to prevent any debonding, slippage and the outbreak of defects.

An adaptation of the well documented Probe-Tack test is proposed to characterize the adhesion, and self-adhesion, properties of the materials for long contact times under a weak contact pressure. Whereas the inter-diffusion mechanism of polymer chains at interfaces is well known and has been the topic of many research projects, all these studies have focused on non-polar, linear polymers. The self-adhesion properties of a polar elastomer, nitrile rubber, are studied and are shown to be very weak compared to those of a classical non-polar SBR elastomer. Our work focuses on the mechanisms responsible for adhesion between polar elastomers with high polydispersity and molar mass. We show that the studied poly(acrylonitrile-co-butadiene) is actually a block copolymer composed of polybutadiene blocks, and blocks of alternating butadiene-acrylonitrile sequences. This composition leads to the formation of a lamellar structure with time, and the strong intermolecular polar interactions create a physical network preventing the polymer chains to diffuse. Such organization is responsible for the weak self-adhesion properties of nitrile rubber, and two strategies are proposed to enhance them. It is shown that the use of polar tackifier is effective, even at low concentration, if sufficient contact time is achieved. The use of solvent to weld both surfaces, called "solvent welding", is investigated and shown to be essential to reach high adhesion levels.

## KEYWORDS

---

Self-adhesion, polar elastomer, tackifier, probe-tack, solvent welding

